Palladium and Transition Metal Based Catalysts for Hydrogen Peroxide Synthesis and Electrocatalytic Applications

A Thesis Submitted for the Degree of

Doctor of Philosophy

By

Sisir Maity

Chemistry and Physics of Materials Unit

Jawaharlal Nehru Centre for Advanced Scientific Research

(A Deemed University)

Jakkur, Bangalore- 560064 (INDIA)

April, 2018

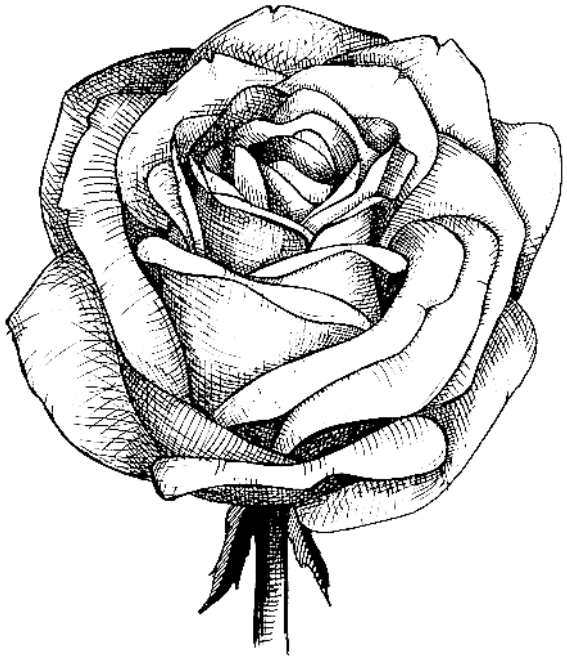

Dedicated to

my parents

DECLARATION

I hereby declare that the thesis entitled ***"Palladium and transition metal based catalysts for hydrogen peroxide synthesis and electrocatalytic applications"*** is an authentic record of research work carried out by me at the Nanomaterials and Catalysis Laboratory, Chemistry and Physics of Materials Unit, Jawaharlal Nehru Centre for Advanced Scientific Research, Bangalore, India under the supervision of **Prof. M. Eswaramoorthy** and that it has not been submitted elsewhere for the award of any degree or diploma.

In keeping with the general practice in reporting scientific observations, due acknowledgment has been made whenever the work described is based on the findings of other investigators. Any omission that might have occurred due to oversight or error in judgment is regretted.

Sisir Maity

Jawaharlal Nehru Centre for Advanced Scientific Research

Prof. M. Eswaramoorthy
Nanomaterials and Catalysis Laboratory
Chemistry and Physics of Materials Unit
Jawaharlal Nehru Centre for Advanced Scientific Research (JNCASR)
Jakkur, Bangalore-560064,India
Phone : +91 80 2208 2870
Fax: + 91 80 22082766
E-mail: eswar@jncasr.ac.in

Date:
April 9, 2018

CERTIFICATE

I hereby certify that the work described in this thesis entitled ***"Palladium and transition metal based catalysts for hydrogen peroxide synthesis and electrocatalytic applications"*** has been carried out by **Sisir Maity** at the Nanomaterials and Catalysis Laboratory, Chemistry and Physics of Materials Unit, Jawaharlal Nehru Centre for Advanced Scientific Research, Bangalore, India under my supervision and it has not been submitted elsewhere for the award of any degree or diploma.

Prof. M. Eswaramoorthy

(Research Supervisor)

ACKNOWLEDGEMENTS

It's my immense pleasure to acknowledge a large number of people for their valuable help and support during the course of my Ph. D. at JNCASR.

Firstly, I would like to express my most sincere gratitude to one person, my research supervisor, ***Prof. M. Eswaramoorthy*** *for introducing me to the field of materials science. I am thankful to him for his help and the freedom given to me to work on various problems from the beginning to the end of my Ph. D. His constant encouragement and valuable suggestions helped me in successful completion of this work. My heartily thanks to him for the opportunity.*

My sincere gratitude to Prof. C. N. R. Rao, FRS for his encouragement and being a constant source of inspiration. I am also grateful to him for creating such a vibrant research atmosphere in the institution to carry out the research work.

I would like to thank the present and past chairmen of CPMU (Prof. N. Chandrabhas, Prof. S. Balasubramanian and Prof. G. U. Kulkarni) for allowing me to use the various facilities of the centre.

I am thankful to the Int. Ph. D. co-ordinators (Prof. S. Balasubramanian and Prof. T. K. Maji) for their help and support during M. S.

Thanks to all the faculties, Prof. S. Balasubramanian, Prof. A. Sundaresen, Prof. M. Ewaramoorthy, Prof. G. U. Kulkarni, Prof. K. S. Narayan, Prof. N. Chandrabhas, Prof. T. K. Maji, Prof. S. M. Shivaprasad, Dr. R. Ganapathy, Dr. R. Dutta, Prof. Swapan K. Pati, Prof. Umesh V. Wagmare, Prof. S. Narasimhan, Prof. H. Ila, Dr. S. Rajaram, Dr. Subi J. George from JNCASR and Prof. S. Sampath from IISc for their useful and informative course work.

It is a great pleasure to thank my collaborators: Prof. S. Sampath from IISc; Prof. Umesh V. Wagmare and Suchitra from JNCASR for fruitful collaborations.

I am thankful to Prof. N. Ravishankar from IISc for TEM imaging.

My special thanks to my labmates, the "Nanocat" group members: Dr. Sai Krishna, Dr. K.K.R. Datta, Dr. B.V.V.S. Pawan Kumar, Dr. Piyush Chaturbedy, Dr. Amritroop Achari, Dheeraj, Sonu, Suchi, Soumita, Momin, Divya, Arunava, Surishi, Himani, Nijita, Dr. Shivanna, Dr. Mehraj, Subramanya, Dr. Sushumna, Dr. Josena, Dr. Krishna, Sahana, all the short term project students and visiting faculties (especially Prof. Varma from University of Trinidad and Tobago and Dr. Harish) for their cooperation, useful discussions and for creating a friendly atmosphere in the lab. Working with them was a real pleasure.

Thanks to the following people for various technical assistance: Mrs. Usha (TEM), Dr. Jay (TEM), Mr. Kanan (TEM), Mrs. Selvi (FESEM), Mr. Anil (XRD), Mr. Vasu (UV, IR, ICP), Mr. Srinath (Technical Assistance) and my friends, Arpan (XPS), Chandan (Magnetic Measurements), Somnath (XRD).

I am thankful to academic, administrative, library, hostel and Dhanvantary (medical) staff of JNCASR for their assistance.

Financial assistance from JNCASR is gratefully acknowledged.

I am thankful to my friends Jia, Saikat, Arpan, Somnath, Chandan and Abhijit for useful discussions (non-scientific also) and creating a wonderful friendly atmosphere. It would have really been difficult staying for me at JNCASR hostel without their company.

Thanks to all my Int. Ph. D. batch mates: Anirban, Arkamita, Chandan De, Chandan Mishra, Koushik and Rajsekhar for their pleasing company during the course work.

I thank all my friends from JNCASR for their company in various activities.

Besides the research life, I am also thankful to Prof. M. Eswaramoorthy and his family members for their hospitality and affection.

Thanks to my all friends from school (especially Abhijit and Suprabhat) and college (especially Ajay, Amit and Manas) for their encouragement and valuable suggestions. Special thanks to Debasmita for her affection and encouragement.

It's a great pleasure to thank all my teachers from my school and college, especially Dr. Subhasis Mallik, Kinkar Prasad Das and Sailendranath Ghosh for sharing their knowledge to a growing student.

I am very pleased to acknowledge the monks from Ramakrishna Mission Vidyamandira, Belur Math for their help, care and encouragement during my college days.

My sincere gratitude to Kuhu Lahiri, Shyamal Basu, Dilip Kumar Mondal and late Bibhutibhusan Parui for their help and support during my school and college life. I am thankful to them for giving me the opportunity to learn how to be honest and a good human being.

Finally, not the least, a deep sense of gratitude to my family for their support, love and affection throughout my life.

Sisir

PREFACE

The thesis is divided into two parts. Part- 1 focuses on the direct synthesis of hydrogen peroxide using bimetallic NiPd catalysts. Part- 2 deals with electrocatalysis like hydrogen and oxygen evolution reactions, oxygen reduction reaction using high surface area transition metal based phosphides and bimetallic NiPd nanostructures.

Part- 1:

Chapter- 1 gives brief introduction about different synthesis techniques for hydrogen peroxide production and their advantages and disadvantages related to the processes. Also, the experimental techniques and brief catalysts background for the direct synthesis of H_2O_2 are also discussed in this chapter.

Chapter- 2 deals with self-supported, bimetallic NiPd nanostructures for direct synthesis of H_2O_2 from molecular H_2 and O_2 in normal pressure conditions. The catalyst exhibits unusually high, three times higher than the normal activity compared to monometallic Pd nanocatalyst. The catalyst also shows high selectivity for H_2O_2 with maximum value of 95% and very long life time, 72h, with high activity in acidic condition.

Chapter- 3 describes about the NiPd nanoparticles supported on activated carbon for direct synthesis of H_2O_2 in normal as well as high pressure conditions. NiPd catalyst shows improvement in its catalytic activity in presence of very little amount of Pt (0.2 wt. % respect to support) as a promoter. The NiPd catalyst in presence of Pt shows one of the best catalytic performance for this reaction among monometallic Pd, bimetallic NiPd. The catalyst shows recyclability up to 5^{th} cycle (total 40h) in normal pressure without losing its initial activity.

Part- 2:

Chapter- 4 discusses about the brief introduction on water splitting and fuel cell technologies as next generation energy resources in near future. This chapter also talks about the costly noble metals, transition metal based electrocatalysts for water splitting reactions (hydrogen and oxygen evolution reactions) and oxygen reduction reaction (mainly employed in fuel cell).

Chapter- 5 describes about a new simple synthetic route to obtain high surface area bimetallic phosphide catalysts, NiCoP (with various Ni and Co compositions) which act as

an efficient electrocatalyst for oxygen evolution reaction (OER) under alkaline conditions as well as for hydrogen evolution reaction (HER) in both alkaline and acidic medium. The bimetallic $Ni_{0.2}Co_{0.8}P$ catalyst shows one of the best performances for OER under alkaline conditions among all the phosphides reported so far in the literature.

Chapter- 6 introduces a novel approach of rapid synthesis of bimetallic NiPd nanostructure by simple $NaBH_4$ reduction followed by a quick dissolution in presence of HCl and H_2O_2. The bimetallic NiPd catalyst shows very high surface area of 136 m^2 gm^{-1} and excellent performance for both hydrogen evolution and oxygen reduction reactions which is almost equivalent to state-of-the-art catalyst, Pt/C.

Chapter- 7 demonstrates a new methodology to quantify the amount of metallic Ni present in the mixed nickel hydroxide/nickel and also to synthesize bimetallic NiPd (with desired loading of Pd) on $Ni(OH)_2$ by simple galvanic replacement of Ni with Pd at different time periods. The nanostructured catalysts prepared by galvanic reaction shows better electrocatalytic activity towards methanol oxidation than commercial Pd/C.

Chapter- 8 gives the summary and conclusion of the thesis.

TABLE OF CONTENTS

PART-2:

Chapter 4: Introduction to electrochemical water splitting and oxygen reduction reaction

Chapter 5: High surface area NiCoP nanostructure as an efficient water splitting electrocatalyst: The oxygen evolution activity

PART-1

Chapter 1: **Introduction to direct synthesis of hydrogen peroxide**

Chapter 2: **Ni-Pd bimetallic catalysts for the direct synthesis of H_2O_2 – unusual enhancement of Pd activity in presence of Ni**

Chapter 3: **Direct synthesis of H_2O_2 by Pt promoted NiPd catalysts supported on carbon**

Chapter - 1

Introduction to direct synthesis of hydrogen peroxide

Summary:

The direct synthesis of hydrogen peroxide from molecular H_2 and O_2 is one of the most important chemical reactions from the industrial point of view. This route is a great alternative to existing anthraquinone (AQ) process which is used commercially for the production of H_2O_2. AQ process produces a lot of environmental hazards and needs to be replaced by some other greener synthetic route like direct pathway from molecular H_2 and O_2. Several advantages and disadvantages related to both the processes are discussed briefly along with other different synthetic routes for H_2O_2 synthesis. Also, the experimental techniques and brief catalyst background for the direct synthesis are described in this chapter.

1.1. Introduction:

Hydrogen peroxide (H_2O_2) was first discovered in 1818 by Louis-Jacques Thernard[1] and it was first synthesized by the hydrolysis of barium peroxide with sulfuric acid. Since its discovery, H_2O_2 is one of the most important chemical widely used in industrial application and for environmental remediation. It is the most promising environment friendly and chlorine free oxidizing agent as its byproduct is only water and therefore extensively used in many large-scale practical applications such as pulp and paper bleaching technologies, textile industries, detergent applications, waste water treatment, electronics industries, medical applications and many other chemical oxidation reactions (Figure 1.1).[2]

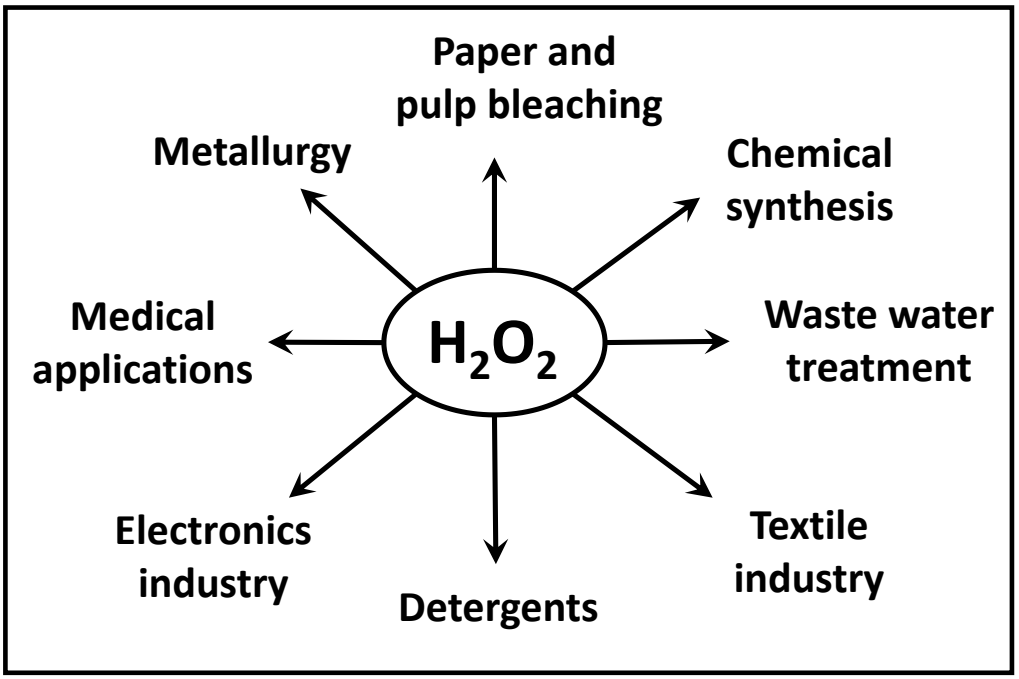

Figure 1.1: *Principal applications of hydrogen peroxide.*

Currently, H_2O_2 is produced mainly via anthraquinone auto-oxidation (AO) process.[3, 4] This method is mainly applicable for a large scale synthesis of H_2O_2 (35-40 wt. %), whereas 3-8 wt. % is only required for practical applications.[5] However, this large scale production suffers from the significant safety issues during transportation of huge amount of H_2O_2 from one place to another.[6] Besides, this process is not considered as green process as a large amount of toxic solvents are used during the synthesis and also hazardous side products are produced. So, as an alternative pathway, direct synthesis of H_2O_2 can be

carried out from molecular hydrogen and oxygen in presence of heterogeneous catalyst in an efficient and economical way which is also considered as an environment friendly process. Though, the direct synthesis of H_2O_2 from molecular H_2 and O_2 looks simple, the major challenges associated with the direct combination of H_2 and O_2 are the hydrogenation and decomposition of formed H_2O_2 in presence of the catalysts, and non-selective formation of H_2O as shown in the Scheme 1.1.[7]

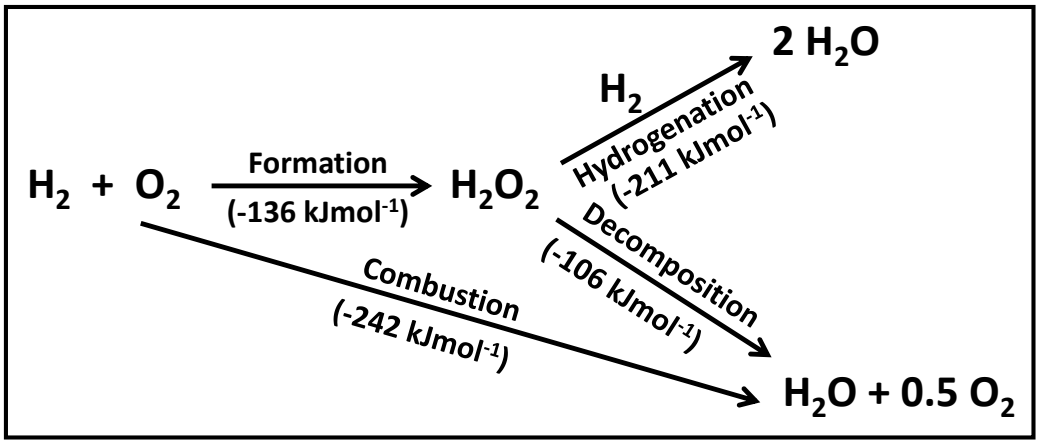

Scheme 1.1: *Reactions involved during the direct synthesis of H_2O_2 from molecular H_2 and O_2 (numbers in the bracket indicate standard enthalpy of the reaction).*

Monometallic Pd and later, bimetallic Pd based (Pd-Pt, Au-Pd, Ni-Pd etc.) heterogeneous catalysts were extensively explored in the last two decades for the direct synthesis of H_2O_2. Various approaches involved in the synthesis of H_2O_2 and the catalysts employed are briefly discussed below.

1.2. Synthesis of H_2O_2:

1.2.1. Indirect synthesis of H_2O_2 using anthraquinones:

The indirect synthesis of H_2O_2 using anthraquinone auto-oxidation (AO) process was first discovered by Riedl and Pfleiderer and commercialized in 1939.[8] Since then, it is the only industrial process to synthesize H_2O_2 in a large scale production. Currently, around 95% of global H_2O_2 production is produced by AO process.[2] The reactions occurred during the indirect synthesis of H_2O_2 via AO process are shown in the Scheme 1.2. The process involves high pressure hydrogenation of anthraquinone (AQ) to form anthrahydroquinone

(AHQ) in presence of Pd or Pt catalyst followed by oxidation in presence of air or O_2 to produce H_2O_2 and the AHQ revert back to AQ. Besides, over hydrogenation of anthrahydroquinone (AHQ) and subsequent oxidation leads to tetrahydroanthraquinone

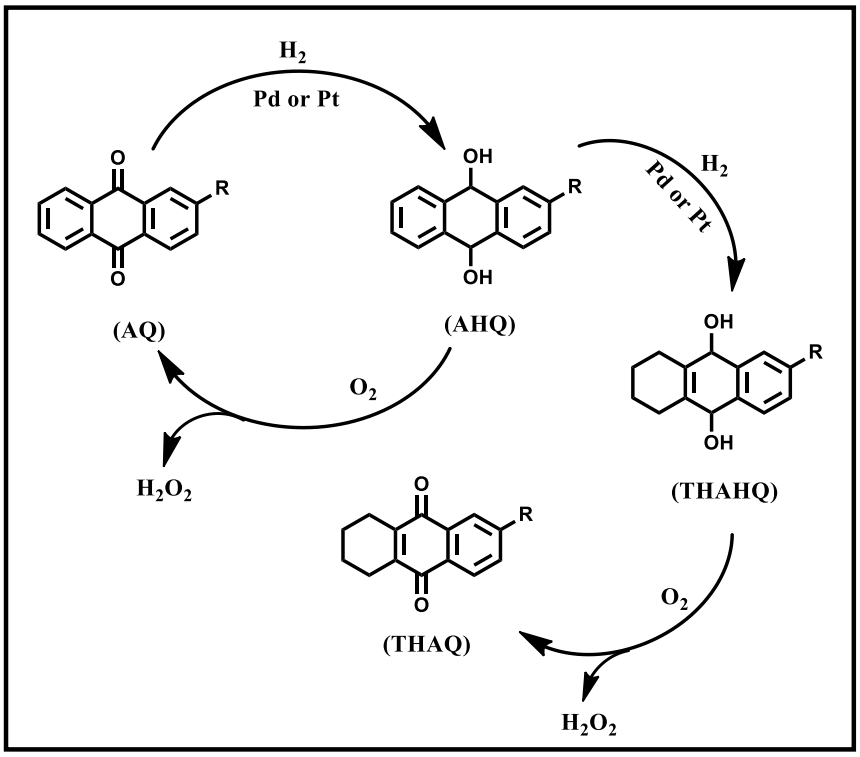

Scheme 1.2: *Reactions involved during the synthesis of H_2O_2 via anthraquinone auto-oxidation process.*

(THAQ) is formed which prevents the reusability of AQ. The overall process is being carried out in a mixture of solvents like esters/hydrocarbon, octanol/methyl-naphthalene etc.[8] Both AHQ and THAQ are active species and are oxidized to form H_2O_2. The H_2O_2 is stripped from organic working phase to aqueous phase in a counter current column to obtain an aqueous solution of H_2O_2. Then the aqueous solution of H_2O_2 is distilled under reduced pressure for further purification and to increase H_2O_2 concentration.

The AO process is extensively used in industries to produce H_2O_2 as it avoids direct mixing of H_2 and O_2 which is an explosive mixture beyond certain concentration. However, AO process has lot of disadvantages, e.g. uses of toxic solvents, non-selective hydrogenation, periodic replacement of costly quinone derivatives, deactivation of hydrogenation catalysts and energy intensive processes for the purification of H_2O_2 produced. Moreover, this is not

an environmentally green process as it produces a lot of hazards during the synthesis. The process is only commercially viable for a large scale synthesis of H_2O_2 but transportation from one place to another suffers from the safety issues[6] as it decomposes easily and also concentrated H_2O_2 is very explosive. Thereby, a high investment and operational cost would prohibit on-site H_2O_2 synthesis at the end user facility by this process. These limitations motivate scientists to develop new synthetic approaches which would more economical and green for the on -site production of H_2O_2.

1.2.2. Direct synthesis of H_2O_2 using heterogeneous catalysts:

The direct synthesis of H_2O_2 from H_2 and O_2 can give greener route compared to indirect way of synthesis as discussed above. Nevertheless, there are several challenges associated with direct synthesis as given in the Scheme 1.1. The catalysts used for direct synthesis reaction may cause the parallel reaction as well as the direct combination reaction which leads to decrease in the selectivity and productivity of H_2O_2.[5] There are various approaches to reduce side reactions, like minimizing the reaction temperature can minimize the direct combustion of H_2. Addition of additives or stabilizers like acids, halides etc. reduces the decomposition and hydrogenation of H_2O_2, thereby, improves the selectivity.[9] Another problem related to the direct synthesis of H_2O_2 is the use of H_2/O_2 mixture as it is explosive in presence of catalyst from 4% to 94% H_2 in O_2.[10] Sufficient safety precautions are required during the reaction and need to be carried out below 4% H_2 in oxygen atmosphere and hence, results in low concentration of H_2O_2.

The direct synthesis of H_2O_2 from molecular H_2 and O_2 using heterogeneous catalysts is quite different from other gas or liquid phase reactions as there are three phases involved during the reaction- the reactant gases (H_2 and O_2) and the diluents (normally inert gases like Ar, N_2 or CO_2) in the gas phase, the reaction medium (H_2O, alcohols or mixture of both) in liquid phase and the catalyst in solid phase. This leads to several steps in transport phenomena- (i) convection in the gas phase, (ii) gas-liquid equilibrium at the interphase of the catalysts, (iii) convection in the bulk liquid phase, (iv) adsorption of H_2 and O_2 on the active catalytic sites, (v) surface reaction between adsorbed species to form H_2O_2, (vi) desorption of H_2O_2 to the bulk liquid phase and finally (vii) convection in the bulk liquid phase as described by Salmi et al.[11] Any of the above steps can limit the overall rate of the reaction and hence the catalyst should be chosen in such a way that it would overcome these limitations.

1.2.3. Other approaches:

1.2.3.1. Fuel cell reactions:

Electrochemical fuel cell technology can be implemented for the synthesis of hydrogen peroxide by the reduction of oxygen in both acidic and alkaline medium.[12-14] A fuel cell method is an electrochemical process where partial reduction of oxygen ($2e^-$ transfer process) produces H_2O_2 at the electrochemical interphase between solid catalyst and aqueous electrolyte. As H_2 and O_2 gases are fed separately into the electrolyte membrane in the fuel cell, it can avoid explosive H_2/O_2 mixing. Also it can generate a lot of electrical power during the synthesis because of the fuel cell set up. Precious metal catalyst, Pt has been used inside the fuel cell for hydrogen activation as well as H_2O_2 synthesis and nafion has also been used as a cationic membrane to prevent the diffusion of H_2O_2. But, the high cost of Pt is still one of the major concerns for practical applications. Though, the fuel cell technology is considered as green process but still not economically viable.

1.2.3.2. Plasma method:

H_2O_2 can also be synthesized from H_2 and O_2 mixture by non-equilibrium plasma. The H_2 and O_2 molecules are activated during the synthesis by silent electric discharge at atmospheric pressure and produces H_2O_2 and H_2O.[15-17] The process has several advantages like it does not require any chemicals other than H_2 and O_2 in single phase (gas phase). It eliminates the diffusivity problem associated with the mass transfer limitations in three-phase direct synthesis reaction in presence of the heterogeneous catalysts.[2, 18] Also, it is considered as green process as it does not produce any other hazardous chemicals.[17]

1.2.3.3. Catalysis under supercritical CO_2 conditions:

Another synthetic approach for H_2O_2 production from H_2 and O_2 is under supercritical CO_2 conditions using both homogeneous [19-21] or Pd-based heterogeneous catalysts.[22] The supercritical CO_2 has many advantages compared to many organic solvents as it is less toxic, non-flammable and naturally abundant. Also, it does not react with the product formed in the reaction system. Moreover, both the reactants (H_2 and O_2) in gas phase are miscible with supercritical CO_2 above its critical temperature[23] (31 ^oC), it would overcome the diffusivity problem associated with three phase system, gas-liquid-solid interphases in the direct synthesis.[18] Thereby, compressed CO_2 either liquid or in supercritical stage above its critical temperature can be a greener[24] and efficient process for H_2O_2 synthesis.[25]

1.2.3.4. Membrane catalysis:

Membrane technology is one of the smart approaches for direct H_2O_2 synthesis. In membrane technology, membrane catalysts keep the reactant gases, H_2 and O_2 separate from each other and thereby, avoid the explosive H_2/O_2 mixing, one of the biggest safety concerns related to direct H_2O_2 synthesis.[26-31] Pd-based catalyst is deposited on a porous membrane shows efficient activity towards the H_2O_2 production in liquid phase synthesis.[26, 31] Pd-based membranes can supply atomic hydrogen on permeation of hydrogen molecules from one side to other which reacts further with the oxygen dissolved in the liquid medium to form H_2O_2. Although membrane technology can avoid explosive H_2/O_2 mixture, the rate of the H_2O_2 synthesis is controlled by the mass transport which is limited in this case, is quite low for the industrial applications.[2]

1.2.3.5. Semiconductor photocatalysts:

Photocatalysis over semi-conductor materials have also been investigated for the synthesis of hydrogen peroxide.[32-36] Irradiation of UV light of energy more than 3.23 eV on an aqueous suspension of TiO_2 nanoparticles (385 nm for anatase phase) excites the electron from valence band (VB) to conduction band (CB), forming a hole (h_{VB}^+) in the VB.[33] The positively charged hole produces OH· radical by oxidizing H_2O while, the electron in the conduction band (e_{CB}^-) reduces O_2 to O^{2-}. Hydrogen peroxide is formed through the recombination of two OH· radicals at the interface.[37]

Two plausible mechanisms proposed for peroxide formation are given below.[33] Equation (i) involves the oxidation of water by the hole generated in the valence band and equation (ii) shows the reduction of oxygen to hydrogen peroxide by the electron in the conduction band.

$$2H_2O + 2h_{VB}^+ \rightarrow H_2O_2 + 2H^+ \quad \text{……. (i)}$$

$$O_2 + 2H^+ + 2e_{CB}^- \rightarrow H_2O_2 \quad \text{……. (ii)}$$

1.2.3.6. $CO/O_2/H_2O$ catalytic process:

Synthesis of hydrogen peroxide from gas mixture of CO, O_2 and H_2O (equation (iii)) in presence of homogeneous catalysts, Pd complexes has also been reported in the literature.[38] The free energy of this reaction is highly negative (-134.3 kJ mol^{-1}) and hence thermodynamically favorable. However, kinetics of the reaction is very slow and hence not

suitable for practical application. Moreover, the catalyst (Pd complexes) is not stable during the reaction and easily leads to deactivation.

$$CO + O_2 + H_2O \rightarrow H_2O_2 + CO_2 \quad \text{……. (iii)}$$

1.3. Experimental techniques for the direct synthesis of H_2O_2:

1.3.1. Batch-type reactor:

Batch-type reactors or autoclaves made of stainless steel or Hastalloy are used extensively for the direct synthesis of H_2O_2 at high pressure.[5, 19, 39-46] Common safety precautions need to be taken during the reaction, as dry Pd-catalyst may result in explosion when it comes in contact with H_2-O_2 gas mixture (beyond 4% H_2 in O_2) during feeding into the reaction chamber.[47, 48] To avoid this issue, solid catalysts should be dispersed well in the solution or distilled water and purged with the H_2-O_2 mixture to equilibrate before feeding into the reactor. The two major advantages of this technique are- (i) controllable mixing of the reactants with the stirring speed which reduces the mass transport limitations, and (ii) low amount of chemicals consumed during the reaction and high production of the experimental outputs.[11] Another impact of this method is that the reaction for direct synthesis of H_2O_2 can be carried in shorter time scale and hence, it does not require any stabilizer (HCl) or inhibitor (Cl^- or Br^-) which are used to prevent the decomposition and hydrogenation of H_2O_2. However, there are several disadvantages of this method, like difficulties in real time kinetic analyses of the gas mixture as the concentration of gas and liquid phases change over time, low H_2O_2 concentration achieved due to limited accessibility of the gases unless a higher volume of gasses are used. The high pressure reactor (Parr reactor) is comparatively costlier, though there are several "home-made designs" available but major concern is related to the safety as this process may lead to explosion and needs careful handling of the instrument.

1.3.2. Flow-type reactor:

Flow-type reactor is one kind of fixed bed reactor where gas and liquid flow simultaneously in downward or upward direction through solid catalyst bed and operates at atmospheric pressure. Flow-type reactor can easily be designed for laboratory use according to desired applications. The flow-type reactor used for H_2O_2 synthesis contains a glass frit (fixed at the bottom of the reactor) over which the catalyst is dispersed. The gas mixture, H_2 and O_2 flows in the upward direction (against gravity) through the catalyst dispersion.[49, 50] A glass

jacket is used to circulate cold water to maintain the reaction at desired temperature. The major advantages of this method are enhanced mass transfer between the gaseous reactants and solid catalyst surfaces, easy control over the liquid and gas phase compositions, user friendly as it works at atmospheric pressure. Also, one can produce higher concentration of H_2O_2 (unlike the batch-type reactor) as H_2-O_2 mixture passes continuously through the catalytic dispersion. The only disadvantage of this method is that it requires relatively longer time for testing the catalytic performance which is the major problem for stabilization of H_2O_2 in presence of the catalyst. And this process additionally needs stabilizer (HCl) and inhibitor (Cl^- or Br^-) to prevent decomposition and hydrogenation of H_2O_2.[9, 49, 51-54]

1.4. Catalysts used in the direct synthesis of H_2O_2:

Since the patent by H. C. H. Henkel and W. Weber in 1914,[55] Pd has been studied extensively as an active component for direct synthesis of H_2O_2. Various support materials for Pd nanoparticles have also been explored to improve its activity and stability in the reaction conditions.[9, 49, 50, 56-60] Among the supports used for Pd, acidic supports like SiO_2 were found to be better than the basic supports such as TiO_2, CeO_2, ZrO_2 etc. oxide materials. Furthermore, it was found that Pd catalysts show improvement in H_2O_2 selectivity in presence of halide ions by inhibiting the direct combustion of H_2 with O_2 to give water.[9, 49, 52-54, 61, 62] The reaction needs to be carried out in mildly acidic medium for longer run as it can reduce the decomposition of H_2O_2 (Scheme 1.1). Also, the hydrogenation of H_2O_2 formed in the reaction mixture could be minimized in presence of halides. Temperature and solvents also play a significant role for this direct synthesis reaction. Direct combustion of H_2 in presence of O_2 can be minimized in presence of catalyst by lowering the temperature and hence, improves the H_2O_2 selectivity. Instead of pure water, water-alcohol mixture was found to be a better solvent due to higher solubility of H_2 and O_2 in the later as compared to pure water.

Recently, Pd-based bimetallic catalysts, Au-Pd (on the support materials) have been developed for the direct synthesis of H_2O_2 in high pressure conditions (which can avoid the additives like acids or halides) by Hutchings and co-workers.[39-43, 46, 63-65] The presence of Au with Pd improves the selectivity of H_2 towards H_2O_2 and enhances the overall catalytic activity. The improved activity in bimetallic Au-Pd catalysts comes from the electronic modification of 3d orbital of Pd in presence of a secondary metal, Au.[66] Pt has also been

studied as a promoter for Au-Pd in the trimetallic system, Au-Pd-Pt, to make the catalysts more efficient.[44] However, the higher cost of the noble metal based catalysts prohibits their large scale use. Lately, low cost elements like Ni, Zn, Sn etc. have been explored with Pd to make it more efficient and stable catalyst and to reduce the cost for practical application.[51, 67, 68]

1.5. Conclusion:

Direct synthesis of H_2O_2 seems to be a promising greener route as an alternative to AQ process in the long run. But the major problem associated with direct synthesis is combustion of H_2 which leads to H_2O formation and decreases the selectivity of H_2O_2. Halides and acids are also required to reduce the hydrogenation and decomposition of H_2O_2 in presence of catalysts under ambient pressure. In high pressure conditions additives are not required, but overall H_2O_2 productivity is comparatively lower. Designing efficient and effective catalysts for the direct synthesis of H_2O_2 is still demanding task for industrial applications. In this investigation, research has been going on to develop efficient and cost effective catalysts to make it commercially viable.

1.6. References:

1. L. J. Thenard, *Ann. Chim. Phys.* , 1818, **8**, 306.
2. J. M. Campos-Martin, G. Blanco-Brieva and J. L. G. Fierro, Hydrogen Peroxide Synthesis: An Outlook beyond the Anthraquinone Process, *Angew. Chem. Int. Ed.*, 2006, **45**, 6962-6984.
3. G. Goor, W. Kunkel and O. Weiberg, UllmannCs Encyclopedia of Industrial Chemistry, Vol. A13 (Eds.: B. Elvers, S. Hawkins, M. Ravenscroft, G. Schulz), *VCH, Weinheim*, 1989, 443 – 466.
4. J. R. Kirchner, in Kirk-Othmer Encyclopedia of Chemical Technology, Vol. **13** (Eds.: M. Grayson, D. Eckroth), *3rd ed., Wiley, New York*, 1979, 12 – 38.
5. J. K. Edwards and G. J. Hutchings, Palladium and Gold–Palladium Catalysts for the Direct Synthesis of Hydrogen Peroxide, *Angew. Chem. Int. Ed.*, 2008, **47**, 9192-9198.
6. http://news.bbc.co.uk/1/hi/england/london/4197500.stm.
7. F. Menegazzo, M. Signoretto, M. Manzoli, F. Boccuzzi, G. Cruciani, F. Pinna and G. Strukul, Influence of the preparation method on the morphological and composition properties of Pd–Au/ZrO_2 catalysts and their effect on the direct

synthesis of hydrogen peroxide from hydrogen and oxygen, *J. Catal.*, 2009, **268**, 122-130.

8. H.-J. Reidl and G. Pfleiderer, *I.G. Farbenindustrie AG*, 1939, US Patent 2158525.
9. Q. Liu and J. H. Lunsford, The roles of chloride ions in the direct formation of H_2O_2 from H_2 and O_2 over a Pd/SiO_2 catalyst in a H_2SO_4/ethanol system, *J. Catal.*, 2006, **239**, 237-243.
10. C. E. Baukal, Oxygen-Enhanced Combustion, *CRC*, 1998.
11. J. Garcia-Serna, T. Moreno, P. Biasi, M. J. Cocero, J.-P. Mikkola and T. O. Salmi, Engineering in direct synthesis of hydrogen peroxide: targets, reactors and guidelines for operational conditions, *Green Chem.*, 2014, **16**, 2320-2343.
12. Y. Ichiro, O. Takeshi, S. Hirobumi, H. Noriko and O. Kiyoshi, Electrocatalysis of Heat-treated Mn–Porphyrin/Carbon Cathode for Synthesis of H_2O_2 Acid Solutions by H_2/O_2 Fuel Cell Method, *Chem. Lett.*, 2006, **35**, 1330-1331.
13. I. Yamanaka, T. Onizawa, S. Takenaka and K. Otsuka, Direct and Continuous Production of Hydrogen Peroxide with 93 % Selectivity Using a Fuel-Cell System, *Angew. Chem. Int. Ed.*, 2003, **42**, 3653-3655.
14. C. H. Choi, H. C. Kwon, S. Yook, H. Shin, H. Kim and M. Choi, Hydrogen Peroxide Synthesis via Enhanced Two-Electron Oxygen Reduction Pathway on Carbon-Coated Pt Surface, *J. Phys. Chem. C*, 2014, **118**, 30063-30070.
15. J. Zhou, H. Guo, X. Wang, M. Guo, J. Zhao, L. Chen and W. Gong, Direct and continuous synthesis of concentrated hydrogen peroxide by the gaseous reaction of H_2/O_2 non-equilibrium plasma, *Chem. Commun.*, 2005, 1631-1633.
16. M. Kihei, The Reaction of Hydrogen and Oxygen through a Silent Electric Discharge. I. The Formation of Hydrogen Peroxide, *Bull. Chem. Soc. Jpn.*, 1962, **35**, 345-348.
17. M. Venugopalan and R. A. Jones, Chemistry of Dissociated Water Vapor and Related Systems, *Chem. Rev.*, 1966, **66**, 133-160.
18. C. Samanta, Direct synthesis of hydrogen peroxide from hydrogen and oxygen: An overview of recent developments in the process, *Appl. Catal. A.: Gen.*, 2008, **350**, 133-149.
19. D. Hancu and E. J. Beckman, Generation of hydrogen peroxide directly from H_2 and O_2 using CO_2 as the solvent, *Green Chem.*, 2001, **3**, 80-86.
20. D. Hâncu, J. Green and E. J. Beckman, H_2O_2 in CO_2: Sustainable Production and Green Reactions, *Acc. Chem. Res.*, 2002, **35**, 757-764.

21. E. J. Beckman, Production of H_2O_2 in CO_2 and its use in the direct synthesis of propylene oxide, *Green Chem.*, 2003, **5**, 332-336.
22. Q. Chen and E. J. Beckman, Direct synthesis of H_2O_2 from O_2 and H_2 over precious metal loaded TS-1 in CO_2, *Green Chem.*, 2007, **9**, 802-808.
23. E. J. Beckman, Supercritical and near-critical CO_2 in green chemical synthesis and processing, *J. Supercrit. Fluids*, 2004, **28**, 121-191.
24. R. Hofer and J. Bigorra, Green chemistry-a sustainable solution for industrial specialties applications, *Green Chem.*, 2007, **9**, 203-212.
25. A. Pashkova and R. Dittmeyer, Carbon dioxide as an alternative solvent for the direct synthesis of hydrogen peroxide: A review of recent activities, *Catal. Today*, 2015, **248**, 128-137.
26. V. R. Choudhary, A. G. Gaikwad and S. D. Sansare, Nonhazardous Direct Oxidation of Hydrogen to Hydrogen Peroxide Using a Novel Membrane Catalyst, *Angew. Chem. Int. Ed.*, 2001, **40**, 1776-1779.
27. G. Centi, R. Dittmeyer, S. Perathoner and M. Reif, Tubular Inorganic catalytic membrane reactors: advantages and performance in multiphase hydrogenation reactions, *Catal. Today*, 2003, **79**, 139-149.
28. G. D. Vulpescu, M. Ruitenbeek, L. L. van Lieshout, L. A. Correia, D. Meyer and P. P. A. C. Pex, One-step selective oxidation over a Pd-based catalytic membrane; evaluation of the oxidation of benzene to phenol as a model reaction, *Catal. Commun.*, 2004, **5**, 347-351.
29. S. Melada, F. Pinna, G. Strukul, S. Perathoner and G. Centi, Palladium-modified catalytic membranes for the direct synthesis of H_2O_2: preparation and performance in aqueous solution, *J. Catal.*, 2005, **235**, 241-248.
30. S. Melada, F. Pinna, G. Strukul, S. Perathoner and G. Centi, Direct synthesis of H_2O_2 on monometallic and bimetallic catalytic membranes using methanol as reaction medium, *J. Catal.*, 2006, **237**, 213-219.
31. S. Abate, G. Centi, S. Melada, S. Perathoner, F. Pinna and G. Strukul, Preparation, performances and reaction mechanism for the synthesis of H_2O_2 from H_2 and O_2 based on palladium membranes, *Catal. Today*, 2005, **104**, 323-328.
32. A. Fujishima, T. N. Rao and D. A. Tryk, Titanium dioxide photocatalysis, *J. Photochem. Photobiol., C: Photochem. Reviews*, 2000, **1**, 1-21.

33. R. Cai, R. Baba, K. Hashimoto, Y. Kubota and A. Fujishima, Photoelectrochemistry of TiO_2 particles: efficient electron transfer from the TiO_2 particles to a redox enzyme, *J. Electroanal. Chem.*, 1993, **360**, 237-245.

34. C. Kormann, D. W. Bahnemann and M. R. Hoffmann, Photocatalytic production of hydrogen peroxides and organic peroxides in aqueous suspensions of titanium dioxide, zinc oxide, and desert sand, *Environ. Sci. Technol.*, 1988, **22**, 798-806.

35. R. Cai, K. Hashimoto, A. Fujishima and Y. Kubota, Conversion of photogenerated superoxide anion into hydrogen peroxide in TiO_2 suspension system, *J. Electroanal. Chem.*, 1992, **326**, 345-350.

36. R. Cai, Y. Kubota and A. Fujishima, Effect of copper ions on the formation of hydrogen peroxide from photocatalytic titanium dioxide particles, *J. Catal.*, 2003, **219**, 214-218.

37. K. Makino, M. M. Mossoba and P. Riesz, Chemical effects of ultrasound on aqueous solutions. Evidence for hydroxyl and hydrogen free radicals (.cntdot.OH and .cntdot.H) by spin trapping, *J. Am. Chem. Soc.*, 1982, **104**, 3537-3539.

38. D. Bianchi, R. Bortolo, R. D'Aloisio and M. Ricci, A novel palladium catalyst for the synthesis of hydrogen peroxide from carbon monoxide, water and oxygen, *J. Mol. Catal. A: Chem.*, 1999, **150**, 87-94.

39. P. Landon, P. J. Collier, A. F. Carley, D. Chadwick, A. J. Papworth, A. Burrows, C. J. Kiely and G. J. Hutchings, Direct synthesis of hydrogen peroxide from H2 and O2 using Pd and Au catalysts, *Phys. Chem. Chem. Phys.*, 2003, **5**, 1917-1923.

40. J. K. Edwards, B. Solsona, P. Landon, A. F. Carley, A. Herzing, M. Watanabe, C. J. Kiely and G. J. Hutchings, Direct synthesis of hydrogen peroxide from H_2 and O_2 using Au-Pd/Fe_2O_3 catalysts, *J. Mater. Chem.*, 2005, **15**, 4595-4600.

41. J. K. Edwards, S. J. Freakley, A. F. Carley, C. J. Kiely and G. J. Hutchings, Strategies for Designing Supported Gold–Palladium Bimetallic Catalysts for the Direct Synthesis of Hydrogen Peroxide, *Acc. Chem. Res.*, 2014, **47**, 845-854.

42. J. K. Edwards, S. J. Freakley, R. J. Lewis, J. C. Pritchard and G. J. Hutchings, Advances in the direct synthesis of hydrogen peroxide from hydrogen and oxygen, *Catal. Today*, 2015, **248**, 3-9.

43. J. K. Edwards, E. Ntainjua N, A. F. Carley, A. A. Herzing, C. J. Kiely and G. J. Hutchings, Direct Synthesis of H_2O_2 from H_2 and O_2 over Gold, Palladium, and Gold–Palladium Catalysts Supported on Acid-Pretreated TiO_2, *Angew. Chem. Int. Ed.*, 2009, **48**, 8512-8515.

44. J. K. Edwards, J. Pritchard, L. Lu, M. Piccinini, G. Shaw, A. F. Carley, D. J. Morgan, C. J. Kiely and G. J. Hutchings, The Direct Synthesis of Hydrogen Peroxide Using Platinum-Promoted Gold–Palladium Catalysts, *Angew. Chem. Int. Ed.*, 2014, **53**, 2381-2384.
45. J. K. Edwards, B. Solsona, E. N. Ntainjua, A. F. Carley, A. A. Herzing, C. J. Kiely and G. J. Hutchings, Switching Off Hydrogen Peroxide Hydrogenation in the Direct Synthesis Process, *Science*, 2009, **323**, 1037-1041.
46. J. K. Edwards, A. Thomas, B. E. Solsona, P. Landon, A. F. Carley and G. J. Hutchings, Comparison of supports for the direct synthesis of hydrogen peroxide from H_2 and O_2 using Au–Pd catalysts, *Catal. Today*, 2007, **122**, 397-402.
47. G. Centi, S. Perathoner and S. Abate, in Modern Heterogeneous Oxidation Catalysis, *Wiley-VCH Verlag GmbH & Co. KGaA*, 2009, 253–287.
48. C. M. Piqueras, J. García-Serna and M. J. Cocero, Estimation of lower flammability limits in high-pressure systems. Application to the direct synthesis of hydrogen peroxide using supercritical and near-critical CO_2 and air as diluents, *J. Supercrit. Fluids*, 2011, **56**, 33-40.
49. S. Chinta and J. H. Lunsford, A mechanistic study of H_2O_2 and H_2O formation from H_2 and O_2 catalyzed by palladium in an aqueous medium, *J. Catal.*, 2004, **225**, 249-255.
50. Q. Liu, J. C. Bauer, R. E. Schaak and J. H. Lunsford, Supported Palladium Nanoparticles: An Efficient Catalyst for the Direct Formation of H_2O_2 from H_2 and O_2, *Angew. Chem. Int. Ed.*, 2008, **47**, 6221-6224.
51. S. Maity and M. Eswaramoorthy, Ni-Pd bimetallic catalysts for the direct synthesis of H_2O_2 - unusual enhancement of Pd activity in the presence of Ni, *J. Mater. Chem. A*, 2016, **4**, 3233-3237.
52. Q. Liu and J. H. Lunsford, Controlling factors in the direct formation of H_2O_2 from H_2 and O_2 over a Pd/SiO_2 catalyst in ethanol, *Appl. Catal. A.: Gen.*, 2006, **314**, 94-100.
53. Y.-F. Han and J. H. Lunsford, Direct formation of H_2O_2 from H_2 and O_2 over a Pd/SiO2 catalyst: the roles of the acid and the liquid phase, *J. Catal.*, 2005, **230**, 313-316.
54. C. Samanta and V. R. Choudhary, Direct formation of H_2O_2 from H_2 and O_2 and decomposition/hydrogenation of H_2O_2 in aqueous acidic reaction medium over halide-containing Pd/SiO_2 catalytic system, *Catal. Commun.*, 2007, **8**, 2222-2228.

55. H. C. H. Henkel and W. Weber, *(Henkel & CIE)*, 1914, US Patent 1108752.

56. E. Ghedini, F. Menegazzo, M. Signoretto, M. Manzoli, F. Pinna and G. Strukul, Mesoporous silica as supports for Pd-catalyzed H_2O_2 direct synthesis: Effect of the textural properties of the support on the activity and selectivity, *J. Catal.*, 2010, **273**, 266-273.

57. N. M. Wilson and D. W. Flaherty, Mechanism for the Direct Synthesis of H_2O_2 on Pd Clusters: Heterolytic Reaction Pathways at the Liquid–Solid Interface, *J. Am. Chem. Soc.*, 2016, **138**, 574-586.

58. T. Deguchi, H. Yamano and M. Iwamoto, Dynamics of direct H_2O_2 synthesis from H_2 and O_2 on a Pd nano-particle catalyst protected with polyvinylpyrrolidone, *J. Catal.*, 2012, **287**, 55-61.

59. G. Blanco-Brieva, E. Cano-Serrano, J. M. Campos-Martin and J. L. G. Fierro, Direct synthesis of hydrogen peroxide solution with palladium-loaded sulfonic acid polystyrene resins, *Chem. Commun.*, 2004, 1184-1185.

60. B. Hu, W. Deng, R. Li, Q. Zhang, Y. Wang, F. Delplanque-Janssens, D. Paul, F. Desmedt and P. Miquel, Carbon-supported palladium catalysts for the direct synthesis of hydrogen peroxide from hydrogen and oxygen, *J. Catal.*, 2014, **319**, 15-26.

61. S. Melada, R. Rioda, F. Menegazzo, F. Pinna and G. Strukul, Direct synthesis of hydrogen peroxide on zirconia-supported catalysts under mild conditions, *J. Catal.*, 2006, **239**, 422-430.

62. V. R. Choudhary, C. Samanta and A. G. Gaikwad, Drastic increase of selectivity for H_2O_2 formation in direct oxidation of H_2 to H_2O_2 over supported Pd catalysts due to their bromination, *Chem. Commun.*, 2004, 2054-2055.

63. P. Landon, P. J. Collier, A. J. Papworth, C. J. Kiely and G. J. Hutchings, Direct formation of hydrogen peroxide from H_2/O_2 using a gold catalyst, *Chem. Commun.*, 2002, 2058-2059.

64. V. Paunovic, V. Ordomsky, M. Fernanda Neira D'Angelo, J. C. Schouten and T. A. Nijhuis, Direct synthesis of hydrogen peroxide over Au–Pd catalyst in a wall-coated microchannel, *J. Catal.*, 2014, **309**, 325-332.

65. V. Paunovic, V. V. Ordomsky, V. L. Sushkevich, J. C. Schouten and T. A. Nijhuis, Direct Synthesis of Hydrogen Peroxide over Au-Pd Catalyst—The Effect of Co-Solvent Addition, *ChemCatChem*, 2015, **7**, 1161-1176.

66. A. Ruban, B. Hammer, P. Stoltze, H. L. Skriver and J. K. Nørskov, Surface electronic structure and reactivity of transition and noble metals1, *J. Mol. Catal. A: Chem.*, 1997, **115**, 421-429.

67. S. Wang, K. Gao, W. Li and J. Zhang, Effect of Zn addition on the direct synthesis of hydrogen peroxide over supported palladium catalysts, *Appl. Catal. A.: Gen.*, 2017, **531**, 89-95.

68. S. J. Freakley, Q. He, J. H. Harrhy, L. Lu, D. A. Crole, D. J. Morgan, E. N. Ntainjua, J. K. Edwards, A. F. Carley, A. Y. Borisevich, C. J. Kiely and G. J. Hutchings, Palladium-tin catalysts for the direct synthesis of H_2O_2 with high selectivity, *Science*, 2016, **351**, 965-968.

Chapter – 2

Ni-Pd bimetallic catalysts for the direct synthesis of H_2O_2 - unusual enhancement of Pd activity in presence of Ni

Summary:

Direct synthesis of hydrogen peroxide from molecular H_2 and O_2 is one of the challenging reactions for several decades in terms of catalyst selection, stability and selectivity. We have demonstrated a bimetallic NiPd nanocatalyst showing unusually high, three times higher activity compared to Pd nanocatalyst. The catalyst also shows high selectivity for H_2O_2 with maximum value of 95% and very long life time, 72h, with high activity in harsh acidic condition.

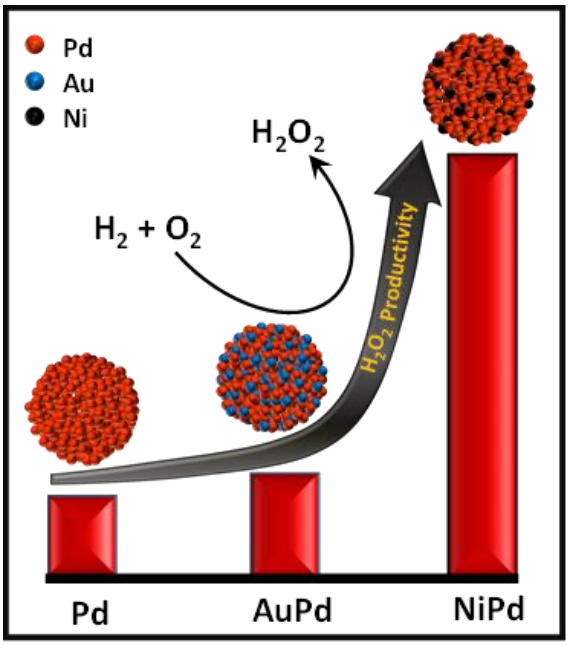

S. Maity and M. Eswaramoorthy, J. Mater. Chem. A, 2016, **4**, 3233-3237.

2.1. Introduction:

Direct synthesis of hydrogen peroxide, an inherently green oxidant obtained from molecular H_2 and O_2 is one of the most sought-after reactions for the past several decades[1-5] though it is not a replacement for the large scale, indirect anthraquinone process which produces concentrated H_2O_2.[6] Understandably, in places where the application demands only dilute H_2O_2 solutions, the storage and transport hazards associated with the concentrated H_2O_2 can be circumvented by the on-site production of hydrogen peroxide through an alternative, green catalytic process using molecular hydrogen and oxygen.[7, 8]

Most of the efforts in this direction mainly focused on the catalyst development and many noble metal catalysts Au, Pd, Pt have been explored for the direct synthesis of H_2O_2.[4, 9-14] Among them, Pd, by and large being the efficient monometallic catalyst for the direct synthesis of H_2O_2[12, 13, 15-18] since the first patent filed by Hugo Henkel and Walter Weber[19] in 1914. The recent findings of bimetallic Pd-Au, as an efficient catalyst for this process over the monometallic Pd or Au generated a lot of interest in exploring new bimetallic and trimetallic systems.[7, 9, 10, 20-27] However, the noble metals Au and Pt explored so far to form bimetallic catalyst with Pd for the efficient productivity of H_2O_2 are costlier than Pd which would prohibit their large scale use in industry. Thus, replacing noble metals (Au and Pt) with cost effective elements or improving the activity of Pd by electronically modifying its active surface with non-noble metals would be of importance to make this green process commercially viable. In this report, we have shown for the first time the presence of a transition element, Ni, phenomenally improving the catalytic activity of Pd. Nickel containing Pd catalyst shows more than 200% enhanced (3 times higher) activity for the direct synthesis of H_2O_2 than the monometallic Pd itself in a mild reaction conditions.

2.2. Scope of the Present Study:

Most of the research carried out in the direct synthesis of H_2O_2 mainly focused on Pd or Pd in combination with other noble metals Au, Pt etc.[3, 7] however, the noble metals Au and Pt are costlier than Pd which limits their large scale use in industry. So, using low cost earth abundant elements with Pd, would make this green process more effective for commercial applications.

2.3. Experimental Section:

2.3.1. Materials and Characterization Techniques:

$PdCl_2$ (Sigma Aldrich), $HAuCl_4.3H_2O$ (Sigma Aldrich), $NiCl_2.6H_2O$ (S D Fine Chemicals), $NaBH_4$ (S D Fine Chemicals), KBr (S D Fine Chemicals), $TiOSO_4$ (Sigma Aldrich), H_2SO_4 (98%, AR grade), HCl (37%, AR grade) were used without any further purification.

Powder X-ray diffraction (PXRD) patterns were recorded using Bruker-D8 diffractometer using Cu Kα radiation, (λ=1.54 Å, step size: 0.02, current: 30 mA and voltage: 40 kV). Field-emission scanning electron microscopy (FESEM) images and energy-dispersive X-ray spectroscopy (EDS) were obtained by using FEI (Nova-Nano SEM-600 Netherlands) equipment. Transmission electron microscope (TEM) imaging was done on a JEOL, JEM 3010 operated at 300 kV. Samples were prepared by putting a drop of very dilute dispersion in ethanol on a TEM grid (carbon polymer, 300 mesh). Electronic absorption spectra were recorded by Perkin Elmer Lambda 900 UV-Vis-NIR Spectrometer. 1 cm path length cuvette was used for recording the spectra. Inductively coupled plasma – atomic emission spectroscopy (ICP-AES) was carried out using a Perkin−Elmer Optima 7000 DV machine. Infra-red (IR) spectra were recorded on a Bruker IFS 66v/S spectrometer. X-ray photoelectron spectroscopy (XPS) has been performed using Omicron EA 125 spectrometer with Al K_α (1486.6 eV) source. The magnetic measurement was carried out by using Quantum Design SQUID VSM magnetometer at 298K. The composition of gas mixture was analysed by Gas Chromatography (Agilent 7890A) using MolSieve 5A 60-80 mesh column 40 ^oC temperature.

2.3.2. Material Synthesis:

Metal nanostructure and bimetallic nanostructures were prepared by the reduction of metal precursor(s) solution by $NaBH_4$ at room temperature.[28] $PdCl_2$, $NiCl_2.6H_2O$ and $HAuCl_4.3H_2O$ were used as metal precursors. The detailed procedure is given below:

2.3.2.1. Synthesis of Pd, Ni, and Au Nanostructure:

In the typical procedure, 10 mL of 0.1 M metal precursor solution ($PdCl_2$ in case of Pd, $NiCl_2.6H_2O$ in case of Ni and $HAuCl_4.3H_2O$ in case of Au) was rapidly added to a 50 mL of 0.1 M aqueous solution of freshly prepared $NaBH_4$ with vigorous stirring. The stirring

was continued for 10 min. The solid product obtained was filtered and washed with distilled water for several times. Finally it was dried at 50 °C for overnight. The as-synthesized Ni nanostructure is mainly consisted of $Ni(OH)_2$ and some of the Ni nanoparticles which have been discussed in the results and discussion section.

2.3.2.2. Synthesis of $Ni_{0.4}Pd_{0.6}$ (containing Ni:Pd wt. ratio 40:60) Nanostructure:

A mixture of 3.4 mL of 0.1 M $NiCl_2.6H_2O$ solution (in aqueous medium) and 2.82 mL of 0.1 M $PdCl_2$ solution (in aqueous medium) was rapidly added to 31.1 mL freshly prepared 0.1 M aqueous solution $NaBH_4$ with continuous stirring. The reaction mixture was allowed to stir for 10 min. The solid product was filtered and washed several times with distilled water and dried at 50 °C for overnight. However, it is to be mentioned that Ni in this composition mostly exists as $Ni(OH)_2$.

To synthesize the other compositions of Ni and Pd, a calculated volume of 0.1 M $NiCl_2.6H_2O$ and 0.1 M $PdCl_2$ solutions (according to desired metal wt. %) were taken and same procedure was followed.

2.3.2.3. Synthesis of $Au_{0.5}Pd_{0.5}$ (wt. ratio) Nanostructure:

In the typical procedure, a mixture of 1.27 mL of 0.1 M $HAuCl_4.3H_2O$ solution (in aqueous medium) and 2.35 mL of 0.1 M $PdCl_2$ solution (in aqueous medium) was rapidly added to 18.1 mL freshly prepared 0.1 M aqueous solution of $NaBH_4$ with vigorous stirring. The stirring was continued for 10 min. The solid product was filtered, washed with distilled water for several times and dried at 50 °C for overnight.

2.3.2.4. Direct Synthesis of H_2O_2:

Direct synthesis of H_2O_2 from gaseous H_2 and O_2 was carried out using a glass jacket reactor described elsewhere.[17] 5 mg catalyst (for Pd, $Au_{0.5}Pd_{0.5}$, $Ni_{0.4}Pd_{0.6}$ and 3 mg for $Ni_{0.1}Pd_{0.9}$) was dispersed by sonication in 30 mL aqueous solution containing 0.1 M HCl and 0.01 M Br^- (introduced as KBr) and added to the glass jacket reactor shown below (Scheme 2.1). The individual gasses, H_2 and O_2 were allowed to bubble through the glass frit in a ratio of 1:4 with a total flow rate of 50 mL min^{-1} using two separate Aera (Hitachi) mass flow controllers. To reduce the dead volume, the below portion of the glass frit was filled with 4 mm glass beads. The reaction temperature was maintained at 10 °C using Julabo water circulation unit.

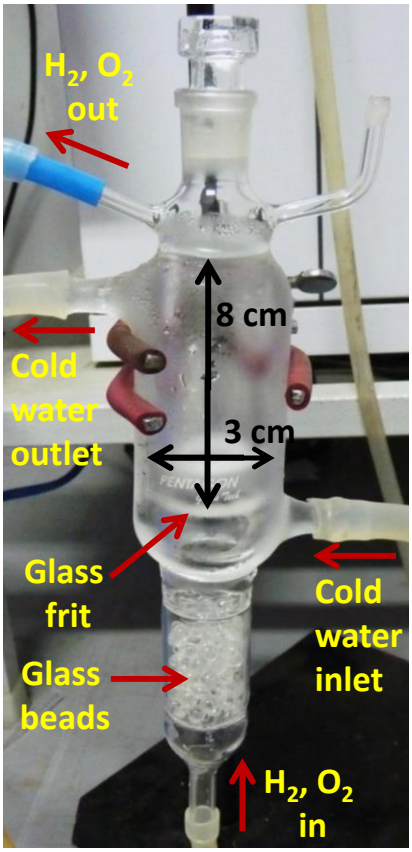

Scheme 2.1: *Reaction set up for direct synthesis of hydrogen peroxide.*

H_2O_2 was analyzed by $TiOSO_4/H_2SO_4$ method using UV-vis spectroscopy.[29] 20 μL of aliquot from the reaction solution was withdrawn at different time interval and diluted with 1.98 mL of previously prepared $TiOSO_4/H_2SO_4$ solution. $TiOSO_4/H_2SO_4$ solution was prepared by dissolving 4.6 gm of $TiOSO_4$ and 20 gm of ammonium sulphate in 100 mL of concentrated H_2SO_4 followed by dilution with 350 mL H_2O. The concentration of H_2O_2 was determined from the calibration curve of absorption at 407 nm by UV-vis spectroscopy after complexation with a $TiOSO_4/H_2SO_4$ solution. The H_2 and O_2 gases were analyzed using MolSieve 5A 60-80 mesh column at 40 ^oC temperature. For selectivity measurement, to get better accuracy, the outlet gas was well diluted with N_2. The selectivity of H_2O_2, $S_{H_2O_2}$ was calculated from the following equation[2]:

$$S_{H_2O_2} = \frac{\text{Rate of hydrogen peroxide production (mmol/min)}}{\text{Rate of hydrogen consumption (mmol/min)}} \times 100.$$

2.3.2.5. Dissolution Study (Synthesis of $Ni_{0.1}Pd_{0.9}$ from $Ni_{0.4}Pd_{0.6}$):

50 mg of $Ni_{0.4}Pd_{0.6}$ catalyst was soaked in aqueous solution containing 0.1 M HCl, 0.01 M Br^- and 0.3 M H_2O_2 in total volume of 30 mL in presence of H_2 flow (20 mL min^{-1}) at 10 °C for different time (0.5h, 1h and 72h). H_2 flow is necessary to avoid the dissolution of Pd as $PdCl_4^{2-}$ in presence of chloride ions. The remaining solid product after dissolution at desired time interval was separated, washed with water and dried. The Ni:Pd ratio after dissolution of different time was found to be 10:90 (wt. ratio) analyzed by inductively coupled plasma (ICP).

2.3.2.6. Decomposition of H_2O_2:

5 mg of catalyst (Pd and $Ni_{0.4}Pd_{0.6}$) was dispersed in 30 mL aqueous solution of 275 mM H_2O_2 and was stirred using magnetic stirrer. The decomposition of H_2O_2 was determined by analyzing the H_2O_2 concentration using UV-vis spectroscopy as described above at different time interval. To study the stability of H_2O_2 in presence of HCl and Br^-, the same reaction was carried out in presence of 0.1 M HCl and 0.01 M Br^- in 30 mL aqueous solution of 275 mM H_2O_2 using Pd and $Ni_{0.4}Pd_{0.6}$ catalysts and the H_2O_2 concentration was monitored at different time.

2.3.2.7. Hydrogenation of H_2O_2:

5 mg of catalyst (Pd and $Ni_{0.4}Pd_{0.6}$) was dispersed in 30 mL aqueous solution of 250 mM H_2O_2 at 10 ^oC and H_2 gas was bubbled in the dispersion with a flow rate of 10 mL min^{-1}. The H_2O_2 concentration was analyzed at different time intervals by UV-vis spectroscopy as described above. The same reaction was carried out in presence of 0.1 M HCl and 0.01 M Br^- with same flow rate of H_2.

2.4. Results and Discussion:

Pd and $Ni_{0.4}Pd_{0.6}$ catalysts prepared in the form of nanostructure at room temperature by a simple borohydride reduction method[28] were characterized by powder X-ray diffraction (PXRD) and transmission electron microscopy (TEM). The PXRD patterns of both Pd and $Ni_{0.4}Pd_{0.6}$ nanostructures shows peaks only for Pd and there is no peak shift in case of $Ni_{0.4}Pd_{0.6}$ (associated with NiPd bimetallic nanostructure) (Figure 2.1). Field-emission scanning electron microscopy (FESEM) and TEM images of Pd nanostructure (Figure 2.2a & b) show network morphology formed by the fusion of nanoparticles of size

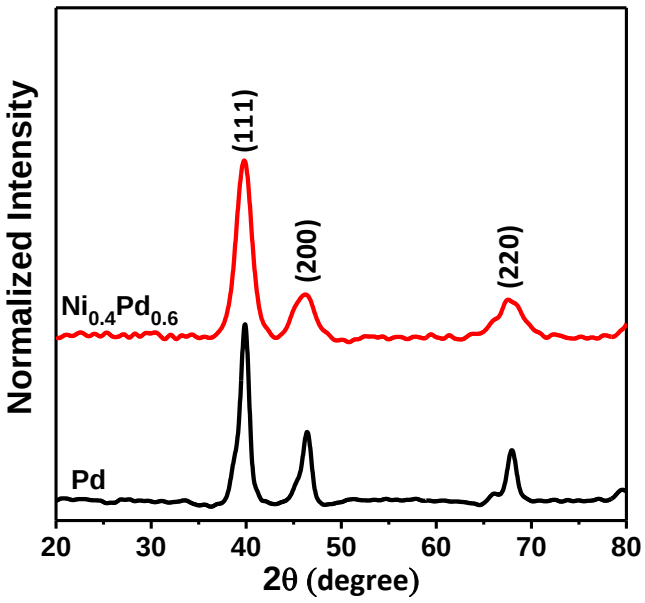

Figure 2.1: *Powder X-ray diffraction (PXRD) patterns of Pd and* $Ni_{0.4}Pd_{0.6}$ *nanostructures.*

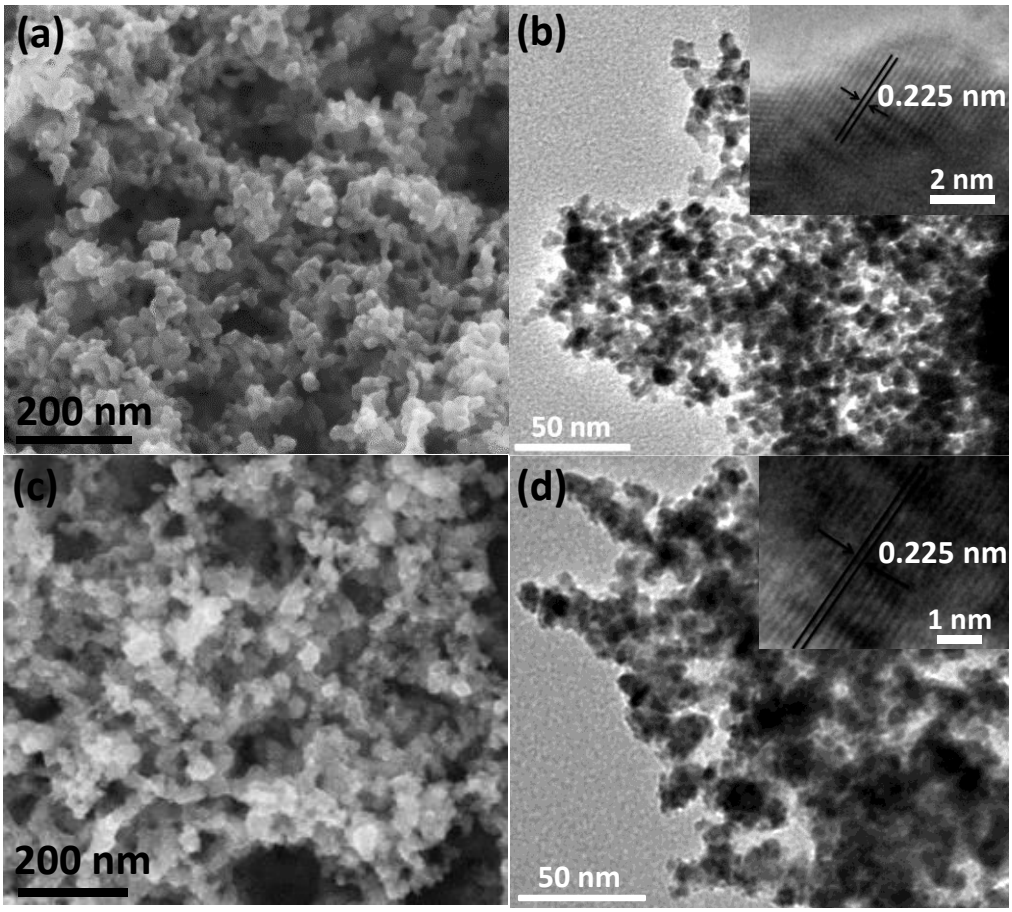

Figure 2.2: *(a) FESEM and (b) TEM images of Pd nanostructure. Inset of (b) shows the*

HRTEM image of Pd. (c) FESEM and (d) TEM images of assynthesized $Ni_{0.4}Pd_{0.6}$ nanostructure. Inset of (d) shows the HRTEM image of $Ni_{0.4}Pd_{0.6}$.

varying from 5 to 8 nm. High resolution TEM (HRTEM) (inset of Figure 2.2b) shows the lattice spacing of 0.225 nm for Pd. Similarly, FESEM and TEM images of assynthesized $Ni_{0.4}Pd_{0.6}$ nanostructure (Figure 2. 2c & d) show fused network morphology interconnected with each other. HRTEM image in the inset of Figure 2.2d shows the lattice spacing, 0.225 associated with Pd.

Direct synthesis of hydrogen peroxide from molecular O_2 and H_2 over Pd and $Ni_{0.4}Pd_{0.6}$ was carried out at normal pressure and at 10 °C temperature in presence of HCl and Br^- as described in the experimental section and the results are shown in Figure 2.3. The HCl and Br^- were added to stabilize the H_2O_2 in the reaction medium.[17] It is to be noted that no H_2O_2 formation occurred in the absence of HCl and Br^- over the catalyst $Ni_{0.4}Pd_{0.6}$ (Figure 2.4a). Furthermore, decomposition studies carried out over known amount of H_2O_2 in presence of catalysts show that in absence of HCl and Br^-, H_2O_2 decomposes very rapidly (Figure 2.4b). Similarly fast hydrogenation of H_2O_2 occurs in absence of HCl and Br^- over Pd and $Ni_{0.4}Pd_{0.6}$ catalysts (Figure 2.4c). The concentration of H_2O_2 over Pd

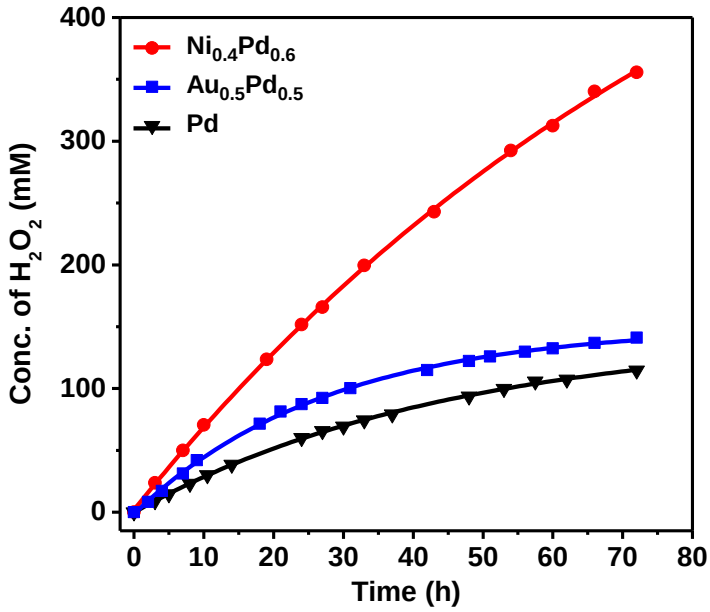

Figure 2.3: *Direct synthesis of H_2O_2 over Pd, $Ni_{0.4}Pd_{0.6}$ and $Au_{0.5}Pd_{0.5}$ catalysts. Reaction conditions: catalyst - 5 mg, 10 °C, 30 mL water containing 0.1 M HCl and 0.01 M Br^-, 1 atm pressure, H_2:O_2 (1:4) gas mixture bubbled with a flow rate, 50 mL min^{-1}.*

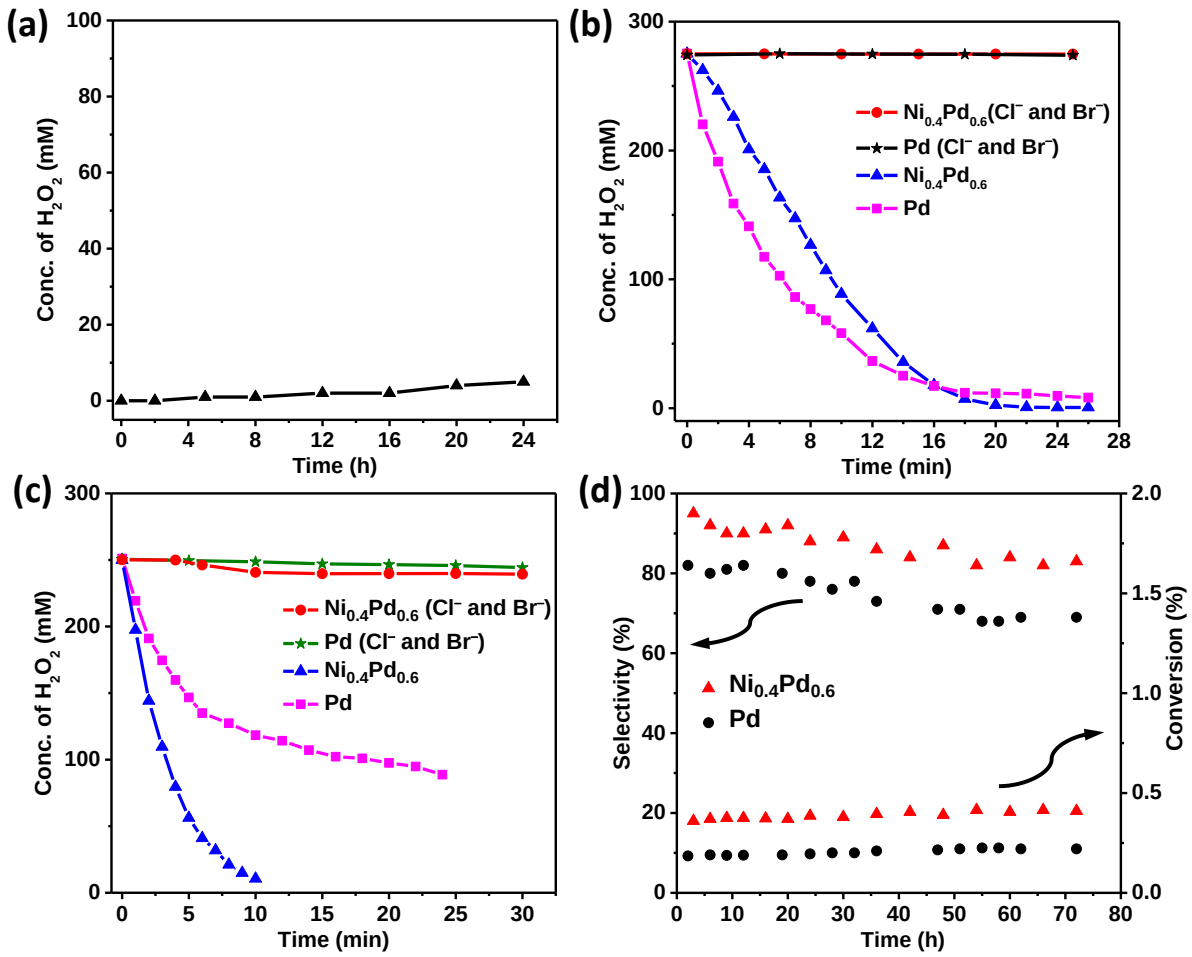

Figure 2.4: *(a) Formation of H_2O_2 by $Ni_{0.4}Pd_{0.6}$ catalyst without HCl and Br^-. (b) Decomposition and (c) Hydrogenation of H_2O_2 by Pd and $Ni_{0.4}Pd_{0.6}$ with and without HCl and Br^-. (d) Selectivity of H_2O_2 (with respect to H_2) and conversion of H_2 for Pd and $Ni_{0.4}Pd_{0.6}$ catalysts.*

increases linearly up to 15h and then slows down leading to an overall concentration of about 114 mM in 72h time (Figure 2.3). On the other hand, $Ni_{0.4}Pd_{0.6}$ shows remarkable activity and the concentration of H_2O_2 increases with time for about 72h. The catalyst shows high selectivity for H_2O_2 with maximum value of 95% at about 0.4% H_2 conversion (Figure 2.4d). The concentration of H_2O_2 is 356 mM (1.2 wt%) in 72h which is about 3 times higher (~200% increase) than that of H_2O_2 obtained over pure Pd catalyst. The $Au_{0.5}Pd_{0.5}$ (Au:Pd composition 50:50) known to be a better catalyst as compared to monometallic Pd,[7, 20, 24] was prepared by the same method without any support (characterization in Figure 2.5) however, showed only a slight increase (25%) in the concentration of H_2O_2 as compared to Pd (Figure 2.3). The H_2O_2 productivity

obtained for $Ni_{0.4}Pd_{0.6}$ catalyst is more than 5 times higher than Pd alone in terms of absolute amount of Pd present in the catalyst (Figure 2.6a). The concentration of H_2O_2 obtained over 5 mg $Ni_{0.4}Pd_{0.6}$ is around five times higher than H_2O_2 obtained over 3 mg Pd after 72h reaction (Figure 2.6b).

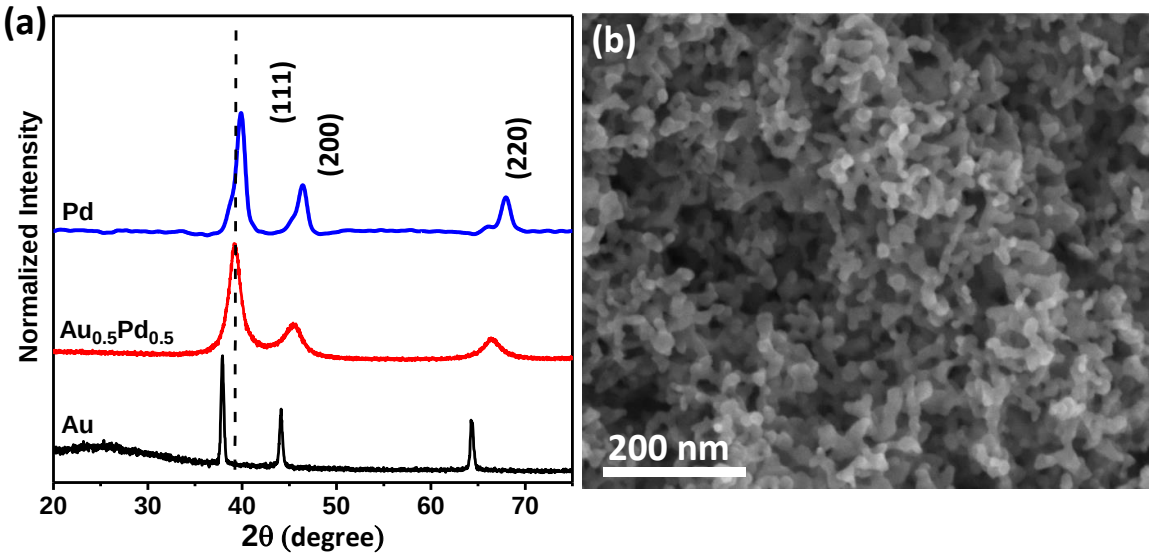

Figure 2.5: *(a) PXRD pattern of $Au_{0.5}Pd_{0.5}$ shows the formation of AuPd alloy and (b) FESEM image of $Au_{0.5}Pd_{0.5}$ shows the network morphology.*

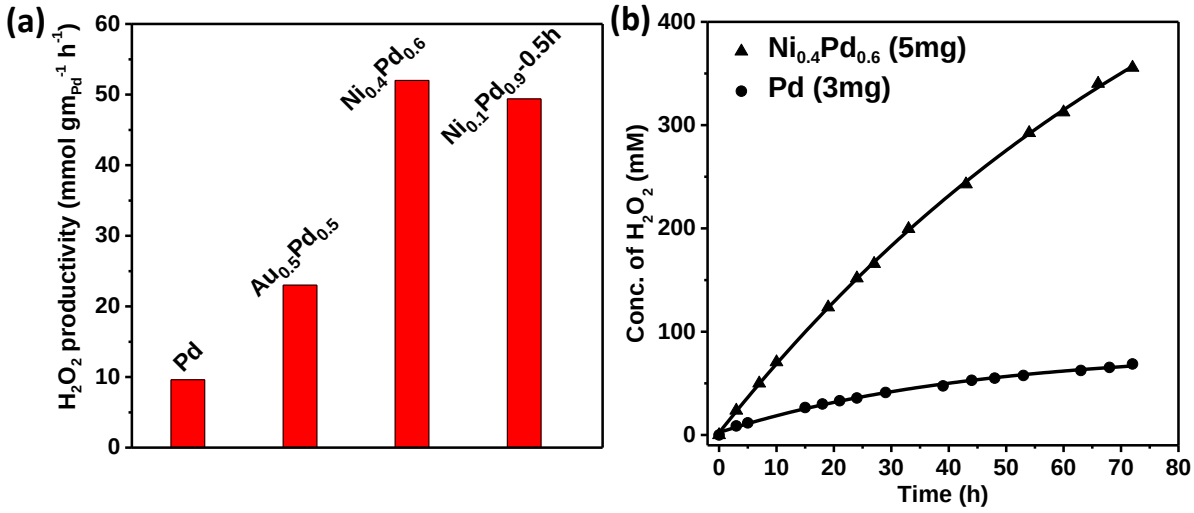

Figure 2.6: *(a) H_2O_2 productivity in terms of mmol gm_{Pd}^{-1} h^{-1}, for all the catalysts after 72h reaction with respect to absolute amount of Pd present in the catalysts. (b) Formation of H_2O_2 over 5 mg $Ni_{0.4}Pd_{0.6}$ and 3 mg Pd catalysts in the same reaction conditions.*

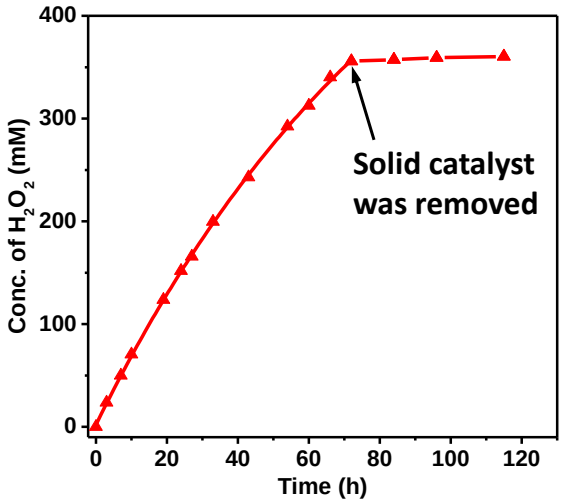

Figure 2.7: *Formation of H_2O_2 after removing the solid catalyst, $Ni_{0.4}Pd_{0.6}$ at 72h.*

The chemical composition of $Ni_{0.4}Pd_{0.6}$ after 72h reaction was found to be around 10:90 (Ni:Pd) estimated through inductively coupled plasma-atomic emission spectroscopy (ICP-AES) analysis which indicates the propensity for nickel to get leached out in an acidic environment. The filtrate obtained after the removal of catalyst shows the presence of Ni, and not Pd in the chemical analysis. This suggests that the Pd did not undergo any leaching in the acidic environment in presence of hydrogen. Moreover, when the reaction was carried out over the filtrate obtained on removal of catalyst after 72h reaction, no hydrogen peroxide formation occurred (Figure 2.7). It is also important to note that assynthesized Ni nanostructure exists mostly in amorphous $Ni(OH)_2$ prepared by $NaBH_4$ reduction. The presence of absorption band at 3556 cm^{-1} in infra-red (IR) spectra (Figure 2.8a) of as synthesized Ni nanostructure associated with O-H stretching confirms the existence of $Ni(OH)_2$. Also, the assynthesized Ni nanostructure heated in Ar atmosphere at 500 ºC for 12h shows the peaks for NiO in PXRD (Figure 2.8b) supports the presence of $Ni(OH)_2$ in as synthesized Ni nanostructure. Magnetic measurements (magnetization (M) vs magnetic field (H) curve) were carried out with as-prepared Ni and $Ni_{0.4}Pd_{0.6}$ nanostructure to confirm the presence of metallic Ni in the assynthesized samples. The relatively higher value of magnetization for assynthesized Ni and $Ni_{0.4}Pd_{0.6}$ as compared to Pd (diamagnetic) confirms the presence of metallic Ni nanoparticles which are not detected by PXRD (Figure 2.8c). Higher magnetization value for assynthesized Ni nanostructure confirms the presence of more metallic Ni nanoparticles than that in $Ni_{0.4}Pd_{0.6}$. X-ray photoelectron spectra (XPS) of $Ni2p_{3/2}$ in as-prepared Ni and $Ni_{0.4}Pd_{0.6}$

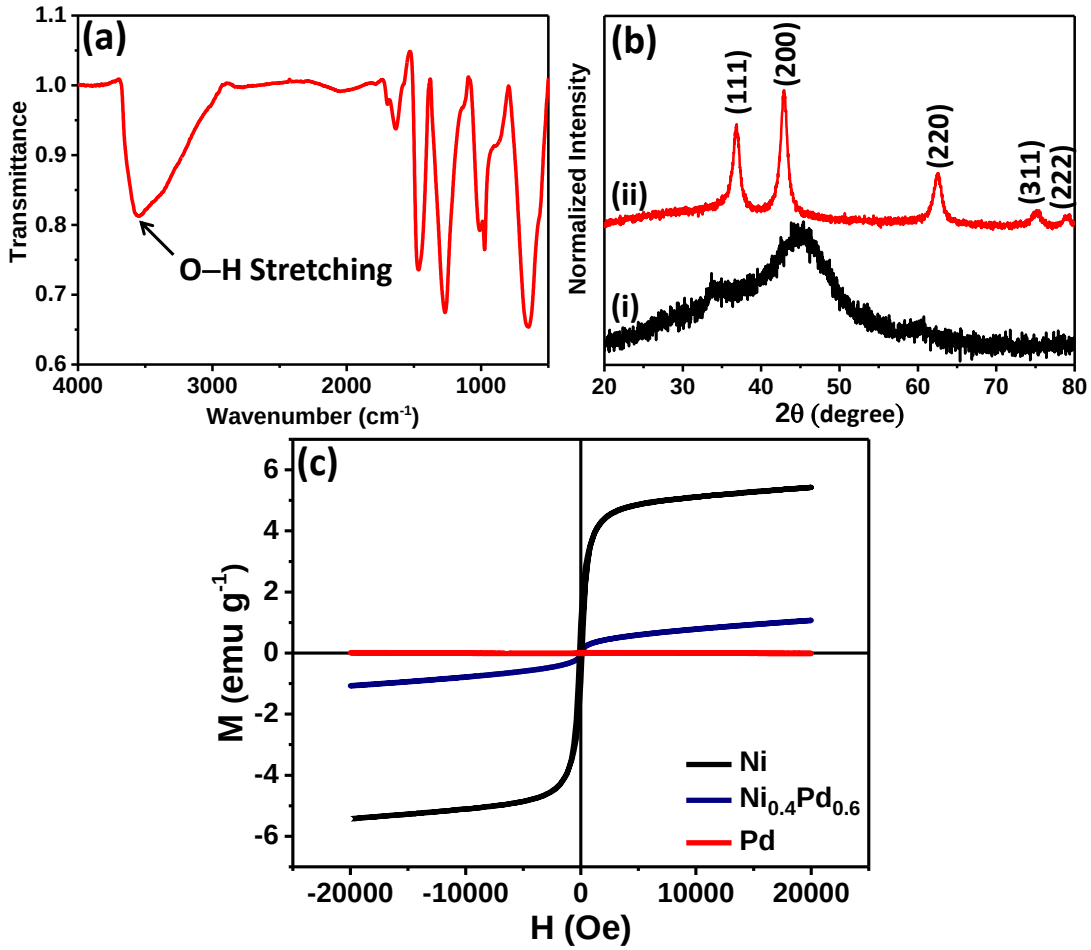

Figure 2.8: *Characterization of assynthesized Ni nanostructure. (a) Infra-red spectra of as synthesized Ni nanostructure. (b) PXRD pattern of (i) assynthesized Ni nanostructure and (ii) after heating in Ar at 500 ºC for 12h. (c) Magnetization (M) vs magnetic field (H) curve of as-prepared Ni, Pd and $Ni_{0.4}Pd_{0.6}$ nanostructure at 298 K.*

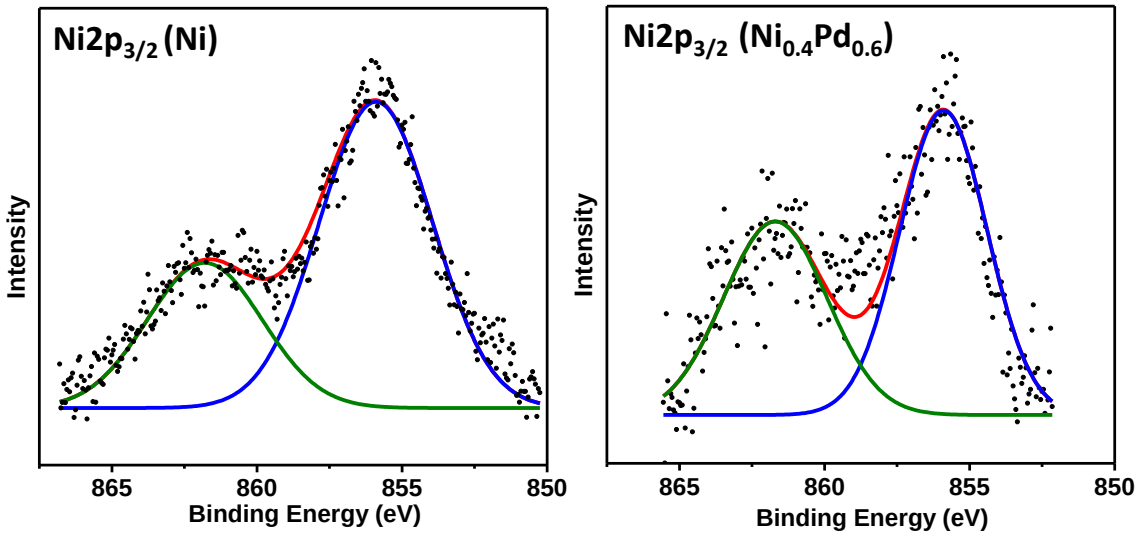

Figure 2.9: *XPS spectra of $Ni2p_{3/2}$ in as-prepared Ni and $Ni_{0.4}Pd_{0.6}$ nanostructure.*

nanostructure shows the appearance of $Ni2p_{3/2}$ peaks at 855.9 eV and 861.8 eV (satellite peak) in both Ni and $Ni_{0.4}Pd_{0.6}$ nanostructures which further confirms the existence of Ni^{+2} in the form of $Ni(OH)_2$ in the samples (Figure 2.9).

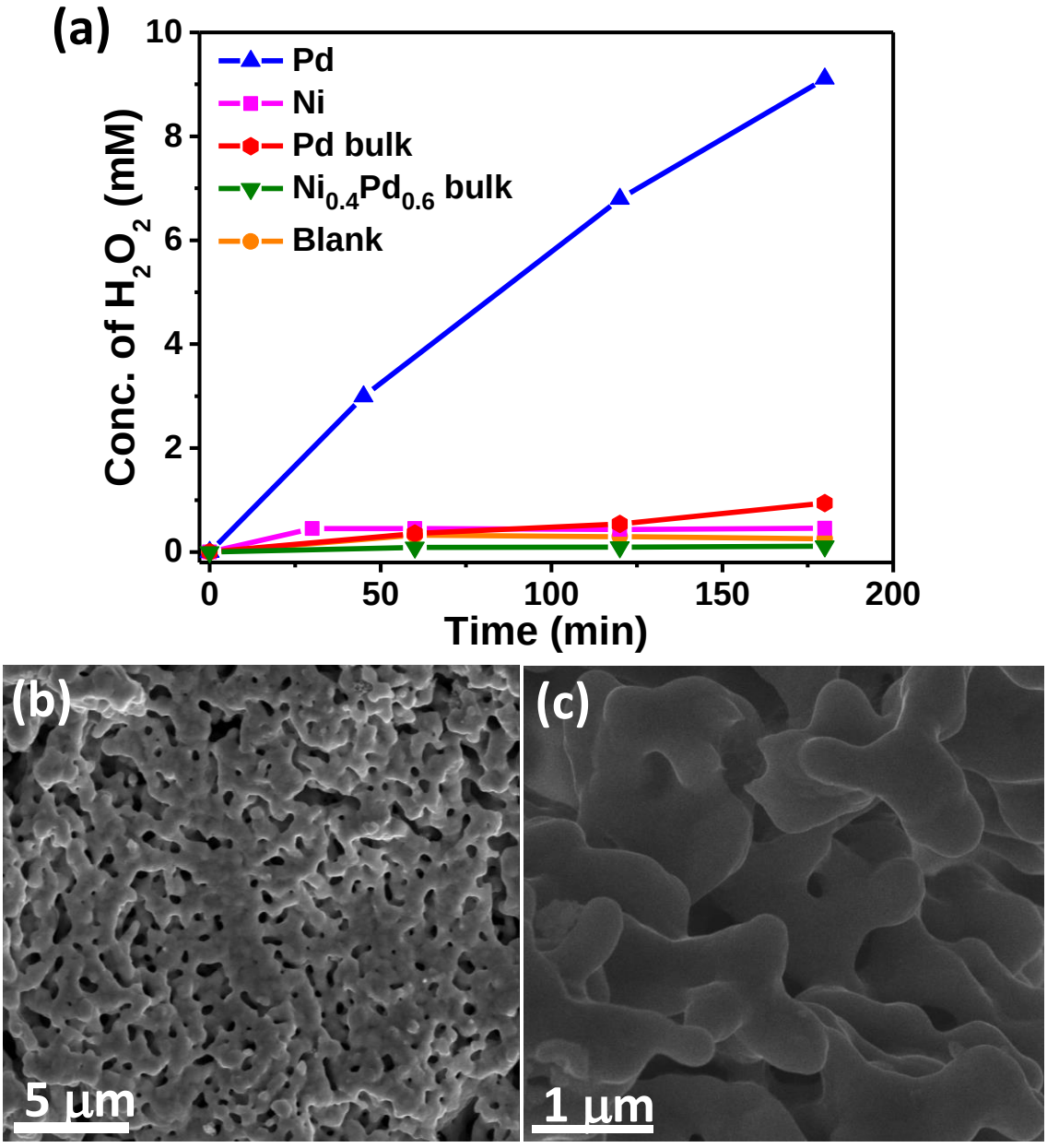

Figure 2.10: *(a) Formation of H_2O_2 by micron size particles. For reference, the activity of Pd nanostructure is shown here along with blank experiment (without any catalyst). FESEM images of micron size particles of (b) Pd and (c) $Ni_{0.4}Pd_{0.6}$.*

The assynthesized Ni nanostructure did not show any activity for the hydrogen peroxide synthesis (Figure 2.10a). The nanoscale phenomenon of Pd and NiPd catalyst is evident from the fact that micron sized particles (prepared by heating the assynthesized samples at 500 ºC for 12h in presence of 5% H_2 in N_2) did not show any activity towards H_2O_2 synthesis (Figure 2.10). As nickel in $Ni_{0.4}Pd_{0.6}$ exists mostly in the form of nickel hydroxide (Figure 2.9), its dissolution in an acidic environment is expected to alter the chemical nature and composition of the catalyst. In order to understand the effect of strong acidic reaction medium on $Ni_{0.4}Pd_{0.6}$ catalyst, we have soaked the catalyst in the same medium ($HCl+H_2O_2$) for different period of time (0.5h, 1h, and 72h) in presence of hydrogen flow (details in experimental section, dissolution study). Hydrogen flow is necessary to avoid the dissolution of Pd as $PdCl_4^{2-}$ in presence of chloride ions.[17] Interestingly, soaking the catalyst for 0.5h dissolves all the free nickel and nickel hydroxide in $Ni_{0.4}Pd_{0.6}$ and the resulting solid is abbreviated as $Ni_{0.1}Pd_{0.9}$-0.5h based on the Ni:Pd composition (1:9) estimated through ICP-AES analysis. This composition remains same and does not undergo any dissolution even after 72h soaking, abbreviated

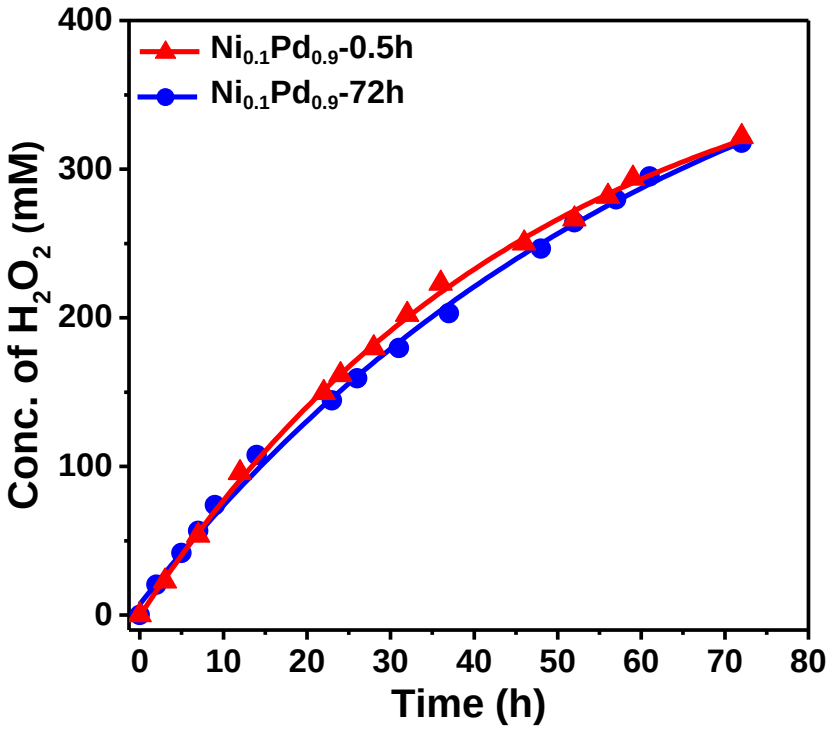

Figure 2.11: *Synthesis of H_2O_2 over $Ni_{0.1}Pd_{0.9}$-0.5h and $Ni_{0.1}Pd_{0.9}$-72h catalysts (catalyst taken: 3 mg for $Ni_{0.1}Pd_{0.9}$, normalized to the amount of Pd present in 5 mg $Ni_{0.4}Pd_{0.6}$).*

as $Ni_{0.1}Pd_{0.9}$-72h, in the reaction medium in presence of hydrogen. The H_2O_2 synthesis carried out over $Ni_{0.1}Pd_{0.9}$-0.5h and $Ni_{0.1}Pd_{0.9}$-72h showed similar trend as that of as-synthesized $Ni_{0.4}Pd_{0.6}$ (Figure 2.11) for 72h reaction and most importantly, both the catalysts does not undergo any leaching of Pd or Ni. It is clear from the above results that the remarkable activity for H_2O_2 production over $Ni_{0.4}Pd_{0.6}$ nanostructure is associated with the presence of NiPd bimetallic nanostructure having Ni:Pd composition, 10:90. The presence of Ni enhances the activity of Pd in bimetallic NiPd. It is known that the d-orbital of Pd is electronically modified in presence of a secondary metal, Ni.[30, 31] Such electronic modifications would influence the Fermi level of Pd metal which in turn would influence the catalytic reactions.[30] Ni modified Pd has been reported to show better electrocatalytic activity for methanol oxidation than Pd alone.[32] This would further support our observation that higher NiPd activity for H_2O_2 formation is due to the presence of Ni which would modify the electronic structure of Pd.

Powder X-ray diffraction (PXRD) pattern (Figure 2.12a) of $Ni_{0.1}Pd_{0.9}$-0.5h does not show any Pd (111) peak shift and is similar to that of Pd (Figure 2.1) and $Ni_{0.4}Pd_{0.6}$ nanostructures. The field emission scanning electron microscopy (FESEM) and transmission electron microscopy (TEM) images of $Ni_{0.1}Pd_{0.9}$-0.5h sample show the network nanostructure formed by the fusion of nanoparticles of size range from 10 to 15 nm (Figure 2.12b & c). High resolution transmission electron microscope (HRTEM) image (Figure 2.12d) shows the lattice spacing of 0.225 nm associated with Pd (111). Elemental mapping (Figure 2.12e) shows uniform distribution of Ni and Pd probably due to the formation of random alloy nanostructure which is not reflected in the PXRD pattern. However, soaking $Ni_{0.4}Pd_{0.6}$ in the reaction medium for 1h, abbreviated as $Ni_{0.1}Pd_{0.9}$-1.0h, shows a marginal shift ($2\theta = 0.24°$) in the Pd (111) peak towards higher diffraction angle associated with NiPd alloy (Figure 2.12a). The XPS analysis of $Ni_{0.1}Pd_{0.9}$-1.0h shows a slight shift in binding energy of Pd $3d_{3/2}$ and Pd $3d_{5/2}$ (0.35 and 0.2 eV respectively) towards lower value as compared to assynthesized Pd suggesting the formation of NiPd alloy (Figure 2.13).[33] The emergence of alloy peak in the PXRD and the retention of same Ni:Pd chemical composition ($Ni_{0.1}Pd_{0.9}$) for 1h dissolution as that of 0.5h dissolution strongly suggests the possible reorganization of nickel atoms which were randomly distributed in the Pd lattice of assynthesized $Ni_{0.4}Pd_{0.6}$, into an ordered nanoalloy domains within 1h dissolution. $Ni_{0.1}Pd_{0.9}$-72h obtained after 72h dissolution showed significant shift towards higher angle for Pd (111) peak in the PXRD (Figure

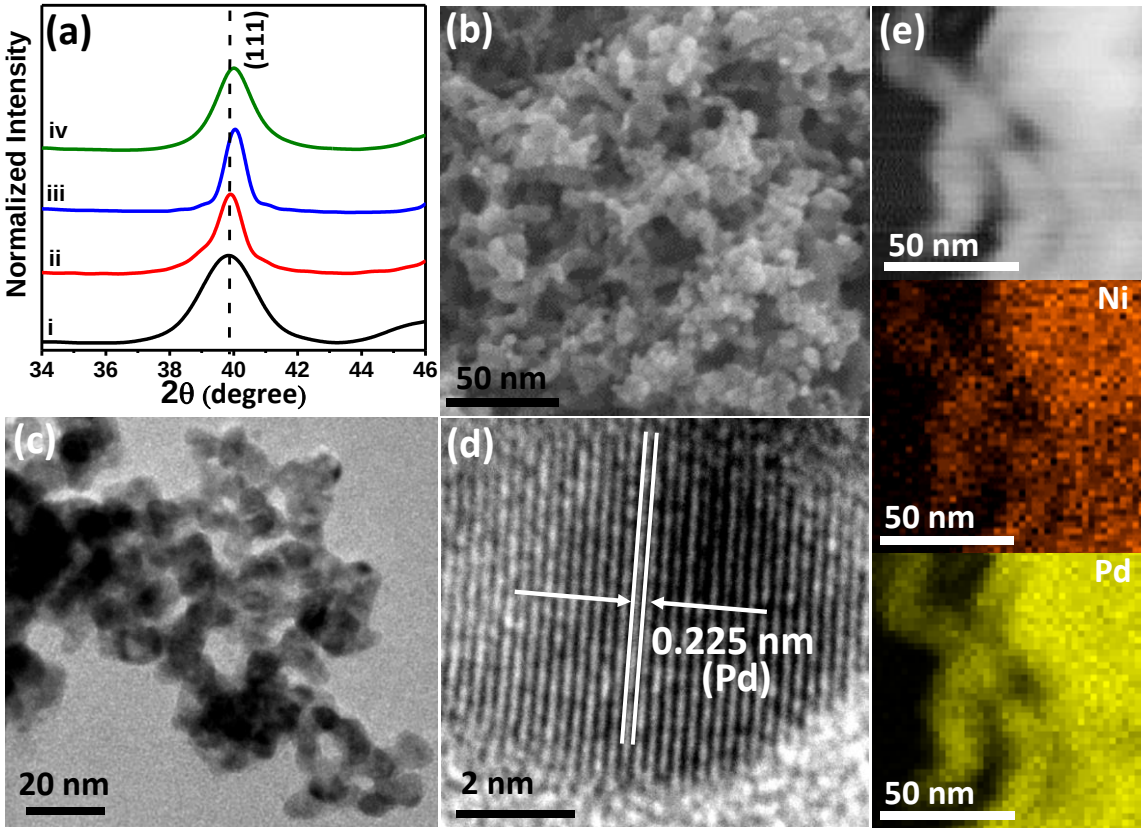

Figure 2.12: *(a) PXRD pattern of (i) $Ni_{0.4}Pd_{0.6}$ and after dissolution at different time interval- (ii) 0.5h, (iii) 1h and (iv) 72h. (b) FESEM and (c) TEM images of $Ni_{0.1}Pd_{0.9}$-0.5h. (d) HRTEM image of $Ni_{0.1}Pd_{0.9}$-0.5h shows lattice spacing for Pd. (e) High angle annular dark-field (HAADF) image and the corresponding elemental mapping of Ni and Pd in $Ni_{0.1}Pd_{0.9}$-0.5h.*

2.12a). The FESEM and TEM images show the retention of network morphology connected with the nanoparticles having size ranging from 20 to 30 nm (Figure 2.14a & b). The elemental mapping (Figure 2.14c) indicates by and large uniform distribution of Ni and Pd, with existence of domains where the composition is enriched with higher amount of Ni or Pd content (marked with the dotted line in Figure 2.14c) probably due to de-alloying nature of NiPd for their high lattice mismatch. Furthermore, the observation of different lattice spacing associated with Pd and NiPd confirms the domain formation (Figure 2.14d). From the above observations it is clear that only 10% of nickel is dissolved in the Pd lattice and the remaining nickel mostly exists as amorphous nickel hydroxide in the assynthesized $Ni_{0.4}Pd_{0.6}$. The free nickel and nickel hydroxide

completely dissolved in the acidic medium within 30 min leaving only the preformed bimetallic NiPd nanostructure having Ni:Pd composition, 1:9.

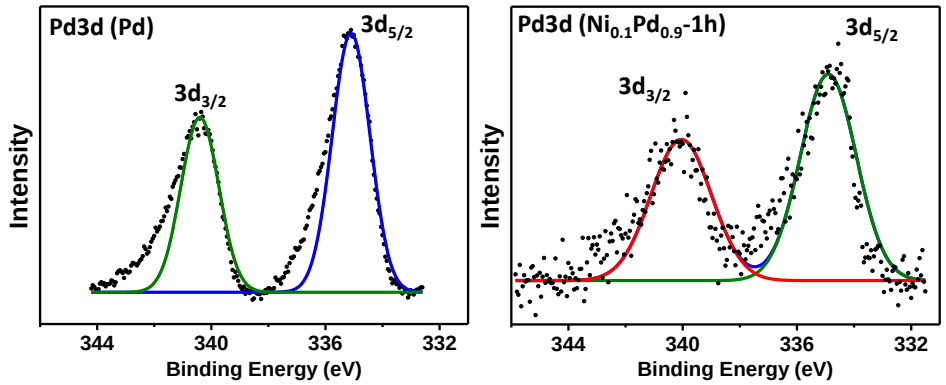

Sample Name	Binding energy of $Pd3d_{3/2}$ (eV)	Binding energy of $Pd3d_{5/2}$ (eV)
Pd	340.4	335.1
$Ni_{0.1}Pd_{0.9}$-1h	340.05	334.9

Figure 2.13: *XPS spectra of Pd3d in Pd and $Ni_{0.1}Pd_{0.9}$-1h nanostructure.*

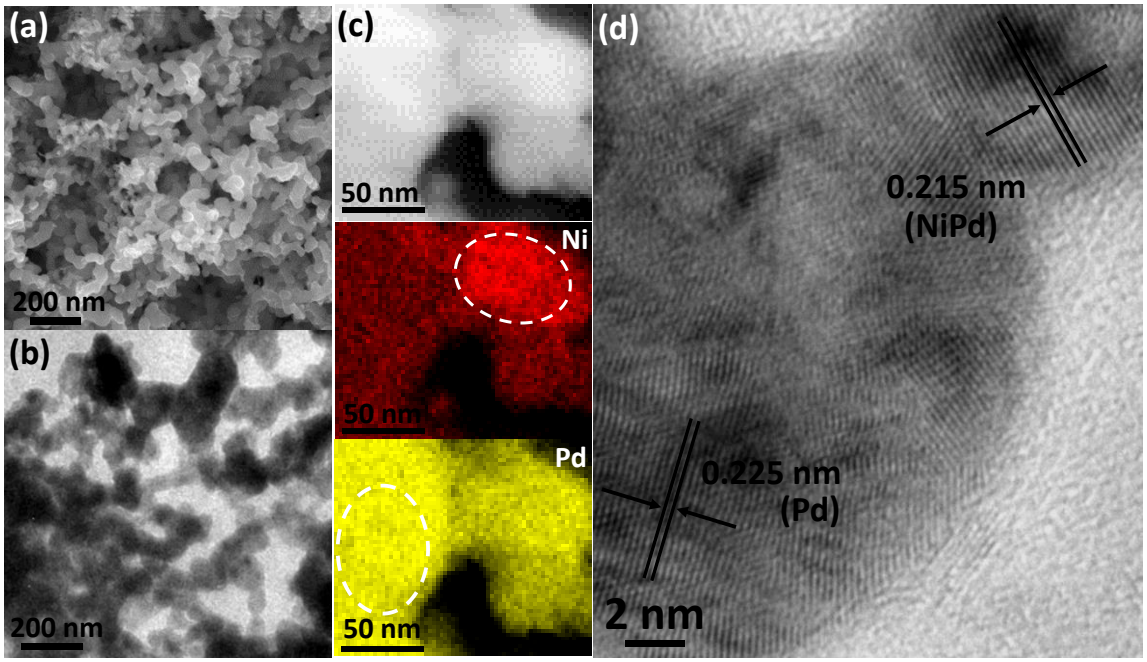

Figure 2.14: Characterization of $Ni_{0.1}Pd_{0.9}$-72h. *(a) FESEM and (b) TEM images show the nanostructure network. (c) High angle annular dark-field (HAADF) image of $Ni_{0.1}Pd_{0.9}$-72h and the corresponding elemental mapping of Ni and Pd. The regions of Ni*

and Pd rich domains are marked in doted lines. (d) HRTEM image shows lattice spacing for both Pd and NiPd.

The formation of NiPd nanoalloy from Ni and Pd nanostructures in the reaction conditions is ruled out, as separate experiment in which a mixture of assynthesized Pd and Ni nanostructures kept in a similar acidic condition failed to produce NiPd alloy and leaves only Pd even after 48h (Figure S14). On the other hand, soaking of assynthesized $Ni_{0.4}Pd_{0.6}$ along with as prepared Pd nanostructure in an acidic environment in presence of hydrogen yields NiPd alloy with Ni:Pd chemical composition, 3:97. This suggests that assynthesized $Ni_{0.4}Pd_{0.6}$ most probably consists of NiPd random alloy (in which 10% of Ni atoms with respect to Pd, mixed in a statistically random manner) nanostructure intermixed with amorphous nickel hydroxide (Scheme 2.2).

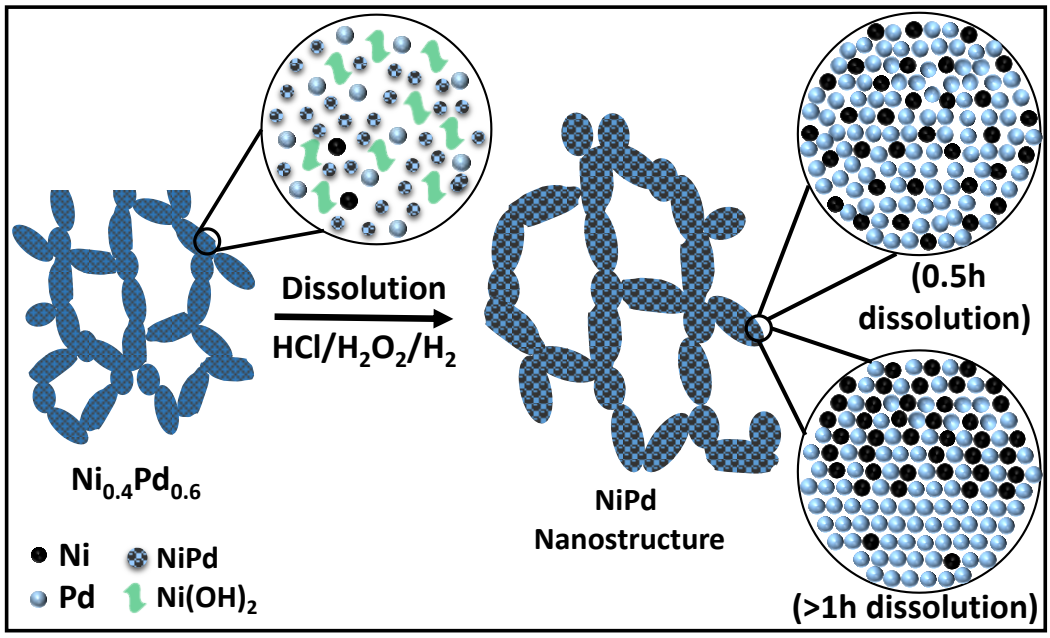

Scheme 2.2: *Schematic represents the formation of bimetallic NiPd nanostructure.*

2.5. Conclusion:

We have shown that the presence of non-noble metal, Ni, enhances the catalytic activity of Pd, three times in comparison to Pd alone. The $Ni_{0.1}Pd_{0.9}$ catalyst is also stable in the harsh reaction conditions and retains its activity for more than 3 days. We believe our observation of phenomenal enhancement in the activity of Pd by Ni for a longer period of

time would pave the way for the development of new catalysts to bring the on-site hydrogen peroxide production a reality.

2.6. References:

1. P. Tundo, P. Anastas, D. S. Black, J. Breen, T. Collins, S. Memoli, J. Miyamoto, M. Polyakoff and W. Tumas, Synthetic pathways and processes in green chemistry. Introductory overview, *Pure Appl. Chem.*, 2000, **72**, 1207–1228.
2. J. M. Campos-Martin, G. Blanco-Brieva and J. L. G. Fierro, Hydrogen Peroxide Synthesis: An Outlook beyond the Anthraquinone Process, *Angew. Chem. Int. Ed.*, 2006, **45**, 6962-6984.
3. C. Samanta, Direct synthesis of hydrogen peroxide from hydrogen and oxygen: An overview of recent developments in the process, *Appl. Catal. A.: Gen.*, 2008, **350**, 133-149.
4. J. K. Edwards, S. J. Freakley, R. J. Lewis, J. C. Pritchard and G. J. Hutchings, Advances in the direct synthesis of hydrogen peroxide from hydrogen and oxygen, *Catal. Today*, 2015, **248**, 3-9.
5. J. Garcia-Serna, T. Moreno, P. Biasi, M. J. Cocero, J.-P. Mikkola and T. O. Salmi, Engineering in direct synthesis of hydrogen peroxide: targets, reactors and guidelines for operational conditions, *Green Chemistry*, 2014, **16**, 2320-2343.
6. H.-J. Reidl and G. Pfleiderer, *I.G. Farbenindustrie AG*, 1939, US Patent 2158525.
7. J. K. Edwards and G. J. Hutchings, Palladium and Gold–Palladium Catalysts for the Direct Synthesis of Hydrogen Peroxide, *Angew. Chem. Int. Ed.*, 2008, **47**, 9192-9198.
8. S. J. Freakley, M. Piccinini, J. K. Edwards, E. N. Ntainjua, J. A. Moulijn and G. J. Hutchings, Effect of Reaction Conditions on the Direct Synthesis of Hydrogen Peroxide with a AuPd/TiO_2 Catalyst in a Flow Reactor, *ACS Catal.*, 2013, **3**, 487-501.
9. F. Menegazzo, M. Signoretto, M. Manzoli, F. Boccuzzi, G. Cruciani, F. Pinna and G. Strukul, Influence of the preparation method on the morphological and composition properties of Pd–Au/ZrO_2 catalysts and their effect on the direct synthesis of hydrogen peroxide from hydrogen and oxygen, *J. Catal.*, 2009, **268**, 122-130.

10. T. Garcia, R. Murillo, S. Agouram, A. Dejoz, M. J. Lazaro, L. Torrente-Murciano and B. Solsona, Highly dispersed encapsulated AuPd nanoparticles on ordered mesoporous carbons for the direct synthesis of H_2O_2 from molecular oxygen and hydrogen, *Chem. Commun.*, 2012, **48**, 5316-5318.
11. J. Xu, L. Ouyang, G.-J. Da, Q.-Q. Song, X.-J. Yang and Y.-F. Han, Pt promotional effects on Pd–Pt alloy catalysts for hydrogen peroxide synthesis directly from hydrogen and oxygen, *J. Catal.*, 2012, **285**, 74-82.
12. V. R. Choudhary, C. Samanta and A. G. Gaikwad, Drastic increase of selectivity for H_2O_2 formation in direct oxidation of H_2 to H_2O_2 over supported Pd catalysts due to their bromination, *Chem. Commun.*, 2004, 2054-2055.
13. G. Blanco-Brieva, E. Cano-Serrano, J. M. Campos-Martin and J. L. G. Fierro, Direct synthesis of hydrogen peroxide solution with palladium-loaded sulfonic acid polystyrene resins, *Chem. Commun.*, 2004, 1184-1185.
14. S. Melada, F. Pinna, G. Strukul, S. Perathoner and G. Centi, Direct synthesis of H_2O_2 on monometallic and bimetallic catalytic membranes using methanol as reaction medium, *J. Catal.*, 2006, **237**, 213-219.
15. T. Deguchi, H. Yamano and M. Iwamoto, Dynamics of direct H_2O_2 synthesis from H_2 and O_2 on a Pd nano-particle catalyst protected with polyvinylpyrrolidone, *J. Catal.*, 2012, **287**, 55-61.
16. Q. Liu, J. C. Bauer, R. E. Schaak and J. H. Lunsford, Supported Palladium Nanoparticles: An Efficient Catalyst for the Direct Formation of H_2O_2 from H_2 and O_2, *Angew. Chem. Int. Ed.*, 2008, **47**, 6221-6224.
17. S. Chinta and J. H. Lunsford, A mechanistic study of H_2O_2 and H_2O formation from H_2 and O_2 catalyzed by palladium in an aqueous medium, *J. Catal.*, 2004, **225**, 249-255.
18. E. Ghedini, F. Menegazzo, M. Signoretto, M. Manzoli, F. Pinna and G. Strukul, Mesoporous silica as supports for Pd-catalyzed H_2O_2 direct synthesis: Effect of the textural properties of the support on the activity and selectivity, *J. Catal.*, 2010, **273**, 266-273.
19. H. C. H. Henkel and W. Weber, *(Henkel & CIE)*, 1914, US Patent 1108752.
20. J. K. Edwards, S. J. Freakley, A. F. Carley, C. J. Kiely and G. J. Hutchings, Strategies for Designing Supported Gold–Palladium Bimetallic Catalysts for the Direct Synthesis of Hydrogen Peroxide, *Acc. Chem. Res.*, 2014, **47**, 845-854.

21. L. Ouyang, G.-j. Da, P.-f. Tian, T.-y. Chen, G.-d. Liang, J. Xu and Y.-F. Han, Insight into active sites of Pd–Au/TiO_2 catalysts in hydrogen peroxide synthesis directly from H_2 and O_2, *J. Catal.*, 2014, **311**, 129-136.
22. J. K. Edwards, B. Solsona, E. N. Ntainjua, A. F. Carley, A. A. Herzing, C. J. Kiely and G. J. Hutchings, Switching Off Hydrogen Peroxide Hydrogenation in the Direct Synthesis Process, *Science*, 2009, **323**, 1037-1041.
23. J. K. Edwards, E. Ntainjua N, A. F. Carley, A. A. Herzing, C. J. Kiely and G. J. Hutchings, Direct Synthesis of H_2O_2 from H_2 and O_2 over Gold, Palladium, and Gold–Palladium Catalysts Supported on Acid-Pretreated TiO2, *Angew. Chem. Int. Ed.*, 2009, **48**, 8512-8515.
24. J. K. Edwards, A. Thomas, B. E. Solsona, P. Landon, A. F. Carley and G. J. Hutchings, Comparison of supports for the direct synthesis of hydrogen peroxide from H_2 and O_2 using Au–Pd catalysts, *Catal. Today*, 2007, **122**, 397-402.
25. V. Paunovic, V. Ordomsky, M. Fernanda Neira D'Angelo, J. C. Schouten and T. A. Nijhuis, Direct synthesis of hydrogen peroxide over Au–Pd catalyst in a wall-coated microchannel, *J. Catal.*, 2014, **309**, 325-332.
26. V. Paunovic, V. V. Ordomsky, V. L. Sushkevich, J. C. Schouten and T. A. Nijhuis, Direct Synthesis of Hydrogen Peroxide over Au-Pd Catalyst—The Effect of Co-Solvent Addition, *ChemCatChem*, 2015, **7**, 1161-1176.
27. F. Menegazzo, P. Burti, M. Signoretto, M. Manzoli, S. Vankova, F. Boccuzzi, F. Pinna and G. Strukul, Effect of the addition of Au in zirconia and ceria supported Pd catalysts for the direct synthesis of hydrogen peroxide, *J. Catal.*, 2008, **257**, 369-381.
28. K. S. Krishna, C. S. S. Sandeep, R. Philip and M. Eswaramoorthy, Mixing Does the Magic: A Rapid Synthesis of High Surface Area Noble Metal Nanosponges Showing Broadband Nonlinear Optical Response, *ACS Nano*, 2010, **4**, 2681-2688.
29. I. R. Cohen, T. C. Purcell and A. P. Altshuller, Analysis of the oxidant in photooxidation reactions, *Environ. Sci. Technol.*, 1967, **1**, 247-252.
30. Z. Yin, W. Zhou, Y. Gao, D. Ma, C. J. Kiely and X. Bao, Supported Pd–Cu Bimetallic Nanoparticles That Have High Activity for the Electrochemical Oxidation of Methanol, *Chem. Eur. J.*, 2012, **18**, 4887-4893.
31. A. Ruban, B. Hammer, P. Stoltze, H. L. Skriver and J. K. Nørskov, Surface electronic structure and reactivity of transition and noble metals1, *J. Mol. Catal. A: Chem.*, 1997, **115**, 421-429.

32. C. Zhu, D. Wen, M. Oschatz, M. Holzschuh, W. Liu, A.-K. Herrmann, F. Simon, S. Kaskel and A. Eychmüller, Kinetically Controlled Synthesis of PdNi Bimetallic Porous Nanostructures with Enhanced Electrocatalytic Activity, *Small*, 2015, **11**, 1430-1434.

33. N. J. S. Costa, M. Guerrero, V. Collière, É. Teixeira-Neto, R. Landers, K. Philippot and L. M. Rossi, Organometallic Preparation of Ni, Pd, and NiPd Nanoparticles for the Design of Supported Nanocatalysts, *ACS Catal.*, 2014, **4**, 1735-1742.

Chapter – 3

Direct synthesis of H_2O_2 by Pt promoted NiPd catalysts supported on carbon

Summary:

Bimetallic NiPd nanoparticles supported on activated carbon was used as a catalyst for the direct synthesis of hydrogen peroxide from molecular H_2 and O_2 in atmospheric as well as in high pressure conditions. The NiPd catalyst supported on carbon shows very high enhancement in activity compared to Pd on carbon. Introduction of Pt (0.2 wt. %) in NiPd, further improves its catalytic activity. NiPdPt on carbon (AC/NiPdPt) catalyst shows stability for 5 cycles (total 40h) in normal pressure without losing its initial activity.

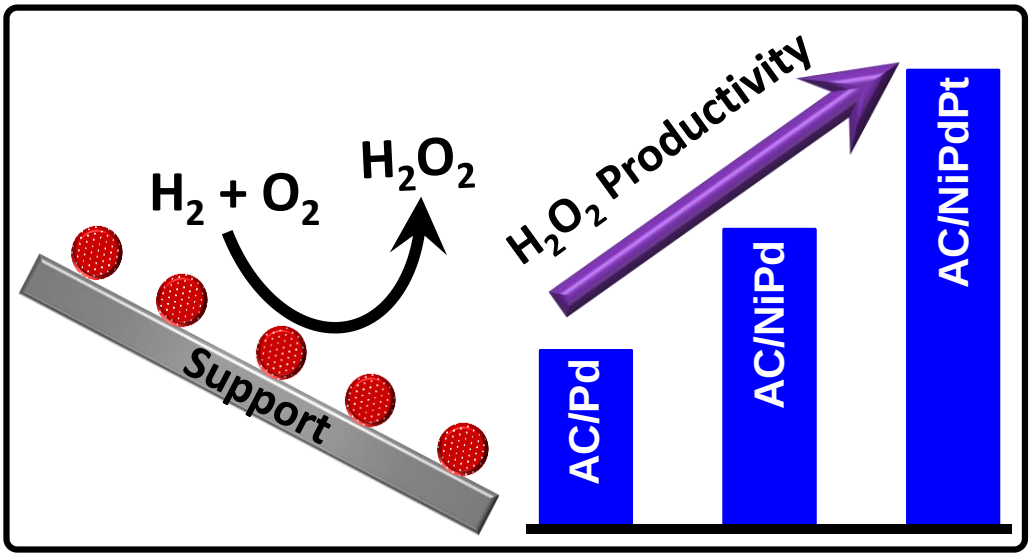

3.1. Introduction:

Direct synthesis of hydrogen peroxide, an eco-friendly oxidizing agent, from molecular H_2 and O_2 has been drawn a lot of attention over the last few decades.[1-4] Its enormous demand in paper and textile industries as a bleaching agent and in modern propylene oxide industries as a green oxidant sees its production surges ahead of 3 million metric tons annually.[4-6] Nevertheless, the only successful commercial synthesis of hydrogen peroxide as of now is indirect anthraquinone process developed by Riedl and Pfleiderer[7] in 1939 which involves hydrogenation of substituted anthraquinone using Pd or Ni catalyst and subsequent air oxidation to obtain original anthraquinone and H_2O_2. This inherently complex process is economically viable only when operated at large scale, and produces concentrated H_2O_2, though most applications demand only dilute solutions. Moreover, the process is not considered as a green process and many unwanted chemicals are formed due to non-selective hydrogenation.[1, 8] The direct synthesis of H_2O_2 would be a great alternative to existing anthraquinone process which can avoid environmentally hazardous, storage and transportation associated with the indirect process.[9]

A lot of studies in the past few decades have been carried out with Pd after the first patent made by Hugo Henkel and Walter Weber[10] in 1914 for the direct synthesis of H_2O_2. Recently, Pd-based bimetallic nanoparticles have been explored in this direction for their improved catalytic properties and stability over a long run.[11-19] Among them, Au and Pt were mostly used with Pd, on various supports (like carbon, zeolite, silica, Fe_2O_3, TiO_2, CeO_2 etc.) to make it more efficient for the direct synthesis of H_2O_2.[8, 20-32] Pt has also been used as a third element in AuPd catalyst to promote its activity for H_2O_2 synthesis.[31] The high cost of noble metals limits their large scale applications and it is important to replace these metals (totally or partially) with earth abundant elements to reduce the cost as well as to improve their efficiency.[33-35]

In this chapter, we have demonstrated the use of bimetallic NiPd nanoparticles supported on carbon towards direct synthesis of H_2O_2 in normal as well as high pressure conditions. The NiPd catalyst shows a significant improvement in catalytic activity in comparison with monometallic Pd on carbon support. When Pt has been introduced as a promoter for NiPd catalyst, the activity is further improved. The catalyst is very stable and shows recyclability up to 5^{th} cycle.

3.2. Scope of the Present Study:

In the previous chapter, we have studied self-supported bimetallic NiPd nanostructured catalysts for direct synthesis of H_2O_2. The bimetallic NiPd catalysts showed three times higher activity compared to monometallic Pd alone. In this study, highly dispersed bimetallic NiPd nanoparticles have been synthesized on activated carbon and the promotional effects of Pt on NiPd catalyst towards H_2O_2 synthesis reaction in normal as well as high pressure conditions were investigated.

3.3. Experimental Section:

3.3.1. Materials and Characterization Techniques:

$PdCl_2$ (Sigma Aldrich), $H_2PtCl_6.6H_2O$ (Sigma Aldrich), $HAuCl_4.3H_2O$ (Sigma Aldrich), $NiCl_2.6H_2O$ (S D Fine Chemicals), $NaBH_4$ (S D Fine Chemicals), KBr (S D Fine Chemicals), $TiOSO_4$ (Sigma Aldrich), H_2SO_4 (98%, AR grade), HCl (37%, AR grade), methanol (AR grade, S D Fine Chemicals), activated carbon (S D Fine Chemicals) were used without any further purification.

Energy-dispersive X-ray spectroscopy (EDS) analyses were carried out using FEI (Nova-Nano SEM-600 Netherlands) equipment. Transmission electron microscope (TEM) imaging was done on a JEOL, JEM 3010 operated at 300 kV. Samples were prepared by putting a drop of very dilute dispersion in ethanol on a TEM grid (carbon polymer, 300 mesh). Electronic absorption spectra were recorded by Perkin Elmer Lambda 900 UV-Vis-NIR Spectrometer. The cuvette with 1 cm path length was used for recording the spectra. Inductively coupled plasma – atomic emission spectroscopy (ICP-AES) was carried out using a Perkin−Elmer Optima 7000 DV machine. The composition of gas mixture was analysed by gas chromatography (Agilent 7890A) using MolSieve 5A 60-80 mesh column at 40 ^oC temperature. High pressure reactions were carried out using high pressure reactor (Amar Equipment, model no- 3601) with 50 mL volume and a maximum working pressure of 200 bar.

3.3.2. Catalysts Synthesis:

Bimetallic NiPd nanoparticles were synthesized on activated carbon (AC, surface area ~1100 $m^2\ g^{-1}$) support (abbreviated as AC/NiPd) at room temperature by the reduction of aqueous metal chloride solutions in presence of $NaBH_4$ as a reducing agent.

To synthesize AC/NiPd, 200 mg of activated carbon was first dispersed in 80 mL water by sonication for 10 minutes. A mixture of 0.68 mL of 0.1 M $NiCl_2.6H_2O$ and 0.57 mL of 0.1 M $PdCl_2$ solution in aqueous medium (5 wt. % loading of NiPd with Ni:Pd wt. ratio 40:60, respect to support) was added to the above dispersion. The dispersion was stirred for 20 minutes. Then 4 mL of 0.1 M $NaBH_4$ solution was added dropwise and stirred for another 30 minutes. The solid product was separated by centrifugation and washed with water for three times and finally dried at 50 ^oC for overnight. The same procedure was followed to synthesize AC/Pd and AC/AuPd (Au:Pd wt. ratio 1:1) for controlled experiment.

To prepare AC/NiPdPt (5 wt. % catalyst loading with Ni:Pd:Pt wt. ratio of 38:57:5), a mixture of 0.65 mL of 0.1 M $NiCl_2.6H_2O$, 0.54 mL of 0.1 M $PdCl_2$ and 26 μL of $H_2PtCl_6.6H_2O$ solution was added to 200 mg activated carbon and stirred for 20 min followed by dropwise addition of 4 mL 0.1 M $NaBH_4$ solution. After 30 min stirring, the solid product was centrifuged, washed and dried at 50 ^oC for overnight.

Acid etching was carried out for AC/NiPd and AC/NiPdPt in KBr/HCl/H_2O_2 mixture in presence of H_2 flow in order to remove the unwanted hydroxide and oxide species of Ni from the as-synthesized catalysts.[33] In a typical procedure, 200 mg of as-synthesized catalyst was dispersed in 30 mL of aqueous solution containing 0.01 M KBr, 0.1 M HCl and 400 mM H_2O_2. The whole dispersion was transferred to a glass jacket reactor and H_2 gas was allowed to bubble through the mixture with a flow rate of 20 mL min^{-1} for an hour at room temperature. Finally, the remaining solid product was separated, washed and dried in oven.

Inductively coupled plasma – atomic emission spectroscopy (ICP-AES) was carried out to calculate the catalyst loading and the metal compositions in the catalysts. The analyses show the total catalyst loading of 3.3 wt. % for all the synthesized catalysts. The final Ni:Pd wt. ratio in AC/NiPd was 10:90 and the Ni:Pd:Pt wt. ratio in AC/NiPdPt was 9:85:6 (0.2 wt. % Pt loading with respect to support) was confirmed by ICP-AES.

3.3.3. Direct Synthesis of H_2O_2:

Direct synthesis of H_2O_2 from gaseous H_2 and O_2 was carried out using a custom made glass jacket reactor described elsewhere[17] in atmospheric pressure conditions. In a typical procedure, 30 mg of catalyst was dispersed by sonication in 30 mL H_2O-methanol (1:5) solution containing 28 mM HCl and 0.01 M Br^- (introduced as KBr) and then transferred

to a glass jacket reactor shown in Scheme 2.1 (Chapter 2). The individual gasses, H_2 and O_2 were allowed to bubble through the glass frit in a ratio of 1:4 v/v with a total flow of 50 mL min^{-1} using two separate mass flow controllers (Aera, Hitachi). To reduce the dead volume, the portion below the glass frit was filled with 4 mm glass beads. The reaction temperature was maintained at 10 °C using Julabo water circulation unit.

Batch type, high pressure synthesis was carried out using high pressure autoclave as reported in the literature.[23] The catalyst testing for direct synthesis of H_2O_2 was carried out at 37 bar using a stainless steel autoclave (made by Amar Equipment) with the reaction capacity of 50 mL (Image 3.1). The autoclave was attached with an overhead external magnetic stirrer (0-2000 rpm) along with temperature and pressure sensors. In a typical procedure, 10 mg catalyst was dispersed in 5.8 gm water and 11.2 gm methanol and the dispersion was purged with CO_2 for 10 min before charging into the autoclave. The autoclave was pressurised with H_2 and O_2 (H_2:O_2 ratio 1:2) at a total pressure of 37 bar using 5% H_2 in CO_2 and 25% O_2 in CO_2 at 10 ^oC (by Julabo water circulating unit). The total content of H_2:O_2:CO_2 are in the ratio of 4:8:88 at 37 bar. The stirring was continued at 1400 rpm and experiment was carried out for 30 min.

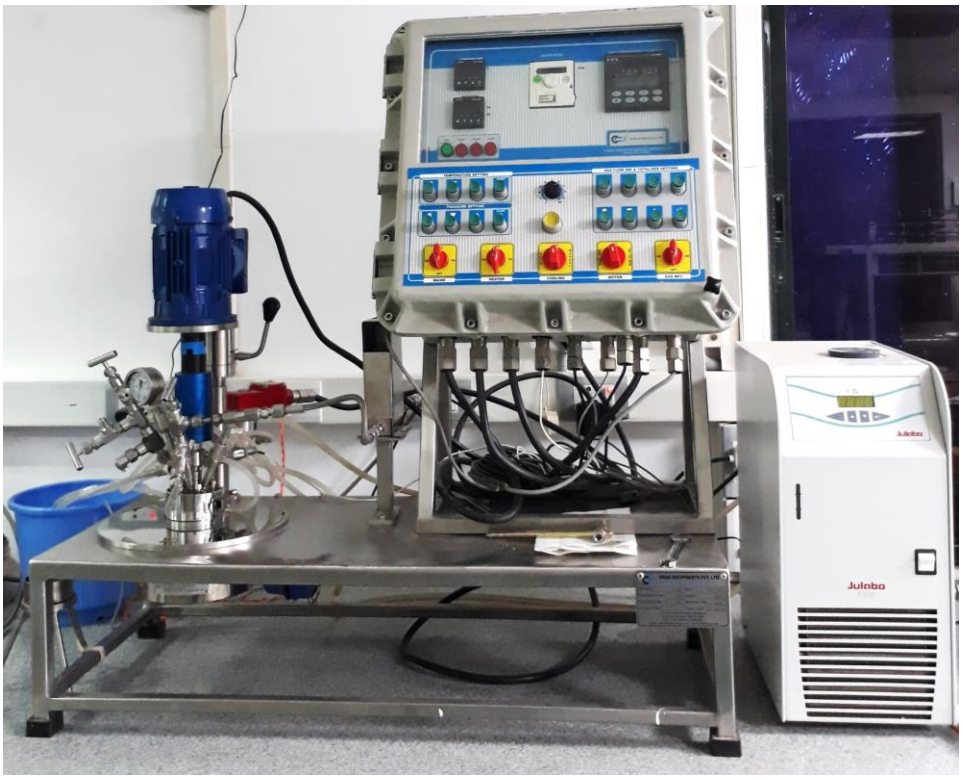

Image 3.1: *Photograph of High pressure reactor.*

H_2O_2 concentration was determined by $TiOSO_4/H_2SO_4$ method[36] using UV-vis spectroscopy as described in the previous chapter (section 2.3.2.4.).

3.4. Results and Discussion:

Bimetallic NiPd (Ni:Pd wt. ratio 10:90) nanoparticles supported on activated carbon (AC/NiPd) were synthesized by simple borohydride reduction method followed by acid washing (details in experimental section- 3.3.2). The transmission electron microscopy (TEM) image shows NiPd nanoparticles of uniform dispersion throughout the carbon support (Figure 3.1). The average particle size is around 4 to 6 nm analysed from the histogram calculated over 200 nanoparticles (Figure 3.1). Inductively coupled plasma – atomic emission spectroscopy (ICP-AES) analysis confirms Ni:Pd ratio of 10:90 with

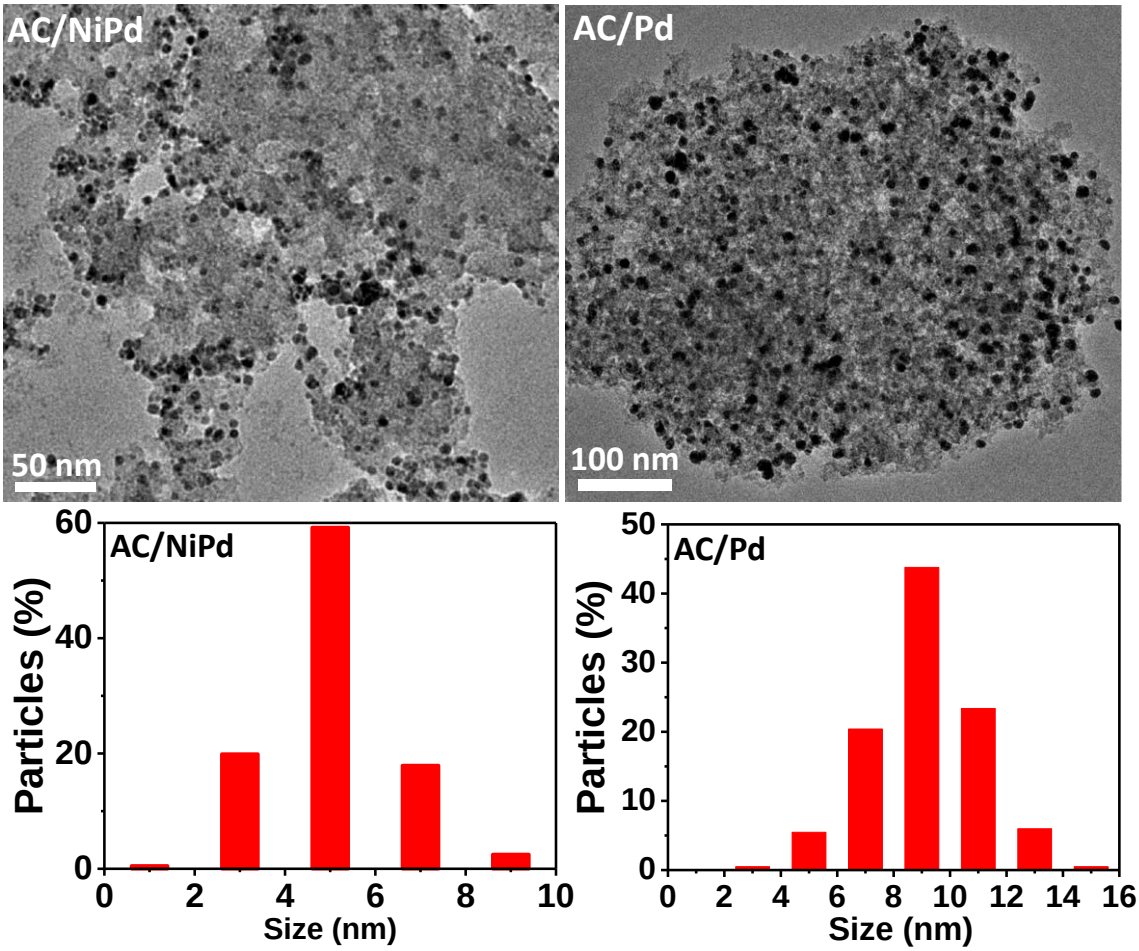

Figure 3.1: *TEM images of NiPd and Pd nanoparticles supported on activated carbon (AC/NiPd and AC/Pd). Corresponding histogram of particle size distribution for NiPd and Pd nanoparticles (calculated over 200 particles).*

overall NiPd loading of 3.3 wt. % with respect to activated carbon. Monometallic Pd nanoparticles prepared on activated carbon show the particle size ranging from 6 to 12 nm (Figure 3.1). AC/NiPdPt catalyst also shows uniformly dispersed metal nanoparticles on carbon as confirmed by the dark-field TEM image (Figure 3.2a). The high resolution TEM (HRTEM) image of AC/NiPdPt shows lattice fringe around 0.22 nm associated with Pd (111) plane (Figure 3.2b). The histogram of NiPdPt nanoparticles (calculated over 200 particles) shows particles of size less than 5 nm (Figure 3.2c).

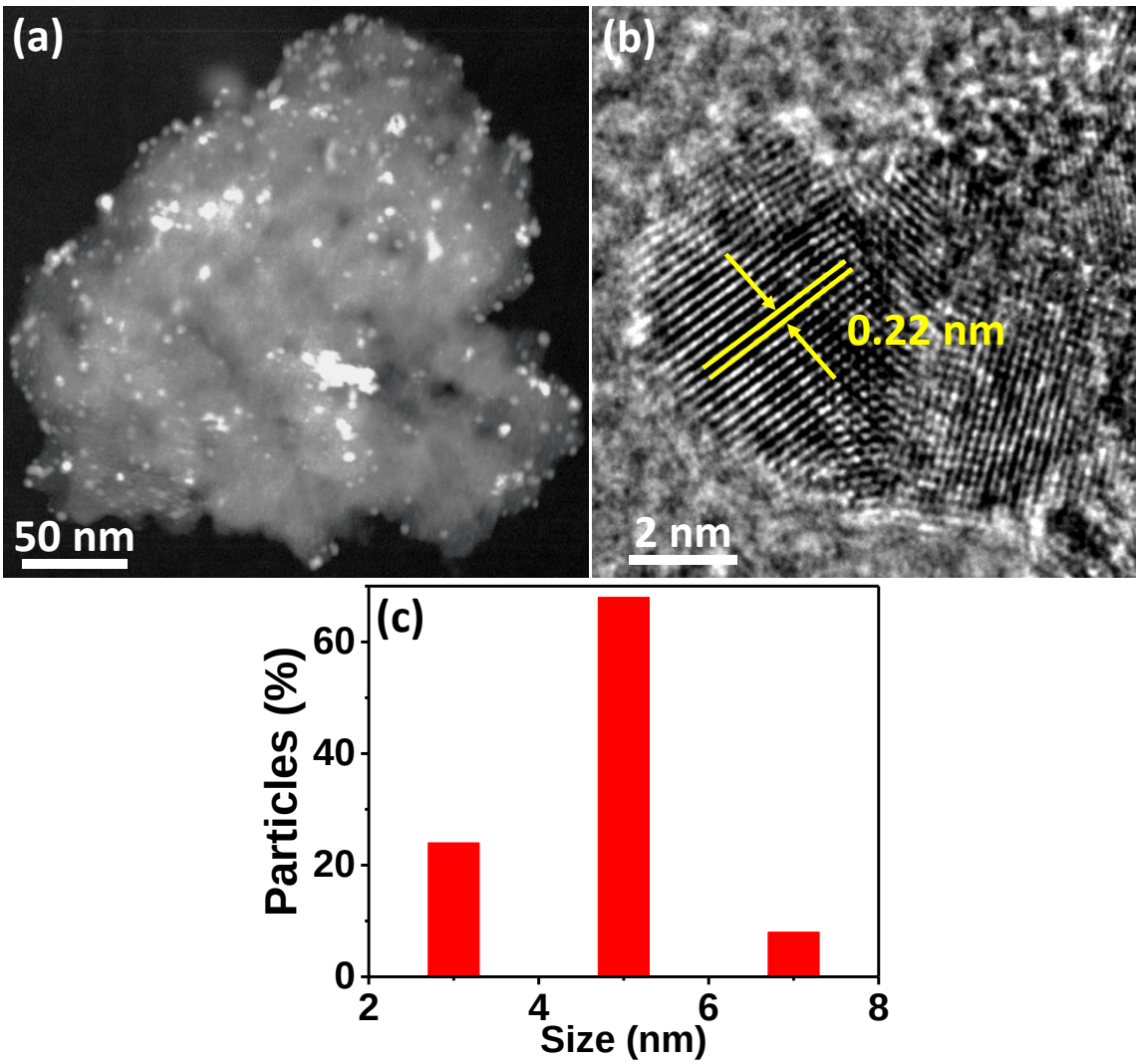

Figure 3.2: *(a)* Dark-field *TEM image of NiPdPt nanoparticles supported on activated carbon (AC/NiPdPt). (b) High resolution TEM (HRTEM) of the same catalyst. (c) Histogram of particle size distribution for NiPdPt nanoparticles (calculated over 200 particles).*

Direct synthesis of H_2O_2 was carried out at atmospheric pressure from molecular H_2 and O_2 in a glass jacket reactor (Scheme 2.1) in presence of Cl^- and Br^- at 10 ^{0}C temperature as described in the experimental section 3.3.3. The H_2O_2 concentration attained for different catalysts after 8h reaction is given in the Figure 3.3a. Bimetallic NiPd on carbon support (AC/NiPd) shows very high activity around 80 % greater than monometallic Pd catalyst (AC/Pd). Moreover, AC/NiPd catalyst shows far better activity than AC/AuPd (Au:Pd ratio is 50:50, prepared by the same procedure) which has been reported earlier in the literature as one of the best catalysts for the direct synthesis of H_2O_2.[8, 27, 28, 30] Incorporation of Pt (about 0.2 wt. %) along with NiPd, shows extraordinary improvement in activity for AC/NiPdPt than AC/NiPd. The final H_2O_2 concentration achieved over AC/NiPdPt after 8h was 590 mM (~2 wt. %) which is about 2.4 times higher (140 % increase) than over AC/Pd and almost 45 % higher over AC/NiPd catalyst (Figure 3.3a). A 95 % selectivity for H_2O_2 was achieved over AC/NiPdPt which is comparatively higher than the selectivity obtained over AC/NiPd (93 %) and AC/Pd (85 %) catalysts (Figure 3.3b). AC/NiPdPt showed conversion of 10.2 % for H_2 which is higher than over AC/NiPd (7.2 %) and AC/Pd (5 %) catalysts (Figure 3.3b).

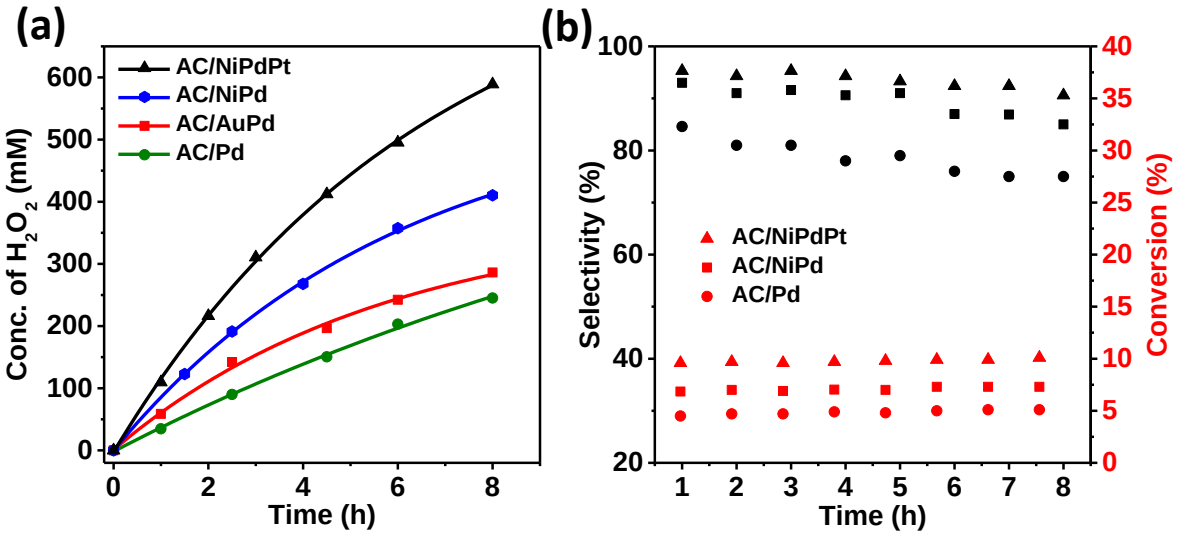

Figure 3.3: *(a) Direct synthesis of H_2O_2 over AC/NiPdPt, AC/NiPd, AC/AuPd and AC/Pd catalysts. Reaction conditions: catalyst - 30 mg, 10 °C, 30 mL water-methanol (1:5) containing 28 mM HCl and 0.01 M Br^-, 1 atm pressure, H_2:O_2 (1:4) gas mixture bubbled with a flow rate, 50 mL min^{-1}. (b) Selectivity of H_2O_2 (with respect to H_2) and conversion of H_2 for AC/NiPdPt, AC/NiPd and AC/Pd catalysts.*

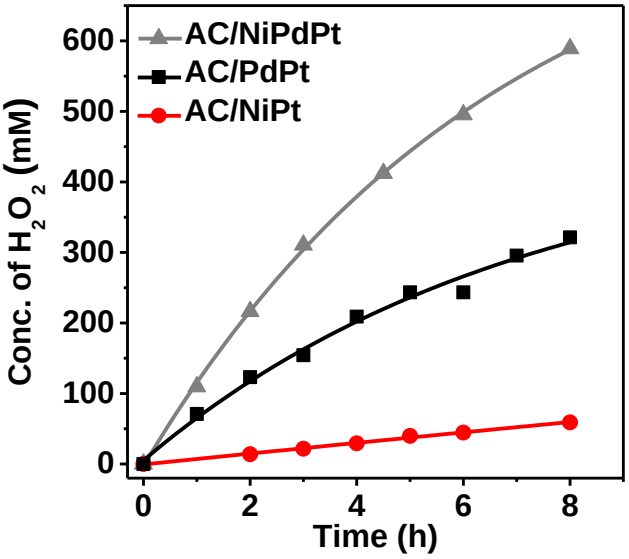

Figure 3.4: *Direct synthesis of H_2O_2 over AC/NiPdPt, AC/PdPt and AC/NiPt catalysts.*

Bimetallic NiPt (3.1 wt. % Ni and 0.2 wt. % Pt with respect to activated carbon) and PdPt (3.1 wt. % Pd and 0.2 wt. % Pt) catalysts were also prepared separately on activated carbon (using same method as described in the experimental section) keeping the Pt loading constant at 0.2 wt. % as in AC/NiPdPt. Both the catalysts AC/NiPt and AC/PdPt showed far lower activity for direct synthesis of H_2O_2 compared to AC/NiPdPt as shown in the Figure 3.4. The above results clearly indicate that the presence of trace amount of Pt acts as a promoter for NiPd catalyst towards direct H_2O_2 synthesis reaction. The H_2O_2 productivity (in mmol g_{Pd}^{-1} min^{-1}) in terms of absolute amount of Pd present in the catalyst is 44, 28 and 17 for AC/NiPdPt, AC/NiPd and AC/Pd respectively (Figure 3.5). NiPd catalyst on activated carbon showed excellent activity towards direct synthesis of H_2O_2, about 33 times (in terms of absolute amount of Pd) higher as compared to self-supported NiPd catalyst[33] (in the previous chapter). The activity has further been enhanced around 51 times (as compared to self-supported NiPd catalyst) by introducing a little amount of Pt on NiPd supported on activated carbon (Figure 3.5).

The catalyst, AC/NiPdPt is very stable in acidic conditions and no catalyst leaching was observed as confirmed by ICP-AES study after 8h reaction. The supernatant after removing the solid catalyst does not show any activity for H_2O_2 production (Figure 3.6a) signifying the absence of colloidal metal nanoparticles leached out in the solution. The catalyst shows

recyclability up to 5 cycle (each cycle carries 8h reaction time) without losing its initial activity (Figure 3.6b).

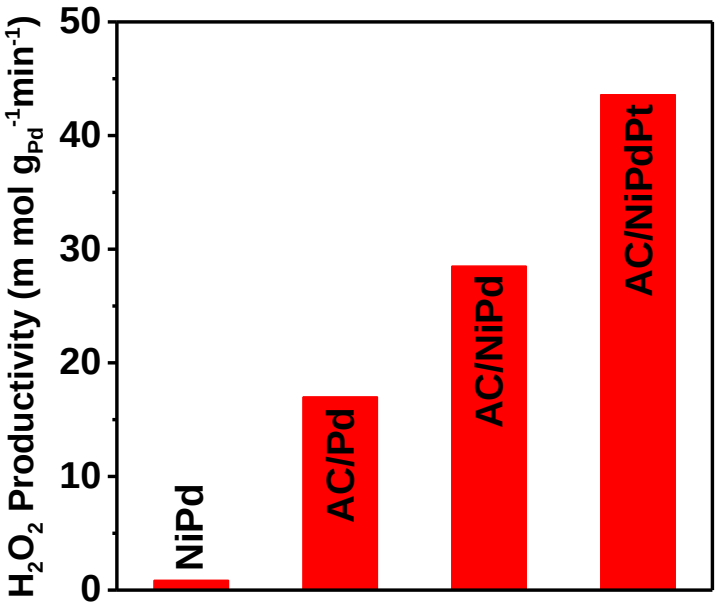

Figure 3.5: *H_2O_2 productivity in terms of* mmol g_{Pd}^{-1} min^{-1}, *for all the catalysts after 8h reaction with respect to absolute amount of Pd present in the catalysts.*

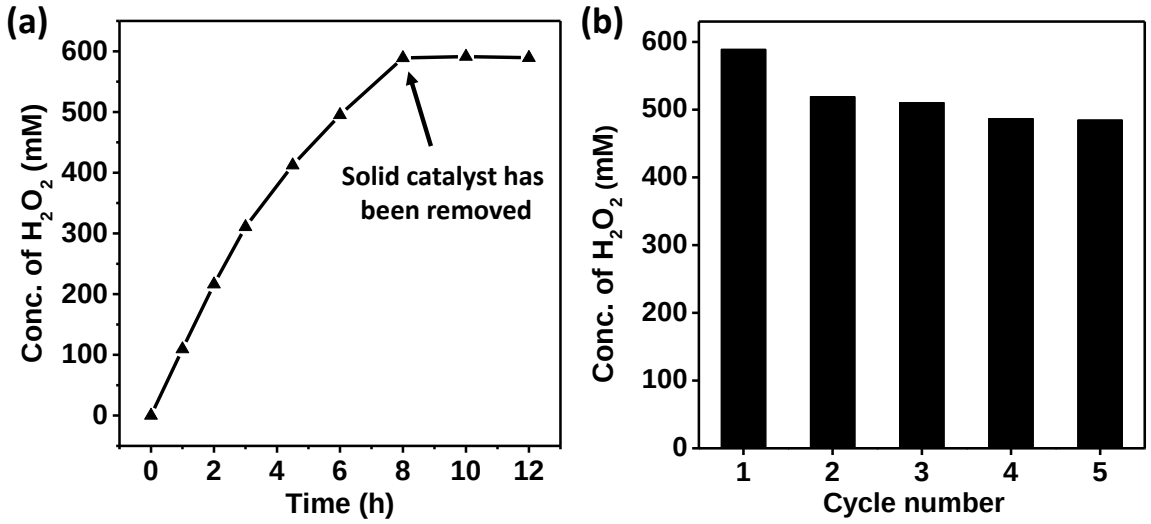

Figure 3.6: *(a) Formation of H_2O_2 after removing the solid catalyst, AC/NiPdPt at 8h. (b) Recyclability of AC/NiPdPt catalyst up to 5^{th} cycle for direct synthesis of H_2O_2.*

The direct synthesis of H_2O_2 was also carried out at high pressure, 37 bar using a high pressure reactor at 10 ^oC temperature. As the reaction was carried out for shorter time scale, 30 min, no additives like halide, acid etc. were required in this conditions unlike the previous one. The results for H_2O_2 synthesis for all the catalysts are given in Table 3.1. AC/NiPdPt shows best activity for H_2O_2 production than AC/NiPd, AC/AuPd and AC/Pd with the trend similar to that observed for flow type reactions at normal pressure. The catalyst also shows one of the best performances for H_2O_2 synthesis at high pressure conditions compared to those reported in the literature (Table 3.2). The promotional effect of Pt has also been prominent for bimetallic NiPd catalyst at high pressure for direct synthesis of H_2O_2. The enhancement in the catalytic activity would be attributed to change in electronic structure of bimetallic NiPd catalyst in presence of the 3rd element like, Pt which has already been observed in the literature for AuPd catalyst.[31]

Table 3.1: *H_2O_2 productivity over different catalysts at high pressure (37 bar) conditions.*

Catalyst	**H_2O_2 Productivity (mol kg_{cat}^{-1} h^{-1})**
AC/NiPdPt	242
AC/NiPd	197
AC/AuPd	134
AC/Pd	46

Table 3.2: *Comparison of H_2O_2 productivity over different catalysts reported in the literature at high pressure (37 bar) conditions.*

Catalyst	**H_2O_2 Productivity (mol kg_{cat}^{-1} h^{-1})**	**References**
AC/0.3% Ni-2.8% Pd-0.2% Pt	**242**	**Present study**
AC/0.3% Ni-3% Pd	**197**	**Present study**
2.5% Au-2.5% Pd/carbon	175	28
1% Pd-4% Sn/SiO_2	76	35

2.5% Au-2.5% Pd/TiO_2	110	27
2.4%Au-2.4%Pd 0.2%Pt/CeO_2	170	31
2.5% Au-2.5% Pd/carbon	110	37
4.2%Au-0.8%Pd/Al_2O_3	21	38
2.5% Au + 1.8% Pd/HZSM-5	138	23

3.5. Conclusion:

Bimetallic NiPd nanoparticles supported on activated carbon showed very high catalytic activity for the direct synthesis of H_2O_2 compared to monometallic Pd in normal pressure as well as under high pressure conditions. Furthermore, the activity of NiPd catalyst was improved by introducing a little amount of Pt (0.2 wt. %) as a promoter. The catalyst is very stable and showed recyclability for 5 cycles (total 40h) retaining its initial activity. Highly active NiPdPt catalyst supported on carbon could be used in near future for on-site production of H_2O_2 for practical applications.

3.6. References:

1. C. Samanta, Direct synthesis of hydrogen peroxide from hydrogen and oxygen: An overview of recent developments in the process, *Appl. Catal. A.: Gen.*, 2008, **350**, 133-149.
2. J. Garcia-Serna, T. Moreno, P. Biasi, M. J. Cocero, J.-P. Mikkola and T. O. Salmi, Engineering in direct synthesis of hydrogen peroxide: targets, reactors and guidelines for operational conditions, *Green Chem.*, 2014, **16**, 2320-2343.
3. Y. Yi, L. Wang, G. Li and H. Guo, A review on research progress in the direct synthesis of hydrogen peroxide from hydrogen and oxygen: noble-metal catalytic method, fuel-cell method and plasma method, *Catal. Sci. Technol.*, 2016, **6**, 1593-1610.
4. J. M. Campos-Martin, G. Blanco-Brieva and J. L. G. Fierro, Hydrogen Peroxide Synthesis: An Outlook beyond the Anthraquinone Process, *Angew. Chem. Int. Ed.*, 2006, **45**, 6962-6984.

5. R. Hage and A. Lienke, Applications of Transition-Metal Catalysts to Textile and Wood-Pulp Bleaching, *Angew. Chem. Int. Ed.*, 2006, **45**, 206-222.
6. E. J. Beckman, Production of H_2O_2 in CO_2 and its use in the direct synthesis of propylene oxide, *Green Chem.*, 2003, **5**, 332-336.
7. H.-J. Reidl and G. Pfleiderer, *I.G. Farbenindustrie AG*, 1939, US Patent 2158525.
8. J. K. Edwards and G. J. Hutchings, Palladium and Gold–Palladium Catalysts for the Direct Synthesis of Hydrogen Peroxide, *Angew. Chem. Int. Ed.*, 2008, **47**, 9192-9198.
9. http://news.bbc.co.uk/1/hi/england/london/4197500.stm.
10. H. C. H. Henkel and W. Weber, *(Henkel & CIE)*, 1914, US Patent 1108752.
11. S. Melada, F. Pinna, G. Strukul, S. Perathoner and G. Centi, Palladium-modified catalytic membranes for the direct synthesis of H_2O_2: preparation and performance in aqueous solution, *J. Catal.*, 2005, **235**, 241-248.
12. Q. Liu, J. C. Bauer, R. E. Schaak and J. H. Lunsford, Supported Palladium Nanoparticles: An Efficient Catalyst for the Direct Formation of H_2O_2 from H_2 and O2, *Angew. Chem. Int. Ed.*, 2008, **47**, 6221-6224.
13. V. R. Choudhary, A. G. Gaikwad and S. D. Sansare, Nonhazardous Direct Oxidation of Hydrogen to Hydrogen Peroxide Using a Novel Membrane Catalyst, *Angew. Chem. Int. Ed.*, 2001, **40**, 1776-1779.
14. C. Samanta and V. R. Choudhary, Direct formation of H_2O_2 from H_2 and O_2 and decomposition/hydrogenation of H_2O_2 in aqueous acidic reaction medium over halide-containing Pd/SiO_2 catalytic system, *Catal. Commun.*, 2007, **8**, 2222-2228.
15. Y.-F. Han and J. H. Lunsford, Direct formation of H_2O_2 from H_2 and O_2 over a Pd/SiO_2 catalyst: the roles of the acid and the liquid phase, *J. Catal.*, 2005, **230**, 313-316.
16. Q. Liu and J. H. Lunsford, Controlling factors in the direct formation of H_2O_2 from H_2 and O_2 over a Pd/SiO_2 catalyst in ethanol, *Appl. Catal. A.: Gen.*, 2006, **314**, 94-100.
17. S. Chinta and J. H. Lunsford, A mechanistic study of H_2O2 and H_2O formation from H_2 and O_2 catalyzed by palladium in an aqueous medium, *J. Catal.*, 2004, **225**, 249-255.
18. E. Ghedini, F. Menegazzo, M. Signoretto, M. Manzoli, F. Pinna and G. Strukul, Mesoporous silica as supports for Pd-catalyzed H_2O_2 direct synthesis: Effect of the

textural properties of the support on the activity and selectivity, *J. Catal.*, 2010, **273**, 266-273.

19. B. Hu, W. Deng, R. Li, Q. Zhang, Y. Wang, F. Delplanque-Janssens, D. Paul, F. Desmedt and P. Miquel, Carbon-supported palladium catalysts for the direct synthesis of hydrogen peroxide from hydrogen and oxygen, *J. Catal.*, 2014, **319**, 15-26.
20. J. Xu, L. Ouyang, G.-J. Da, Q.-Q. Song, X.-J. Yang and Y.-F. Han, Pt promotional effects on Pd–Pt alloy catalysts for hydrogen peroxide synthesis directly from hydrogen and oxygen, *J. Catal.*, 2012, **285**, 74-82.
21. P. Landon, P. J. Collier, A. J. Papworth, C. J. Kiely and G. J. Hutchings, Direct formation of hydrogen peroxide from H_2/O_2 using a gold catalyst, *Chem. Commun.*, 2002, 2058-2059.
22. J. K. Edwards, B. Solsona, P. Landon, A. F. Carley, A. Herzing, M. Watanabe, C. J. Kiely and G. J. Hutchings, Direct synthesis of hydrogen peroxide from H_2 and O_2 using Au-Pd/Fe_2O_3 catalysts, *J. Mater. Chem.*, 2005, **15**, 4595-4600.
23. G. Li, J. Edwards, A. F. Carley and G. J. Hutchings, Direct synthesis of hydrogen peroxide from H_2 and O_2 using zeolite-supported Au-Pd catalysts, *Catal. Today*, 2007, **122**, 361-364.
24. V. Paunovic, V. V. Ordomsky, V. L. Sushkevich, J. C. Schouten and T. A. Nijhuis, Direct Synthesis of Hydrogen Peroxide over Au-Pd Catalyst—The Effect of Co-Solvent Addition, *ChemCatChem*, 2015, **7**, 1161-1176.
25. J. K. Edwards, A. Thomas, B. E. Solsona, P. Landon, A. F. Carley and G. J. Hutchings, Comparison of supports for the direct synthesis of hydrogen peroxide from H_2 and O_2 using Au–Pd catalysts, *Catal. Today*, 2007, **122**, 397-402.
26. F. Menegazzo, P. Burti, M. Signoretto, M. Manzoli, S. Vankova, F. Boccuzzi, F. Pinna and G. Strukul, Effect of the addition of Au in zirconia and ceria supported Pd catalysts for the direct synthesis of hydrogen peroxide, *J. Catal.*, 2008, **257**, 369-381.
27. J. K. Edwards, E. Ntainjua N, A. F. Carley, A. A. Herzing, C. J. Kiely and G. J. Hutchings, Direct Synthesis of H_2O_2 from H_2 and O_2 over Gold, Palladium, and Gold–Palladium Catalysts Supported on Acid-Pretreated TiO_2, *Angew. Chem. Int. Ed.*, 2009, **48**, 8512-8515.

28. J. K. Edwards, B. Solsona, E. N. Ntainjua, A. F. Carley, A. A. Herzing, C. J. Kiely and G. J. Hutchings, Switching Off Hydrogen Peroxide Hydrogenation in the Direct Synthesis Process, *Science*, 2009, **323**, 1037-1041.

29. F. Menegazzo, M. Signoretto, M. Manzoli, F. Boccuzzi, G. Cruciani, F. Pinna and G. Strukul, Influence of the preparation method on the morphological and composition properties of Pd–Au/ZrO_2 catalysts and their effect on the direct synthesis of hydrogen peroxide from hydrogen and oxygen, *J. Catal.*, 2009, **268**, 122-130.

30. J. K. Edwards, S. J. Freakley, A. F. Carley, C. J. Kiely and G. J. Hutchings, Strategies for Designing Supported Gold–Palladium Bimetallic Catalysts for the Direct Synthesis of Hydrogen Peroxide, *Acc. Chem. Res.*, 2014, **47**, 845-854.

31. J. K. Edwards, J. Pritchard, L. Lu, M. Piccinini, G. Shaw, A. F. Carley, D. J. Morgan, C. J. Kiely and G. J. Hutchings, The Direct Synthesis of Hydrogen Peroxide Using Platinum-Promoted Gold–Palladium Catalysts, *Angew. Chem. Int. Ed.*, 2014, **53**, 2381-2384.

32. J. K. Edwards, S. J. Freakley, R. J. Lewis, J. C. Pritchard and G. J. Hutchings, Advances in the direct synthesis of hydrogen peroxide from hydrogen and oxygen, *Catal. Today*, 2015, **248**, 3-9.

33. S. Maity and M. Eswaramoorthy, Ni-Pd bimetallic catalysts for the direct synthesis of H_2O_2 - unusual enhancement of Pd activity in the presence of Ni, *J. Mater. Chem. A*, 2016, **4**, 3233-3237.

34. S. Wang, K. Gao, W. Li and J. Zhang, Effect of Zn addition on the direct synthesis of hydrogen peroxide over supported palladium catalysts, *Appl. Catal. A.: Gen.*, 2017, **531**, 89-95.

35. S. J. Freakley, Q. He, J. H. Harrhy, L. Lu, D. A. Crole, D. J. Morgan, E. N. Ntainjua, J. K. Edwards, A. F. Carley, A. Y. Borisevich, C. J. Kiely and G. J. Hutchings, Palladium-tin catalysts for the direct synthesis of H_2O_2 with high selectivity, *Science*, 2016, **351**, 965-968.

36. I. R. Cohen, T. C. Purcell and A. P. Altshuller, Analysis of the oxidant in photooxidation reactions, *Environ. Sci. Technol.*, 1967, **1**, 247-252.

37. J. K. Edwards, A. Thomas, A. F. Carley, A. A. Herzing, C. J. Kiely and G. J. Hutchings, Au-Pd supported nanocrystals as catalysts for the direct synthesis of hydrogen peroxide from H_2 and O_2, *Green Chem.*, 2008, **10**, 388-394.

38. B. E. Solsona, J. K. Edwards, P. Landon, A. F. Carley, A. Herzing, C. J. Kiely and G. J. Hutchings, Direct Synthesis of Hydrogen Peroxide from H_2 and O_2 Using Al_2O_3 Supported Au−Pd Catalysts, *Chem. Mater.*, 2006, **18**, 2689-2695.

PART-2

Chapter 4: **Introduction to electrochemical water splitting and oxygen reduction reaction**

Chapter 5: **High surface area NiCoP nanostructure as an efficient water splitting electrocatalyst: The oxygen evolution activity**

Chapter 6: **High surface area Ni containing Pd nanostructure: Pt like activity for hydrogen evolution and oxygen reduction reactions**

Chapter 7: **Controlled galvanic replacement of Ni in $Ni(OH)_2$ by Pd: a method to quantify metallic Ni and to synthesize bimetallic catalysts for methanol oxidation**

Chapter - 4

Introduction to electrochemical water splitting and oxygen reduction reaction

Summary:

The global energy consumption is increasing drastically due to rapid growth of world population over the last few decades. However, the depletion of fossil fuels, the fundamental energy source for last two centuries and the environmental concerns associated with their combustion forcing the scientific community to think about alternative green energy sources. Water splitting and fuel cell technologies are going to be next promising energy resources in near future. Costly noble metals are still being used as the best electrocatalysts in hydrogen and oxygen evolution reactions (water splitting) and oxygen reduction reaction (in fuel cell). Many non-noble metals are being explored in this direction and still there is a lot of room to design and synthesize new materials for efficient catalytic activity in this area.

4.1. Introduction:

Rapid growth of world population demands huge global energy consumption. Fossil fuels have been served as crucial energy sources in industrial and technological applications over the last two centuries because of their high energy density. Though, coal and natural gas are still being used to fulfil the global energy demand, there are lot of environmental concerns due to huge carbon emissions associated with their inefficient combustion.[1] Though, renewable energy sources like solar, wave, wind etc. are being used as alternatives, most of them are seasonal and requires batteries or other storage materials for long-term usability.[2]

Molecular hydrogen is one of the most promising renewable chemical fuels due to its zero carbon footprint and can be used as an alternative to fossil fuels because of its very high energy density.[3] H_2 is also a main feedstock in hydrogen based fuel cell technologies for large scale applications as its only byproduct is environment friendly water.[4] Currently, H_2 is produced in huge quantity by industrial steam reforming method which requires very high temperature and in addition, the process produces significant amount of CO_2 in the atmosphere.[5] Moreover, the method often adds sulphur-containing impurities which leads to a lot of environmental problems as well as poisoning of the fuel cell catalysts.[6]

Hydrogen can be largely produced with almost 100% purity through electrochemical water splitting process. The process consists of two half-cell reactions (Scheme 4.1): hydrogen evolution reaction (HER) in cathode ($2H^+ + 2e^- \rightarrow H_2$)[7, 8] and oxygen evolution reaction (OER) in anode ($2H_2O \rightarrow O_2 + 4H^+ + 4e^-$).[9, 10] Though, it seems that water splitting is easier process to generate H_2 but one cannot neglect the counter OER reaction which makes the overall water splitting very sluggish because of its four electron transfer kinetics.[11] Another issue is related to the use of expensive noble metals and their compounds for HER (like Pt)[12, 13] and OER (Ru, Ir catalysts)[11, 14] which need to be replaced by earth-abundant and cost-effective non-noble metals or their compounds. Recently, transition metal (i.e. Mn, Fe, Co, Ni etc.) based phosphides,[15-32] selenides,[33-35] sulphides[36-38] etc. have been developed for OER. Similarly compounds of Mo[39-42] and W[43-45] have been studied for HER.

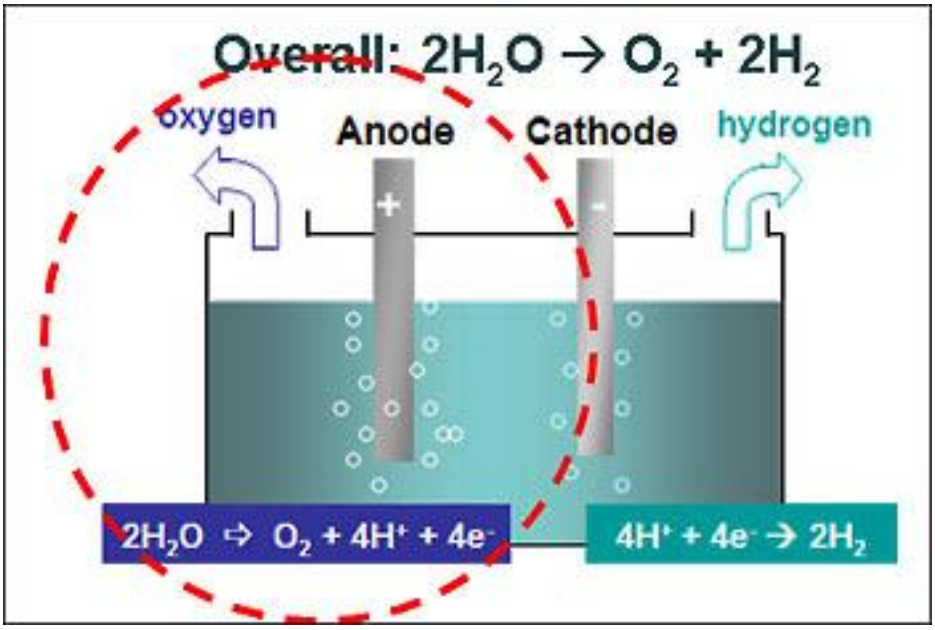

Scheme 4.1: *Electrochemical water splitting reaction.*[†]

Fuel cell technologies and metal-air batteries have also been drawn a lot of attraction as a renewable and green energy resources for global energy demands.[46, 47] Just like, HER is the key step in water splitting reaction to produce H_2, oxygen reduction reaction (ORR) is the major step in hydrogen fuel cell (Scheme 4.2) and metal-air batteries.[48] Again, the best catalyst for ORR is Pt which limits it wide scale application due to high cost and less availability. Attempts are being made to develop non-Pt based materials and transition metal based bimetallic nanostructured catalysts to reduce their overall cost.[47]

[†]*(Image source: http://www.berkeley.edu/news/media/releases/2009/10/08_sustainable_chemistry.shtml).*

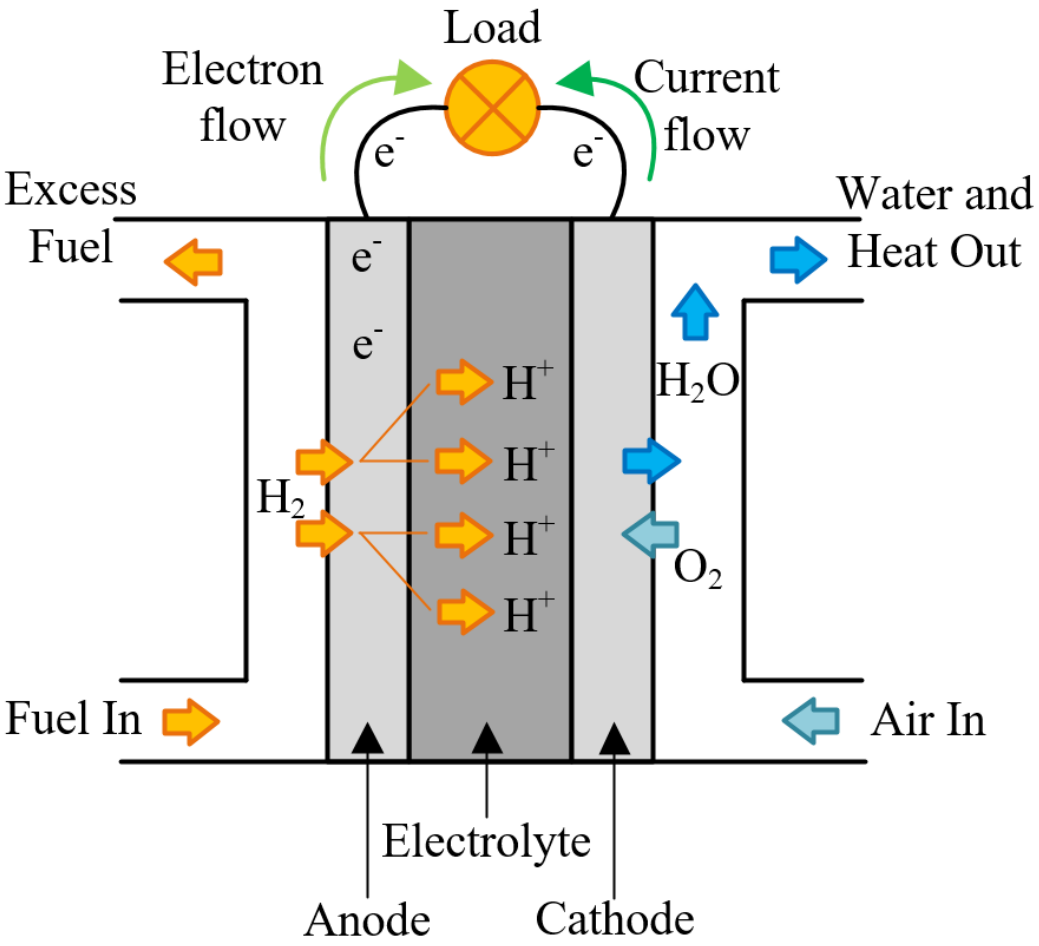

Scheme 4.2: *Scheme of a proton-conducting fuel cell.*[†]

4.2. Hydrogen evolution reaction (HER):

HER proceeds by two, or multi-step reaction pathways irrespective of acidic or basic medium.[49, 50] HER is facile in acidic pH as large number of protons available in the reaction medium. The first step in HER mechanism involves adsorption of hydrogen (H_{ads}) on the electrode surface by the reduction of proton from the solution which is known as Volmer step. The second step is the desorption of hydrogen molecule from the electrode surface. This could proceed in two ways: (i) electrochemical desorption, or (ii) chemical desorption depending on the coverage of H_{ads}. If the coverage of H_{ads} is low, electrochemical desorption of H_2 molecule is favored in which the adsorbed H on the active site of the

[†]*(Image source: https://www.rtds.com/wp-content/uploads/2015/12/Figure-1-Functional-diagram-of-fuel-cell.png).*

electrode preferably takes one proton from the solution to form H_2 molecule. This step is known as Heyrovsky step. On the other hand, if the coverage of H_{ads} is more, chemical desorption is favored in which two surroundings adsorbed hydrogen atom joins together chemically to form H_2 molecule. This is known as Tafel step. The first one, Volmer step is common for all the HER mechanisms. The value of Tafel slope is used to ascertain the steps involved in HER mechanism. The calculated Tafel slopes, 118 mV dec^{-1}, 39 mV dec^{-1} and 29 mV dec^{-1} are assigned for Volmer, Heyrovsky and Tafel step respectively. Depending upon the coverage of H_{ads}, HER mechanisms undergo either Volmer-Heyrovsky or Volmer-Tafel pathways. That means, lower the H_{ads} coverage Volmer-Heyrovsky steps predominates and higher the H_{ads} coverage Volmer-Tafel steps dominates. In general Pt-based catalysts (show strong hydrogen binding affinity) exhibit Volmer-Tafel pathway and carbon-based materials (weak hydrogen binding affinity) show Volmer-Heyrovsky mechanism. Certain materials falls in between and undergo both the pathways during HER. Thus the mechanism of HER can be evaluated by experimentally obtained Tafel slope value.[7]

On the other hand, HER under alkaline conditions is comparatively sluggish as it directly depends upon the opposite electrode (anode) where OER occurs which supplies the proton to cathode after deprotonation from hydroxyl anions and thereby, affects the HER kinetics. Also, the protons further combine with the hydroxyl anions available plenty in the alkaline medium to form water and makes HER struggling to move forward.

HER mechanism in acidic condition[51]:

1. Volmer step: $* + H_3O^+ + e^- \rightarrow *H_{ads} + H_2O$
2. Heyrovsky step: $*H_{ads} + H_3O^+ + e^- \rightarrow * + H_2 + H_2O$
3. Tafel step: $*H_{ads} + *H_{ads} \rightarrow 2* + H_2$

HER mechanism in alkaline condition[52]:

1. Volmer step: $* + H_2O + e^- \rightarrow *H_{ads} + OH^-$
2. Heyrovsky step: $*H_{ads} + H_2O + e^- \rightarrow * + H_2 + OH^-$
3. Tafel step: $*H_{ads} + *H_{ads} \rightarrow 2* + H_2$

Where, '*' is the representation of active catalytic site.

4.3. Oxygen evolution reaction (OER):

The OER is totally different from HER. The kinetics of the OER in acidic or alkaline medium depends upon the characteristics of the material used as electrocatalyst. For example, noble metal Ru, Ir and their compounds show better OER activity in acidic medium than under alkaline medium.[11] On the other hand, 3d transition metals like Fe, Co, Ni etc. catalyzes the OER better in alkaline medium than under acidic medium. One reason behind this is the poor stability of the transition metal based systems under acidic conditions as it is known to leach out in the acidic electrolyte solution.

Unlike HER, OER mechanism is more complicated and involved more number of reaction pathways in both acidic as well as alkaline medium. In alkaline condition, all the proposed mechanism begin with the elementary step of hydroxide co-ordination on the active catalytic site followed by other elementary reaction pathways.[53-55] The energy barrier associated with each and every elementary step leads to increase in over potential of the catalysts and makes OER more kinetically sluggish. The peroxide intermediate formed on the catalytic interface plays an important role in delivering the dioxygen molecules during the reaction.[56] The most accepted OER mechanism[48] in alkaline condition is given below.

(i) $* + OH^- \rightarrow OH^* + e^-$

(ii) $OH^* + OH^- \rightarrow O^* + H_2O\,(l) + e^-$

(iii) $O^* + OH^- \rightarrow OOH^* + e^-$

(iv) $OOH^* + OH^- \rightarrow * + O_2\,(g) + H_2O + e^-$

Where, '*' represents the active catalytic site.

4.4. Oxygen reduction reaction (ORR):

ORR is the most important reaction in proton exchange membrane fuel cells (PEMFCs).[48] ORR catalyst in cathode is used to reduce O_2 to water with the production of electricity and heat when H_2 is used as a fuel, (as shown in Fig. 4.2). ORR in the aqueous medium undergoes two reaction pathways– (i) two electron reduction pathway to form H_2O_2 and (ii) direct four electron reduction pathway to form H_2O from O_2.[57] Sometimes, it can also undergo one electron pathway to form superoxide species (O_2^-) in non-aqueous aprotic solvents or in alkaline medium. Normally the electrochemical ORR is kinetically very sluggish and needs efficient cathode catalyst to make it faster. The mechanism of ORR is quite complicated and involve many intermediates depending upon the electrocatalyst and

the electrolyte solution which are not well understood still now. In aqueous alkaline medium, the ORR mechanism[57] (Eley-Rideal mechanism, given below) is just inverse of the OER mechanism in the same medium.

(i) $* + O_2 \rightarrow O_2*$

(ii) $O_2* + H_2O\ (l) + e^- \rightarrow OOH* + OH^-$

(iii) $OOH* + e^- \rightarrow O* + OH^-$

(iv) $O* + H_2O\ (l) + e^- \rightarrow OH* + OH^-$

(v) $OH* + e^- \rightarrow * + OH^-$

Where, '*' represents the active catalytic site.

4.5. Phosphide based materials as water splitting catalysts:

The transition metal based phosphides have been recently studied for electrochemical water splitting due to their high conducting nature, stability and better electrocatalytic activity for both HER and OER.[58] The presence of heteroatom, P in metal lattices improves the overall activity for transition metal phosphide systems not only for HER but also for OER.[7]

In a metal phosphide system, the P-terminated surface contains polarization-induced partial negative charge which acts as a proton adsorption centre (as a base)[11] and also weakens hydrogen binding energy for easy desorption of H_2 molecule and thereby, increases the overall HER activity.[7, 11] As a result, it is expected that the phosphide materials having higher P content, show better HER performance. It is reported that the transition metal (mainly Co, Ni and Fe) based phosphide materials and their polymorphs with higher percentage of P showed better HER activity.[11] For example, among CoP and Co_2P, CoP was found to be more active for HER as it contains more phosphorous.[59] Similarly, among all the polymorphs of nickel phosphides (Ni_2P, Ni_5P_4, $Ni_{12}P_5$), Ni_5P_4 with higher P content shows very good activity as compared to other polymorphs.[60] Recently, density function theory (DFT) study shows that the P centres acting as a base which traps the proton, also facilitates the H_2 desorption at higher H_{ads} coverage.[61]

In case of OER, the presence of P centres in metal phosphides do not have any direct impact like HER.[11] The 3d metal ions in transition metal phosphides show better OER activity due to the increased 3d-2p repulsion between metal d-band centre and p-band centre of co-ordinated oxygen in the peroxide intermediate species.[56] In presence of heteroatom, P, the

release of oxygen molecule is enhanced by 3p-2p repulsion between P and the peroxide species after formation of the peroxide intermediate and hence increases the OER activity.

4.6. Bimetallic catalysts for ORR:

Noble metal Pt, the state-of-the-art catalyst for ORR is prohibitively expensive and needs to be replaced by cost-effective materials.[46, 48] Another noble metal Pd from Pt-group which is comparatively cheaper than Pt, has been studied as potential catalyst for ORR as an alternative to Pt, but its ORR activity is far lower than expected to replace Pt.[62-65] Recently, bimetallic nanostructured materials (mainly Pd or Pt with low cost transition metals) are drawing attention to be explored for ORR in order to reduce the overall cost of the catalyst.[66-69] Efforts are being made in this direction to improve their catalytic activity by controlling their composition, particle size and morphology.[70-72]

Among all, transition metal based bimetallic catalysts, M-Pd and M-Pt (M- Fe, Co, Ni, Mn, Mo, Ti etc.) not only improve the ORR activity, but also make it relatively cheaper for their widespread use.[3, 47, 62, 63] The bimetallic nanostructures can be prepared in the form of homogeneous alloys, heterogeneous core-shell nanoparticles or, ordered intermetallic phases. From theoretical calculations, it has been reported that the surface electronic properties of the noble metals (Pd or Pt) in presence of secondary metal in bimetallic nanostructured catalysts changes a lot compared to their pure state and leads to overall increase in the ORR activity.[73-75] In presence of second element, d-orbital of Pd or Pt is electronically modified and leads towards lower energy of d-band centre in the bimetallic nanostructure.[76, 77] For example, in pure Pt nanostructure oxygen binds too strongly which suggests that its d-band centre is too high. Alloying Pt with transition metal, nickel, lowers the d-band centre and hence the oxygen binds more weakly in Pt_3Ni system than pure Pt.[67-69]

4.7. Conclusion:

The rapid depletion of conventional fossil fuels and their negative impacts on environment have forced the government and researchers to think alternative green energy resources. The most promising energy source hydrogen and its natural abundance in water makes the electrochemical water splitting as a more attractive technology to produce hydrogen in which two electrochemical reactions, HER and OER, operate in tandem. Still now, Pt has been used as state-of-the-art electrocatalyst for HER and ORR; Ir and Ru are the best catalysts for OER, but the high cost of those noble metals limits their large scale

applications. Though, several approaches have been explored to design a new set of electrocatalyst for future energy applications as their performances are far lower than expected and need to be improved in order to use them at large scale as low cost and stable electrocatalysts.

4.8. References:

1. N. S. Lewis and D. G. Nocera, Powering the planet: Chemical challenges in solar energy utilization, *Proc. Natl. Acad. Sci.*, 2006, **103**, 15729-15735.
2. B. M. Hunter, J. D. Blakemore, M. Deimund, H. B. Gray, J. R. Winkler and A. M. Müller, Highly Active Mixed-Metal Nanosheet Water Oxidation Catalysts Made by Pulsed-Laser Ablation in Liquids, *J. Am. Chem. Soc.*, 2014, **136**, 13118-13121.
3. S. E. Habas, H. A. S. Platt, M. F. A. M. van Hest and D. S. Ginley, Low-Cost Inorganic Solar Cells: From Ink To Printed Device, *Chem. Rev.*, 2010, **110**, 6571-6594.
4. J. F. Callejas, C. G. Read, C. W. Roske, N. S. Lewis and R. E. Schaak, Synthesis, Characterization, and Properties of Metal Phosphide Catalysts for the Hydrogen-Evolution Reaction, *Chem. Mater.*, 2016, **28**, 6017-6044.
5. A. Haryanto, S. Fernando, N. Murali and S. Adhikari, Current Status of Hydrogen Production Techniques by Steam Reforming of Ethanol: A Review, *Energy Fuels*, 2005, **19**, 2098-2106.
6. X. Cheng, Z. Shi, N. Glass, L. Zhang, J. Zhang, D. Song, Z.-S. Liu, H. Wang and J. Shen, A review of PEM hydrogen fuel cell contamination: Impacts, mechanisms, and mitigation, *J. Power Sources*, 2007, **165**, 739-756.
7. Y. Shi and B. Zhang, Recent advances in transition metal phosphide nanomaterials: synthesis and applications in hydrogen evolution reaction, *Chem. Soc. Rev.*, 2016, **45**, 1529-1541.
8. P. C. K. Vesborg, B. Seger and I. Chorkendorff, Recent Development in Hydrogen Evolution Reaction Catalysts and Their Practical Implementation, *J. Phys. Chem. Lett.*, 2015, **6**, 951-957.
9. E. Fabbri, A. Habereder, K. Waltar, R. Kotz and T. J. Schmidt, Developments and perspectives of oxide-based catalysts for the oxygen evolution reaction, *Catal. Sci. Technol.*, 2014, **4**, 3800-3821.

10. M.-R. Gao, Y.-F. Xu, J. Jiang and S.-H. Yu, Nanostructured metal chalcogenides: synthesis, modification, and applications in energy conversion and storage devices, *Chem. Soc. Rev.*, 2013, **42**, 2986-3017.
11. S. Anantharaj, S. R. Ede, K. Sakthikumar, K. Karthick, S. Mishra and S. Kundu, Recent Trends and Perspectives in Electrochemical Water Splitting with an Emphasis on Sulfide, Selenide, and Phosphide Catalysts of Fe, Co, and Ni: A Review, *ACS Catal.*, 2016, **6**, 8069-8097.
12. Z. Zeng, C. Tan, X. Huang, S. Bao and H. Zhang, Growth of noble metal nanoparticles on single-layer TiS_2 and TaS_2 nanosheets for hydrogen evolution reaction, *Energy Environ. Sci.*, 2014, **7**, 797-803.
13. C. Wang, K. E. deKrafft and W. Lin, Pt Nanoparticles@Photoactive Metal–Organic Frameworks: Efficient Hydrogen Evolution via Synergistic Photoexcitation and Electron Injection, *J. Am. Chem. Soc.*, 2012, **134**, 7211-7214.
14. L. Y. Chen, Y. Hou, J. L. Kang, A. Hirata, T. Fujita and M. W. Chen, Toward the Theoretical Capacitance of RuO_2 Reinforced by Highly Conductive Nanoporous Gold, *Adv. Energy Mater.*, 2013, **3**, 851-856.
15. A. Han, H. Zhang, R. Yuan, H. Ji and P. Du, Crystalline Copper Phosphide Nanosheets as an Efficient Janus Catalyst for Overall Water Splitting, *ACS Appl. Mater. Interfaces*, 2017, **9**, 2240-2248.
16. C.-C. Hou, S. Cao, W.-F. Fu and Y. Chen, Ultrafine CoP Nanoparticles Supported on Carbon Nanotubes as Highly Active Electrocatalyst for Both Oxygen and Hydrogen Evolution in Basic Media, *ACS Appl. Mater. Interfaces*, 2015, **7**, 28412-28419.
17. Y. Li, J. Liu, C. Chen, X. Zhang and J. Chen, Preparation of NiCoP Hollow Quasi-Polyhedra and Their Electrocatalytic Properties for Hydrogen Evolution in Alkaline Solution, *ACS Appl. Mater. Interfaces*, 2017, **9**, 5982-5991.
18. M. Liu and J. Li, Cobalt Phosphide Hollow Polyhedron as Efficient Bifunctional Electrocatalysts for the Evolution Reaction of Hydrogen and Oxygen, *ACS Appl. Mater. Interfaces*, 2016, **8**, 2158-2165.
19. C. Xuan, J. Wang, W. Xia, Z. Peng, Z. Wu, W. Lei, K. Xia, H. L. Xin and D. Wang, Porous Structured Ni–Fe–P Nanocubes Derived from a Prussian Blue Analogue as an Electrocatalyst for Efficient Overall Water Splitting, *ACS Appl. Mater. Interfaces*, 2017, **9**, 26134-26142.

20. J. Yu, Q. Li, N. Chen, C.-Y. Xu, L. Zhen, J. Wu and V. P. Dravid, Carbon-Coated Nickel Phosphide Nanosheets as Efficient Dual-Electrocatalyst for Overall Water Splitting, *ACS Appl. Mater. Interfaces*, 2016, **8**, 27850-27858.
21. T. Zhang, J. Du, P. Xi and C. Xu, Hybrids of Cobalt/Iron Phosphides Derived from Bimetal–Organic Frameworks as Highly Efficient Electrocatalysts for Oxygen Evolution Reaction, *ACS Appl. Mater. Interfaces*, 2017, **9**, 362-370.
22. J. Chang, Y. Xiao, M. Xiao, J. Ge, C. Liu and W. Xing, Surface Oxidized Cobalt-Phosphide Nanorods As an Advanced Oxygen Evolution Catalyst in Alkaline Solution, *ACS Catal.*, 2015, **5**, 6874-6878.
23. J. Ryu, N. Jung, J. H. Jang, H.-J. Kim and S. J. Yoo, In Situ Transformation of Hydrogen-Evolving CoP Nanoparticles: Toward Efficient Oxygen Evolution Catalysts Bearing Dispersed Morphologies with Co-oxo/hydroxo Molecular Units, *ACS Catal.*, 2015, **5**, 4066-4074.
24. A. Dutta, A. K. Samantara, S. K. Dutta, B. K. Jena and N. Pradhan, Surface-Oxidized Dicobalt Phosphide Nanoneedles as a Nonprecious, Durable, and Efficient OER Catalyst, *ACS Energy Lett.*, 2016, **1**, 169-174.
25. S. Fu, C. Zhu, J. Song, M. H. Engelhard, X. Li, D. Du and Y. Lin, Highly Ordered Mesoporous Bimetallic Phosphides as Efficient Oxygen Evolution Electrocatalysts, *ACS Energy Lett.*, 2016, **1**, 792-796.
26. P. Xiao, W. Chen and X. Wang, A Review of Phosphide-Based Materials for Electrocatalytic Hydrogen Evolution, *Adv. Energy Mater.*, 2015, **5**, 1500985-1500997.
27. C. Wang, J. Jiang, T. Ding, G. Chen, W. Xu and Q. Yang, Monodisperse Ternary NiCoP Nanostructures as a Bifunctional Electrocatalyst for Both Hydrogen and Oxygen Evolution Reactions with Excellent Performance, *Adv. Mater. Int.*, 2016, **3**, 1500454-1500458.
28. W. Cui, Q. Liu, Z. Xing, A. M. Asiri, K. A. Alamry and X. Sun, MoP nanosheets supported on biomass-derived carbon flake: One-step facile preparation and application as a novel high-active electrocatalyst toward hydrogen evolution reaction, *Appl. Catal., B*, 2015, **164**, 144-150.
29. Y. Feng, X.-Y. Yu and U. Paik, Nickel cobalt phosphides quasi-hollow nanocubes as an efficient electrocatalyst for hydrogen evolution in alkaline solution, *Chem. Commun.*, 2016, **52**, 1633-1636.

30. D. Xiong, X. Wang, W. Li and L. Liu, Facile synthesis of iron phosphide nanorods for efficient and durable electrochemical oxygen evolution, *Chem. Commun.*, 2016, **52**, 8711-8714.
31. E. J. Popczun, J. R. McKone, C. G. Read, A. J. Biacchi, A. M. Wiltrout, N. S. Lewis and R. E. Schaak, Nanostructured Nickel Phosphide as an Electrocatalyst for the Hydrogen Evolution Reaction, *J. Am. Chem. Soc.*, 2013, **135**, 9267-9270.
32. D. Li, H. Baydoun, C. N. Verani and S. L. Brock, Efficient Water Oxidation Using CoMnP Nanoparticles, *J. Am. Chem. Soc.*, 2016, **138**, 4006-4009.
33. J. Masud, A. T. Swesi, W. P. R. Liyanage and M. Nath, Cobalt Selenide Nanostructures: An Efficient Bifunctional Catalyst with High Current Density at Low Coverage, *ACS Appl. Mater. Interfaces*, 2016, **8**, 17292-17302.
34. T. Liu, Q. Liu, A. M. Asiri, Y. Luo and X. Sun, An amorphous CoSe film behaves as an active and stable full water-splitting electrocatalyst under strongly alkaline conditions, *Chem. Commun.*, 2015, **51**, 16683-16686.
35. Z. Wang, J. Li, X. Tian, X. Wang, Y. Yu, K. A. Owusu, L. He and L. Mai, Porous Nickel–Iron Selenide Nanosheets as Highly Efficient Electrocatalysts for Oxygen Evolution Reaction, *ACS Appl. Mater. Interfaces*, 2016, **8**, 19386-19392.
36. C. Di Giovanni, W.-A. Wang, S. Nowak, J.-M. Grenèche, H. Lecoq, L. Mouton, M. Giraud and C. Tard, Bioinspired Iron Sulfide Nanoparticles for Cheap and Long-Lived Electrocatalytic Molecular Hydrogen Evolution in Neutral Water, *ACS Catal.*, 2014, **4**, 681-687.
37. M. Chauhan, K. P. Reddy, C. S. Gopinath and S. Deka, Copper Cobalt Sulfide Nanosheets Realizing a Promising Electrocatalytic Oxygen Evolution Reaction, *ACS Catal.*, 2017, **7**, 5871-5879.
38. H. Qian, J. Tang, Z. Wang, J. Kim, J. H. Kim, S. M. Alshehri, E. Yanmaz, X. Wang and Y. Yamauchi, Synthesis of Cobalt Sulfide/Sulfur Doped Carbon Nanocomposites with Efficient Catalytic Activity in the Oxygen Evolution Reaction, *Chem. Eur. J.*, 2016, **22**, 18259-18264.
39. V. Kiran, D. Mukherjee, R. N. Jenjeti and S. Sampath, Active guests in the MoS2/MoSe2 host lattice: efficient hydrogen evolution using few-layer alloys of MoS2(1-x)Se2x, *Nanoscale*, 2014, **6**, 12856-12863.
40. Y. Li, H. Wang, L. Xie, Y. Liang, G. Hong and H. Dai, MoS2 Nanoparticles Grown on Graphene: An Advanced Catalyst for the Hydrogen Evolution Reaction, *J. Am. Chem. Soc.*, 2011, **133**, 7296-7299.

41. J. M. McEnaney, T. L. Soucy, J. M. Hodges, J. F. Callejas, J. S. Mondschein and R. E. Schaak, Colloidally-synthesized cobalt molybdenum nanoparticles as active and stable electrocatalysts for the hydrogen evolution reaction under alkaline conditions, *J. Mater. Chem. A*, 2016, **4**, 3077-3081.

42. W.-F. Chen, K. Sasaki, C. Ma, A. I. Frenkel, N. Marinkovic, J. T. Muckerman, Y. Zhu and R. R. Adzic, Hydrogen-Evolution Catalysts Based on Non-Noble Metal Nickel–Molybdenum Nitride Nanosheets, *Angew. Chem. Int. Ed.*, 2012, **51**, 6131-6135.

43. D. Voiry, H. Yamaguchi, J. Li, R. Silva, D. C. B. Alves, T. Fujita, M. Chen, T. Asefa, V. B. Shenoy, G. Eda and M. Chhowalla, Enhanced catalytic activity in strained chemically exfoliated WS2 nanosheets for hydrogen evolution, *Nat. Mater.*, 2013, **12**, 850-855.

44. Z. Jin, P. Li, X. Huang, G. Zeng, Y. Jin, B. Zheng and D. Xiao, Three-dimensional amorphous tungsten-doped nickel phosphide microsphere as an efficient electrocatalyst for hydrogen evolution, *J. Mater. Chem. A*, 2014, **2**, 18593-18599.

45. G. Huang, H. Liu, S. Wang, X. Yang, B. Liu, H. Chen and M. Xu, Hierarchical architecture of WS2 nanosheets on graphene frameworks with enhanced electrochemical properties for lithium storage and hydrogen evolution, *J. Mater. Chem. A*, 2015, **3**, 24128-24138.

46. J. Zhang, L. Qu, G. Shi, J. Liu, J. Chen and L. Dai, N,P-Codoped Carbon Networks as Efficient Metal-free Bifunctional Catalysts for Oxygen Reduction and Hydrogen Evolution Reactions, *Angew. Chem. Int. Ed.*, 2016, **55**, 2230-2234.

47. M. Shao, Q. Chang, J.-P. Dodelet and R. Chenitz, Recent Advances in Electrocatalysts for Oxygen Reduction Reaction, *Chem. Rev.*, 2015, **116**, 3594-3657.

48. J. Zhang, Z. Zhao, Z. Xia and L. Dai, A metal-free bifunctional electrocatalyst for oxygen reduction and oxygen evolution reactions, *Nat. Nanotechnol.*, 2015, **10**, 444-452.

49. A. J. Bard and L. R. Faulkner, *Electrochemical Methods: Fundamentals and Applications, Wiley: New York*, 2001.

50. J. O. Bockris, A. K. N. Reddy and M. E. Gamboa-Aldeco, *Modern Electrochemistry; Plenum Press: New York*, 1998.

51. A. B. Laursen, A. S. Varela, F. Dionigi, H. Fanchiu, C. Miller, O. L. Trinhammer, J. Rossmeisl and S. Dahl, Electrochemical Hydrogen Evolution: Sabatier's Principle and the Volcano Plot, *J. Chem. Educ.*, 2012, **89**, 1595-1599.
52. W. Sheng, M. Myint, J. G. Chen and Y. Yan, Correlating the hydrogen evolution reaction activity in alkaline electrolytes with the hydrogen binding energy on monometallic surfaces, *Energy Environ. Sci.*, 2013, **6**, 1509-1512.
53. Y. Matsumoto and E. Sato, Electrocatalytic properties of transition metal oxides for oxygen evolution reaction, *Mater. Chem. Phys.*, 1986, **14**, 397-426.
54. J. O. Bockris and T. Otagawa, Mechanism of oxygen evolution on perovskites, *J. Phys. Chem.*, 1983, **87**, 2960-2971.
55. W. H. Wade and N. Hackerman, Anodic phenomena at an iron electrode, *Trans. Faraday Soc.*, 1957, **53**, 1636-1647.
56. R. Subbaraman, D. Tripkovic, K.-C. Chang, D. Strmcnik, A. P. Paulikas, P. Hirunsit, M. Chan, J. Greeley, V. Stamenkovic and N. M. Markovic, Trends in activity for the water electrolyser reactions on 3d M(Ni,Co,Fe,Mn) hydr(oxy)oxide catalysts, *Nat. Mater.*, 2012, **11**, 550-557.
57. J. Hafner, Ab-initio simulations of materials using VASP: Density-functional theory and beyond, *J. Comput. Chem.*, 2008, **29**, 2044-2078.
58. T. Wu, M. Pi, D. Zhang and S. Chen, 3D structured porous CoP3 nanoneedle arrays as an efficient bifunctional electrocatalyst for the evolution reaction of hydrogen and oxygen, *J. Mater. Chem. A*, 2016, **4**, 14539-14544.
59. J. F. Callejas, C. G. Read, E. J. Popczun, J. M. McEnaney and R. E. Schaak, Nanostructured Co2P Electrocatalyst for the Hydrogen Evolution Reaction and Direct Comparison with Morphologically Equivalent CoP, *Chem. Mater.*, 2015, **27**, 3769-3774.
60. Y. Pan, Y. Liu, J. Zhao, K. Yang, J. Liang, D. Liu, W. Hu, D. Liu, Y. Liu and C. Liu, Monodispersed nickel phosphide nanocrystals with different phases: synthesis, characterization and electrocatalytic properties for hydrogen evolution, *J. Mater. Chem. A*, 2015, **3**, 1656-1665.
61. P. Xiao, M. A. Sk, L. Thia, X. Ge, R. J. Lim, J.-Y. Wang, K. H. Lim and X. Wang, Molybdenum phosphide as an efficient electrocatalyst for the hydrogen evolution reaction, *Energy Environ. Sci.*, 2014, **7**, 2624-2629.
62. A. Chen and C. Ostrom, Palladium-Based Nanomaterials: Synthesis and Electrochemical Applications, *Chem. Rev.*, 2015, **115**, 11999-12044.

63. L. Zhang, Q. Chang, H. Chen and M. Shao, Recent advances in palladium-based electrocatalysts for fuel cell reactions and hydrogen evolution reaction, *Nano Energy*, 2016, **29**, 198-219.

64. Y. Nie, L. Li and Z. Wei, Recent advancements in Pt and Pt-free catalysts for oxygen reduction reaction, *Chem. Soc. Rev.*, 2015, **44**, 2168-2201.

65. M. Shao, Palladium-based electrocatalysts for hydrogen oxidation and oxygen reduction reactions, *J. Power Sources*, 2011, **196**, 2433-2444.

66. J. Jiang, H. Gao, S. Lu, X. Zhang, C.-Y. Wang, W.-K. Wang and H.-Q. Yu, Ni-Pd core-shell nanoparticles with Pt-like oxygen reduction electrocatalytic performance in both acidic and alkaline electrolytes, *J. Mater. Chem. A*, 2017, **5**, 9233-9240.

67. J. Zhang, H. Yang, J. Fang and S. Zou, Synthesis and Oxygen Reduction Activity of Shape-Controlled Pt3Ni Nanopolyhedra, *Nano Lett.*, 2010, **10**, 638-644.

68. J. Wu and H. Yang, Study of the Durability of Faceted Pt3Ni Oxygen–Reduction Electrocatalysts, *ChemCatChem*, 2012, **4**, 1572-1577.

69. J. Wu, J. Zhang, Z. Peng, S. Yang, F. T. Wagner and H. Yang, Truncated Octahedral Pt3Ni Oxygen Reduction Reaction Electrocatalysts, *J. Am. Chem. Soc.*, 2010, **132**, 4984-4985.

70. S. Cao, F. Tao, Y. Tang, Y. Li and J. Yu, Size- and shape-dependent catalytic performances of oxidation and reduction reactions on nanocatalysts, *Chem. Soc. Rev.*, 2016, **45**, 4747-4765.

71. M. Shao, T. Yu, J. H. Odell, M. Jin and Y. Xia, Structural dependence of oxygen reduction reaction on palladium nanocrystals, *Chem. Commun.*, 2011, **47**, 6566-6568.

72. Y. Xia, Y. Xiong, B. Lim and S. E. Skrabalak, Shape-Controlled Synthesis of Metal Nanocrystals: Simple Chemistry Meets Complex Physics?, *Angew. Chem. Int. Ed.*, 2009, **48**, 60-103.

73. V. Stamenkovic, B. S. Mun, K. J. J. Mayrhofer, P. N. Ross, N. M. Markovic, J. Rossmeisl, J. Greeley and J. K. Nørskov, Changing the Activity of Electrocatalysts for Oxygen Reduction by Tuning the Surface Electronic Structure, *Angew. Chem. Int. Ed.*, 2006, **45**, 2897-2901.

74. A. Ruban, B. Hammer, P. Stoltze, H. L. Skriver and J. K. Nørskov, Surface electronic structure and reactivity of transition and noble metals, *J. Mol. Catal. A: Chem.*, 1997, **115**, 421-429.

75. A. U. Nilekar, Y. Xu, J. Zhang, M. B. Vukmirovic, K. Sasaki, R. R. Adzic and M. Mavrikakis, Bimetallic and Ternary Alloys for Improved Oxygen Reduction Catalysis, *Top. Catal.*, 2007, **46**, 276-284.

76. Z. Yin, W. Zhou, Y. Gao, D. Ma, C. J. Kiely and X. Bao, Supported Pd–Cu Bimetallic Nanoparticles That Have High Activity for the Electrochemical Oxidation of Methanol, *Chem. Eur. J.*, 2012, **18**, 4887-4893.

77. B. Hammer and J. K. Nørskov, Theoretical surface science and catalysis - calculations and concepts, *Adv. Catal.*, 2000, **45**, 71-129.

Chapter – 5

High surface area NiCoP nanostructure as an efficient water splitting electrocatalyst: The oxygen evolution activity

Summary:

High surface area metal phosphide, $Ni_{0.2}Co_{0.8}P$ shows excellent oxygen evolution reaction (OER) performance in alkaline condition. It requires very low overpotential, 230 mV to achieve an anodic current density of 10 mA cm^{-2} with a Tafel slope of 44 mV dec^{-1}. The catalyst also shows good activity for hydrogen evolution reaction (HER) under both alkaline and acidic conditions. The higher activity may come from the synergistic effect of Ni and Co in $Ni_{0.2}Co_{0.8}P$ lattice which is further assisted by rapid mass transport due to porous architecture in three dimensional network morphology.

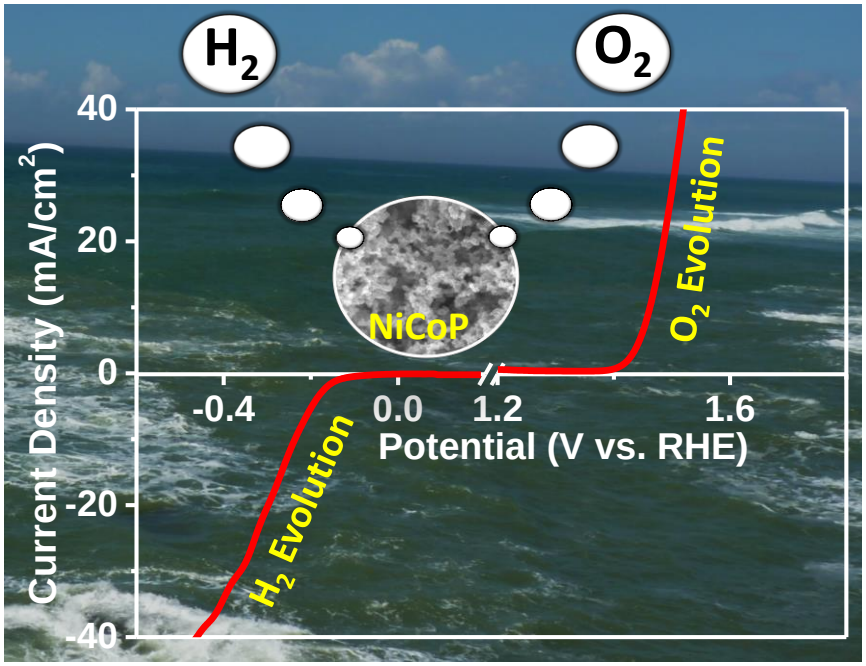

5.1. Introduction:

Electrochemical water splitting (to H_2 and O_2) is an attractive sustainable technology for tapping renewable energy resources with negligible carbon footprints.[1-4] However, the high cost and low earth abundance of the best performing oxygen evolution reaction (OER) and hydrogen evolution reaction (HER) catalysts (RuO_2, IrO_2 etc. for OER and Pt based catalysts for HER) limit their widespread application.[5-8] Practical prototypes surpassing industrial threshold for water splitting demands not only effective but also earth abundant electrocatalysts to carry out hydrogen and oxygen generation at opposite electrodes efficiently.[3, 9] The sluggish electron transfer kinetics associated with OER is the major impediment to overcome with the earth abundant catalysts before we realize water splitting as the source of renewable energy.[10-12] Several transition metal oxides,[13-16] hydroxides,[17-19] sulfides,[8, 20-22] selenides,[23-25] nitrides,[26-28] phosphides[29-36] etc. are being explored in this direction as monofunctional/bifunctional electrocatalysts for HER and OER studies. Among them; Mo, Fe, Ni and Co based transition metal phosphides are emerging as a new class of electrocatalysts for OER owing to their good electrical conductivity[33, 37] as compared to their oxide counterparts and excellent stability under wide range of pH.[9] Furthermore, their ability to show proton and hydride acceptor properties over metal and phosphorus sites respectively aids their performance in HER activity.[9, 36-39] Nevertheless, still a lot of improvement in terms of their structure and composition is required to match their performance with RuO_2, IrO_2 and Pt based catalysts in their respective OER and HER reactions.[9]

For example, in comparison to one and two dimensional structures, three dimensional nanoporous architectures of CoP_3 nanoneedles facilitate mass transport dynamics and efficient charge-transfer kinetics at electrode-electrolyte interfaces which in turn enhances their electrocatalytic activity.[37] Furthermore, the presence of hetero-metals in close proximity is known to tune the local electronic environment significantly leading to unusual OER and HER activities.[40, 41] Therefore, a synergistically designed catalyst having balanced pore architecture along with optimally tailored electronic structure is expected to further boost its performance in electrochemical reactions.

In this chapter, we demonstrated a self-supported, three-dimensional nanoporous NiCoP catalysts prepared by a simple strategy showing a very low overpotential, excellent high current density and small Tafel slope for OER reaction. The overpotential required to

achieve an anodic current density of 10 mA cm^{-2} for $Ni_{0.2}Co_{0.8}P$ (subscripts indicate wt. % of respective element) catalyst is only 230 mV with a very small Tafel slope of 44 mV dec^{-1}.

5.2. Scope of the Present Study:

Due to limitations of existing fossil fuels, renewable energy resources have been drawing a lot of attention for future energy sources. Among them, water splitting is one of the most promising, green and sustainable energy technology which can generate pure hydrogen and oxygen. However, this uphill reaction needs to be catalysed by earth abundant elements to make this process economically viable. Though several approaches are being explored over the last few decades, still designing an efficient catalyst for kinetically sluggish oxygen evolution reaction (in the overall water splitting) is a challenging task. In this study, we report bimetallic phosphides made from earth abundant elements acting as a highly efficient bifunctional catalyst for both OER and HER performance. This finding may be very useful and can open the path for technological application in future.

5.3. Experimental Section:

5.3.1. Materials and Characterization Techniques:

$NiCl_2.6H_2O$ (S D Fine Chemicals), $CoCl_2.6H_2O$ (S D Fine Chemicals), $NaBH_4$ (S D Fine Chemicals), NaH_2PO_2 (Sigma-Aldrich), KOH (Merck Chemicals), H_2SO_4 (98%, AR grade), HCl (37%, AR grade) were used as received without any further purification.

Powder X-ray diffraction (PXRD) patterns were recorded using Bruker-D8 diffractometer using Cu Kα radiation, (λ=1.54 Å, step size: 0.02, current: 30 mA and voltage: 40 kV). Field-emission scanning electron microscopy (FESEM) images and energy-dispersive X-ray spectroscopy (EDS) were obtained by using FEI (Nova-Nano SEM-600 Netherlands) equipment. Transmission electron microscope (TEM) imaging was done using Technai F30 UHR electron microscope operating at an accelerating voltage of 200 kV. Samples were prepared by putting a drop of very dilute dispersion in ethanol on a TEM grid (carbon polymer, 300 mesh). Inductively coupled plasma – atomic emission spectroscopy (ICP-AES) was carried out using a Perkin−Elmer Optima 7000 DV machine. X-ray photoelectron spectroscopy (XPS) has been performed using Omicron EA 125 spectrometer with Al K_α (1486.6 eV) source. Gas adsorption-desorption measurements

were performed on Autosorb-iQ2 (Quantachrome corp.) at 77 K. The samples were degassed before starting the nitrogen gas sorption analysis under a high vacuum (10^{-8} torr) for 12 h at 423 K. Electrochemical measurements were carried out using electrochemical work station obtained from CH instruments (660C, USA) for evaluating the electrochemical activities of the catalysts for hydrogen evolution reaction (HER) and oxygen evolution reaction (OER).

5.3.2. Experimental Details:

5.3.2.1. Catalyst Synthesis:

Ni_2P, CoP and mixed metal phosphides (Ni_xCo_yP, x and y indicates the wt. % of respective metal present in the sample) with different Ni and Co compositions, were prepared by the reaction of metal hydroxides and phosphide precursor (NaH_2PO_2) at 300 ^oC in Ar atmosphere.

Metal hydroxides were prepared by the reaction of aqueous metal chloride solution in presence of excess amount of $NaBH_4$ at room temperature.[42, 43] In a typical procedure, 20 mL of metal chloride solution of 0.1 M concentration was rapidly added to a freshly prepared 100 mL of 0.5 M $NaBH_4$ aqueous solution with vigorous stirring. The stirring was continued for another 30 minute. Finally the solid product obtained was washed with water for several times and dried at 60 ^oC in an oven for overnight. For the synthesis of bimetallic nickel-cobalt hydroxide, nickel and cobalt chloride solutions were mixed according to their desired compositions (different Ni:Co wt. ratio) and reduced with $NaBH_4$ solution with the same procedure described above for nickel and cobalt hydroxide synthesis.

Metal phosphide nanostructures were synthesized by the procedure reported elsewhere.[44-46] To synthesize the metal phosphide, 200 mg of as-synthesized metal hydroxide (nickel or cobalt hydroxide) was mixed with 1 g (5 times) of NaH_2PO_2 by grinding in a motor-pestle. The solid powder was transferred into a ceramic boat and heated in a tube furnace at 300 ^oC for 1 h in Ar atmosphere (heating and cooling rate was 3 ^oC per minute). Then the solid product was soaked in 60 ml 0.1 M HCl solution for 3 h in order to remove unreacted metal particles which were formed during the borohydride reduction. Finally, the remaining solid was washed with water for several times and dried at 60 ^oC in an oven for overnight. The bimetallic nickel-cobalt phosphides, Ni_xCo_yP were synthesized from

the reaction of nickel-cobalt hydroxide with NaH_2PO_2 in the same reaction condition as mentioned above followed by acid washing. Nickel-cobalt phosphides having different Ni and Co compositions, $Ni_{0.2}Co_{0.8}P$, $Ni_{0.4}Co_{0.6}P$, $Ni_{0.6}Co_{0.4}P$ and $Ni_{0.8}Co_{0.2}P$ were also prepared using the above procedure. The composition of all the samples were analyzed by inductively-coupled plasma atomic emission spectroscopy (ICP-AES). Among them, $Ni_{0.2}Co_{0.8}P$ catalyst showed very high activity and rest of the experiments were carried out using this catalyst.

5.3.2.2. Synthesis of $Ni_{0.2}Co_{0.8}P$ Doped with 2 wt. % Fe ($Ni_{0.2}Co_{0.8}P$-2% Fe):

During the synthesis of mixed hydroxide of Ni and Co (Ni:Co wt. ratio is 20:40) from the chloride precursors solution, iron chloride ($FeCl_2.\ 4H_2O$) was added accordingly so that Fe wt. percentage is 2 with respect to total weight of Ni and Co in the sample. In a typical procedure, 3.4 mL 0.1 M $NiCl_2$, 13.58 mL 0.1 M $CoCl_2$ and 0.36 mL 0.1 M $FeCl_2$ solutions were mixed properly and rapidly added to 100 mL freshly prepared 1 M $NaBH_4$ solution with vigorous stirring. The stirring was continued for another 30 minute. Finally the solid product obtained was washed with water for several times and dried at 60 ^oC in oven for overnight. Then the solid product was mixed with NaH_2PO_2 (5 times) and heated in a tube furnace at 300 ^oC for 1 h in Ar atmosphere followed by acid washing as mentioned above. The compositions of Ni, Co and Fe were confirmed by inductively-coupled plasma atomic emission spectroscopy (ICP-AES).

5.3.2.3. Removal of Fe from 1 M KOH Solution:

Trace amount of Fe present in the commercial grade KOH was removed by $Co(OH)_2$ absorption method reported in the literature.[18] In a typical procedure, $Co(OH)_2$ was prepared first by dissolving 2 gm of $Co(NO_3)_2$ in 4 mL mili Q water followed by the addition of 20 mL 0.1 M KOH solution with stirring. The precipitated $Co(OH)_2$ was separated out after 5 min by centrifugation and washed with mili Q water by mechanical agitation for 5 times. Finally obtained $Co(OH)_2$ was used for Fe removal to purify 1 M KOH. As-prepared $Co(OH)_2$ was added to 50 mL of 1 M KOH solution and the mixture was mechanically agitated for another 10 min to absorb Fe impurities. Then the brown colored suspension was removed by centrifugation for 1 h and the purified KOH was separated out. The process was repeatedly done for another three times with the same purified KOH solution and finally used as Fe-free KOH electrolyte for electrochemical

measurements. Also, the absence of Fe in 1 M KOH solution was confirmed by ICP-AES analysis.

5.3.2.4. Electrochemical Measurements:

The electro active material (2 mg) was dispersed in a mixture of mili Q water (0.7 mL) and isopropanol (0.3 mL) containing 10 μL of 5 wt. % nafion solution and ultrasonicated to obtain a homogeneous catalyst ink. Then, 8 μL of the catalyst ink was drop casted on a cleaned glassy carbon (GC) electrode having 3 mm diameter resulting a catalyst loading of ~0.22 mg cm^{-2}. The GC electrode was dried in ambient conditions and used as working electrode in the electrochemical studies.

Electrochemical measurements were carried out using a standard three-electrode cells using a graphite rod having large area as a counter electrode and saturated calomel electrode (SCE) as reference electrode in acidic medium (0.5 M H_2SO_4) for HER activity and mercury-mercuric oxide (Hg/HgO) electrode as also a reference electrode in basic medium (0.1 M and 1 M KOH) for both HER and OER activity. All the polarization curves were recorded after the correction of iR compensation arising due to ohmic resistance of the cell. The measured potentials vs. SCE or Hg/HgO were calibrated with respect to reversible hydrogen electrode (RHE). The obtained current densities were normalized to the geometrical surface area of the GC electrode. The linear sweep voltammograms (LSVs) were recorded in 1 M KOH /0.1 M KOH /0.5 M H_2SO_4 at 5 mV s^{-1} under Ar saturated aqueous electrolytes. Cyclic voltammograms (CV) were recorded under similar conditions and at different scan rates (20-200 mV s^{-1}) within the potential range from -0.1 to 0.3 V (vs. RHE) in order to evaluate electrochemical double layer capacitance (C_{dl}), representing electrochemically active surface area (ECSA).

5.3.2.5. Calibration of Reference Electrodes:

The reference electrodes Hg/HgO used in alkaline electrolyte (KOH solution) and SCE used in acidic solution, were calibrated with respect to reversible hydrogen electrode (RHE) using large area Pt foil as a working electrode and long Pt wire as counter electrode. High purity hydrogen gas was purged in the respective solutions for 1 h before the experiment and a constant overhead purge was maintained during the measurements. Cyclic voltammograms were recorded at a scan rate of 1 mV s^{-1} (Figure 5.1).

For 1 M KOH, $E_{RHE} = E_{Hg/HgO} + 0.935$ V

For 0.1 M KOH, $E_{RHE} = E_{Hg/HgO} + 0.894$ V

For 0.5 M H_2SO_4, $E_{RHE} = E_{SCE} + 0.274$ V

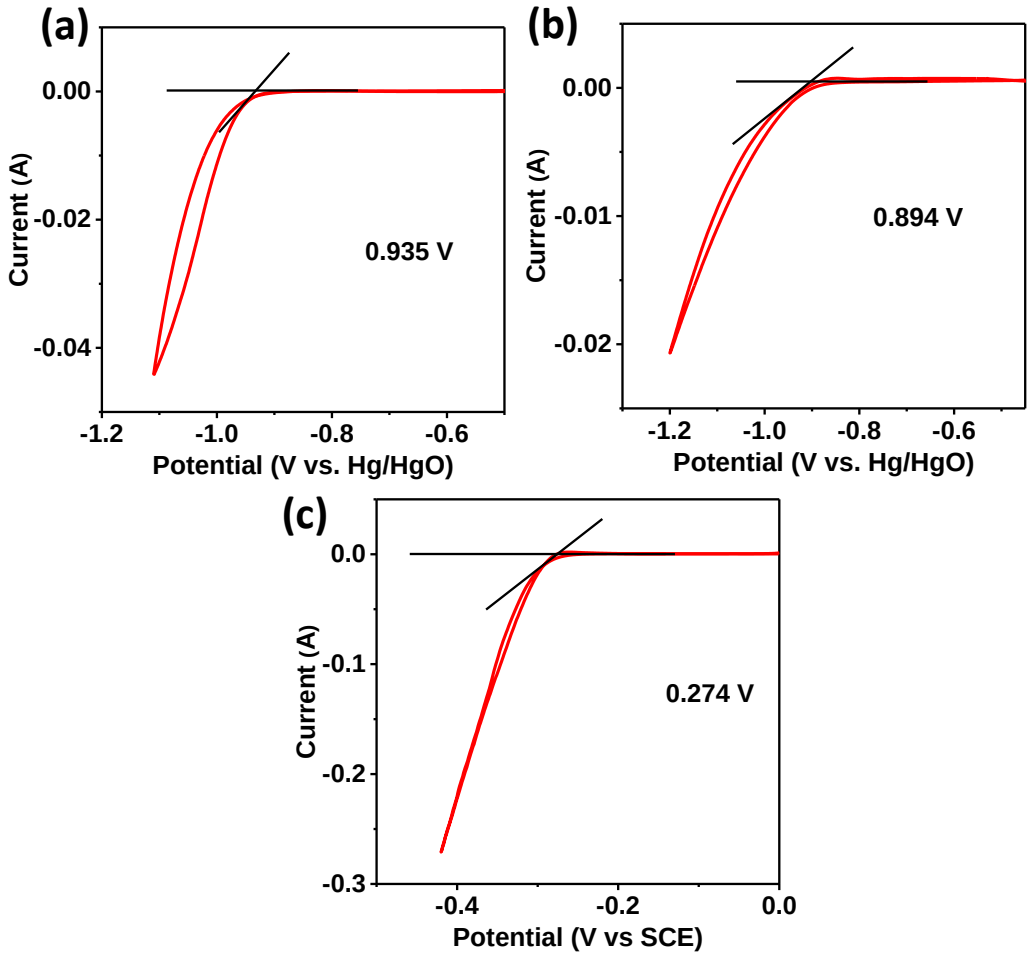

Figure 5.1: *Calibration plot of mercury/mercury oxide (Hg/HgO) electrode with respect to reversible hydrogen electrode (RHE) in (a) 1 M KOH and (b) 0.1 M KOH. (c) Calibration plot of saturated calomel electrode (SCE) with respect to RHE in 0.5 M H_2SO_4. All the cases measurements were carried out at a scan rate of 1 mV s^{-1}.*

5.4. Results and Discussion:

Bimetallic, pore engineered, mixed metal phosphide, $Ni_{0.2}Co_{0.8}P$ was synthesized by reaction of nickel-cobalt hydroxide with NaH_2PO_2 at 300 ^oC under Ar atmosphere followed by acid washing (details in the experimental section).[44, 45] Acid washing is required in order to remove unreacted metal particles which were formed during the synthesis of metal hydroxide. The powder X-ray diffraction (PXRD) pattern of Ni_2P

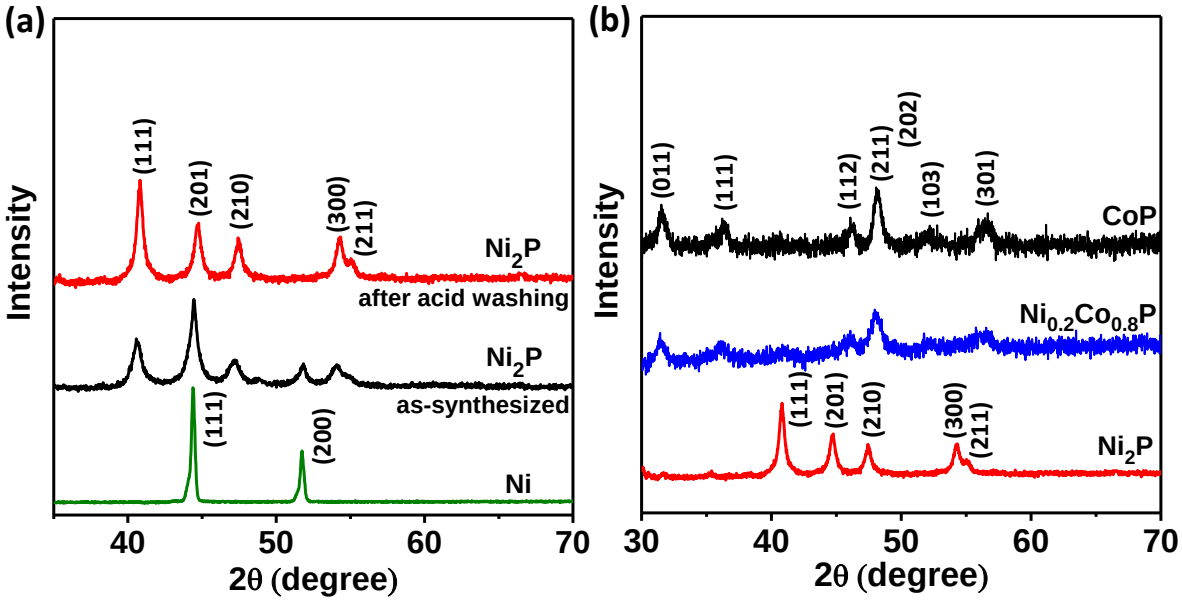

Figure 5.2: *(a) Powder X-ray diffraction (PXRD) patterns of as-synthesized Ni_2P and after acid etching. As-synthesized Ni_2P contains some amount of Ni nanoparticles which can be removed by acid treatment as discussed in the experimental section. (b) PXRD patterns of Ni_2P, CoP and $Ni_{0.2}Co_{0.8}P$. It shows $Ni_{0.2}Co_{0.8}P$ structure is governed by CoP as it contains 80 wt. % of Co.*

(Figure 5.2a) after acid washing shows the complete removal of unreacted Ni nanoparticles. The precursors, nanoporous Ni, Co and Ni-Co hydroxides having high surface area were prepared by $NaBH_4$ reduction of the respective salt solutions, a method adopted by us earlier to prepare high surface area noble metal nanostructures.[42, 43] The phase purity and chemical composition of Ni_2P, CoP and $Ni_{0.2}Co_{0.8}P$ electrocatalysts were analyzed by PXRD pattern (Figure 5.2b) and inductively-coupled plasma atomic emission spectroscopy (ICP-AES). The PXRD pattern of $Ni_{0.2}Co_{0.8}P$ confirms that the lattice structure mainly consists of CoP phase (orthorhombic) predominantly governed by the relative weightage of the metal. The transmission electron microscopic (TEM) image of $Ni_{0.2}Co_{0.8}P$ (Figure 5.3a) shows that it has a network, sponge-like structure made up of interconnected particles of size about 10 nm. High resolution- TEM (HRTEM) image of $Ni_{0.2}Co_{0.8}P$ (Figure 5.3b) indicates a lattice spacing of 0.26 nm which is in between Ni_2P

(0.513 nm, hexagonal structure) and CoP (0.19 nm, orthorhombic structure) (Figure 5.4) confirming the formation of bimetallic Ni-Co phase. Furthermore, energy dispersive X-ray spectroscopic (EDS) elemental mapping (Figure 5.3c) shows uniform dispersion of Ni, Co and P in $Ni_{0.2}Co_{0.8}P$ sample which indicates phase uniformity of the material.

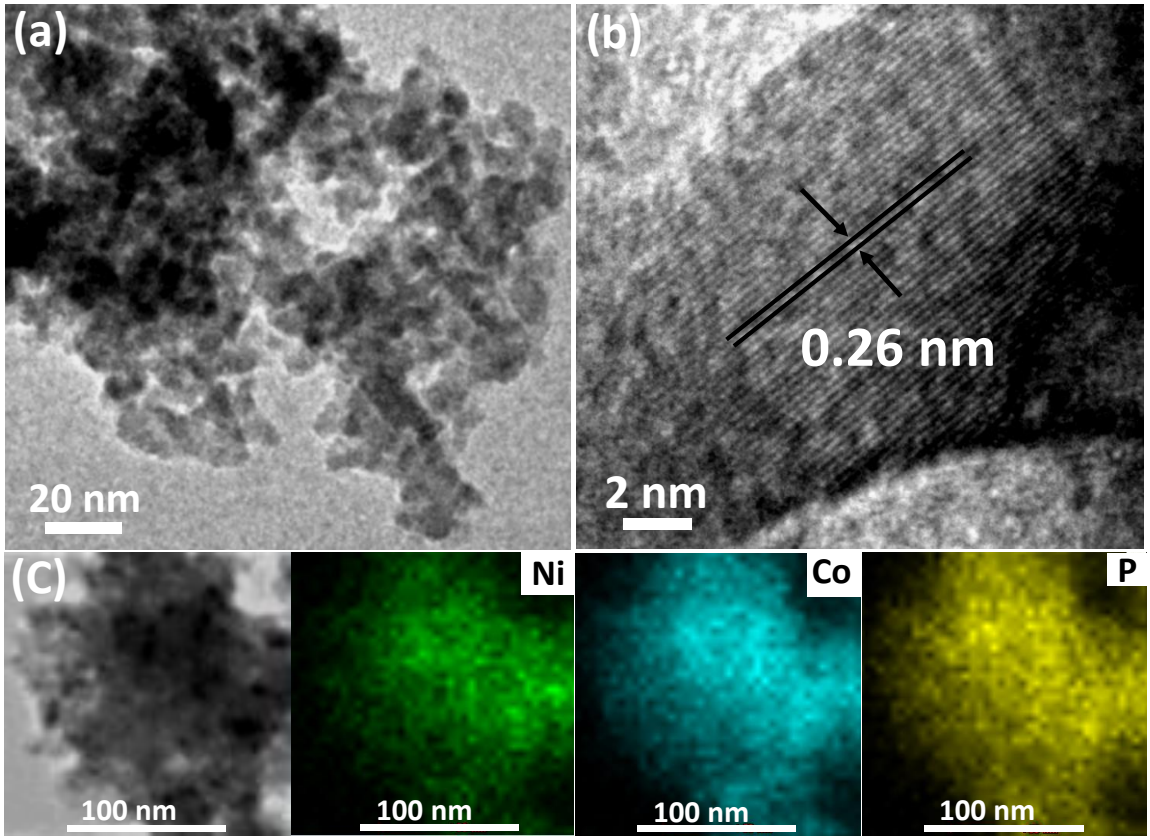

Figure 5.3: *Characterization of $Ni_{0.2}Co_{0.8}P$. (a) TEM image and (b) high resolution-TEM (HRTEM) image of $Ni_{0.2}Co_{0.8}P$ phase. (c) Corresponding elemental mapping for Ni, Co and P in $Ni_{0.2}Co_{0.8}P$.*

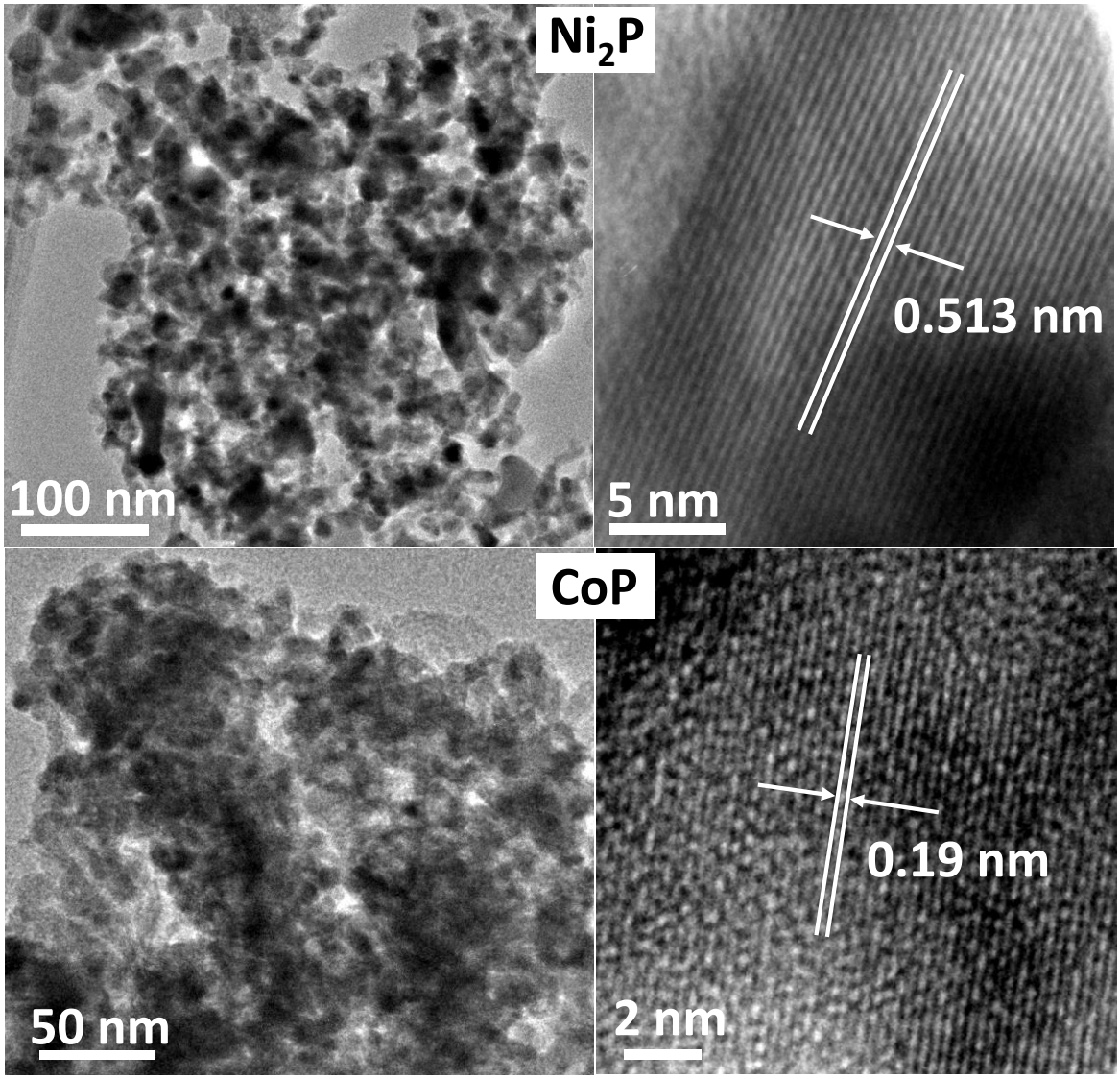

Figure 5.4: *Transmission electron microscopy (TEM) images of Ni_2P and CoP. High resolution TEM (HRTEM) images show the lattice fringes of Ni_2P (hexagonal phase) and CoP (orthorhombic phase).*

The field emission scanning electron microscopic (FESEM) images (Figure 5.5) further confirms the three dimensional network morphology of phosphides. N_2 sorption analyses in Figure 5.6 indicate significant nitrogen condensation at higher P/P_o and the pore size analyses shows the presence of wide range of mesopores (3-12 nm) which matches well with TEM observation. The surface areas calculated from N_2 isotherms at 77 K for $Ni_{0.2}Co_{0.8}P$, Ni_2P and CoP were found to be 38, 33 and 48 $m^2\ g^{-1}$ respectively which is significantly higher compared to previously reported literature values (Table 5.1).

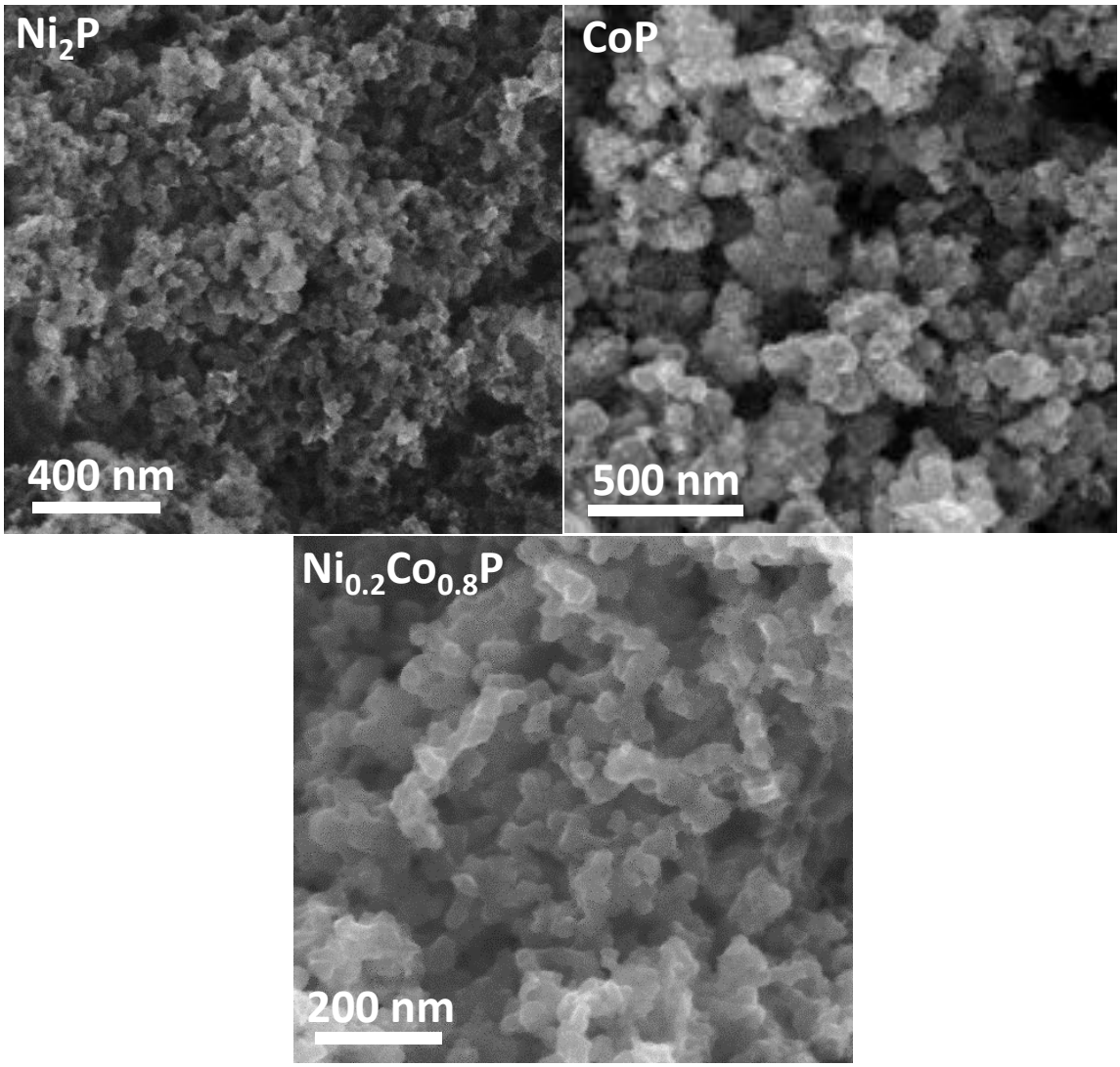

Figure 5.5: *Field-emission scanning electron microscopy (FESEM) images of Ni_2P, CoP and $Ni_{0.2}Co_{0.8}P$. The images show three dimensional network morphology made up of interconnected nanoparticles during the synthesis.*

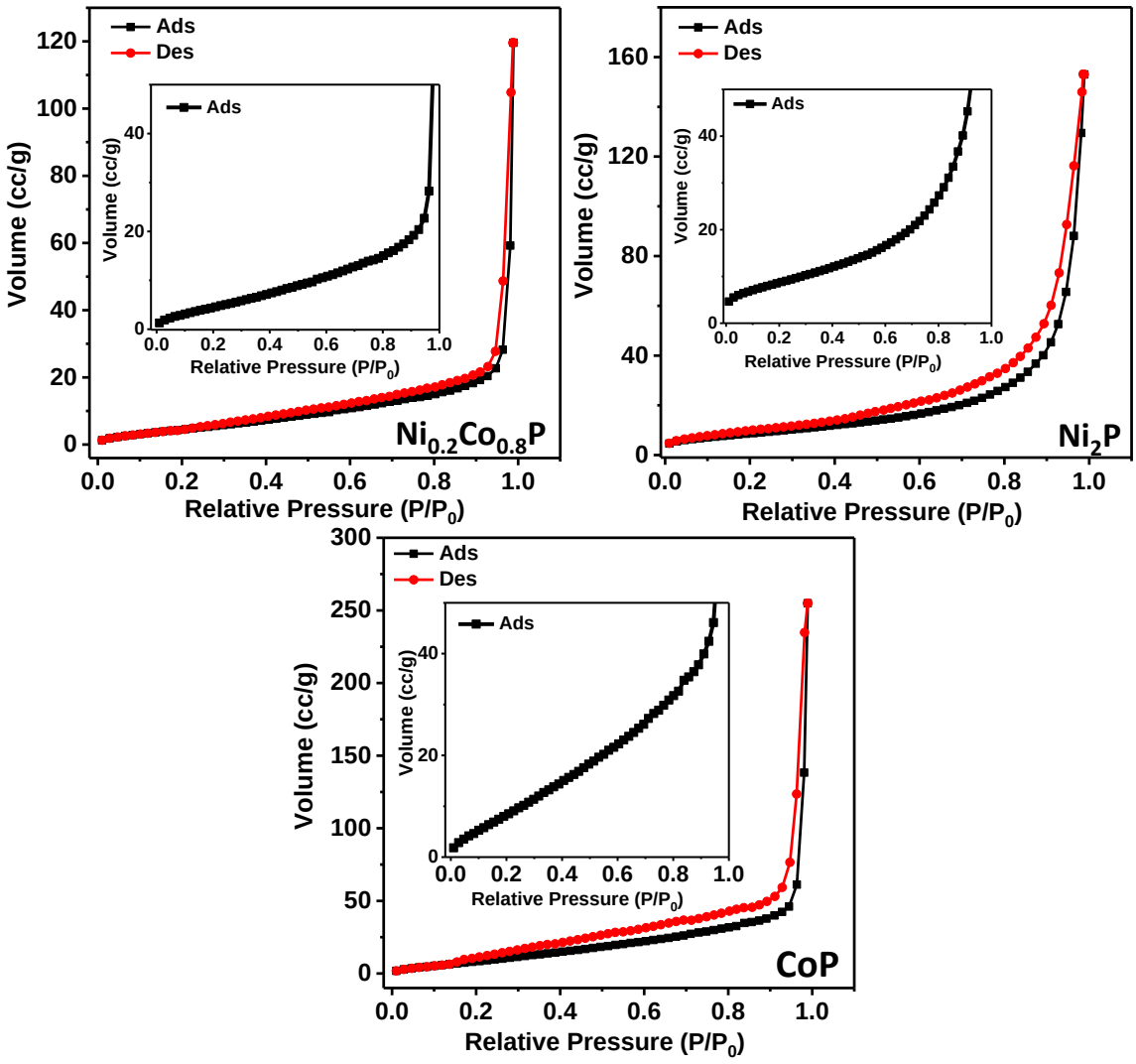

Figure 5.6: *N_2 adsorption-desorption isotherms of $Ni_{0.2}Co_{0.8}P$, Ni_2P and CoP measured at 77 K. Inset of all shows the enlarged view of adsorption.*

Table 5.1: *Comparison of Brunauer–Emmett–Teller (BET) surface area of assynthesized catalysts with the literature reports.*

Catalyst	Surface Area (m^2 g^{-1})	References
$Ni_{0.2}Co_{0.8}P$	38	Present Study
Ni_2P	33	Present Study

CoP	48	Present Study
$Ni_{0.4}Co_{0.6}P$	37	Present Study
$Ni_{0.6}Co_{0.4}P$	40	Present Study
$Ni_{0.8}Co_{0.2}P$	39	Present Study
Ni-Co-P	22	40
CoP_3 nanoneedles	21.4	37
CoP_3 nanoparticles	4.7	37
CoP nanowire	36.5	47
CoP hollow polyhedron	46.9	48

X-ray photoelectron spectroscopy (XPS) analyses were carried in order to evaluate the chemical nature of elements and to correlate with electroactivity. Survey spectrum of $Ni_{0.2}Co_{0.8}P$ (Figure 5.7a) indicates the surface presence of Ni, Co, P and O (existence of O on the surface is due to exposure of the sample in air), commensurate with EDS analyses. The deconvolution of high resolution Ni 2p spectrum (Figure 5.7b) shows peaks at 853.1 eV (for Ni $2p_{3/2}$) and at 870.1 eV (for Ni $2p_{1/2}$) ascribed to partially positive $Ni^{\delta+}$ in Ni-P bond.[49] The peak at 856.6 eV and the corresponding satellite peak at 861.9 eV for Ni $2p_{3/2}$ (also the peak at 874.8 eV and its corresponding satellite peak at 880.5 eV for Ni $2p_{1/2}$) could be attributed to Ni^{2+} species.[40, 50, 51] The deconvoluted high resolution spectrum for Co 2p also shows peaks corresponding to $Co^{\delta+}$ in Co-P bond[49] as well as Co^{2+} species[40, 50] (Figure 5.7c). The binding energy values for P $2p_{3/2}$ and P $2p_{1/2}$ are 128.8 eV and 129.8 eV (Figure 5.7d) respectively in $Ni_{0.2}Co_{0.8}P$ show a negative shift compared to elemental

P (130.2 eV) supports the presence of $P^{\delta-}$.[52] In addition, the presence of a broad peak at higher binding energy, 133.2 eV, could be ascribed to oxidation of P species.[53] The peaks corresponding to partially oxidized Ni and Co and partially reduced P in XPS analysis suggest that a certain amount of electron density transfers from Ni and Co site towards P.[54]

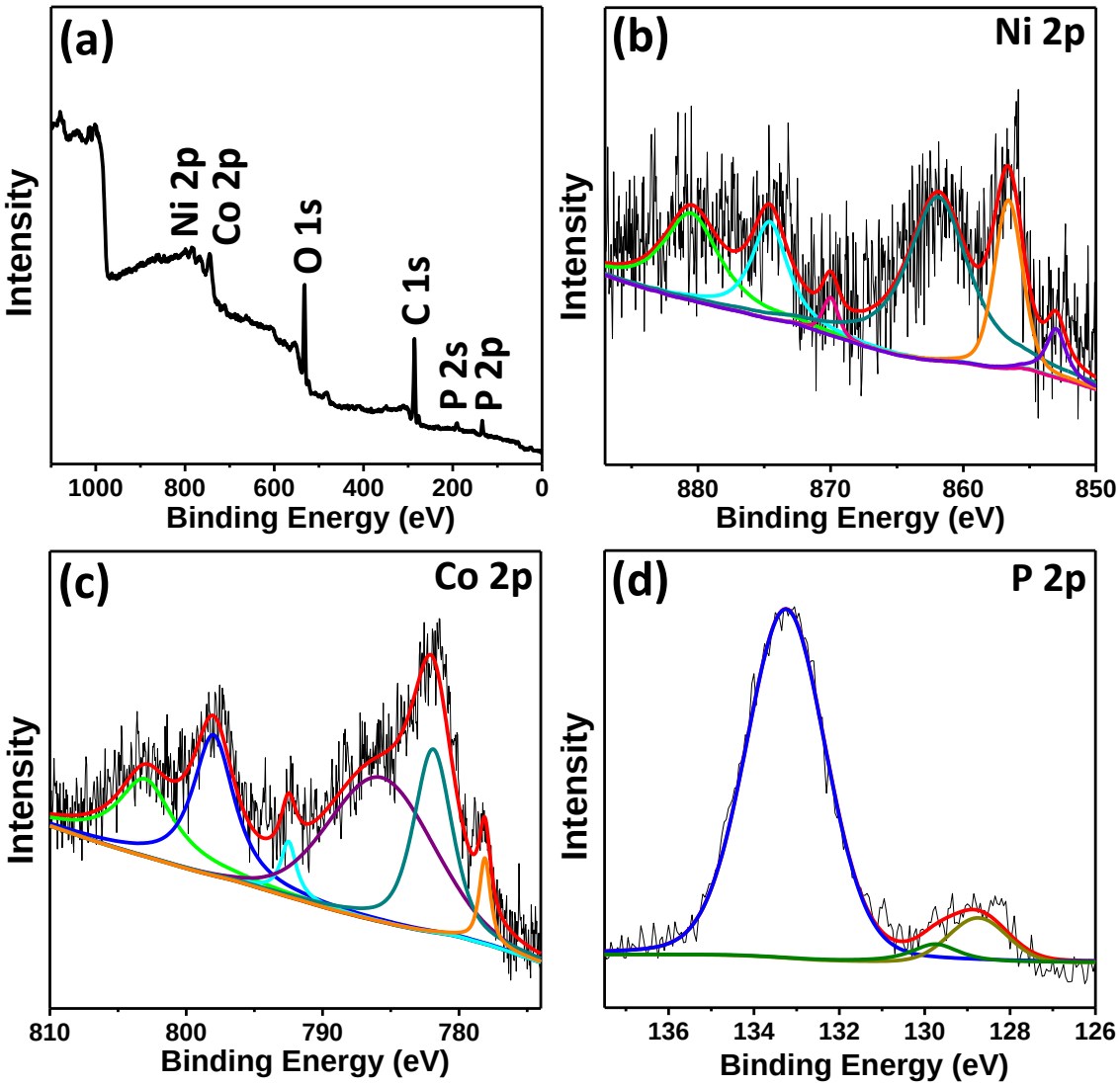

Figure 5.7: *X-ray photoelectron spectroscopic (XPS) analyses of $Ni_{0.2}Co_{0.8}P$. (a) XPS survey spectrum of $Ni_{0.2}Co_{0.8}P$ and corresponding high resolution deconvoluted spectra of (b) Ni 2p, (c) Co 2p and (d) P 2p respectively.*

The OER performance of the samples were investigated using a rotating disk electrode (RDE) as the working electrode at 1600 rpm in 1 M KOH solution. The performance of Ni_2P, CoP and commercial RuO_2 catalysts were also measured for comparison with $Ni_{0.2}Co_{0.8}P$. Polarized linear sweep voltammograms (LSVs) of different phosphides studied at 5 mV s^{-1} under Ar saturated conditions indicate superior performance for

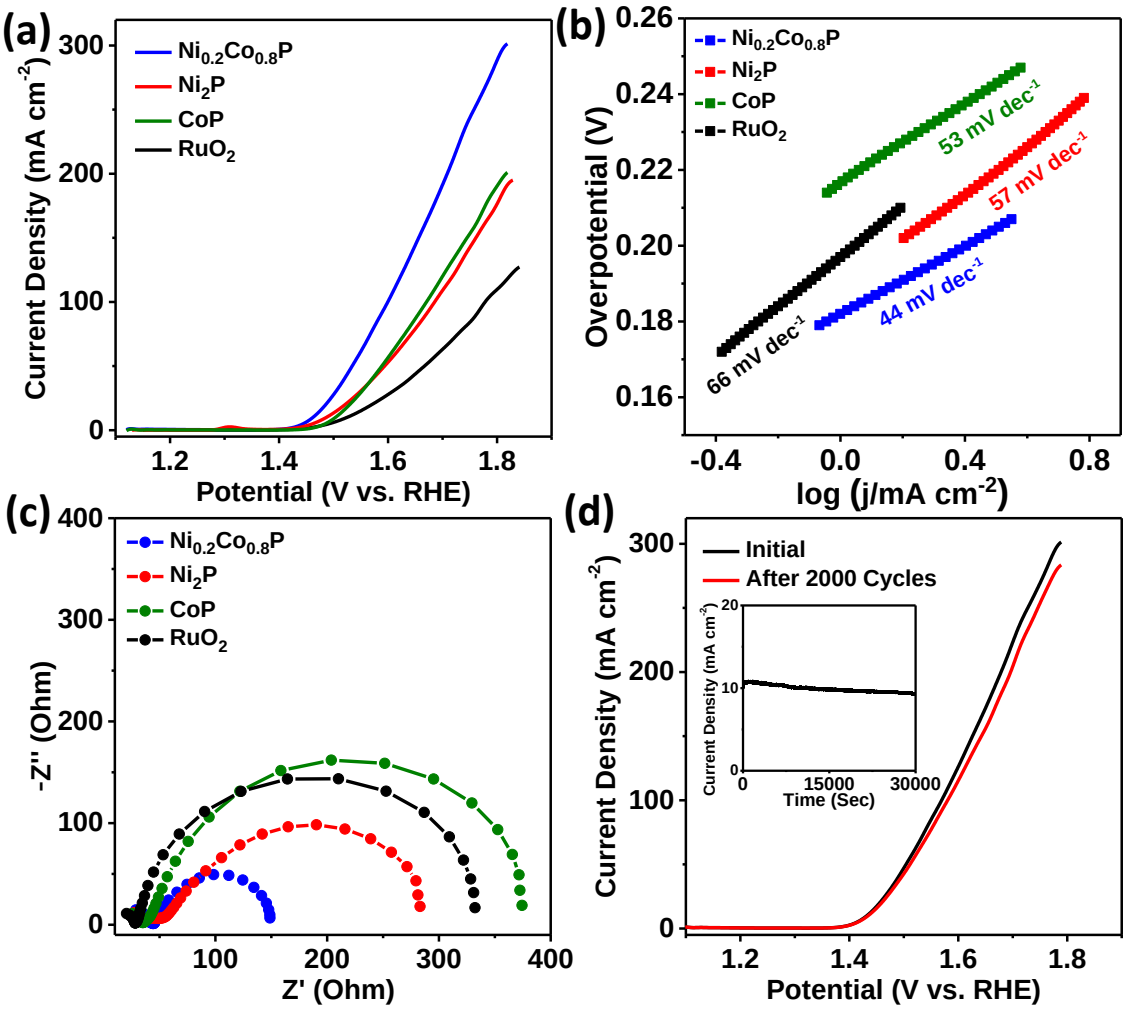

Figure 5.8: *(a) The polarized linear sweep voltammograms of different catalysts for evaluating OER activity at 5 mV s^{-1} after iR compensation in 1 M KOH solution. (b) Corresponding Tafel analyses extracted from (a), compared with state-of-the-art RuO_2. (c) Nyquist plots of all the electrocatalysts at their respective onset potentials. (d) Stability studies of $Ni_{0.2}Co_{0.8}P$ before and after 2000 cycles indicating stable performance. Inset shows chronoamperometry (the current density vs time plot) for the same catalyst.*

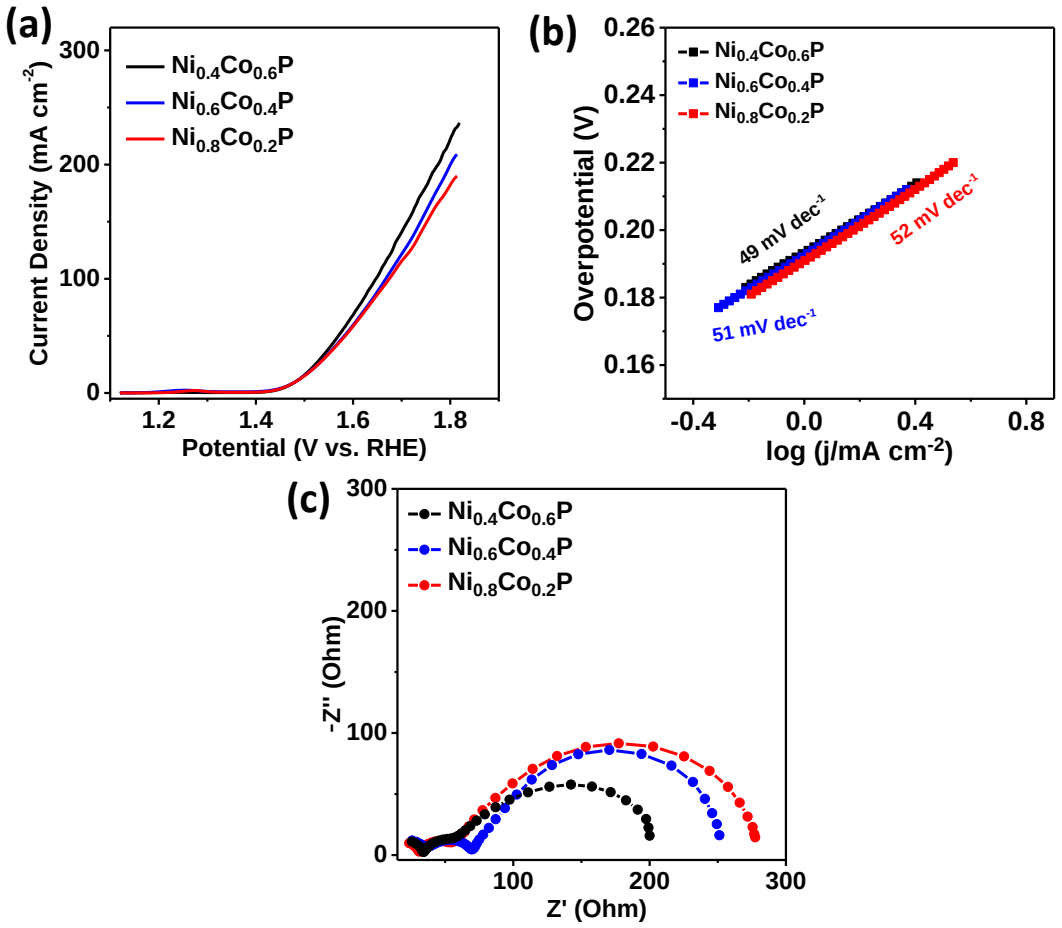

Figure 5.9: *The polarized linear sweep voltammograms of different catalysts for evaluating OER activity at 5 mV s^{-1} after iR compensation in 1 M KOH solution. (b) Corresponding Tafel analyses extracted from (a). (c) Nyquist plots of all the electrocatalysts at their respective onset potentials.*

Table 5.2: *Comparison table of electrochemical parameters obtained for OER performance in 1 M KOH solution among all phosphide catalysts and state-of-the-art RuO_2 catalyst.*

	$Ni_{0.2}Co_{0.8}P$	CoP	Ni_2P	$Ni_{0.4}Co_{0.6}P$	$Ni_{0.6}Co_{0.4}P$	$Ni_{0.8}Co_{0.2}P$	RuO_2
Onset overpotential (mV)	190	230	200	200	200	200	240
Overpotential at 10 mA cm^{-2} (mV)	230	280	270	255	255	255	300
Overpotential at 100 mA cm^{-2} (mV)	360	440	460	420	440	445	550
Tafel Slope (mV dec^{-1})	44	53	57	49	51	52	66

$Ni_{0.2}Co_{0.8}P$ compared to other mixed/monometallic phosphides (Figure 5.8a, 5.9a and Table 5.2). The LSVs (Figure 5.8a) indicate very high oxygen evolution activity for bimetallic $Ni_{0.2}Co_{0.8}P$ catalyst with lowest onset potential of 1.42 V as compared to Ni_2P (1.43 V), CoP (1.46 V), and the standard RuO_2 catalyst (1.47 V). The overpotential required for $Ni_{0.2}Co_{0.8}P$ to reach a current density of 10 mA cm^{-2} is 230 mV (360 mV to generate 100 mA cm^{-2}) which is one of the lowest values reported so far for any transition metal phosphide materials (Table 5.3). On the other hand, Ni_2P and CoP show overpotentials of 270 and 280 mV respectively at 10 mA cm^{-2} (460 and 440 mV at 100 mA cm^{-2} respectively). Reaction kinetics were studied in kinetically controlled region using Tafel analysis (Figure 5.8b). $Ni_{0.2}Co_{0.8}P$ exhibits lowest Tafel slope of only 44 mV dec^{-1} compared to Ni_2P (57 mV dec^{-1}), CoP (53 mV dec^{-1}) and RuO_2 (66 mV dec^{-1}) and many transition metal phosphides reported so far (Figure 5.8b, 5.9b and Table 5.3). As expected, electrochemical impedance spectroscopic (EIS) analyses show lower charge transfer resistance (R_{ct}) for $Ni_{0.2}Co_{0.8}P$ catalyst compared to other NiCoP catalysts prepared at varying compositions (Figure 5.8c and 5.9c). Moreover, $Ni_{0.2}Co_{0.8}P$ shows hardly any loss in activity even after 2000 cycles (after accelerated cycling test) (Figure 5.8d) and no sign of degradation of current density even after a long time of 30000 s at fixed potential at a current density of 10 mA cm^{-2} (inset of Figure 5.8d). There is no significant change in the morphology of $Ni_{0.2}Co_{0.8}P$ catalysts observed in TEM after the OER performance (Figure 5.10). It is to be noted that a physical mixture of Ni_2P and CoP (mixed in a wt. ratio to obtain $Ni_{0.2}Co_{0.8}P$ stoichiometry) showed the OER activity far lower than the activity of $Ni_{0.2}Co_{0.8}P$ further confirming the synergistic effect[40] of Ni and Co in $Ni_{0.2}Co_{0.8}P$ lattice (Figure 5.11).

Table 5.3: *Comparison table of OER activity in alkaline medium among the transition metal based phosphide catalysts recently reported in the literature.*

Catalysts	Overpotential (mV) at @10 mA cm^{-2}	***Tafel Slope (mV dec^{-1})***	***References***
$Ni_{20}Co_{80}P$	230	44	Present Study
CoP	280	53	Present Study
Ni_2P	270	57	Present Study

CoP/CNT	~330	50	[33]
CoP	400	80	[33]
Ni_2P nanowires	290	47	[32]
Ni_2P nanoparticles	330	59	[32]
Ni_1Co_3P	280	66.5	[41]
$C@Ni_8P_3$	267	51	[35]
Ni_8P_3	283	78	[35]
Cu_3P/ Ni Foam	320	54	[55]
Core-oxidized amorphous CoP	287	70	[30]
CoP NR /Carbon	320	71	[56]
CoP NP /Carbon	340	99	[56]
Co_2P nanoneedles	310	50	[31]
CoMnP	330	61	[11]
Co_2P	370	128	[11]
Co-Fe-P-1.7	319	58	[57]
CoP/C	360	66	[58]
Ni_2P nanowires	400	60	[59]
FeMnP nanoplates /FTO	300	65	[60]
NiCoP/Ti	310	52	[54]

carbon coated NiP nanoplates	300	64	[34]
Ni-Fe-P nanocubes	271	53	[61]
CP@FeP	350	63.6	[62]
CoP_2/RGO	300	96	[63]
CoP_2	370	103	[63]
$Fe_{0.2}Ni_{0.8}P_2$ /carbon paper	241	49.3	[64]

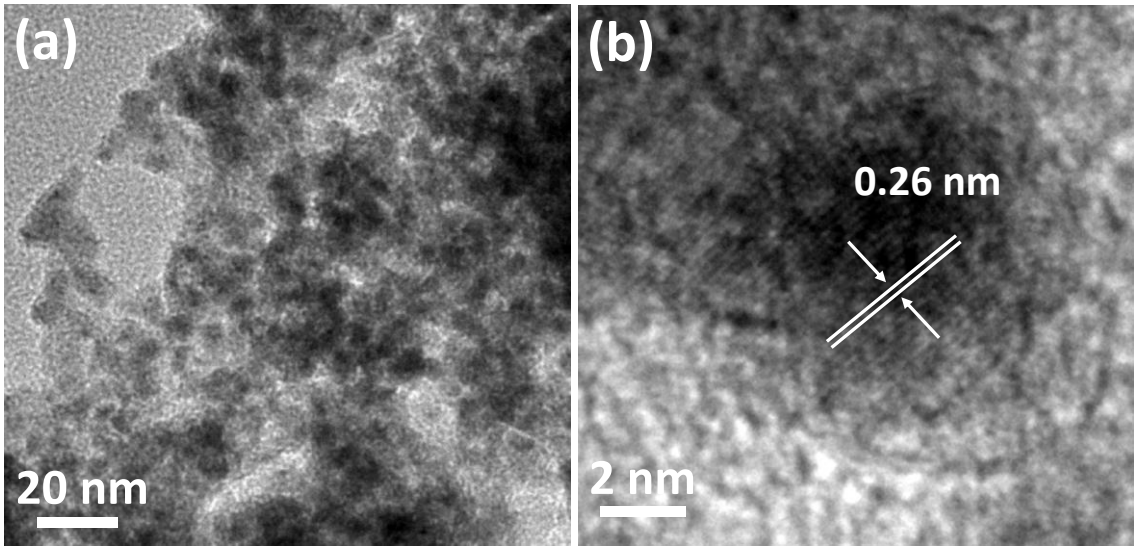

Figure 5.10: *(a) TEM and (b) HRTEM images of $Ni_{0.2}Co_{0.8}P$ catalyst after the OER performance in 1 M KOH solution.*

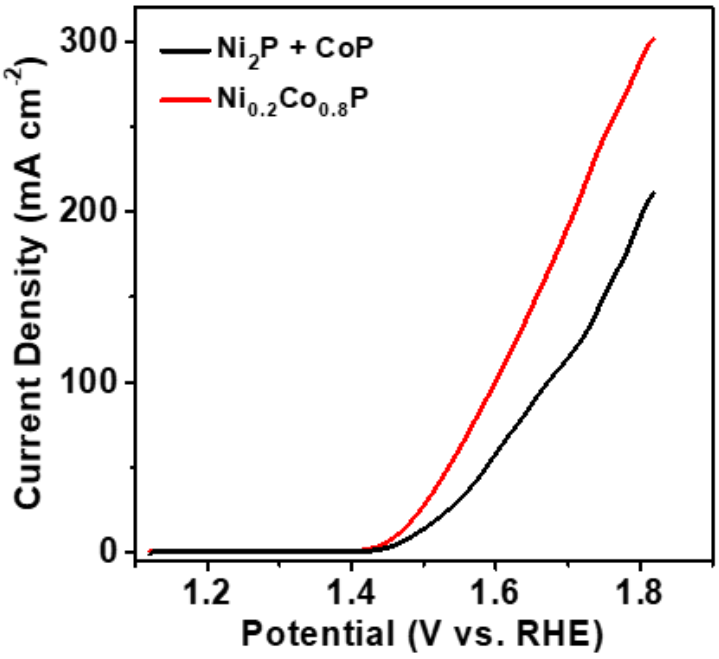

Figure 5.11: *The polarized linear sweep voltammogram of a physical mixture of Ni_2P and CoP (mixed in a wt. ratio to obtain $Ni_{0.2}Co_{0.8}P$ stoichiometry) for OER performance at 5 mV s^{-1} after iR compensation in 1 M KOH solution which shows far lower OER activity compared to $Ni_{0.2}Co_{0.8}P$ catalyst.*

Hu et al. in a recent report observed that higher activity of Ni_2P nanoparticles for OER (overpotential of 290 mV at 10 mA cm^{-2}) in alkaline medium is associated with the presence of trace amount of Fe impurities (~40 ppb, present in commercial KOH electrolyte).[32] Removal of iron from KOH showed a huge increase in overpotential, 410 mV at a current density of 10 mA cm^{-2}. However, in our case, there was no such change in the performance of $Ni_{0.2}Co_{0.8}P$ catalyst (Figure 5.12) when the OER was carried out in 1 M KOH electrolyte before (commercial grade containing ~40 ppb Fe analyzed by ICP-AES) and after removing the trace iron (by using $Co(OH)_2$ absorption,[18] details in the experimental section). Furthermore, addition of Fe (10 ppm concentration) into iron-free 1 M KOH electrolyte did not show any enhancement in OER activity for $Ni_{0.2}Co_{0.8}P$ (Figure 5.12). Besides, $Ni_{0.2}Co_{0.8}P$ prepared with 2 wt. % Fe (details in experimental section) also shows no significant enhancement for OER activity in 1 M KOH electrolyte (Figure 5.12). This experiment further confirms that the lower overpotential displayed by $Ni_{0.2}Co_{0.8}P$ catalyst is rather intrinsic and not resulting from the iron impurities. The

synergistic effect of Ni and Co in $Ni_{0.2}Co_{0.8}P$ can be understood as this ternary phosphide shows excellent performance for OER compared to the binary Ni_2P and CoP catalysts as described above.

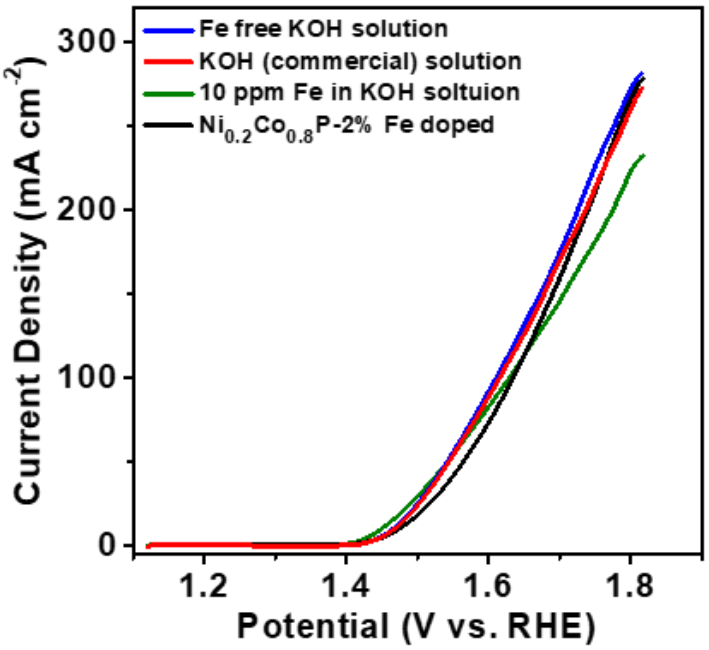

Figure 5.12: *OER performance of $Ni_{0.2}Co_{0.8}P$ catalyst in 1 M KOH electrolyte before and after removing the trace amount of iron. Same measurement was carried out in presence of 10 ppm Fe (added separately) in 1 M KOH solution. Also, OER was done for $Ni_{0.2}Co_{0.8}P$-2% Fe doped (prepared separately as described before in the experimental section).*

The HER studies of Ni_2P, CoP and $Ni_{0.2}Co_{0.8}P$ catalysts were investigated in 0.1 M KOH in a standard three electrode assembly with a mass loading of 0.22 mg cm^{-2} on glassy carbon (GC) electrode and was compared with state-of-the-art catalyst 40 wt. % Pt/C. The LSVs of different phosphides (Figure 5.13a and 5.14a) indicate superior performance for $Ni_{0.2}Co_{0.8}P$ compared to other mixed/monometallic phosphides (Table 5.4). $Ni_{0.2}Co_{0.8}P$ requires an overpotential (η) of 237 mV to achieve a cathodic current density 10 mA cm^{-2} which is much lower compared to CoP (η = 401 mV), Ni_2P (η = 443). Furthermore,

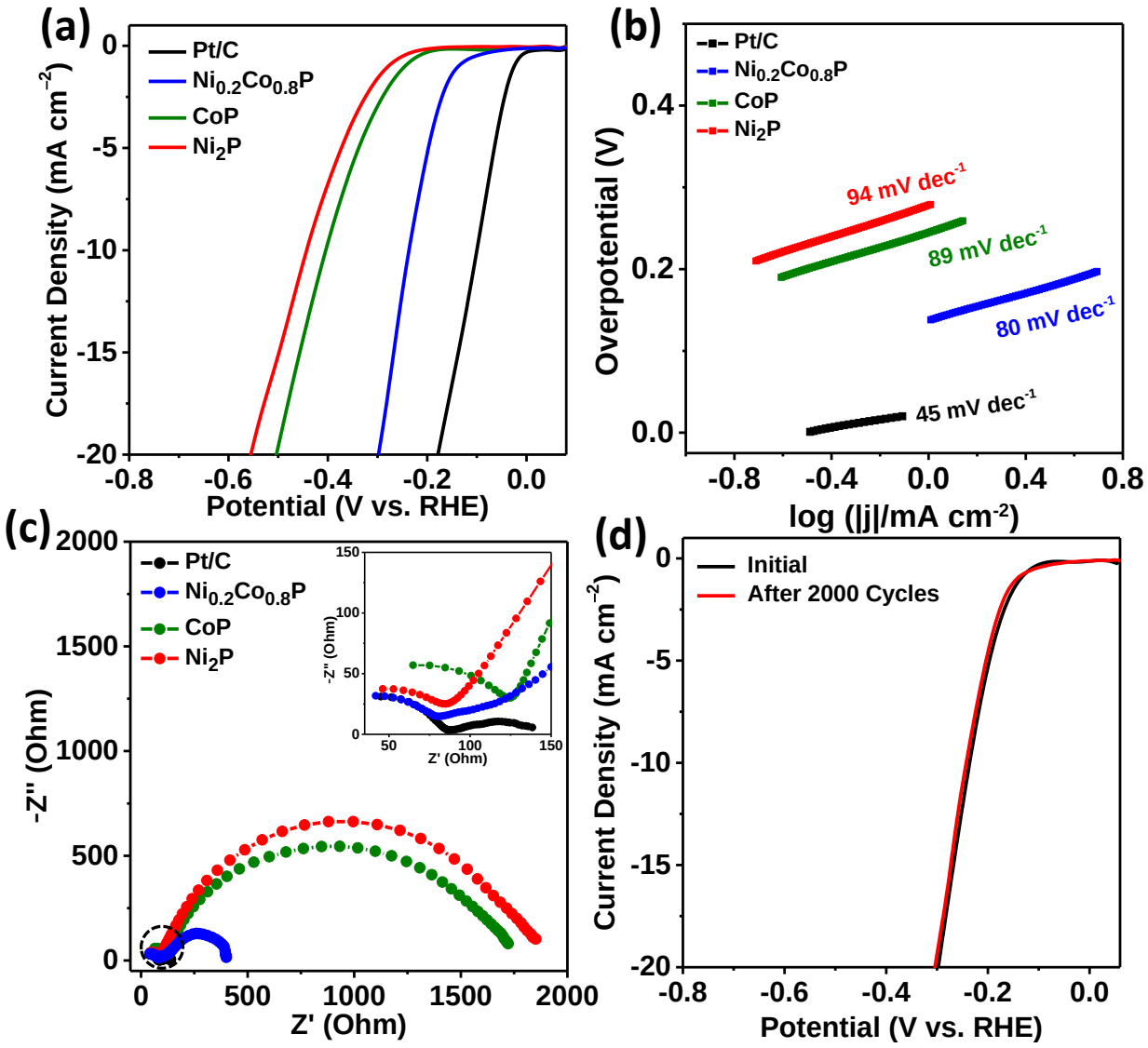

Figure 5.13: *(a) The polarized linear sweep voltammograms of different catalysts for evaluating HER activity at 5 mV s^{-1} after iR compensation in 0.1 M KOH solution. (b) Corresponding Tafel analyses extracted from (a), compared with state-of-the-art Pt/C. (c) Nyquist plots of all the electrocatalysts at their respective onset potentials. Inset shows the magnified view of the region marked in doted circle in higher frequency regime. (d) Stability performance of $Ni_{0.2}Co_{0.8}P$ before and after 2000 cycles indicating stable performance.*

$Ni_{0.2}Co_{0.8}P$ exhibits a Tafel slope of 80 mV dec^{-1} as compared to CoP (89 mV dec^{-1}) and Ni_2P (94 mV dec^{-1}) and other mixed phosphides (Figure 5.13b and 5.14b). To investigate the interfacial HER phenomenon, electrochemical impedance spectroscopic (EIS) analyses (Figure 5.13c and 5.14c) were carried out at their respective onset potentials.

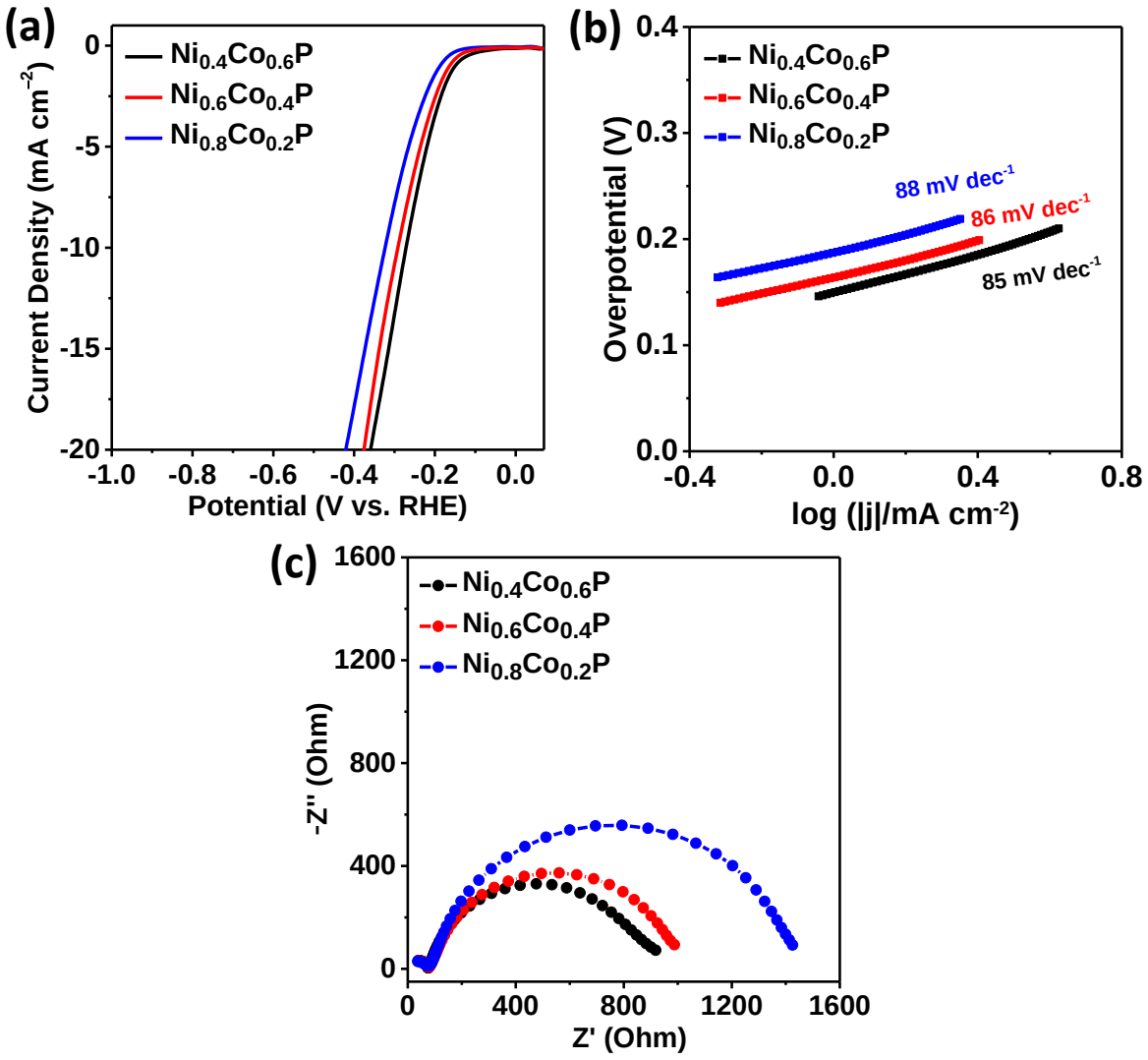

Figure 5.14: *(a) The polarized linear sweep voltammograms of NiCoP of different Ni and Co compositions for evaluating HER activity at 5 mV s^{-1} after iR compensation in 0.1 M KOH solution. (b) Corresponding Tafel analyses extracted from (a). (c) Nyquist plots of all the electrocatalysts at their respective onset potentials.*

Table 5.4: *Comparison table of electrochemical parameters obtained for HER performance in 0.1 M KOH solution among all phosphide catalysts and state-of-the-art Pt/C catalyst.*

	$Ni_{0.2}Co_{0.8}P$	CoP	Ni_2P	$Ni_{0.4}Co_{0.6}P$	$Ni_{0.6}Co_{0.4}P$	$Ni_{0.8}Co_{0.2}P$	40% Pt/C
Onset overpotential (mV)	70	199	229	91	123	150	7
Overpotential at 10 mA cm^{-2} (mV)	237	401	443	272	292	324	100
Tafel Slope (mV dec^{-1})	80	89	94	85	86	88	45

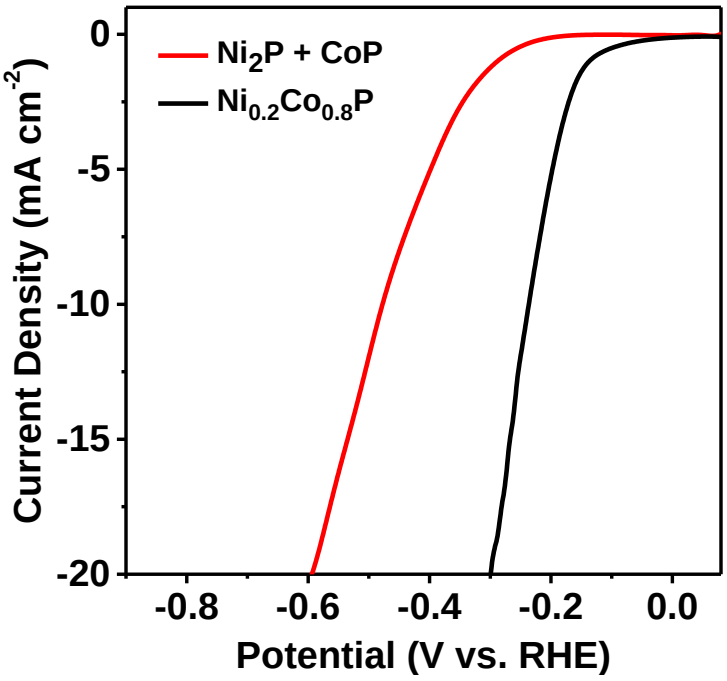

Figure 5.15: *The polarized linear sweep voltammogram of a physical mixture of Ni_2P and CoP (mixed in a wt. ratio to obtain $Ni_{0.2}Co_{0.8}P$ stoichiometry) for HER performance at 5 mV s^{-1} after iR compensation in 0.1 M KOH solution which shows far lower HER activity than $Ni_{0.2}Co_{0.8}P$ catalyst.*

$Ni_{0.2}Co_{0.8}P$ shows lowest charge transfer resistance (R_{ct}) among all the binary and ternary metal phosphides indicating facile electron transfer kinetics for the electrochemical reactions. Nevertheless, the curves obtained from EIS measurement suggest more than a single step involved for HER in the basic medium. The faster kinetics for bimetallic $Ni_{0.2}Co_{0.8}P$ catalyst compared to single/mixed metal phosphide systems is probably due to the contribution from higher surface area of the catalysts and the synergistic effect of both Ni and Co present in a three dimensional, highly porous interconnected network which allows easy electron transfer across the electrochemical interfaces. The HER performance carried over the physical mixture of CoP and Ni_2P (mixed in the wt. % ratio to obtain $Ni_{0.2}Co_{0.8}P$ as mentioned earlier) was far lower than the performance of $Ni_{0.2}Co_{0.8}P$ confirming the synergistic effect of Ni and Co in $Ni_{0.2}Co_{0.8}P$ lattice (Figure 5.15). $Ni_{0.2}Co_{0.8}P$ does exhibit superior stability for over 2000 cycles after accelerated cyclic testing (Figure 5.13d) indicating durability of such systems for long term electrochemical performance. However, the HER performance of $Ni_{0.2}Co_{0.8}P$ in 1 M KOH is lower than expected and the reason is not clear.

The catalysts, $Ni_{0.2}Co_{0.8}P$, Ni_2P and CoP were also tested for HER activity in acidic medium (0.5 M H_2SO_4 solution). $Ni_{0.2}Co_{0.8}P$ shows much lower onset potential of 33 mV, Further it shows an overpotential (η) of 116 mV to achieve a cathodic current density 10 mA cm^{-2} with a Tafel slope of 51 mV dec^{-1} significantly lower than the value observed for Ni_2P, CoP and other compositions of NiCoP (Figure 5.16, 5.17 and Table 5.5). Furthermore, $Ni_{0.2}Co_{0.8}P$ is also very stable and its activity remains same even after 2000 cycles in 0.5 M H_2SO_4 solution (Figure 5.16d).

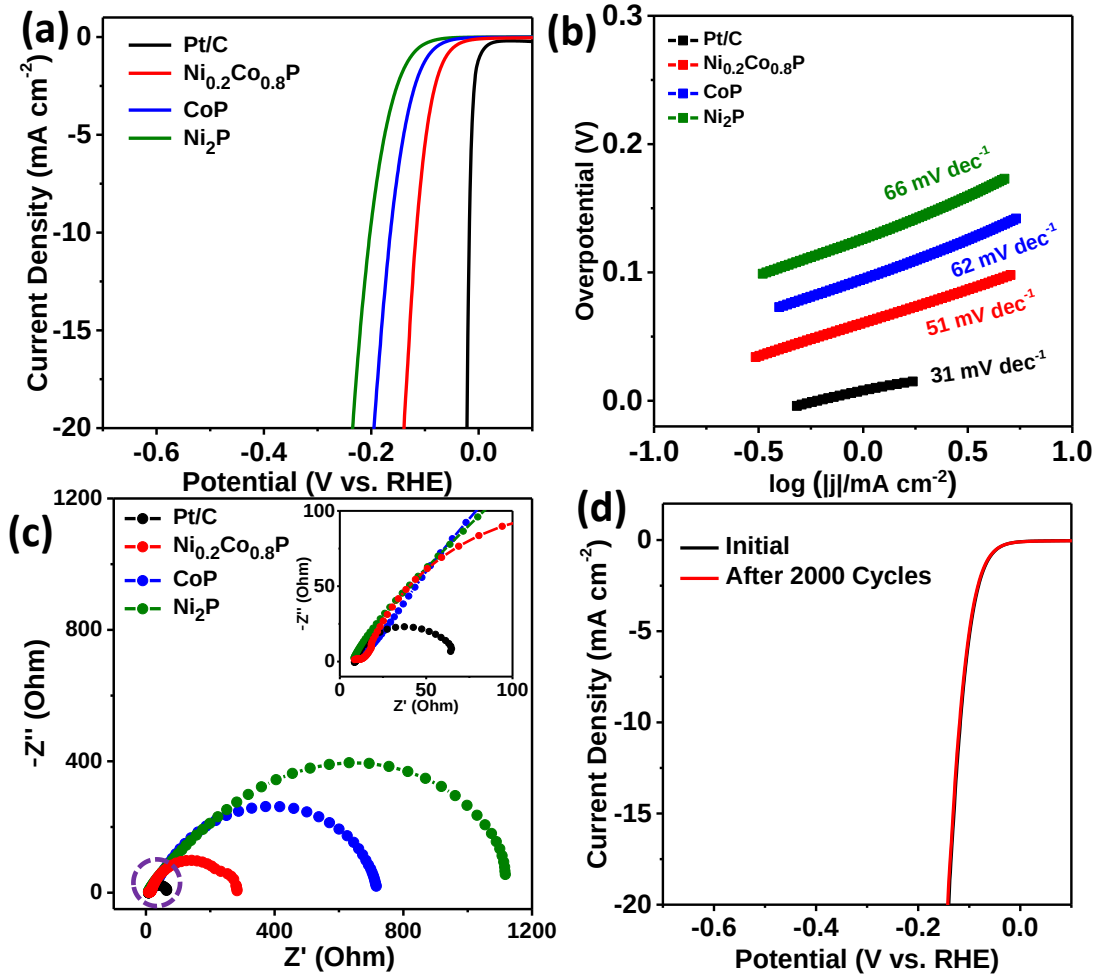

Figure 5.16: *(a) The polarized linear sweep voltammograms of different catalysts for evaluating HER activity at 5 mV s^{-1} after iR compensation in 0.5 M H_2SO_4 solution. (b) Corresponding Tafel analyses extracted from (a), compared with state-of-the-art Pt/C. (c) Nyquist plots of all the electrocatalysts at their respective onset potentials. Inset shows the magnified view of the region marked in doted circle in higher frequency regime. (d) Stability performance of $Ni_{0.2}Co_{0.8}P$ before and after 2000 cycles indicating stable performance.*

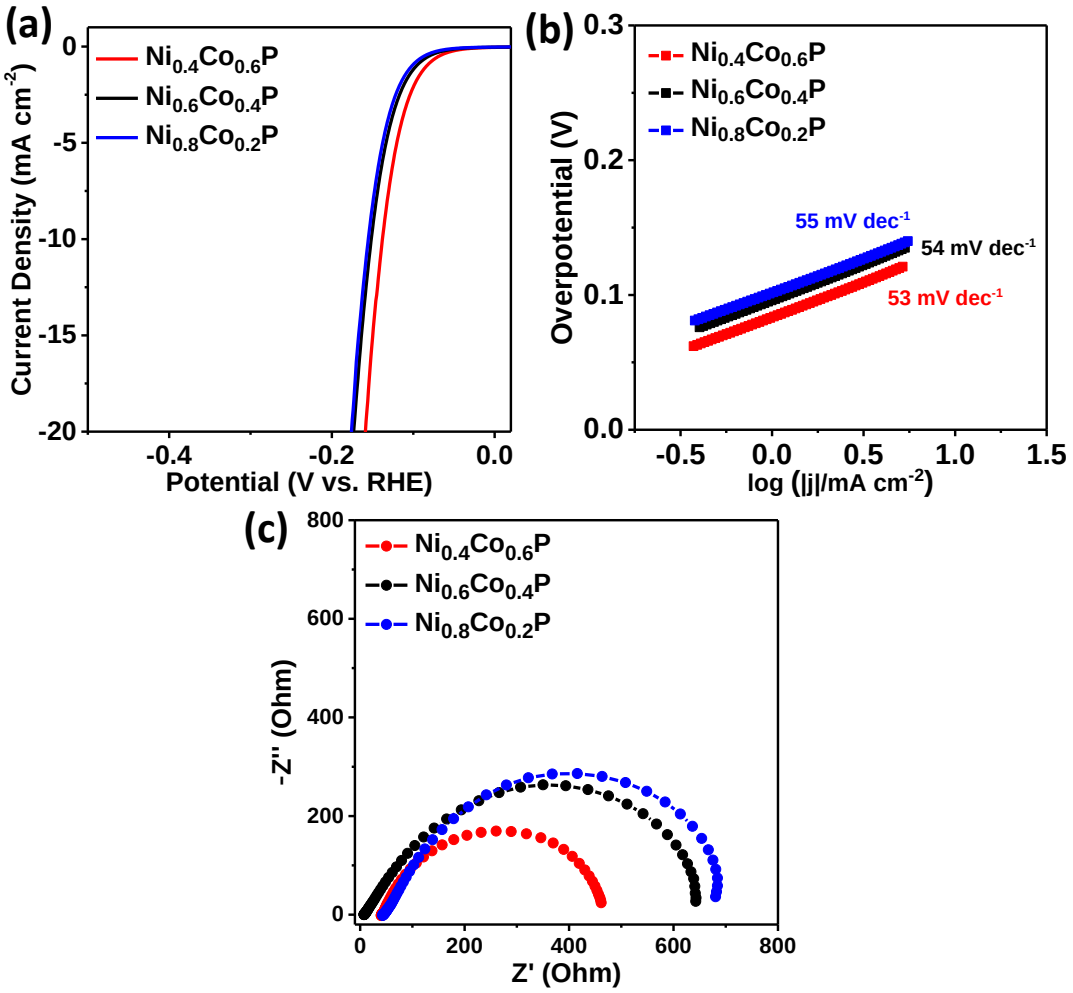

Figure 5.17: *(a) The polarized linear sweep voltammograms of different catalysts for evaluating HER activity at 5 mV s^{-1} after iR compensation in 0.5 M H_2SO_4 solution. (b) Corresponding Tafel analyses extracted from (a). (c) Nyquist plots of all the electrocatalysts at their respective onset potentials.*

Table 5.5: *Comparison table of electrochemical parameters obtained for HER performance in 0.5 M H_2SO_4 solution among all phosphide catalysts and state-of-the-art Pt/C catalyst.*

	$Ni_{0.2}Co_{0.8}P$	CoP	Ni_2P	$Ni_{0.4}Co_{0.6}P$	$Ni_{0.6}Co_{0.4}P$	$Ni_{0.8}Co_{0.2}P$	40% Pt/C
Onset overpotential (mV)	**33**	**67**	**97**	**58**	**70**	**76**	**5**
Overpotential at 10 mA cm^{-2} (mV)	**116**	**165**	**203**	**138**	**152**	**156**	**17**
Tafel Slope (mV dec^{-1})	**51**	**62**	**66**	**53**	**54**	**55**	**31**

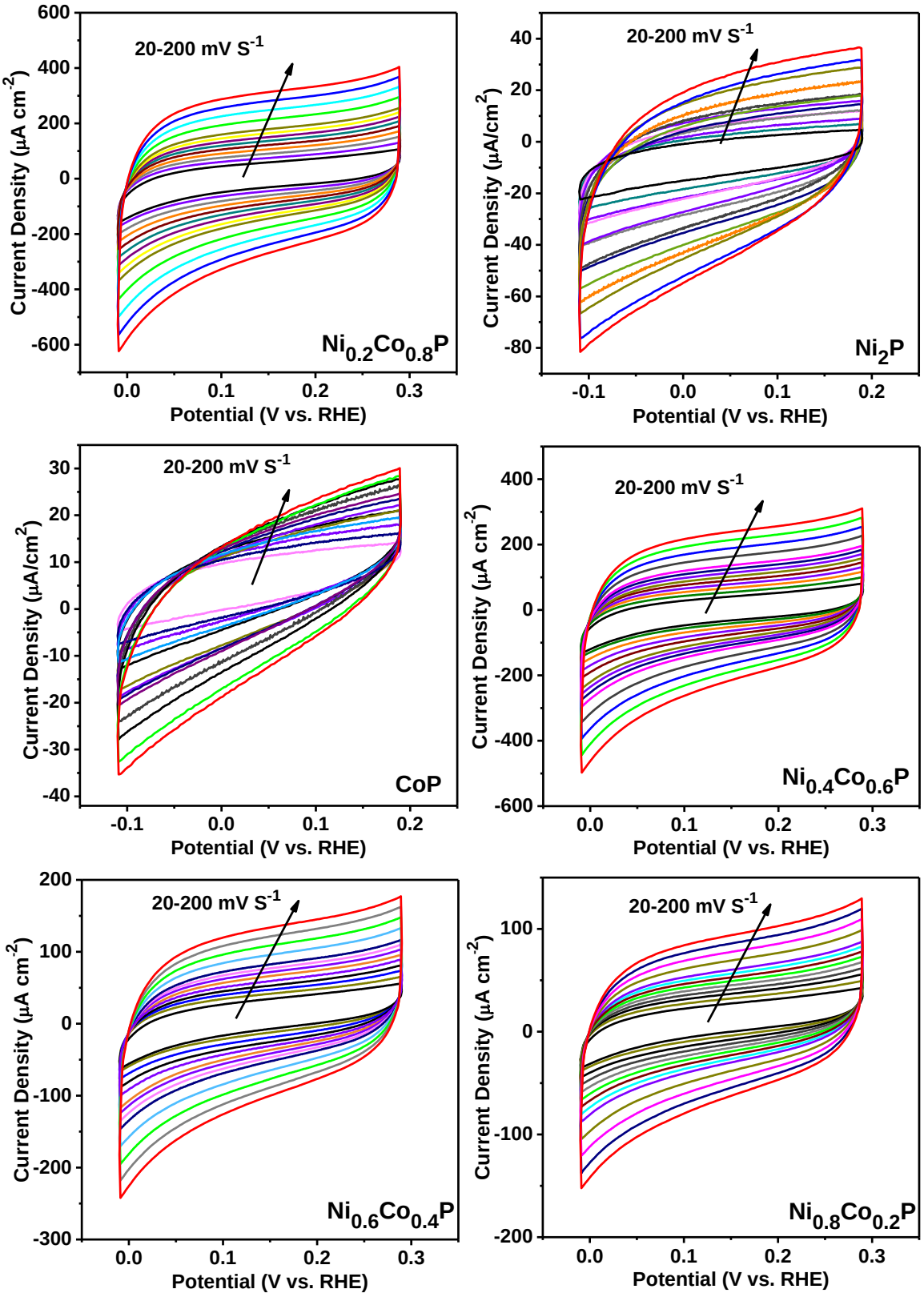

Figure 5.18: *Cyclic voltammograms of all the phosphide catalysts at different scan rates ranging from 20 to 200 mV* s^{-1}.

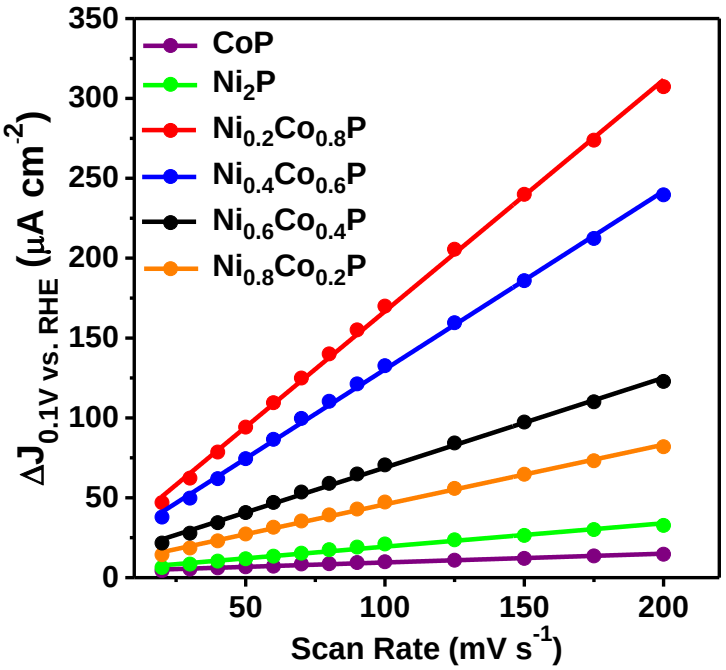

Catalysts	Double layer capacitance (mF cm^{-2})
$Ni_{0.2}Co_{0.8}P$	1.45
Ni_2P	0.146
CoP	0.055
$Ni_{0.4}Co_{0.6}P$	1.11
$Ni_{0.6}Co_{0.4}P$	0.56
$Ni_{0.8}Co_{0.2}P$	0.37

Figure 5.19: *Evaluation of the double-layer capacitance of different phosphide samples at 0.1 V (vs. RHE). Double layer capacitance are calculated from the slope and tabulated in the table.*

In order to understand the strong electrochemical activity of $Ni_{0.2}Co_{0.8}P$, measurement of double layer capacitance (C_{dl}), signifying the electrochemically active surface area (ECSA) was evaluated. Needless to mention, $Ni_{0.2}Co_{0.8}P$ exhibits higher double layer capacitance compared to other mono/mixed metallic phosphide phases indicating higher number of active sites of the former. The C_{dl} of $Ni_{0.2}Co_{0.8}P$ is 1.45 mF cm^{-2} which is around 10 times higher than Ni_2P (0.146 mF cm^{-2}), 26 times higher compared to CoP (0.055 mF cm^{-2}). This value is also higher than other mixed phosphide systems (Figure 5.18, 5.19) and previously reports.[32, 33] The origin of HER and OER activity can also be attributed to the presence of higher density of catalytically active sites in $Ni_{0.2}Co_{0.8}P$. It must however be noted that electrochemically active surface area is different from geometrical surface area; even though CoP has greater surface area compared to $Ni_{0.2}Co_{0.8}P$ but its activity is lower compared to that of the former. It clearly points out the fact that the local synergism aided by the presence of other metal atoms[40] would locally tune the electrochemical properties in a favorable way as it is known that such elements could lower the activation energy barrier for adsorption as well as electronic conductivity

as evident from EIS data (Figure 5.8c, 5.13c and 5.16c). Moreover, the performance metrics of our catalysts is far better than previously reported transition metal based systems for OER under alkaline conditions. Such performance can be rationalized in terms of better mass transport properties aided by high surface area (wider mesopores) and appropriate engineering of local electronic structure.

5.5. Conclusion:

In summary, a simple route was developed to obtain high surface area, pore engineered bimetallic phosphide catalysts, NiCoP (with various Ni and Co compositions) which act as a superior electrocatalyst for OER under alkaline conditions as well as HER activity in both alkaline and acidic medium. It is demonstrated that $Ni_{0.2}Co_{0.8}P$ catalyst (having an η@10 mA cm^{-2} of only 230 mV) is one of the best performing OER catalysts, compared to previously reported transition metal phosphide catalysts. The synergistic effect of Ni and Co present in the bimetallic phosphide catalysts improves the overall activity compared to their monometallic phosphides. The pore-engineering in three dimensional network morphology provides the higher active surface area facilitating the electron transfer at the interface during the electrochemical reactions. This kind of non-noble metal based low-cost material as bifunctional catalyst for both OER and HER can open the path for real application in future.

5.6. References:

1. H. B. Gray, Powering the planet with solar fuel, *Nat. Chem.*, 2009, **1**, 7.
2. M. G. Walter, E. L. Warren, J. R. McKone, S. W. Boettcher, Q. Mi, E. A. Santori and N. S. Lewis, Solar Water Splitting Cells, *Chem. Rev.*, 2010, **110**, 6446-6473.
3. I. Roger, M. A. Shipman and M. D. Symes, Earth-abundant catalysts for electrochemical and photoelectrochemical water splitting, *Nat. Rev. Chem.*, 2017, **1**, 0003.
4. T. R. Cook, D. K. Dogutan, S. Y. Reece, Y. Surendranath, T. S. Teets and D. G. Nocera, Solar Energy Supply and Storage for the Legacy and Nonlegacy Worlds, *Chem. Rev.*, 2010, **110**, 6474-6502.
5. Y. Lee, J. Suntivich, K. J. May, E. E. Perry and Y. Shao-Horn, Synthesis and Activities of Rutile IrO_2 and RuO_2 Nanoparticles for Oxygen Evolution in Acid and Alkaline Solutions, *J. Phys. Chem. Lett.*, 2012, **3**, 399-404.

6. M. E. G. Lyons and S. Floquet, Mechanism of oxygen reactions at porous oxide electrodes. Part 2-Oxygen evolution at RuO_2, IrO_2 and $Ir_xRu_{1-x}O_2$ electrodes in aqueous acid and alkaline solution, *Phys. Chem. Chem. Phys.*, 2011, **13**, 5314-5335.
7. D. Voiry, H. Yamaguchi, J. Li, R. Silva, D. C. B. Alves, T. Fujita, M. Chen, T. Asefa, V. B. Shenoy, G. Eda and M. Chhowalla, Enhanced catalytic activity in strained chemically exfoliated WS_2 nanosheets for hydrogen evolution, *Nat. Mater.*, 2013, **12**, 850-855.
8. D. Merki and X. Hu, Recent developments of molybdenum and tungsten sulfides as hydrogen evolution catalysts, *Energy Environ. Sci.*, 2011, **4**, 3878-3888.
9. S. Anantharaj, S. R. Ede, K. Sakthikumar, K. Karthick, S. Mishra and S. Kundu, Recent Trends and Perspectives in Electrochemical Water Splitting with an Emphasis on Sulfide, Selenide, and Phosphide Catalysts of Fe, Co, and Ni: A Review, *ACS Catal.*, 2016, **6**, 8069-8097.
10. J. Suntivich, K. J. May, H. A. Gasteiger, J. B. Goodenough and Y. Shao-Horn, A Perovskite Oxide Optimized for Oxygen Evolution Catalysis from Molecular Orbital Principles, *Science*, 2011, **334**, 1383-1385.
11. D. Li, H. Baydoun, C. N. Verani and S. L. Brock, Efficient Water Oxidation Using CoMnP Nanoparticles, *J. Am. Chem. Soc.*, 2016, **138**, 4006-4009.
12. Y. Zhao, R. Nakamura, K. Kamiya, S. Nakanishi and K. Hashimoto, Nitrogen-doped carbon nanomaterials as non-metal electrocatalysts for water oxidation, *Nat. Commun.*, 2013, **4**, 2390.
13. I. C. Man, H.-Y. Su, F. Calle-Vallejo, H. A. Hansen, J. I. Martínez, N. G. Inoglu, J. Kitchin, T. F. Jaramillo, J. K. Nørskov and J. Rossmeisl, Universality in Oxygen Evolution Electrocatalysis on Oxide Surfaces, *ChemCatChem*, 2011, **3**, 1159-1165.
14. M. S. Burke, L. J. Enman, A. S. Batchellor, S. Zou and S. W. Boettcher, Oxygen Evolution Reaction Electrocatalysis on Transition Metal Oxides and (Oxy)hydroxides: Activity Trends and Design Principles, *Chem. Mater.*, 2015, **27**, 7549-7558.
15. M. García-Mota, M. Bajdich, V. Viswanathan, A. Vojvodic, A. T. Bell and J. K. Nørskov, Importance of Correlation in Determining Electrocatalytic Oxygen Evolution Activity on Cobalt Oxides, *J. Phys. Chem. C*, 2012, **116**, 21077-21082.

16. Y. Zhao, X. Jia, G. Chen, L. Shang, G. I. N. Waterhouse, L.-Z. Wu, C.-H. Tung, D. O'Hare and T. Zhang, Ultrafine NiO Nanosheets Stabilized by TiO2 from Monolayer NiTi-LDH Precursors: An Active Water Oxidation Electrocatalyst, *J. Am. Chem. Soc.*, 2016, **138**, 6517-6524.
17. M. Gong, Y. Li, H. Wang, Y. Liang, J. Z. Wu, J. Zhou, J. Wang, T. Regier, F. Wei and H. Dai, An Advanced Ni–Fe Layered Double Hydroxide Electrocatalyst for Water Oxidation, *J. Am. Chem. Soc.*, 2013, **135**, 8452-8455.
18. M. S. Burke, M. G. Kast, L. Trotochaud, A. M. Smith and S. W. Boettcher, Cobalt–Iron (Oxy)hydroxide Oxygen Evolution Electrocatalysts: The Role of Structure and Composition on Activity, Stability, and Mechanism, *J. Am. Chem. Soc.*, 2015, **137**, 3638-3648.
19. L. Trotochaud, S. L. Young, J. K. Ranney and S. W. Boettcher, Nickel–Iron Oxyhydroxide Oxygen-Evolution Electrocatalysts: The Role of Intentional and Incidental Iron Incorporation, *J. Am. Chem. Soc.*, 2014, **136**, 6744-6753.
20. Y. Li, H. Wang, L. Xie, Y. Liang, G. Hong and H. Dai, MoS2 Nanoparticles Grown on Graphene: An Advanced Catalyst for the Hydrogen Evolution Reaction, *J. Am. Chem. Soc.*, 2011, **133**, 7296-7299.
21. V. Kiran, D. Mukherjee, R. N. Jenjeti and S. Sampath, Active guests in the MoS2/MoSe2 host lattice: efficient hydrogen evolution using few-layer alloys of MoS2(1-x)Se2x, *Nanoscale*, 2014, **6**, 12856-12863.
22. C. Di Giovanni, W.-A. Wang, S. Nowak, J.-M. Grenèche, H. Lecoq, L. Mouton, M. Giraud and C. Tard, Bioinspired Iron Sulfide Nanoparticles for Cheap and Long-Lived Electrocatalytic Molecular Hydrogen Evolution in Neutral Water, *ACS Catal.*, 2014, **4**, 681-687.
23. A. T. Swesi, J. Masud and M. Nath, Nickel selenide as a high-efficiency catalyst for oxygen evolution reaction, *Energy Environ. Sci.*, 2016, **9**, 1771-1782.
24. J. Masud, A. T. Swesi, W. P. R. Liyanage and M. Nath, Cobalt Selenide Nanostructures: An Efficient Bifunctional Catalyst with High Current Density at Low Coverage, *ACS Appl. Mater. Interfaces*, 2016, **8**, 17292-17302.
25. T. Liu, Q. Liu, A. M. Asiri, Y. Luo and X. Sun, An amorphous CoSe film behaves as an active and stable full water-splitting electrocatalyst under strongly alkaline conditions, *Chem. Commun.*, 2015, **51**, 16683-16686.

26. P. Chen, K. Xu, Y. Tong, X. Li, S. Tao, Z. Fang, W. Chu, X. Wu and C. Wu, Cobalt nitrides as a class of metallic electrocatalysts for the oxygen evolution reaction, *Inorg Chem Front*, 2016, **3**, 236-242.
27. P. Chen, K. Xu, Z. Fang, Y. Tong, J. Wu, X. Lu, X. Peng, H. Ding, C. Wu and Y. Xie, Metallic Co4N Porous Nanowire Arrays Activated by Surface Oxidation as Electrocatalysts for the Oxygen Evolution Reaction, *Angew. Chem. Int. Ed.*, 2015, **54**, 14710-14714.
28. K. Xu, P. Chen, X. Li, Y. Tong, H. Ding, X. Wu, W. Chu, Z. Peng, C. Wu and Y. Xie, Metallic Nickel Nitride Nanosheets Realizing Enhanced Electrochemical Water Oxidation, *J. Am. Chem. Soc.*, 2015, **137**, 4119-4125.
29. E. J. Popczun, J. R. McKone, C. G. Read, A. J. Biacchi, A. M. Wiltrout, N. S. Lewis and R. E. Schaak, Nanostructured Nickel Phosphide as an Electrocatalyst for the Hydrogen Evolution Reaction, *J. Am. Chem. Soc.*, 2013, **135**, 9267-9270.
30. S. Anantharaj, P. N. Reddy and S. Kundu, Core-Oxidized Amorphous Cobalt Phosphide Nanostructures: An Advanced and Highly Efficient Oxygen Evolution Catalyst, *Inorg. Chem.*, 2017, **56**, 1742-1756.
31. A. Dutta, A. K. Samantara, S. K. Dutta, B. K. Jena and N. Pradhan, Surface-Oxidized Dicobalt Phosphide Nanoneedles as a Nonprecious, Durable, and Efficient OER Catalyst, *ACS Energy Lett.*, 2016, **1**, 169-174.
32. L.-A. Stern, L. Feng, F. Song and X. Hu, Ni2P as a Janus catalyst for water splitting: the oxygen evolution activity of Ni_2P nanoparticles, *Energy Environ. Sci.*, 2015, **8**, 2347-2351.
33. C.-C. Hou, S. Cao, W.-F. Fu and Y. Chen, Ultrafine CoP Nanoparticles Supported on Carbon Nanotubes as Highly Active Electrocatalyst for Both Oxygen and Hydrogen Evolution in Basic Media, *ACS Appl. Mater. Interfaces*, 2015, **7**, 28412-28419.
34. X.-Y. Yu, Y. Feng, B. Guan, X. W. Lou and U. Paik, Carbon coated porous nickel phosphides nanoplates for highly efficient oxygen evolution reaction, *Energy Environ. Sci.*, 2016, **9**, 1246-1250.
35. J. Yu, Q. Li, N. Chen, C.-Y. Xu, L. Zhen, J. Wu and V. P. Dravid, Carbon-Coated Nickel Phosphide Nanosheets as Efficient Dual-Electrocatalyst for Overall Water Splitting, *ACS Appl. Mater. Interfaces*, 2016, **8**, 27850-27858.

36. P. Xiao, W. Chen and X. Wang, A Review of Phosphide-Based Materials for Electrocatalytic Hydrogen Evolution, *Adv. Energy Mater.*, 2015, **5**, 1500985-1500997.

37. T. Wu, M. Pi, D. Zhang and S. Chen, 3D structured porous CoP3 nanoneedle arrays as an efficient bifunctional electrocatalyst for the evolution reaction of hydrogen and oxygen, *J. Mater. Chem. A*, 2016, **4**, 14539-14544.

38. J. Kibsgaard, C. Tsai, K. Chan, J. D. Benck, J. K. Norskov, F. Abild-Pedersen and T. F. Jaramillo, Designing an improved transition metal phosphide catalyst for hydrogen evolution using experimental and theoretical trends, *Energy Environ. Sci.*, 2015, **8**, 3022-3029.

39. A. Dutta and N. Pradhan, Developments of Metal Phosphides as Efficient OER Precatalysts, *J. Phys. Chem. Lett.*, 2017, **8**, 144-152.

40. Y. Feng, X.-Y. Yu and U. Paik, Nickel cobalt phosphides quasi-hollow nanocubes as an efficient electrocatalyst for hydrogen evolution in alkaline solution, *Chem. Commun.*, 2016, **52**, 1633-1636.

41. S. Fu, C. Zhu, J. Song, M. H. Engelhard, X. Li, D. Du and Y. Lin, Highly Ordered Mesoporous Bimetallic Phosphides as Efficient Oxygen Evolution Electrocatalysts, *ACS Energy Lett.*, 2016, **1**, 792-796.

42. K. S. Krishna, C. S. S. Sandeep, R. Philip and M. Eswaramoorthy, Mixing Does the Magic: A Rapid Synthesis of High Surface Area Noble Metal Nanosponges Showing Broadband Nonlinear Optical Response, *ACS Nano*, 2010, **4**, 2681-2688.

43. S. Maity and M. Eswaramoorthy, Ni-Pd bimetallic catalysts for the direct synthesis of H_2O_2 - unusual enhancement of Pd activity in the presence of Ni, *J. Mater. Chem. A*, 2016, **4**, 3233-3237.

44. E. J. Popczun, C. G. Read, C. W. Roske, N. S. Lewis and R. E. Schaak, Highly Active Electrocatalysis of the Hydrogen Evolution Reaction by Cobalt Phosphide Nanoparticles, *Angew. Chem. Int. Ed.*, 2014, **53**, 5427-5430.

45. Q. Liu, J. Tian, W. Cui, P. Jiang, N. Cheng, A. M. Asiri and X. Sun, Carbon Nanotubes Decorated with CoP Nanocrystals: A Highly Active Non-Noble-Metal Nanohybrid Electrocatalyst for Hydrogen Evolution, *Angew. Chem.*, 2014, **126**, 6828-6832.

46. S. Cao, Y. Chen, C.-C. Hou, X.-J. Lv and W.-F. Fu, Cobalt phosphide as a highly active non-precious metal cocatalyst for photocatalytic hydrogen production under visible light irradiation, *J. Mater. Chem. A*, 2015, **3**, 6096-6101.

47. J. Tian, Q. Liu, A. M. Asiri and X. Sun, Self-Supported Nanoporous Cobalt Phosphide Nanowire Arrays: An Efficient 3D Hydrogen-Evolving Cathode over the Wide Range of pH 0–14, *J. Am. Chem. Soc.*, 2014, **136**, 7587-7590.

48. M. Liu and J. Li, Cobalt Phosphide Hollow Polyhedron as Efficient Bifunctional Electrocatalysts for the Evolution Reaction of Hydrogen and Oxygen, *ACS Appl. Mater. Interfaces*, 2016, **8**, 2158-2165.

49. C. D. Wagner, G. Muilenberg, L. E. Davis, J. F. Moulder and G. E.Muilenberg, *Handbook of X-Ray Photoelectron Spectroscopy; Perkin Elmer: Eden Prairie*, 1979.

50. Y. Li, J. Liu, C. Chen, X. Zhang and J. Chen, Preparation of NiCoP Hollow Quasi-Polyhedra and Their Electrocatalytic Properties for Hydrogen Evolution in Alkaline Solution, *ACS Appl. Mater. Interfaces*, 2017, **9**, 5982-5991.

51. Z. Yao, G. Wang, Y. Shi, Y. Zhao, J. Jiang, Y. Zhang and H. Wang, One-step synthesis of nickel and cobalt phosphide nanomaterials via decomposition of hexamethylenetetramine-containing precursors, *Dalton Trans.*, 2015, **44**, 14122-14129.

52. W. Cui, Q. Liu, Z. Xing, A. M. Asiri, K. A. Alamry and X. Sun, MoP nanosheets supported on biomass-derived carbon flake: One-step facile preparation and application as a novel high-active electrocatalyst toward hydrogen evolution reaction, *Appl. Catal., B*, 2015, **164**, 144-150.

53. Y. Pan, Y. Chen, Y. Lin, P. Cui, K. Sun, Y. Liu and C. Liu, Cobalt nickel phosphide nanoparticles decorated carbon nanotubes as advanced hybrid catalysts for hydrogen evolution, *J. Mater. Chem. A*, 2016, **4**, 14675-14686.

54. C. Wang, J. Jiang, T. Ding, G. Chen, W. Xu and Q. Yang, Monodisperse Ternary NiCoP Nanostructures as a Bifunctional Electrocatalyst for Both Hydrogen and Oxygen Evolution Reactions with Excellent Performance, *Adv. Mater. Int.*, 2016, **3**, 1500454-1500458.

55. A. Han, H. Zhang, R. Yuan, H. Ji and P. Du, Crystalline Copper Phosphide Nanosheets as an Efficient Janus Catalyst for Overall Water Splitting, *ACS Appl. Mater. Interfaces*, 2017, **9**, 2240-2248.

56. J. Chang, Y. Xiao, M. Xiao, J. Ge, C. Liu and W. Xing, Surface Oxidized Cobalt-Phosphide Nanorods As an Advanced Oxygen Evolution Catalyst in Alkaline Solution, *ACS Catal.*, 2015, **5**, 6874-6878.

57. T. Zhang, J. Du, P. Xi and C. Xu, Hybrids of Cobalt/Iron Phosphides Derived from Bimetal–Organic Frameworks as Highly Efficient Electrocatalysts for Oxygen Evolution Reaction, *ACS Appl. Mater. Interfaces*, 2017, **9**, 362-370.

58. J. Ryu, N. Jung, J. H. Jang, H.-J. Kim and S. J. Yoo, In Situ Transformation of Hydrogen-Evolving CoP Nanoparticles: Toward Efficient Oxygen Evolution Catalysts Bearing Dispersed Morphologies with Co-oxo/hydroxo Molecular Units, *ACS Catal.*, 2015, **5**, 4066-4074.

59. A. Han, H. Chen, Z. Sun, J. Xu and P. Du, High catalytic activity for water oxidation based on nanostructured nickel phosphide precursors, *Chem. Commun.*, 2015, **51**, 11626-11629.

60. D. E. Schipper, Z. Zhao, A. P. Leitner, L. Xie, F. Qin, M. K. Alam, S. Chen, D. Wang, Z. Ren, Z. Wang, J. Bao and K. H. Whitmire, A TiO_2/FeMnP Core/Shell Nanorod Array Photoanode for Efficient Photoelectrochemical Oxygen Evolution, *ACS Nano*, 2017, **11**, 4051-4059.

61. C. Xuan, J. Wang, W. Xia, Z. Peng, Z. Wu, W. Lei, K. Xia, H. L. Xin and D. Wang, Porous Structured Ni–Fe–P Nanocubes Derived from a Prussian Blue Analogue as an Electrocatalyst for Efficient Overall Water Splitting, *ACS Appl. Mater. Interfaces*, 2017, **9**, 26134-26142.

62. D. Xiong, X. Wang, W. Li and L. Liu, Facile synthesis of iron phosphide nanorods for efficient and durable electrochemical oxygen evolution, *Chem. Commun.*, 2016, **52**, 8711-8714.

63. J. Wang, W. Yang and J. Liu, CoP_2 nanoparticles on reduced graphene oxide sheets as a super-efficient bifunctional electrocatalyst for full water splitting, *J. Mater. Chem. A*, 2016, **4**, 4686-4690.

64. J. D. Costa, J. L. Lado, E. Carbó-Argibay, E. Paz, J. Gallo, M. F. Cerqueira, C. Rodríguez-Abreu, K. Kovnir and Y. V. Kolen'ko, Electrocatalytic Performance and Stability of Nanostructured Fe–Ni Pyrite-Type Diphosphide Catalyst Supported on Carbon Paper, *J. Phys. Chem. C*, 2016, **120**, 16537-16544.

Chapter-6

High surface area Ni containing Pd nanostructure: Pt like activity for hydrogen evolution and oxygen reduction reactions

Summary:

We report a novel approach for rapid synthesis of NiPd nanostructure by simple $NaBH_4$ reduction followed by quick dissolution in HCl and H_2O_2. The NiPd catalyst shows a very high surface area of 136 m^2 gm^{-1} and excellent catalytic performance for both hydrogen evolution and oxygen reduction reactions. The catalyst requires only 39 mV overpotential at current density, 10 mA cm^{-2} with a Tafel slope 32 mV dec^{-1} which is almost equivalent to the state-of-the-art Pt/C catalyst.

6.1. Introduction:

Synthesis of noble metal nanostructures of high surface area has generated a great deal of interest owing to their potential applications in fuel cells,[1-3] catalysis,[4-6] sensors[7, 8] and membranes.[9] Among all, Pd based nanostructures have attracted much attention for their role as a catalyst in many industrially important chemical reactions.[10-14] In recent years, Pd is increasingly being recognized as a better alternative to high cost platinum electrocatalyst used for hydrogen evolution reaction (HER)[15-19] and oxygen reduction reaction (ORR),[19-21] the most indispensable processes in the renewable energy technologies, water electrolysis and fuel cell respectively. However, the performance of Pd based catalysts for electrochemical HER and ORR is far lower than Pt[3, 18, 19, 22, 23] and a lot of efforts are being made to improve their activity by manipulating its size, structure, surface area and electronic properties. [21, 24-26]

For example, the presence of secondary elements like Ni, Cu etc. are known to modify the electronic structure of Pd which in turn influences its catalytic properties.[12, 14] The electrocatalytic activity of Pd could also be enhanced by having high surface area and porous nanostructures as they provide large number of active sites and effective mass transport at the electrode-electrolyte interface. Mass transport is an important parameter for electrochemical activity and materials with wider pores would result in unaided transport of adsorbate towards or away from the electrode-electrolyte interfaces resulting in effective utilization of active sites located deep inside the catalysts.[27-29]

Herein, we report a new and scalable method to make Pd nanostructures with remarkably high surface area and porosity incorporated with little amount of transition metal, nickel, to modify its electronic structure. High surface area Pd nanostructure was synthesized by a modified procedure reported by us earlier[14] by reducing the Pd and Ni salt precursor with sodium borohydride solution, $NaBH_4$, followed by a quick dissolution (less than 2 minutes) in HCl/H_2O_2 mixture. The assynthesized nickel containing (6wt%<) Pd nanostructure shows extraordinary high surface area of 136 $m^2\ gm^{-1}$, the highest ever reported so far and a benchmarking performance for both hydrogen evolution reaction (HER) and oxygen reduction reaction(ORR) on par with platinum. The catalyst requires only 39 mV overpotential for HER at current density, 10 mA cm^{-2} with a Tafel slope 32 mV dec^{-1} which is almost equivalent to the state-of-the-art catalyst Pt/C.

6.2. Scope of the Present Study:

Drastic increase in the world population is leading to the rapid depletion of existing fossil fuels. Water splitting, fuel cell technologies and electrochemical energy storage have recently been drawn a huge attraction as promising and efficient future energy applications. Noble metal, Pt has been studied extensively as the best electrocatalyst for electrochemical reactions but the high cost inhibits its global application. Developing low cost catalysts is highly necessitated for widespread and commercial applications. In this chapter, we have demonstrated the synthesis of high surface area nickel containing Pd (abbreviated as NiPd) catalyst which showed Pt-like activity for HER and ORR.

6.3. Experimental Section:

6.3.1. Materials and Characterization Techniques:

$PdCl_2$ (Sigma Aldrich), $NiCl_2.6H_2O$ (S D Fine Chemicals), $NaBH_4$ (S D Fine Chemicals), H_2O_2 (S D Fine Chemicals, AR grade), KOH (Merck Chemicals), H_2SO_4 (98%, AR grade), HCl (37%, AR grade) were used as received without any further purification.

Powder X-ray diffraction (PXRD) patterns were recorded using Bruker-D8 diffractometer using Cu Kα radiation, (λ=1.54 Å, step size: 0.02, current: 30 mA and voltage: 40 kV). Field-emission scanning electron microscopy (FESEM) images and energy-dispersive X-ray spectroscopy (EDS) were obtained by using FEI (Nova-Nano SEM-600 Netherlands) equipment. Transmission electron microscope (TEM) imaging was done using Technai F30 UHR electron microscope operating at an accelerating voltage of 200 kV. Samples were prepared by putting a drop of very dilute dispersion in ethanol on a TEM grid (carbon polymer, 300 mesh). Inductively coupled plasma – atomic emission spectroscopy (ICP-AES) was carried out using a Perkin−Elmer Optima 7000 DV machine. X-ray photoelectron spectroscopy (XPS) has been performed using Omicron EA 125 spectrometer with Al K_α (1486.6 eV) source. Gas adsorption-desorption measurements were performed on Autosorb-iQ2 (Quantachrome corp.) at 77 K. The samples were degassed before starting the nitrogen gas sorption analysis under a high vacuum for 12 h at 373 K. Electrochemical measurements were carried out using electrochemical work station obtained from CH instruments (660C, USA) for evaluating the electrochemical activities

of the catalysts for hydrogen evolution reaction (HER) and oxygen reduction reaction (ORR).

6.3.2. Synthesis of NiPd Nanostructure Catalyst:

NiPd nanostructure was prepared by the reduction of aqueous metal chloride solution by $NaBH_4$ at room temperature followed by acid etching in presence of HCl and H_2O_2. H_2O_2 was used to increase the rate of acid etching.[14, 30] In the first step $Ni_{0.8}Pd_{0.2}$ (number indicates the wt. % of respective metal) was synthesized and then etching was done to remove unwanted hydroxide/oxyhydroxide species of nickel to get NiPd nanostructure which contains 6 wt. % Ni confirmed by ICP-AES analyses.

In a typical procedure, 27.26 mL 0.1 M aqueous solution of $NiCl_2.6H_2O$ and 3.76 mL 0.1 M aqueous solution of $PdCl_2$ solution was rapidly added to 150 mL of 0.1 M aqueous solution of freshly prepared $NaBH_4$ with vigorous stirring. The black coloured dispersion was stirred for 20 min. The solid product was separated and washed thoroughly with distilled water. The solid product was transferred to 120 mL 0.1 M HCl followed by the addition of 2 mL H_2O_2 (28%, commercially available). The dispersion was stirred for another 2 min and the solid product was separated quickly by decantation. Finally, it was washed several times with distilled water and dried at 40 ^oC for overnight. It is important to note that, the acid leaching should be carried out only for a very short time if there is no insitu flow of hydrogen. Otherwise, palladium will be leached out into the solution in addition to Ni and $Ni(OH)_2$. Similarly Pd nanostructure without nickel was also synthesized by the reduction of $PdCl_2$ (no addition of nickel salt) in presence of $NaBH_4$ following the same procedure.

6.3.3. Electrochemical Measurements:

To prepare the catalyst ink, 2 mg of electrocatalyst was dispersed in a mixture of mili Q water (0.8 mL) and isopropanol (0.2 mL) containing 10 μL of 5 wt. % nafion solution and ultrasonicated for 1 h to obtain a homogeneous dispersion. Then, 5 μL of the catalyst ink was drop casted on a cleaned glassy carbon (GC) electrode having 3 mm diameter (for hydrogen evolution reaction (HER)) resulting a catalyst loading of ~0.14 mg cm^{-2}. The GC electrode was dried in ambient conditions and used as working electrode in the

electrochemical studies. For oxygen reduction reaction (ORR), rotating disk electrode (RDE) having 3 mm diameter was used.

Electrochemical measurements were carried out using a standard three-electrode cells using a graphite rod having large area as a counter electrode and a saturated calomel electrode (SCE) as reference electrode in acidic medium (0.5 M H_2SO_4) for HER activity and mercury-mercuric oxide (Hg/HgO) electrode as a reference electrode in basic medium (0.1 M KOH) for ORR activity. All the polarization curves were recorded after the correction of iR compensation arising due to ohmic resistance of the cell. The measured potentials vs. SCE or Hg/HgO were calibrated with respect to reversible hydrogen electrode (RHE). The obtained current densities were normalized to the geometrical surface area of the GC electrode. The linear sweep voltammograms (LSVs) for HER performance were recorded in 0.5 M H_2SO_4 at 5 mV s^{-1} under argon (Ar) gas saturated aqueous electrolytes. Similarly, the LSVs for ORR performance were recorded in 0.1 M KOH at 5 mV s^{-1} with different rotations under O_2 saturated conditions. Cyclic voltammograms (CVs) were recorded under Ar saturated conditions at different scan rates (20-200 mV s^{-1}) within the potential range from 0.35 to 0.6 V (vs. RHE) in order to evaluate electrochemical double layer capacitance (C_{dl}), representing electrochemically active surface area (ECSA).

6.3.4. Calculation of Number of Electron Transfer for ORR:

The number of electron transfer was calculated from Koutecky-Levich equation for oxygen reduction reaction (ORR). The linear sweep voltammograms (LSVs) were recorded on rotating disk electrode at different rotations and these data were used to determine the number of electrons transferred per O_2 molecule.

$$\frac{1}{j} = \frac{1}{j_k} + \frac{1}{j_l} = \frac{1}{j_k} + \frac{1}{B\omega^{1/2}} \quad \text{..... (1)}$$

Where, j is the measured current density, j_k and j_l are kinetic and diffusion limited current densities respectively, ω is the electrode rotation speed and B is the Levich slope determined from Koutecky-Levich equation given below (2):

$$B = 0.62nFC_{O_2}(D_{O_2})^{\frac{2}{3}}\nu^{-\frac{1}{6}} \quad \text{..... (2)}$$

Where, n is the number of electron transferred per O_2 molecule, F is the Faraday constant (96485 C mol^{-1}), C_{O_2} is the bulk concentration of O_2 in the electrolyte (1.2 x 10^{-6} mol cm^{-3}), D_{O_2} is the diffusion coefficient of O_2 (1.9 x 10^{-5} cm^2 s^{-1}) and v is the kinematic viscosity of the electrolyte (0.01 cm^2 s^{-1}). The values are used for an aqueous electrolyte, 0.1 M KOH solution.

6.3.5. Calibration of Reference Electrodes:

The reference electrodes Hg/HgO used in alkaline electrolyte (KOH solution) and SCE used in acidic solution, were calibrated with respect to reversible hydrogen electrode (RHE) using large area Pt foil as a working electrode and long Pt wire as counter electrode. High purity hydrogen gas was purged in the respective solutions for 1 h before the experiments and a constant overhead purge was maintained during the measurements. Cyclic voltammograms were recorded at a scan rate of 1 mV s^{-1} (Figure 5.1)

For 0.1 M KOH, $E_{RHE} = E_{Hg/HgO} + 0.894$ V

For 0.5 M H_2SO_4, $E_{RHE} = E_{SCE} + 0.274$ V

6.4. Results and Discussion:

High surface area NiPd was prepared by the reduction of aqueous metal chloride solution in presence of $NaBH_4$ which has been developed earlier by our group followed by rapid washing in H_2O_2 and HCl solution (details in the experimental section).[14, 30] The washing in presence of H_2O_2 and HCl is very important in order to remove unwanted hydroxide/oxyhydroxide species of nickel which has been used as a sacrificial template to get high surface area of NiPd.[14] Powder X-ray diffraction (PXRD) pattern of NiPd shows the formation of face centred cubic (fcc) structure like Pd (Figure 6.1). The broadening in the diffraction peaks of NiPd signifies the presence of smaller crystallites as compared to Pd alone. The inductively- coupled plasma atomic emission spectroscopy (ICP-AES) analyses shows the presence of 6 wt. % Ni and 94 wt. % Pd in the NiPd nanostructure. The field emission scanning electron microscopy (FESEM) images of Pd (figure 6.2a) and NiPd (Figure 6.2c) show the three dimensional porous network structure formed during the reduction process. The transmission electron microscopy (TEM) image of NiPd shows the

particles having size around 5-15 nm fused together to form spongy network morphology (Figure 6.2d). The high angle annular dark field (HAADF) TEM image of NiPd (Figure 6.2e) shows lattice spacing of 0.22 nm which is similar to that of Pd (111) in pure Pd nanostructure (Figure 6.2b). Electron mapping of NiPd shows uniform dispersion of Ni and Pd throughout the sample (Figure 6.3). N_2 sorption analysis of NiPd carried out at 77 K shows type-II behaviour with very high uptake of N_2 at higher P/P_o (Figure 6.4a) and the pore size distribution calculate using BJH (Barrett-Joyner-Halenda) method shows the pore size range of 4 to 15 nm (Figure 6.4b) which is in agreement with TEM observation. The Brunauer-Emmett-Teller (BET) surface area calculated from N_2 isotherm was found to be 136 $m^2\ g^{-1}$ for NiPd nanostructure which is the highest one among all the noble metal nanostructures reported so far. Considering the mass ratio of Pd to SiO_2, the surface area will be about 240 $m^2\ g^{-1}$ which is quite significant.

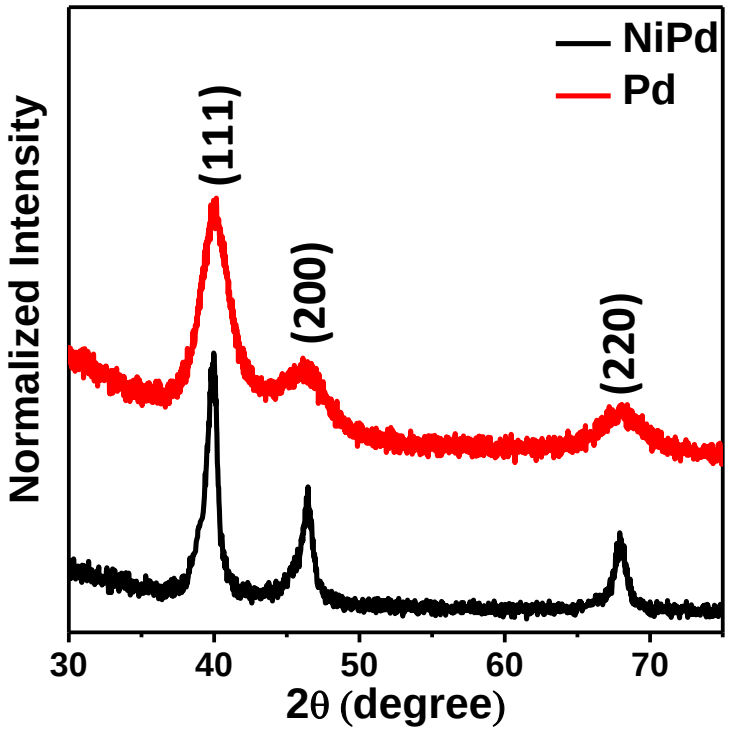

Figure 6.1: *Powder X-ray diffraction (PXRD) pattern of NiPd and Pd.*

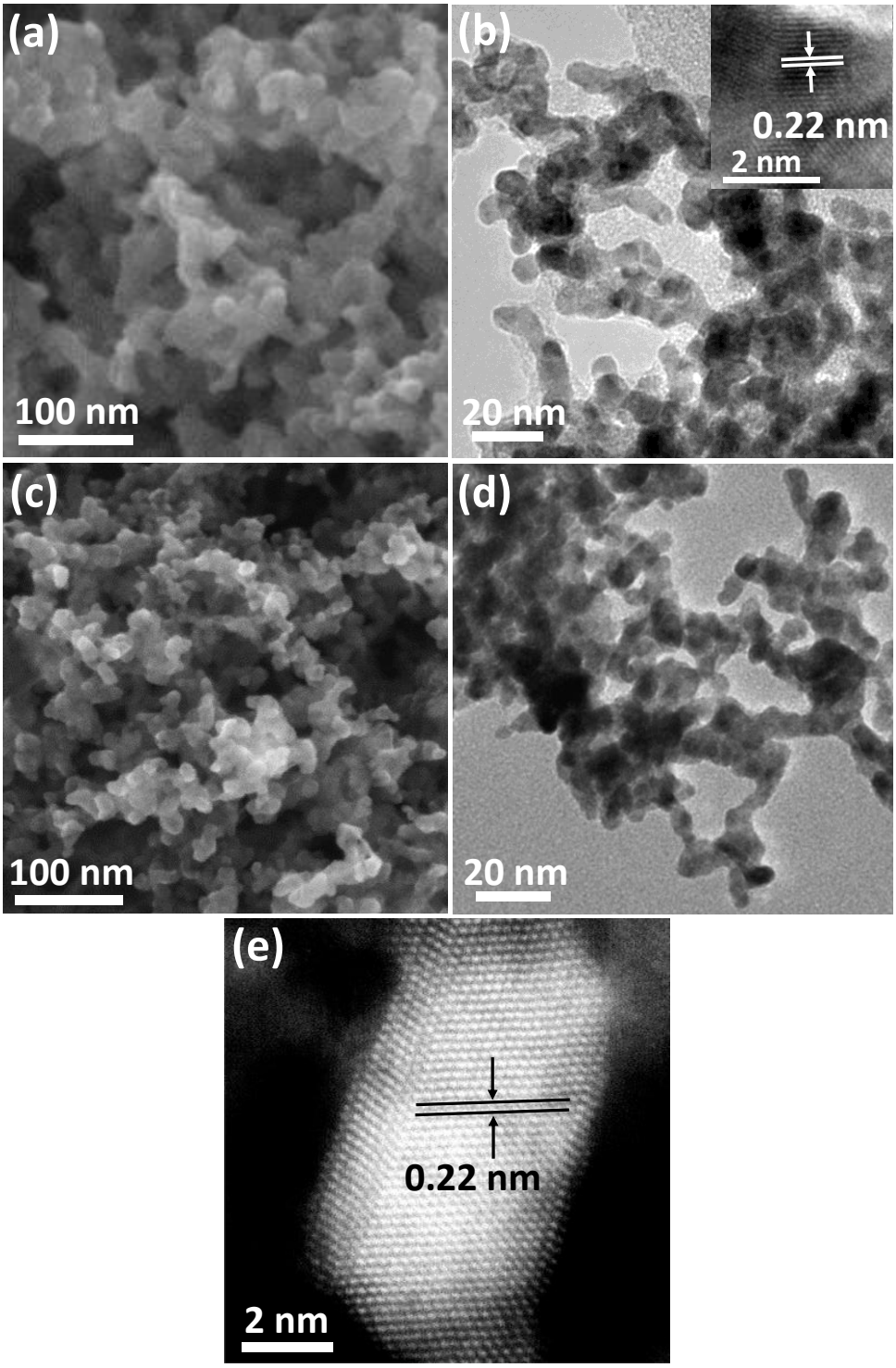

Figure 6.2: *(a) Field emission scanning electron microscopy (FESEM) and (b) transmission electron microscopy (TEM) images of image of Pd nanostructure. Inset of (b) shows the high-resolution TEM (HRTEM) of Pd. (c) FESEM and (d) TEM images of NiPd. (e) High angle annular dark-field (HAADF) image of NiPd.*

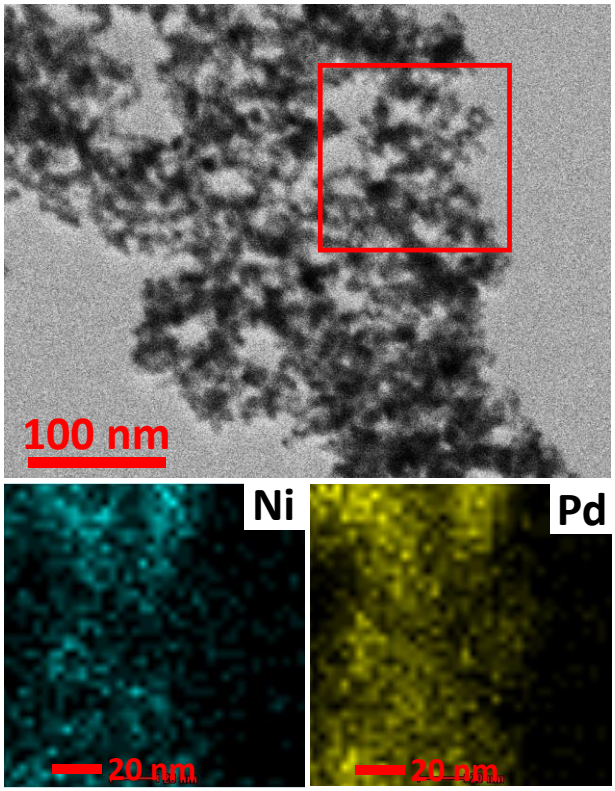

Figure 6.3: *TEM image of NiPd and the corresponding elemental mapping of Ni and Pd.*

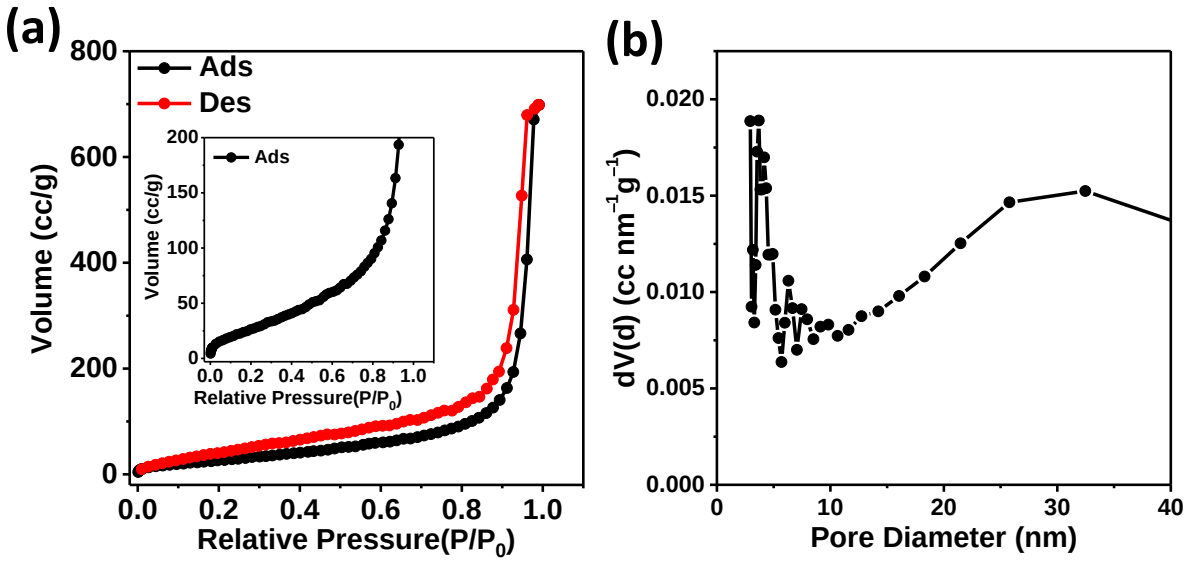

Figure 6.4: *(a) N_2 adsorption-desorption isotherm of NiPd measured at 77 K and (b) corresponding pore size distribution of NiPd analyzed using BJH method from (a). Inset of (a) shows the enlarged view of adsorption.*

The HER performance for all the catalysts was carried out using standard three electrode set up with a mass loading of ~0.14 mg cm^{-2} on glassy carbon as a working electrode and high surface area graphite rod as a counter electrode in 0.5 M aqueous H_2SO_4 solution.

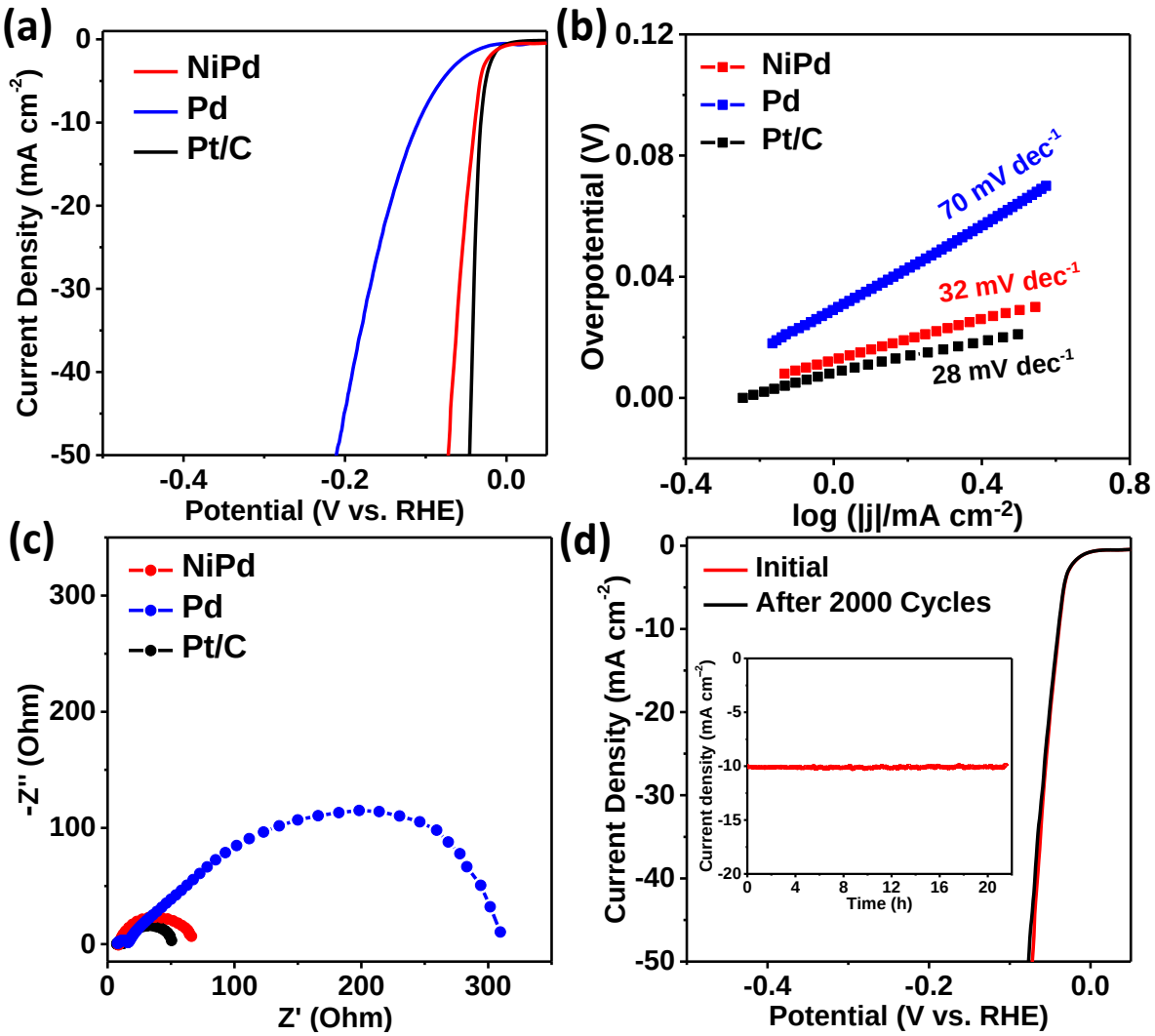

Figure 6.5: *(a) The polarized linear sweep voltammograms of different catalysts for evaluating HER activity at 5 mV s^{-1} after iR compensation in 0.5 M H_2SO_4 solution. (b) Corresponding Tafel analyses extracted from (a), compared with the state-of-the-art Pt/C catalyst. (c) Nyquist plots of all the electrocatalysts at their respective onset potentials. (d) Stability performance of NiPd catalyst before and after 2000 cycles indicating stable performance. Inset shows chronoamperometry (the current density vs time plot) for the same catalyst.*

Polarized linear sweep voltammograms (LSVs) (Figure 6.5a) of Pd and NiPd nanostructures were studied at 5 mV s^{-1} under Ar saturated conditions and their electrocatalytic activity was compared with state-of-the-art commercial catalyst, 40 wt.% Pt/C. The HER polarization curve shows one of the best performances for NiPd catalyst that requires an onset overpotential (η) of 8 mV which is almost comparable to that of Pt. To achieve a cathodic current density at 10 mA cm^{-2}, NiPd needs an overpotential of only 39 mV which is far lower than monometallic Pd (η = 110 mV) and similar to Pt catalyst (η = 33 mV). NiPd nanostructure shows one of the best HER performances like Pt among all other Pd-based or transition metal based catalysts reported so far in the literature (Table 6.1). In order to understand the HER kinetics, Tafel analysis has been carried out in the kinetically controlled region (Figure 6.5b) and the NiPd catalyst shows lower Tafel slope of 32 mV dec^{-1}, a value far lower than Pd (70 mV dec^{-1}) and is comparable to that of Pt (28 mV dec^{-1}) signifying the faster charge transfer kinetics in Volmer-Tafel reaction pathway.[15, 17, 31, 32] Furthermore, electrochemical impedance spectroscopy (EIS) analyses (Figure 6.5c) were carried out at their respective onset potentials to understand the interfacial charge transfer phenomenon and as expected, NiPd shows lower charge transfer resistance (R_{ct}) than Pd indicating facile electron transfer at the electrode-electrolyte interfaces. Moreover, the catalyst shows excellent stability over 2000 cycles after accelerated cyclic testing (Figure 6.5d) and there is hardly any loss in current density @10 mA cm^{-2} at fixed potential over 22 h (inset of Figure 6.5d) indicating a very good performance for long term electrochemical applications.

Table 6.1: *Comparison in HER activity for different metal catalysts in acidic medium:*

Catalyst	Catalyst Loading on the Electrode (mg cm^{-2})	Overpotential at @10 mA cm^{-2} (mV)	Tafel Slope (mV dec^{-1})	**References**
NiPd	**0.14**	**-39**	**32**	**Present Study**
PdPS	2.5	-90	46	17
Pd_4Se	0.2	-94	57	16

PdCu	0.28	-50	34	33
Pd_2Si	1	-192	131	34
WS_2 nanoflakes	0.35	~-410	48	35
MoS_2/rGO	0.28	-150	41	36
Mo_2C	1.4	-210	56	37
MoB	2.5	-240	55	37
CoS_2/RGO-CNT	1.15	-142	51	38
Ni_2P	1	-130 @20 mA cm^{-2}	46	39
MoP	0.86	~-150	54	40
C@Ni_8P_3	___	-110	46	41
Ni_8P_3	___	-152	86	41
Ni_5P_4-Ni_2P Nanosheet	0.283	-120	79.1	42
Co/CoP	___	-135	66	43
Cu_3P	15.2	-143	67	44

The electrochemical activity towards ORR for NiPd catalyst was also carried out in O_2 saturated 0.1 M aqueous KOH solution using high surface area graphite rod as counter electrode in standard three electrode set up and compared its activity with the state-of-the-art catalyst, 40 wt.% Pt/C. The cyclic voltammogram (CV) of NiPd shows the prominent oxygen reduction peak in O_2 saturated solution which is absent for Ar saturated conditions (Figure 6.6). The polarized linear sweep voltammograms (LSVs) of NiPd catalyst (Figure 6.7a) at rotating disk electrode (RDE, 3 mm diameter) with a mass loading of 0.14 mg cm^{-2} shows the onset potential of 0.91 V (vs. RHE) which is nearly close to that of Pt (0.97 V vs. RHE). The limiting current densities at lower potential region is more for NiPd as compared to monometallic Pd and Pt/C catalyst. The ORR activity of NiPd catalysts is better than other literature reports and also equivalent to the Pt/C catalyst (Table 6.2).

Further to investigate the kinetics and mechanism for ORR, the LSVs were recorded at different rotations which shows increase in current densities at the limiting regions with increase of rotation speed (Figure 6.7b, 6.8a and 6.8c). The Koutecky-Levich (K-L) plots[45, 46] between j^{-1} (mA^{-1} cm^2) vs. $w^{-1/2}$ (r. p. $s.^{-1/2}$) (details in the experimental section) extracted from the LSVs in the limiting current density regions at different rotation shows the linear relationship (Figure 6.7c, 6.8b and 6.8d). The similar slopes obtained from the K-L plots at different potentials signifies the first order kinetics with respect to dissolved O_2 in the electrolyte solution. The kinetic current density (j_k), a measure of inherent catalytic property of the catalysts, signifies the highest activity for NiPd with j_k of 150 mA cm^{-2} at 0.4 V as compared to Pt/C (63 mA cm^{-2}). The number of electrons (n) transferred per O_2 molecule (at 0.4 V) calculated from the slopes of K-L plots for Pd (n = 4.0) and NiPd (n = 4.2) indicates the efficient $4e^-$ reduction pathway to form OH^- directly from O_2, a pathway similar to the one reported for Pt/C catalyst (Figure 6.7d) used in metal-air

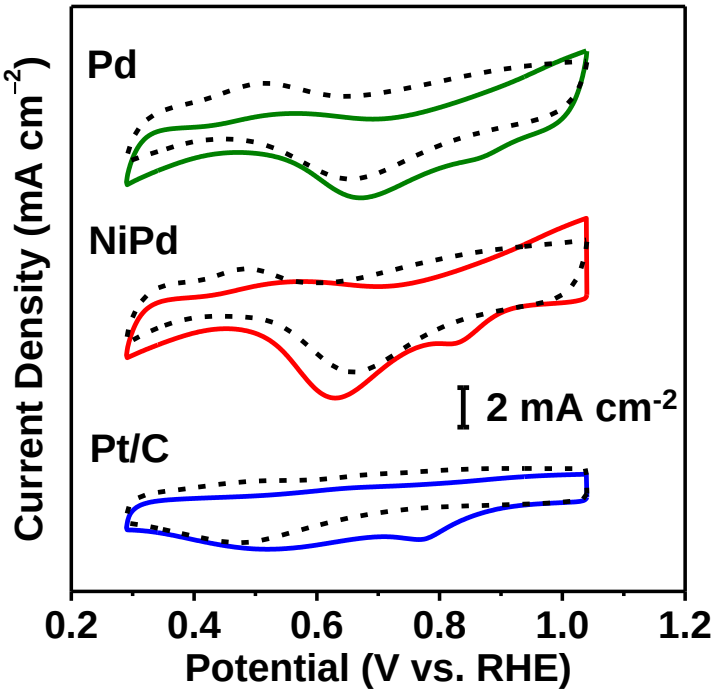

Figure 6.6: *Cyclic voltammograms (CV) of Pd, NiPd and Pt/C in O_2 saturated (solid line) and argon saturated (dashed line) 0.1 M KOH at 50 mV s^{-1}. The broad peak for Pd and NiPd nanostructures around 0.63 V (vs. RHE) arise due to palladium oxide reduction.*

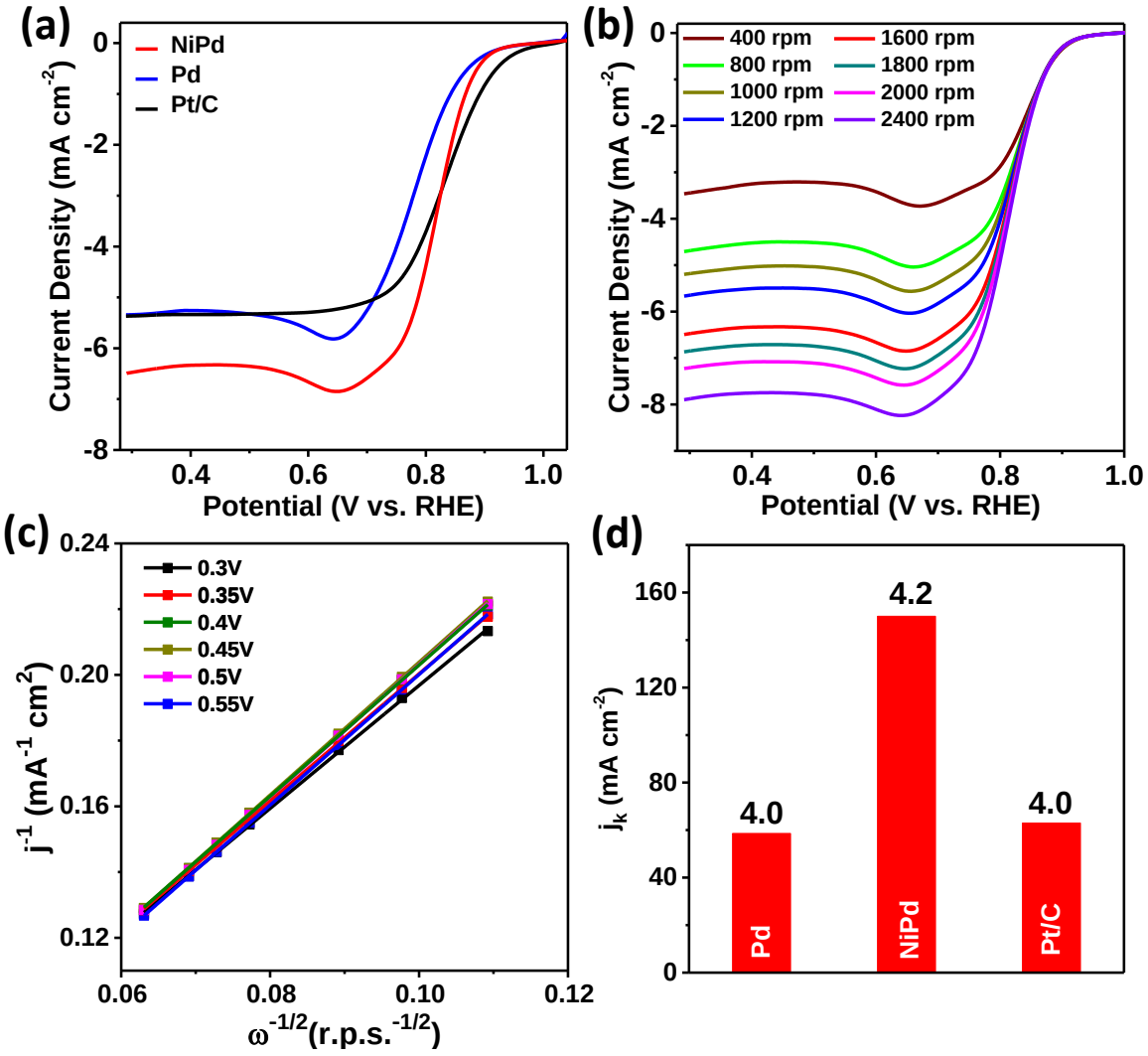

Figure 6.7: *(a) Comparison in linear sweep voltammograms (LSVs) of NiPd, Pd and state-of-the-art Pt/C towards ORR in O_2 saturated 0.1 M KOH at 1600 rpm at 5 mV s^{-1}. (b) Rotating disk electrode (RDE) voltammograms at different rotations for NiPd catalyst in 0.1 M KOH at 5 mV s^{-1}. (c) Koutecky–Levich (K-L) plots extracted from RDE voltammograms for NiPd. (d) The kinetic current density (j_k) along with the number of electrons transferred per O_2 molecule (given on the top of the bar) for Pd, NiPd and Pt/C at 0.4 V.*

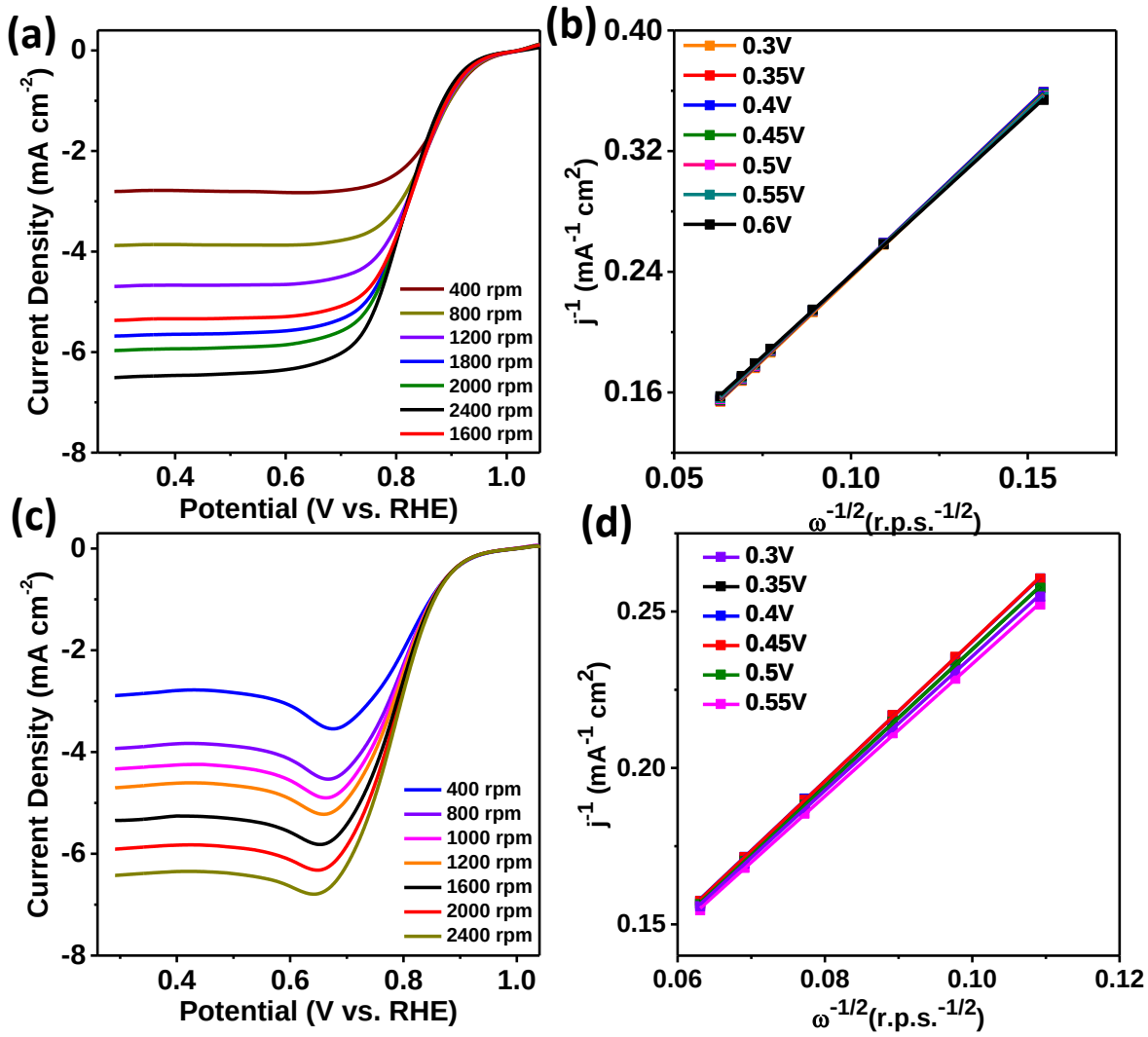

Figure 6.8: *(a) Rotating disk electrode (RDE) voltammograms at different rotations for state-of-the-art Pt/C catalyst in 0.1 M KOH at 5 mV s^{-1} and (b) corresponding Koutecky–Levich (K-L) plots extracted from RDE voltammograms in (a). (c) Rotating disk electrode (RDE) voltammograms of Pd measured in same conditions and (d) corresponding Koutecky–Levich (K-L) plots extracted from (c).*

batteries and fuel cells. In addition, NiPd catalyst is very stable in the reaction conditions and retains its initial ORR activity after 2000 cycles (Figure 6.9) signifying its stability for long term uses. The high activity of NiPd can be attributed to the presence of wide mesopores coupled with unusually high surface area facilitating better mass transports for the electrochemical reactions.

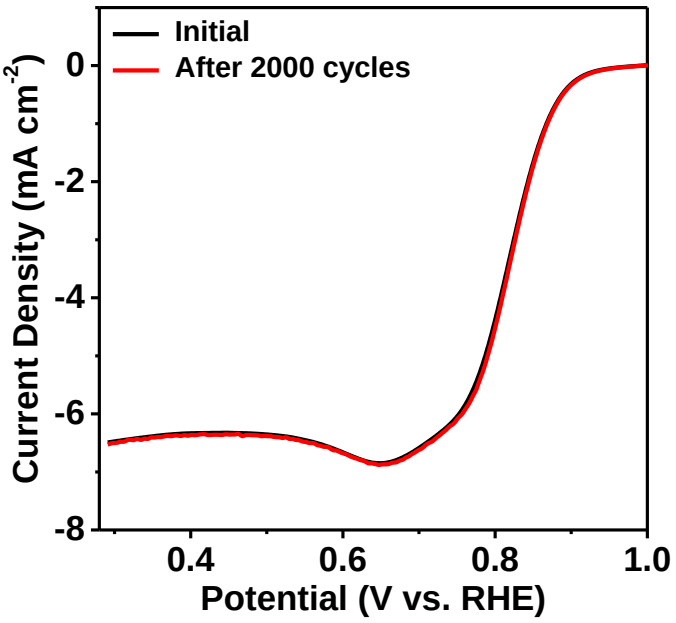

Figure 6.9: *Stability performance of NiPd before and after 2000 cycles for ORR.*

Table 6.2: *Comparison in ORR activity for different catalysts reported in the literature:*

Catalysts	Electrolyte	Onset potential (V vs. RHE)	$E_{1/2}$ potential (V vs. RHE)	References
NiPd nanostructure	**0.1 M KOH**	**0.91**	**0.82**	**Present study**
Pd nanostructure	**0.1 M KOH**	**0.90**	**0.78**	**Present study**
Pt/C commercial	**0.1 M KOH**	**0.97**	**0.82**	**Present study**
Pd bulk	0.1 M KOH	0.860	0.790	47
Pd/C	0.1 M KOH	0.741	0.674	48

AuPd/C	0.1 M NaOH	1.063	0.932	49
Pt/C	0.1 M NaOH	1.048	0.891	49
Pt/C	0.1 M KOH	0.851	0.581	50
Pt/C	0.1 M KOH	0.951	0.906	51
N-doped CNT	0.1 M KOH	~0.981	0.831	52
N-doped CNC	0.1 M KOH	0.851	0.806	51
B-doped CNT	0.1 M KOH	0.848	0.728	52
Graphene	0.1 M KOH	0.831	0.541	52
N-doped graphene	0.1 M KOH	0.964	0.814	52
B-doped graphene	0.1 M KOH	0.851	0.681	52

Electrochemically active surface area (ECSA) for NiPd and Pd nanostructures were calculated by evaluating their double layer capacitance (C_{dl}) in order to understand their catalytic activities. NiPd catalyst showed very high double layer capacitance, 3.3 mF cm^{-2} (Figure 6.10) which is 11 times higher compared to the Pd nanostructure (0.3 mF cm^{-2}) of having BET surface area around 70 m^2 g^{-1} indicating higher number of electrochemically active sites (higher ECSA value). This can be directly correlated to the origin of unusual activity for HER and ORR performance of NiPd than Pd as the former contains high density of catalytically active sites. The efficient HER and ORR activities of NiPd can also be attributed to synergistic effect of Ni present with the Pd in NiPd. Furthermore, the presence of Ni in NiPd leads to the electronically modification of d-orbital of Pd which influences in Fermi level shifting towards lower activation energy as better adsorption sites.[53-56] The presence of Ni in Pd has been already explored for better catalytic activity in electrocatalytic applications and hydrogen peroxide synthesis compared to monometallic Pd.[12, 14] These reports would further support our studies for enhanced electrocatalytic activity of Pd in presence of Ni which would lead to electronic modification of Pd electronic structure.

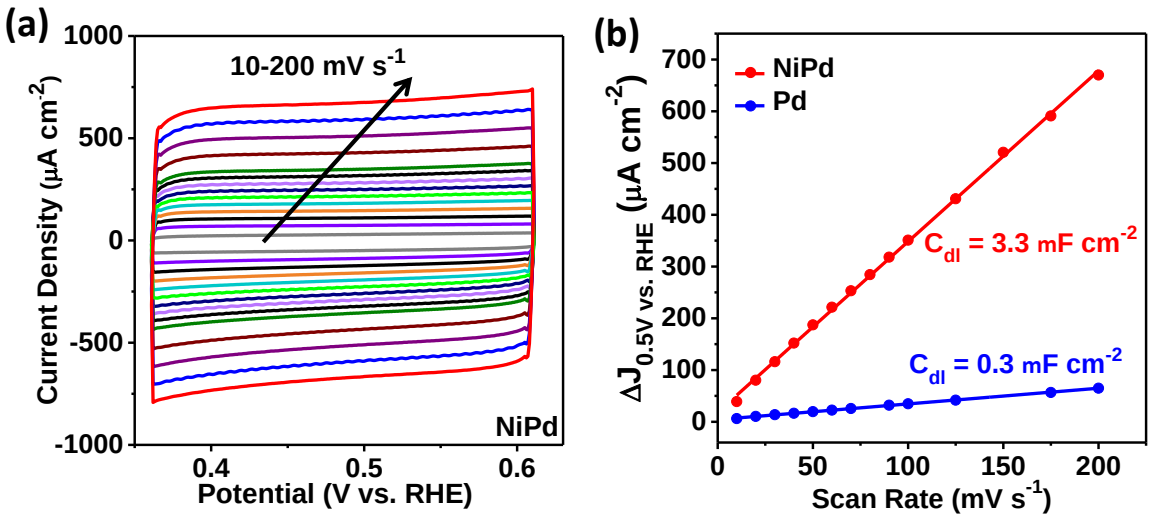

Figure 6.10: *(a) Cyclic voltammograms for NiPd at different scan rates ranging from 10-200 mV* s^{-1}*. (b) Evaluation of the double-layer capacitance (*C_{dl}*) for NiPd and Pd nanostructures at 0.5 V (vs. RHE). Double layer capacitance are calculated from the slopes in (b).*

6.5. Conclusion:

A novel simple and rapid method was developed to synthesize NiPd nanostructure exhibiting very high surface area, 136 m^2 g^{-1} by borohydride reduction method followed by quick dissolution in presence of HCl and H_2O_2. The NiPd catalyst thus obtained shows extraordinary activity and stability towards HER performance in 0.5 M H_2SO_4 solution. The NiPd catalyst also showed Pt-like activity for ORR. The shift in the d-band centre of Pd by electronic modification in presence of Ni leads to the enhancement in the electrocatalytic activity for HER and ORR. The wide mesopores present in NiPd catalyst provides higher number of active sites which aid the mass transport in the electrochemical interfaces and hence lowers the overpotential. The highly active NiPd catalyst could be a promising alternative to Pt for future applications.

6.6. References:

1. B. C. H. Steele and A. Heinzel, Materials for fuel-cell technologies, *Nature*, 2001, **414**, 345.

2. Y. Ding, M. Chen and J. Erlebacher, Metallic Mesoporous Nanocomposites for Electrocatalysis, *J. Am. Chem. Soc.*, 2004, **126**, 6876-6877.
3. L. Zhang, Q. Chang, H. Chen and M. Shao, Recent advances in palladium-based electrocatalysts for fuel cell reactions and hydrogen evolution reaction, *Nano Energy*, 2016, **29**, 198-219.
4. B. Zugic, L. Wang, C. Heine, D. N. Zakharov, B. A. J. Lechner, E. A. Stach, J. Biener, M. Salmeron, R. J. Madix and C. M. Friend, Dynamic restructuring drives catalytic activity on nanoporous gold–silver alloy catalysts, *Nat. Mater.*, 2016, **16**, 558.
5. D. R. Rolison, Catalytic Nanoarchitectures--the Importance of Nothing and the Unimportance of Periodicity, *Science*, 2003, **299**, 1698-1701.
6. C. Zhu, D. Wen, M. Oschatz, M. Holzschuh, W. Liu, A.-K. Herrmann, F. Simon, S. Kaskel and A. Eychmüller, Kinetically Controlled Synthesis of PdNi Bimetallic Porous Nanostructures with Enhanced Electrocatalytic Activity, *Small*, 2015, **11**, 1430-1434.
7. Y.-Y. Song, D. Zhang, W. Gao and X.-H. Xia, Nonenzymatic Glucose Detection by Using a Three-Dimensionally Ordered, Macroporous Platinum Template, *Chem. Eur. J.*, 2005, **11**, 2177-2182.
8. K. Bonroy, J.-M. Friedt, F. Frederix, W. Laureyn, S. Langerock, A. Campitelli, M. Sára, G. Borghs, B. Goddeeris and P. Declerck, Realization and Characterization of Porous Gold for Increased Protein Coverage on Acoustic Sensors, *Anal. Chem.*, 2004, **76**, 4299-4306.
9. A. Pérez Padilla, J. A. Rodríguez and H. A. Saitúa, Synthesis and water ultrafiltration properties of silver membrane supported on porous ceramics, *Desalination*, 1997, **114**, 203-208.
10. H. Göksu, S. F. Ho, Ö. Metin, K. Korkmaz, A. Mendoza Garcia, M. S. Gültekin and S. Sun, Tandem Dehydrogenation of Ammonia Borane and Hydrogenation of Nitro/Nitrile Compounds Catalyzed by Graphene-Supported NiPd Alloy Nanoparticles, *ACS Catal.*, 2014, **4**, 1777-1782.
11. Y. She, Z. Lu, W. Fan, S. Jewell and M. K. H. Leung, Facile preparation of PdNi/rGO and its electrocatalytic performance towards formic acid oxidation, *J. Mater. Chem. A*, 2014, **2**, 3894-3898.

12. Z. Yin, W. Zhou, Y. Gao, D. Ma, C. J. Kiely and X. Bao, Supported Pd–Cu Bimetallic Nanoparticles That Have High Activity for the Electrochemical Oxidation of Methanol, *Chem. Eur. J.*, 2012, **18**, 4887-4893.
13. J. Ge, P. Wei, G. Wu, Y. Liu, T. Yuan, Z. Li, Y. Qu, Y. Wu, H. Li, Z. Zhuang, X. Hong and Y. Li, Ultrathin Palladium Nanomesh for Electrocatalysis, *Angew. Chem. Int. Ed.*, 2018, **57**, 3435-3438.
14. S. Maity and M. Eswaramoorthy, Ni-Pd bimetallic catalysts for the direct synthesis of H_2O_2 - unusual enhancement of Pd activity in the presence of Ni, *J. Mater. Chem. A*, 2016, **4**, 3233-3237.
15. N. Pentland, J. O. M. Bockris and E. Sheldon, Hydrogen Evolution Reaction on Copper, Gold, Molybdenum, Palladium, Rhodium, and Iron: Mechanism and Measurement Technique under High Purity Conditions, *J. Electrochem. Soc.*, 1957, **104**, 182-194.
16. S. Kukunuri, P. M. Austeria and S. Sampath, Electrically conducting palladium selenide (Pd_4Se, $Pd_{17}Se_{15}$, Pd_7Se_4) phases: synthesis and activity towards hydrogen evolution reaction, *Chem. Commun.*, 2016, **52**, 206-209.
17. S. Sarkar and S. Sampath, Equiatomic ternary chalcogenide: PdPS and its reduced graphene oxide composite for efficient electrocatalytic hydrogen evolution, *Chem. Commun.*, 2014, **50**, 7359-7362.
18. A. Chen and C. Ostrom, Palladium-Based Nanomaterials: Synthesis and Electrochemical Applications, *Chem. Rev.*, 2015, **115**, 11999-12044.
19. M. Shao, Palladium-based electrocatalysts for hydrogen oxidation and oxygen reduction reactions, *J. Power Sources*, 2011, **196**, 2433-2444.
20. M. Shao, T. Yu, J. H. Odell, M. Jin and Y. Xia, Structural dependence of oxygen reduction reaction on palladium nanocrystals, *Chem. Commun.*, 2011, **47**, 6566-6568.
21. J. Jiang, H. Gao, S. Lu, X. Zhang, C.-Y. Wang, W.-K. Wang and H.-Q. Yu, Ni-Pd core-shell nanoparticles with Pt-like oxygen reduction electrocatalytic performance in both acidic and alkaline electrolytes, *J. Mater. Chem. A*, 2017, **5**, 9233-9240.
22. A. Morozan, B. Jousselme and S. Palacin, Low-platinum and platinum-free catalysts for the oxygen reduction reaction at fuel cell cathodes, *Energy Environ. Sci.*, 2011, **4**, 1238-1254.

23. H. Liu, C. Koenigsmann, R. R. Adzic and S. S. Wong, Probing Ultrathin One-Dimensional Pd–Ni Nanostructures As Oxygen Reduction Reaction Catalysts, *ACS Catal.*, 2014, **4**, 2544-2555.
24. Y.-X. Huang, J.-F. Xie, X. Zhang, L. Xiong and H.-Q. Yu, Reduced Graphene Oxide Supported Palladium Nanoparticles via Photoassisted Citrate Reduction for Enhanced Electrocatalytic Activities, *ACS Appl. Mater. Interfaces*, 2014, **6**, 15795-15801.
25. L. Xiong, J.-J. Chen, Y.-X. Huang, W.-W. Li, J.-F. Xie and H.-Q. Yu, An oxygen reduction catalyst derived from a robust Pd-reducing bacterium, *Nano Energy*, 2015, **12**, 33-42.
26. A. U. Nilekar, Y. Xu, J. Zhang, M. B. Vukmirovic, K. Sasaki, R. R. Adzic and M. Mavrikakis, Bimetallic and Ternary Alloys for Improved Oxygen Reduction Catalysis, *Top. Catal.*, 2007, **46**, 276-284.
27. D. K. Singh, R. N. Jenjeti, S. Sampath and M. Eswaramoorthy, Two in one: N-doped tubular carbon nanostructure as an efficient metal-free dual electrocatalyst for hydrogen evolution and oxygen reduction reactions, *J. Mater. Chem. A*, 2017, **5**, 6025-6031.
28. H. B. Yang, J. Miao, S.-F. Hung, J. Chen, H. B. Tao, X. Wang, L. Zhang, R. Chen, J. Gao, H. M. Chen, L. Dai and B. Liu, Identification of catalytic sites for oxygen reduction and oxygen evolution in N-doped graphene materials: Development of highly efficient metal-free bifunctional electrocatalyst, *Science Advances*, 2016, **2**.
29. J. Zhang, L. Qu, G. Shi, J. Liu, J. Chen and L. Dai, N,P-Codoped Carbon Networks as Efficient Metal-free Bifunctional Catalysts for Oxygen Reduction and Hydrogen Evolution Reactions, *Angew. Chem. Int. Ed.*, 2016, **55**, 2230-2234.
30. K. S. Krishna, C. S. S. Sandeep, R. Philip and M. Eswaramoorthy, Mixing Does the Magic: A Rapid Synthesis of High Surface Area Noble Metal Nanosponges Showing Broadband Nonlinear Optical Response, *ACS Nano*, 2010, **4**, 2681-2688.
31. W. Sheng, H. A. Gasteiger and Y. Shao-Horn, Hydrogen Oxidation and Evolution Reaction Kinetics on Platinum: Acid vs Alkaline Electrolytes, *J. Electrochem. Soc.*, 2010, **157**, B1529-B1536.

32. B. E. Conway and B. V. Tilak, Interfacial processes involving electrocatalytic evolution and oxidation of H_2, and the role of chemisorbed H, *Electrochim. Acta*, 2002, **47**, 3571-3594.

33. R. Jana, A. Bhim, P. Bothra, S. K. Pati and S. C. Peter, Electrochemical Dealloying of $PdCu_3$ Nanoparticles to Achieve Pt-like Activity for the Hydrogen Evolution Reaction, *ChemSusChem*, 2016, **9**, 2922-2927.

34. J. M. McEnaney and R. E. Schaak, Solution Synthesis of Metal Silicide Nanoparticles, *Inorg. Chem.*, 2015, **54**, 707-709.

35. L. Cheng, W. Huang, Q. Gong, C. Liu, Z. Liu, Y. Li and H. Dai, Ultrathin WS2 Nanoflakes as a High-Performance Electrocatalyst for the Hydrogen Evolution Reaction, *Angew. Chem. Int. Ed.*, 2014, **53**, 7860-7863.

36. Y. Li, H. Wang, L. Xie, Y. Liang, G. Hong and H. Dai, MoS_2 Nanoparticles Grown on Graphene: An Advanced Catalyst for the Hydrogen Evolution Reaction, *J. Am. Chem. Soc.*, 2011, **133**, 7296-7299.

37. H. Vrubel and X. Hu, Molybdenum Boride and Carbide Catalyze Hydrogen Evolution in both Acidic and Basic Solutions, *Angew. Chem.*, 2012, **124**, 12875-12878.

38. S. Peng, L. Li, X. Han, W. Sun, M. Srinivasan, S. G. Mhaisalkar, F. Cheng, Q. Yan, J. Chen and S. Ramakrishna, Cobalt Sulfide Nanosheet/Graphene/Carbon Nanotube Nanocomposites as Flexible Electrodes for Hydrogen Evolution, *Angew. Chem.*, 2014, **126**, 12802-12807.

39. E. J. Popczun, J. R. McKone, C. G. Read, A. J. Biacchi, A. M. Wiltrout, N. S. Lewis and R. E. Schaak, Nanostructured Nickel Phosphide as an Electrocatalyst for the Hydrogen Evolution Reaction, *J. Am. Chem. Soc.*, 2013, **135**, 9267-9270.

40. P. Xiao, M. A. Sk, L. Thia, X. Ge, R. J. Lim, J.-Y. Wang, K. H. Lim and X. Wang, Molybdenum phosphide as an efficient electrocatalyst for the hydrogen evolution reaction, *Energy Environ. Sci.*, 2014, **7**, 2624-2629.

41. J. Yu, Q. Li, N. Chen, C.-Y. Xu, L. Zhen, J. Wu and V. P. Dravid, Carbon-Coated Nickel Phosphide Nanosheets as Efficient Dual-Electrocatalyst for Overall Water Splitting, *ACS Appl. Mater. Interfaces*, 2016, **8**, 27850-27858.

42. X. Wang, Y. V. Kolen'ko, X.-Q. Bao, K. Kovnir and L. Liu, One-Step Synthesis of Self-Supported Nickel Phosphide Nanosheet Array Cathodes for Efficient

Electrocatalytic Hydrogen Generation, *Angew. Chem. Int. Ed.*, 2015, **54**, 8188-8192.

43. H. Wang, S. Min, Q. Wang, D. Li, G. Casillas, C. Ma, Y. Li, Z. Liu, L.-J. Li, J. Yuan, M. Antonietti and T. Wu, Nitrogen-Doped Nanoporous Carbon Membranes with Co/CoP Janus-Type Nanocrystals as Hydrogen Evolution Electrode in Both Acidic and Alkaline Environments, *ACS Nano*, 2017, **11**, 4358-4364.
44. J. Tian, Q. Liu, N. Cheng, A. M. Asiri and X. Sun, Self-Supported Cu3P Nanowire Arrays as an Integrated High-Performance Three-Dimensional Cathode for Generating Hydrogen from Water, *Angew. Chem. Int. Ed.*, 2014, **53**, 9577-9581.
45. A. J. Bard and L. R. Faulkner, *Electrochemical Methods: Fundamentals and Applications, Wiley: New York*, 2nd edn, 2000.
46. S. Treimer, A. Tang and D. C. Johnson, A Consideration of the Application of Koutecký-Levich Plots in the Diagnoses of Charge-Transfer Mechanisms at Rotated Disk Electrodes, *Electroanalysis*, 2002, **14**, 165-171.
47. H. Erikson, M. Liik, A. Sarapuu, J. Kozlova, V. Sammelselg and K. Tammeveski, Oxygen reduction on electrodeposited Pd coatings on glassy carbon, *Electrochim. Acta*, 2013, **88**, 513-518.
48. L. Kuai, X. Yu, S. Wang, Y. Sang and B. Geng, Au–Pd Alloy and Core–Shell Nanostructures: One-Pot Coreduction Preparation, Formation Mechanism, and Electrochemical Properties, *Langmuir*, 2012, **28**, 7168-7173.
49. A. Cha, J. H. Shim, A. Jo, S. C. Lee, Y. Lee and C. Lee, Facile Synthesis of AuPd Nanochain Networks on Carbon Supports and Their Application as Electrocatalysts for Oxygen Reduction Reaction, *Electroanalysis*, 2014, **26**, 723-731.
50. J.-J. Lv, J.-X. Feng, S.-S. Li, Y.-Y. Wang, A.-J. Wang, Q.-L. Zhang, J.-R. Chen and J.-J. Feng, Ionic liquid crystal-assisted synthesis of PtAg nanoflowers on reduced graphene oxide and their enhanced electrocatalytic activity toward oxygen reduction reaction, *Electrochim. Acta*, 2014, **133**, 407-413.
51. S. Chen, J. Bi, Y. Zhao, L. Yang, C. Zhang, Y. Ma, Q. Wu, X. Wang and Z. Hu, Nitrogen-Doped Carbon Nanocages as Efficient Metal-Free Electrocatalysts for Oxygen Reduction Reaction, *Adv. Mater.*, 2012, **24**, 5593-5597.
52. L. Dai, Y. Xue, L. Qu, H.-J. Choi and J.-B. Baek, Metal-Free Catalysts for Oxygen Reduction Reaction, *Chem. Rev.*, 2015, **115**, 4823-4892.

53. B. Hammer and J. K. Nørskov, Theoretical surface science and catalysis - calculations and concepts, *Adv. Catal.*, 2000, **45**, 71-129.

54. X. Chen, D. Xia, Z. Shi and J. Zhang, Theoretical Study of Oxygen Reduction Reaction Catalysts: From Pt to Non-precious Metal Catalysts. In: Shao M. (eds) Electrocatalysis in Fuel Cells., *Lecture Notes in Energy, vol 9. Springer, London*, 2013, 339-373

55. M. T. Gorzkowski and A. Lewera, Probing the Limits of d-Band Center Theory: Electronic and Electrocatalytic Properties of Pd-Shell–Pt-Core Nanoparticles, *The Journal of Physical Chemistry C*, 2015, **119**, 18389-18395.

56. M. V. Castegnaro, W. J. Paschoalino, M. R. Fernandes, B. Balke, M. C. M. Alves, E. A. Ticianelli and J. Morais, Pd–M/C (M = Pd, Cu, Pt) Electrocatalysts for Oxygen Reduction Reaction in Alkaline Medium: Correlating the Electronic Structure with Activity, *Langmuir*, 2017, **33**, 2734-2743.

Chapter-7

Controlled galvanic replacement of Ni in $Ni(OH)_2$ by Pd: a method to quantify metallic Ni and to synthesize bimetallic catalysts for methanol oxidation

Summary:

In this chapter we have demonstrated a new and simple methodology to quantify the amount of metallic Ni present in the mixed nickel hydroxide/nickel surface using galvanic replacement reaction. This method was also used to manipulate the formation of NiPd on $Ni(OH)_2$ support by controlling the extent of galvanic replacement of Ni by Pd. The bimetallic NiPd nanoparticles supported on $Ni(OH)_2$ prepared by galvanic reaction showed better electrocatalytic activity for methanol oxidation than commercial Pd/C. This approach can be extended to synthesize various nickel containing bimetallic nanoparticles essential for different catalysis.

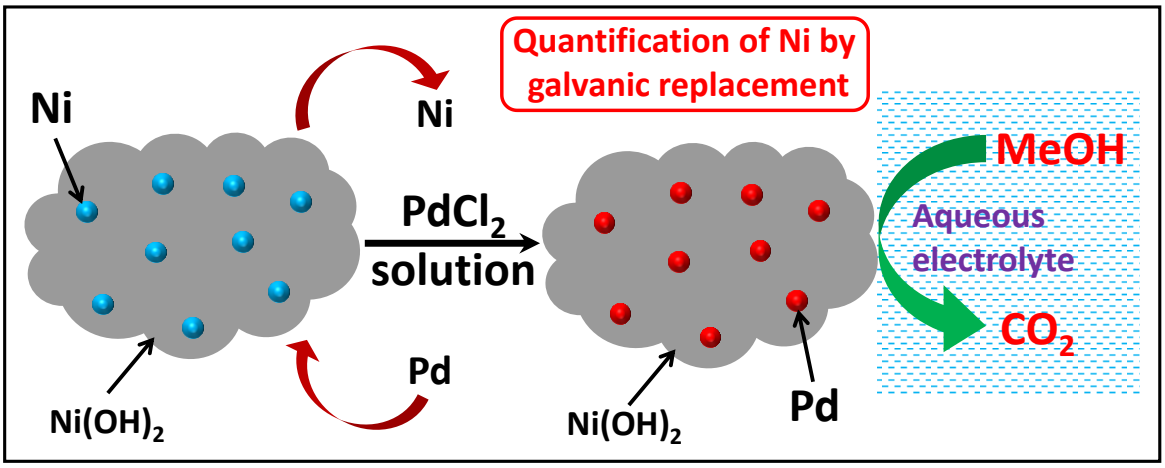

7.1. Introduction:

Bimetallic NiPd catalysts gained a lot of attention in recent years owing to their improved performance than the Pd catalysts in many industrially significant reactions such as hydrogen evolution reaction,[1, 2] oxygen reduction reaction,[3, 4] formic acid oxidation,[1, 5-7] methanol oxidation[8-12] and direct synthesis of hydrogen peroxide.[13] One of the methods often used to obtain NiPd nanostructure is the borohydride reduction of Ni and Pd salt precursors.[9, 13-17] In borohydride reduction, although Pd salt is fully reduced to Pd nanostructure, Ni salt mostly gets converted to $Ni(OH)_2$ and Ni due to higher pH associated with the addition of borohydride.[9, 13] As a corollary, the obtained nanostructures mostly composed of $Ni(OH)_2$ and Ni nanoparticles in addition to NiPd bimetallic nanoparticles. Quantification of metallic Ni present in the $Ni(OH)_2$ is one of the challenging tasks, although metallic Ni (in zero oxidation state) can be analysed using magnetic measurement due to its ferromagnetic behaviour.[13] The Ni nanoparticles in $Ni(OH)_2$ can be further estimated by converting it into Pd nanoparticles through galvanic replacement reaction.[1, 12] This method not only allows us to estimate the total amount of Ni present in zero oxidation state in $Ni(OH)_2$, but also allows us to have a good control on the formation of NiPd bimetallic nanoparticles on $Ni(OH)_2$ support by controlling the time of galvanic replacement reaction.

In this work, we attempted to utilize high surface area porous $Ni(OH)_2$/Ni nanostructure prepared by borohydride reduction method developed by our group[13, 18] as a substrate for galvanic replacement reaction with Pd. The as-synthesized nanostructure, $Ni(OH)_2$/Ni was used as a template for the galvanic replacement of Ni present in $Ni(OH)_2$/Ni by Pd. The resulting NiPd loaded on $Ni(OH)_2$ nanostructure was tested for the electrocatalytic activity for methanol oxidation as the test reaction.

7.2. Scope of the Present Study:

Our previous study (in chapter 1) shows the presence of metallic Ni in $Ni(OH)_2$ can be qualitatively analysed using magnetic measurement. However, quantitative estimation of metallic Ni present in the $Ni(OH)_2$ is quite difficult. In this work, the idea is to develop a new method to quantify the amount of metallic Ni present in the mixed nickel/nickel hydroxide surface by simple galvanic replacement with Pd. This method has also been used to synthesize bimetallic NiPd nanostructure on $Ni(OH)_2$ support.

7.3. Experimental Section:

7.3.1. Materials and Characterization Techniques:

$NiCl_2.6H_2O$ (S D Fine Chemicals), $NaBH_4$ (S D Fine Chemicals), $PdCl_2$ (Sigma Aldrich), NaOH (S D Fine Chemicals), Methanol (S D Fine Chemicals, AR grade), Nafion (5 wt%, Sigma Aldrich), Pd/C (5 wt%, Alfa Aesar) were used as such without any further purification.

Powder X-ray diffraction (PXRD) patterns were recorded using Bruker-D8 diffractometer using Cu Kα radiation, (λ=1.54 Å, step size: 0.02, current: 30 mA and voltage: 40 kV). Field-emission scanning electron microscopy (FESEM) images and energy-dispersive X-ray spectroscopy (EDS) were obtained by using FEI (Nova-Nano SEM-600 Netherlands) equipment. Transmission electron microscope (TEM) imaging was done on a JEOL, JEM 3010 operated at 200 kV. Samples were prepared by putting a drop of very dilute dispersion in ethanol on a TEM grid (carbon polymer, 300 mesh). Inductively coupled plasma – atomic emission spectroscopy (ICP-AES) was carried out using a Perkin−Elmer Optima 7000 DV machine. Gas adsorption-desorption measurements were performed on Autosorb-iQ2 (Quantachrome corp.) at 77 K. The samples were degassed before starting the nitrogen gas sorption analysis under a high vacuum for 12 h at 373 K.

7.3.2. Synthesis of $Ni(OH)_2$/Ni nanostructure:

The $Ni(OH)_2$/Ni nanostructure was synthesized via one step process by the reduction of aqueous $NiCl_2$ solution in presence of $NaBH_4$ at room temperature.[13, 18] In a typical procedure, 20 mL 0.1 M aqueous solution of $NiCl_2$ was rapidly added to a 100 mL 0.1 M aqueous solution of freshly prepared $NaBH_4$ with vigorous stirring. The mixture was allowed to stir for 30 min. The solid product obtained after stirring was separated out and washed with water for several times and finally dried at 50 ^oC for overnight.

7.3.3. Galvanic Replacement of Ni by Pd in $Ni(OH)_2$/Ni Nanostructure:

In a typical procedure, 50 mg of as-synthesized $Ni(OH)_2$/Ni nanostructure was soaked in 10 mL of 10 mM $PdCl_2$ solution with stirring for different time periods (5, 10, 30, 60 and 720 min). The solid product thus obtained was centrifuged and washed thoroughly with distilled water to make sure the complete removal of $PdCl_2$. Finally, the sample was dried at 50 ^oC for overnight. The Pd loading in all the galvanic replacement samples were

analyzed by ICP-AES. The blank experiment was also carried out with $Ni(OH)_2$/Ni in absence of $PdCl_2$ and no leaching of Ni from the sample was observed in the similar conditions.

7.3.4. Electrochemical Measurements:

All the electrochemical measurements were carried out using electrochemical work station obtained from CH instruments (660C, USA) using a three electrode set-up. The measurements were carried out using long Pt-wire having large area as a counter electrode, mercury-mercuric oxide (MMO) electrode as a reference electrode in strong alkaline medium (1 M NaOH) and glassy carbon (GC) electrode having 3 mm diameter (geometric area 0.07068 cm^2) as working electrode. All the electrochemical experiments were carried out in deaerated solution by bubbling Ar gas for 30 minutes with a scan rate of 20 mV s^{-1}. The mass-current densities for all the samples are given with respect to the electrochemically active-mass calculated from Faraday's law.

7.3.5. Electrode Preparation and Methanol Oxidation:

2 mg of the sample was dispersed in a mixture of milli Q water (0.9 mL) and 5 wt. % nafion (0.1 mL) solution and ultrasonicated to obtain a homogeneous catalyst ink. Then, 3 μL of the catalyst ink was drop casted on a cleaned glassy carbon (GC) electrode (3 mm diameter) with a catalyst loading of ~0.085 mg cm^{-2}. The GC electrode was dried in ambient conditions and used as working electrode in the electrochemical studies. The methanol oxidation was carried out using 0.5 M methanol in 1 M aqueous solution of NaOH.

7.4. Results and Discussion:

The $Ni(OH)_2$/Ni nanostructure was synthesized by reduction of $NiCl_2$ in presence of $NaBH_4$ (as discussed in the experimental section). This method produces mostly $Ni(OH)_2$ along with Ni nanoparticles as nickel is prone to hydrolyze to its hydroxide at higher pH produced by the presence of $NaBH_4$.[13] The Ni nanoparticles dispersed in the $Ni(OH)_2$ nanostructure are difficult to detect using powder X-ray diffraction (PXRD) study and can't be quantified by inductively coupled plasma – atomic emission spectroscopic (ICP-AES) analysis.[13] The $Ni(OH)_2$/Ni nanostructure shows a broad X-ray diffraction peak (Figure 7.1a) which confirms the amorphous nature of the sample. The field emission scanning electron microscopy (FESEM) image of $Ni(OH)_2$/Ni shows sponge like morphology (Figure 7.1b).

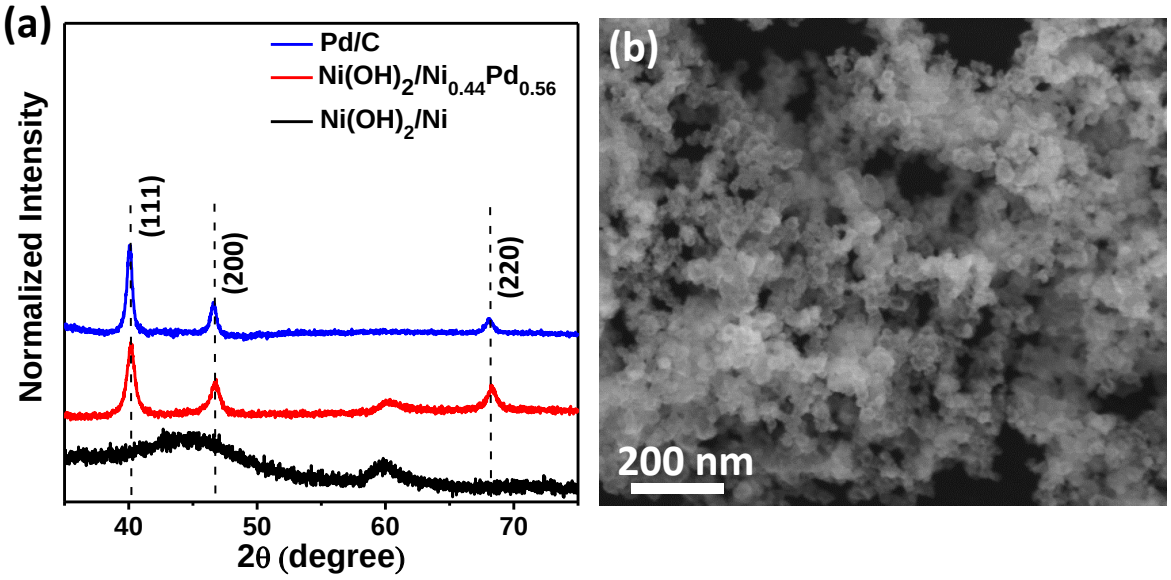

Figure 7.1: *(a) Powder X-ray diffraction (PXRD) patterns of $Ni(OH)_2/Ni$, $Ni(OH)_2/Ni_{0.44}Pd_{0.56}$ (after 5 min galvanic replacement) and compared with commercial Pd/C. (b) Field emission scanning electron microscopy (FESEM) image of $Ni(OH)_2/Ni$.*

Galvanic replacement (details in the experimental section) was carried out by soaking of $Ni(OH)_2/Ni$ in $PdCl_2$ salt solution (10 mM) at different periods of time (5, 10, 30, 60 and 720 min). During the galvanic replacement, Ni metal nanoparticles dispersed in $Ni(OH)_2$ nanostructure were replaced by Pd metal as the reduction potential of Pd^{2+}/Pd (E^o= +0.915 V) is higher than Ni^{2+}/Ni (E^o= –0.25 V). Since the galvanic replacement reactions occur with non-noble metal of zero oxidation state,[19] the amount of metallic Ni present in the mixed metal hydroxide/metal surface can be directly correlated with amount of Pd (Table 7.1). The amount of Pd loading with time by galvanic replacement was quantitatively estimated by ICP-AES and the results are given in Table 7.1. From the table, it is observed that all the metallic Ni was replaced by Pd within 60 min which mostly corresponds to around 0.05 mol% of Ni present in $Ni(OH)_2$. Beyond 60 min time of galvanic replacement, no increase in the Pd loading confirmed from ICP-AES, suggesting that all the nickel (zero valent state) present in the as-prepared sample are replaced by Pd (Table 7.1).

Table 7.1: *Estimation of Pd and Ni in $Ni(OH)_2$ sample at different time intervals of galvanic replacement reaction (analyzed from ICP-AES).*

Time for galvanic replacement (min)	Pd loading in $Ni(OH)_2$/Ni (wt. %)	Pd loading in $Ni(OH)_2$/Ni (mol %)[a]	Remaining Ni in $Ni(OH)_2$/Ni[b] (mol %)	Ni:Pd (mol ratio)	Sample name[c]
5	2.9	0.027	0.021	44:56	$Ni(OH)_2/Ni_{0.44}Pd_{0.56}$
10	3	0.028	0.020	42:58	$Ni(OH)_2/Ni_{0.42}Pd_{0.58}$
30	3.8	0.036	0.012	25:75	$Ni(OH)_2/Ni_{0.25}Pd_{0.75}$
60	5.1	0.048	0	0:100	$Ni(OH)_2$/Pd
720	5.1	0.048	0	0:100	$Ni(OH)_2$/Pd

[a]Pd loading (mol %) with respect to wt. of the catalyst. [b]Remaining Ni in metallic state (mol %) calculated by subtraction from complete galvanic replacement of Ni by Pd beyond 60 min. [c]Ni and Pd mol % is given in the sample name as calculated in the table.

The galvanic replacement reaction carried out for different time periods (10, 30, 60 and 720 min) shows diffraction patterns similar to that of Pd in Pd/C (Figure 7.2). FESEM analysis shows similar morphology as that of $Ni(OH)_2$/Ni nanostructure for all the synthesized samples. $Ni(OH)_2/Ni_{0.25}Pd_{0.75}$ (after 30 min galvanic replacement) was chosen for further studies as it shows better electrocatalytic performance towards methanol oxidation among all the samples. The $Ni(OH)_2/Ni_{0.25}Pd_{0.75}$ (abbreviated as $Ni(OH)_2$/NiPd) sample shows bright spots in FESEM (Figure 7.3a) associated with Pd (lighter element Ni is replaced by heavier Pd). Further, the energy dispersive X-ray spectroscopic (EDS) analysis shows the presence of Pd distributed over the $Ni(OH)_2$/NiPd nanostructure (Figure 7.3a). The transmission electron microscopy (TEM) analysis of $Ni(OH)_2$/NiPd (Figure 7.3b) further confirms the Pd dispersion over $Ni(OH)_2$ nanostructure. The Pd particles are polydispersed in nature and the particles size are in the range of 30 to 50 nm. The Brunauer-Emmett-Teller (BET) surface area calculated from N_2 adsorption-desorption isotherm for $Ni(OH)_2$/Ni (Figure 7.4) at 77 K is around 64 m^2/g which did not change significantly for $Ni(OH)_2$/NiPd sample. This suggests that in galvanic replacement reaction the morphology and surface area of the template, $Ni(OH)_2$ is retained.[12]

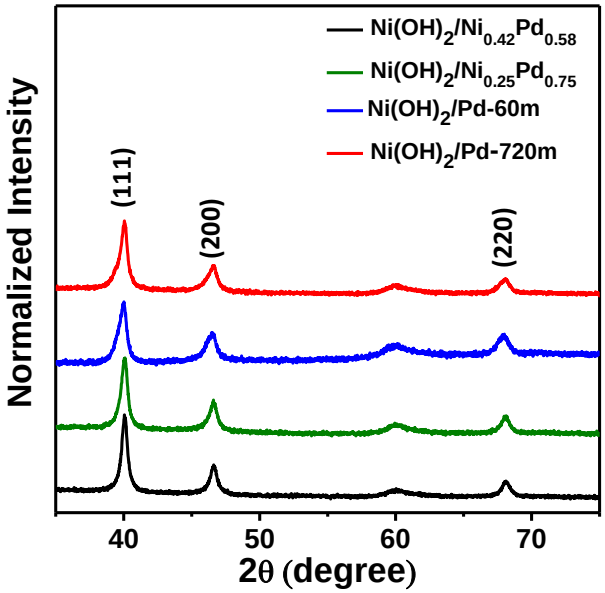

Figure 7.2: *PXRD patterns of different galvanic replacement samples prepared at different time periods (10, 30, 60 and 720 min).*

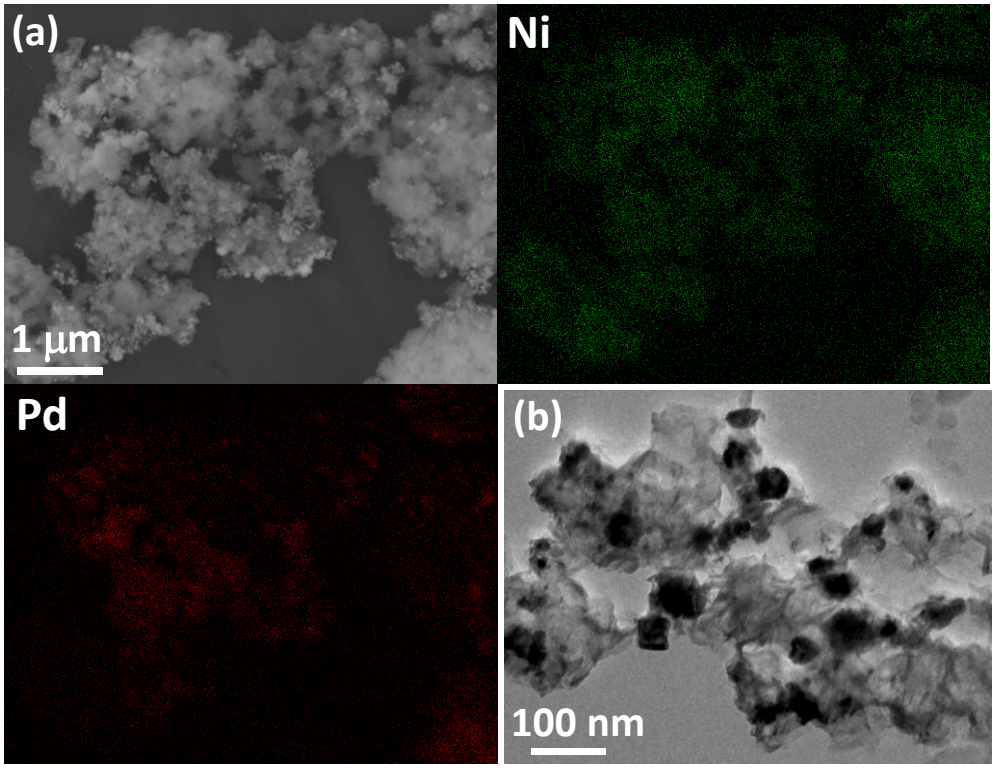

Figure 7.3: *Characterization of $Ni(OH)_2$/NiPd sample after 30 min of galvanic replacement. (a) Field emission scanning electron microscopy (FESEM) image of $Ni(OH)_2$/NiPd and the corresponding electron mapping of Ni and Pd respectively. (b) Transmission electron microscopy (TEM) image of $Ni(OH)_2$/NiPd.*

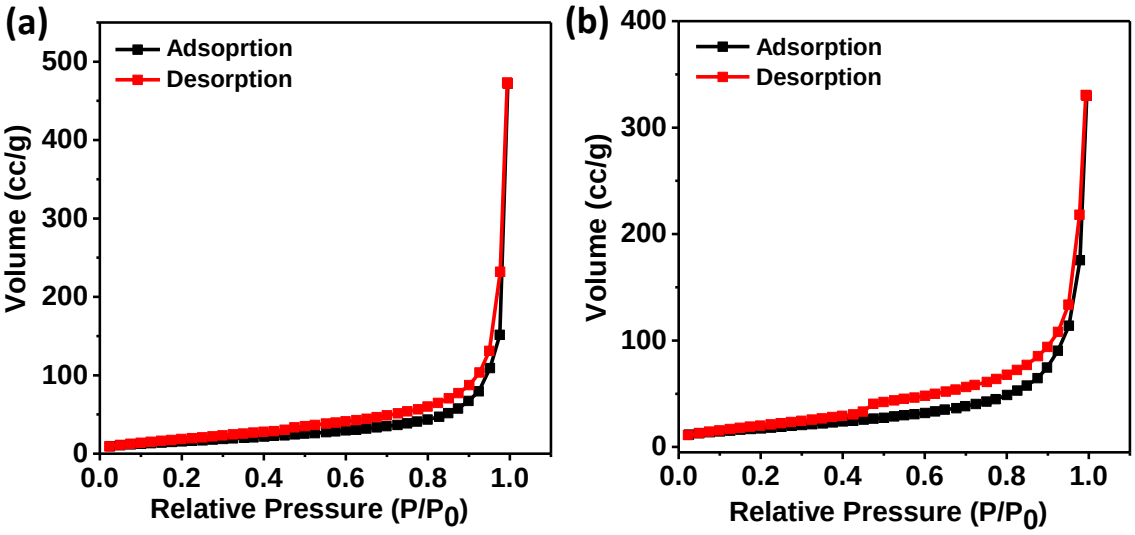

Figure 7.4: *N_2 adsorption-desorption isotherms of (a) $Ni(OH)_2$/Ni and (b) $Ni(OH)_2$/NiPd (after 30 min galvanic replacement) nanostructure measured at 77 K.*

The electrochemical response of $Ni(OH)_2$/Ni nanostructure was studied in deaerated 1 M NaOH solution (purged with Ar gas for 30 min) using long Pt-wire having large area as a counter electrode, mercury-mercuric oxide (MMO) electrode as a reference electrode. The cyclic voltammogram (CV) of $Ni(OH)_2$/Ni nanostructure shows a couple of redox peaks at 1.4 V and 1.73 V (vs. RHE, reversible hydrogen electrode) (Figure 7.5a) associated with the formation of NiOOH from $Ni(OH)_2$ as reported in the literature.[20] The characteristic response of Pd in CV was observed (like hydrogen adsorption-desorption behavior) in the potential regime –0.06 V to 0.35 V (vs. RHE) and PdO reduction peak at 0.68 V (vs. RHE) (Figure 7.5b). The amount of active Pd present in each sample was calculated from coulombic charge for the reduction of PdO using Faraday's law. The coulombic charge for mono layer desorption of oxygen from the Pd surface is 405 μC cm^{-2}.[21] These values were compared with ICP-AES analyses and it was observed that the amount of Pd calculated from Faraday's law is very less than the ICP-AES analysis (Figure 7.6). This can be attributed to the fact that the Faraday's method takes into account only the electrochemically active Pd present in the sample whereas, the ICP-AES gives the total amount of Pd present in the sample. It is important to note that Pd loading due to galvanic reaction is very fast as complete replacement occurs in 60 min as estimated from ICP-AES (Table 7.1). The reaction time (galvanic replacement) versus the amount of Pd deposited on $Ni(OH)_2$ shows that all the nickel in zero valent state is replaced within 60 minutes as

there is no significant difference in the amount of Pd loading beyond 60 minutes of galvanic reaction (Figure 7.6).

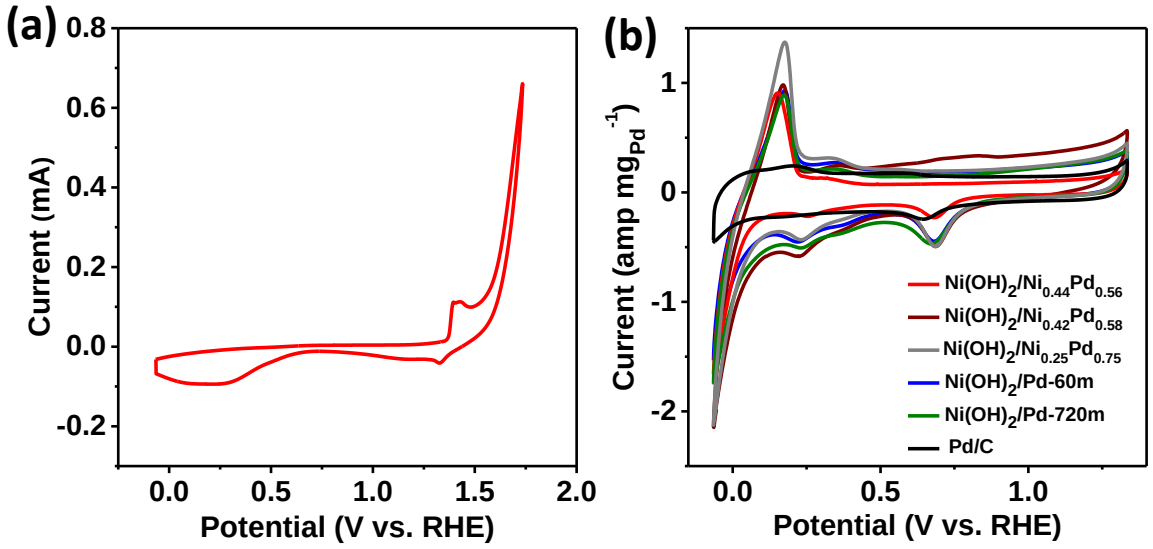

Figure 7.5: *Electrochemical characterization of all the samples. Cyclic voltammograms of (a) Ni(OH)$_2$/Ni and (b) different galvanic replacement samples and Pd/C measured in 1 M aqueous solution of NaOH with a scan rate of 20 mV s^{-1}.*

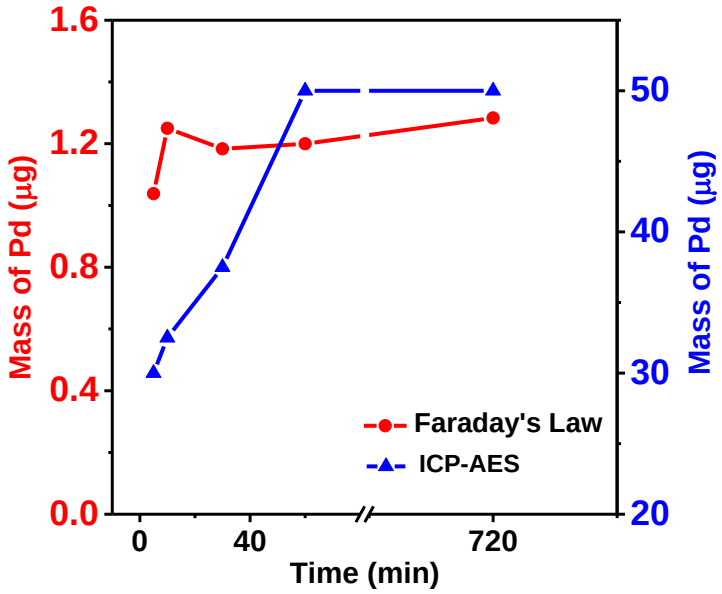

Figure 7.6: *The time (for galvanic replacement) versus amount of Pd (per mg of catalyst) analyzed from Faraday's law and inductively coupled plasma - atomic emission spectroscopy (ICP-AES) analyses.*

Methanol oxidation was carried out using 0.5 M methanol in 1 M NaOH solution for all the synthesized catalysts and compared with commercially purchased Pd/C. $Ni(OH)_2$/Ni nanostructure shows methanol oxidation at the potential where NiOOH/$Ni(OH)_2$ transformation and oxygen evolution reaction occurs (Figure 7.7a) as observed in the literature.[14, 20] By replacing of Ni by Pd using galvanic replacement reaction, methanol oxidation was observed at very low potential of 0.79 V vs. RHE for $Ni(OH)_2$/NiPd (Figure 7.7b). On comparison to Pd/C, it shows large potential shift, 18 mV towards lower potential signifying the role of synergistic effect of Ni with Pd for the oxidation of methanol (Figure 7.7b). $Ni(OH)_2$/NiPd catalyst with different Ni and Pd compositions also show relatively better activity for methanol oxidation as compared to Pd/C. It is also interesting to note that there is almost no change in the onset potential of methanol oxidation for the catalysts prepared by 5, 10 and 30 min galvanic replacements (Table 7.1), whereas the catalysts obtained beyond 60 min show similar onset potential as that of Pd/C (Figure 7.7b). This indicates that the catalysts contain only Pd nanoparticles (no NiPd) is less active for methanol oxidation compared to other catalysts prepared at shorter time periods.

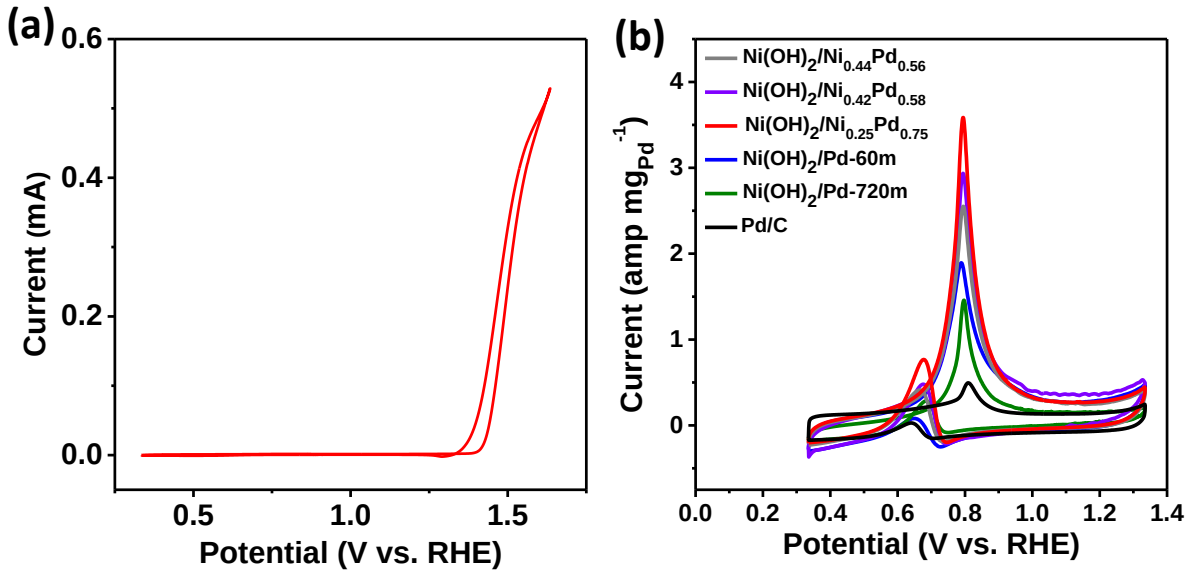

Figure 7.7: *Cyclic voltammograms of (a) $Ni(OH)_2$/Ni and (b) different galvanic replacement samples and Pd/C towards methanol oxidation carried out using 0.5 M methanol in 1 M NaOH.*

The catalyst stability towards methanol oxidation is studied using current-time study at fixed potential for 1h period. Figure 7.8 shows $Ni(OH)_2$/NiPd catalyst is as stable as Pd/C. In addition, the current observed is higher in $Ni(OH)_2$/NiPd than Pd/C which is also reflected in cyclic voltammetry studies.

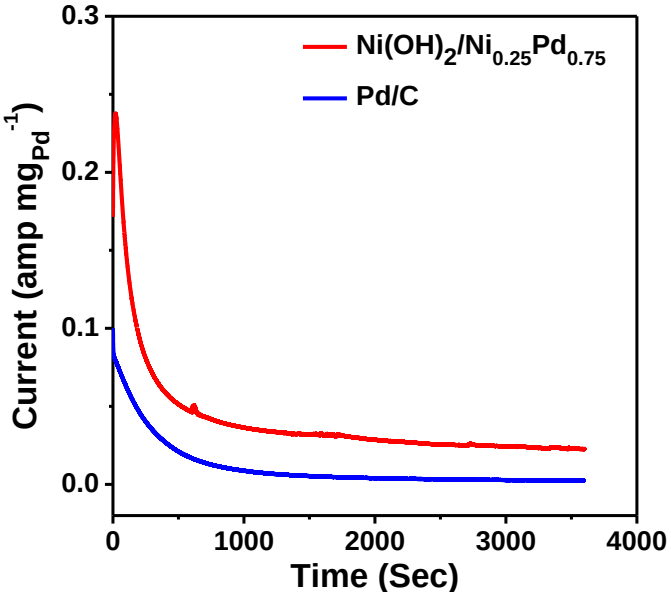

Figure 7.8: *Current-time (i-t) curve of $Ni(OH)_2$/NiPd and Pd/C catalyst to check the stability towards methanol oxidation reaction.*

7.5. Conclusion:

In conclusion, galvanic replacement was successfully employed to quantitatively estimate the amount of Ni present in the $Ni(OH)_2$/Ni. This method was also used to synthesize bimetallic NiPd supported on $Ni(OH)_2$ which can be used as a "carbon-free" catalyst. NiPd nanoparticles (with different Ni:Pd ratio) supported on $Ni(OH)_2$ were prepared by controlling the galvanic replacement time. Bimetallic NiPd ($Ni(OH)_2$/NiPd) prepared by 30 min galvanic replacement reaction showed better performance towards oxidation of methanol as compared to commercial Pd/C catalyst. As this method of preparation is simple and doesn't require any additional additives, this can be extended to prepare other nickel containing noble metal nanostructures for various electrochemical applications.

7.6. References:

1. H. Rasouli, S. H. Tabaian and M. Rezaei, Galvanic replacement of electrodeposited nickel by palladium and investigation of the electrocatalytic activity of synthesized Pd/(Ni) for hydrogen evolution and formic acid oxidation, *R. Soc. Chem. Adv*, 2016, **6**, 22500-22510.
2. J. Li, P. Zhou, F. Li, R. Ren, Y. Liu, J. Niu, J. Ma, X. Zhang, M. Tian, J. Jin and J. Ma, Ni@Pd/PEI-rGO stack structures with controllable Pd shell thickness as advanced electrodes for efficient hydrogen evolution, *J. Mater. Chem. A*, 2015, **3**, 11261-11268.
3. J. Jiang, H. Gao, S. Lu, X. Zhang, C.-Y. Wang, W.-K. Wang and H.-Q. Yu, Ni-Pd core-shell nanoparticles with Pt-like oxygen reduction electrocatalytic performance in both acidic and alkaline electrolytes, *J. Mater. Chem. A*, 2017, **5**, 9233-9240.
4. H. Liu, C. Koenigsmann, R. R. Adzic and S. S. Wong, Probing Ultrathin One-Dimensional Pd–Ni Nanostructures As Oxygen Reduction Reaction Catalysts, *ACS Catal.*, 2014, **4**, 2544-2555.
5. Y. She, Z. Lu, W. Fan, S. Jewell and M. K. H. Leung, Facile preparation of PdNi/rGO and its electrocatalytic performance towards formic acid oxidation, *J. Mater. Chem. A*, 2014, **2**, 3894-3898.
6. D. Bin, B. Yang, F. Ren, K. Zhang, P. Yang and Y. Du, Facile synthesis of PdNi nanowire networks supported on reduced graphene oxide with enhanced catalytic performance for formic acid oxidation, *J. Mater. Chem. A*, 2015, **3**, 14001-14006.
7. R. Li, Z. Wei, T. Huang and A. Yu, Ultrasonic-assisted synthesis of Pd–Ni alloy catalysts supported on multi-walled carbon nanotubes for formic acid electrooxidation, *Electrochim. Acta*, 2011, **56**, 6860-6865.
8. B. Cai, D. Wen, W. Liu, A.-K. Herrmann, A. Benad and A. Eychmüller, Function-Led Design of Aerogels: Self-Assembly of Alloyed PdNi Hollow Nanospheres for Efficient Electrocatalysis, *Angew. Chem. Int. Ed.*, 2015, **54**, 13101-13105.
9. C. Zhu, D. Wen, M. Oschatz, M. Holzschuh, W. Liu, A.-K. Herrmann, F. Simon, S. Kaskel and A. Eychmüller, Kinetically Controlled Synthesis of PdNi Bimetallic Porous Nanostructures with Enhanced Electrocatalytic Activity, *Small*, 2015, **11**, 1430-1434.
10. J. C. Calderón, M. J. Nieto-Monge, S. Pérez-Rodríguez, J. I. Pardo, R. Moliner and M. J. Lázaro, Palladium–nickel catalysts supported on different chemically-treated

carbon blacks for methanol oxidation in alkaline media, *Int. J. Hydrogen Energy*, 2016, **41**, 19556-19569.

11. P. Xi, Y. Cao, F. Yang, C. Ma, F. Chen, S. Yu, S. Wang, Z. Zeng and X. Zhang, Facile synthesis of Pd-based bimetallic nanocrystals and their application as catalysts for methanol oxidation reaction, *Nanoscale*, 2013, **5**, 6124-6130.
12. X. Niu, H. Zhao and M. Lan, Palladium deposits spontaneously grown on nickel foam for electro-catalyzing methanol oxidation: Effect of precursors, *J. Power Sources*, 2016, **306**, 361-368.
13. S. Maity and M. Eswaramoorthy, Ni-Pd bimetallic catalysts for the direct synthesis of H_2O_2 - unusual enhancement of Pd activity in the presence of Ni, *J. Mater. Chem. A*, 2016, **4**, 3233-3237.
14. L. Trotochaud, S. L. Young, J. K. Ranney and S. W. Boettcher, Nickel–Iron Oxyhydroxide Oxygen-Evolution Electrocatalysts: The Role of Intentional and Incidental Iron Incorporation, *J. Am. Chem. Soc.*, 2014, **136**, 6744-6753.
15. R. N. Singh, A. Singh and Anindita, Electrocatalytic activity of binary and ternary composite films of Pd, MWCNT and Ni, Part II: Methanol electrooxidation in 1M KOH, *Int. J. Hydrogen Energy*, 2009, **34**, 2052-2057.
16. R. N. Singh, A. Singh and Anindita, Electrocatalytic activity of binary and ternary composite films of Pd, MWCNT, and Ni for ethanol electro-oxidation in alkaline solutions, *Carbon*, 2009, **47**, 271-278.
17. R. S. Amin, R. M. Abdel Hameed, K. M. El-Khatib and M. Elsayed Youssef, Electrocatalytic activity of nanostructured Ni and Pd–Ni on Vulcan XC-72R carbon black for methanol oxidation in alkaline medium, *Int. J. Hydrogen Energy*, 2014, **39**, 2026-2041.
18. K. S. Krishna, C. S. S. Sandeep, R. Philip and M. Eswaramoorthy, Mixing Does the Magic: A Rapid Synthesis of High Surface Area Noble Metal Nanosponges Showing Broadband Nonlinear Optical Response, *ACS Nano*, 2010, **4**, 2681-2688.
19. A. Papaderakis, I. Mintsouli, J. Georgieva and S. Sotiropoulos, Electrocatalysts Prepared by Galvanic Replacement, *Catalysts*, 2017, **7**, 80.
20. C. Qiu, R. Shang, Y. Xie, Y. Bu, C. Li and H. Ma, Electrocatalytic activity of bimetallic Pd–Ni thin films towards the oxidation of methanol and ethanol, *Mater. Chem. Phys.*, 2010, **120**, 323-330.

21. D. A. J. Rand and R. Woods, The nature of adsorbed oxygen on rhodium, palladium and gold electrodes, *J. Electroanal. Chem. Interfacial Electrochem.*, 1971, **31**, 29-38.

Chapter-8

Summary and conclusion

The thesis deals with new materials for heterogeneous catalysis, hydrogen peroxide synthesis and electrocatalysis. The first part of the thesis is focused on NiPd based bimetallic catalysts for the direct synthesis of hydrogen peroxide, a possible alternative to the existing anthraquinone method. The unusual enhancement in the catalytic activity of Pd in presence of Ni was observed for hydrogen peroxide synthesis. Introduction of a small amount of Pt as a promoter in NiPd catalyst (synthesized on carbon support) further improved the catalytic activity for hydrogen peroxide synthesis.

Energy related materials are another emerging area of research in the field of science and technology. Enormous efforts have been made in designing and developing efficient electrocatalysts from the cost-effective earth abundant elements. The second part of the thesis focuses on new approaches for the synthesis of high surface area transition metal and Pd based materials for various electrocatalytic applications. In the chapter 5, a new method to synthesize high surface area ternary phosphides (NiCoP) is described and these phosphides show very good performance for oxygen evolution reaction. A rapid synthesis of high surface area, Ni containing Pd nanostructure is demonstrated in chapter 6. The bimetallic NiPd shows Pt-like activity for hydrogen evolution and oxygen reduction reaction which could be utilized as an alternative to Pt. Chapter 7 discusses about a simple method to prepare NiPd nanostructures on $Ni(OH)_2$ support by galvanic replacement reaction and their electrochemical activity for methanol oxidation.

Overall, the thesis is mainly focused on transition metal and Pd based bimetallic catalysts for heterogeneous catalysis (hydrogen peroxide synthesis) and electrocatalytic applications. We have shown that the activity of Pd, improved phenomenally in presence of transition metal, Ni which would reduce the cost of the catalysts.